THÈSE

présentée
pour obtenir le titre de

DOCTEUR DE L'UNIVERSITÉ DE BORDEAUX

Spécialité : Automatique, Productique, Signal et Image

par **Héctor Enrique Poveda Poveda**

Techniques d'Estimation de Canal et de Décalage de Fréquence Porteuse pour Systèmes Sans-fil Multiporteuses en Liaison Montante

Soutenue le 14 décembre 2011 devant le jury composé de :

Jean-Pierre CANCES	Professeur des Universités, ENSIL	Rapporteurs
Nicolaï CHRISTOV	Professeur des Universités, Université de Lille	
Christophe JEGO	Professeur des Universités, IPB-ENSEIRB-MATMECA	
Sébastien HOUCKE	Maître des Conférences, Telecom Bretagne	
Eric GRIVEL	Professeur des Universités, IPB-ENSEIRB-MATMECA	Directeur de thèse
Guillaume FERRÉ	Maître des Conférences, IPB-ENSEIRB-MATMECA	Co-encadrant

Acknowledgments

Abstract

Multicarrier modulation is the common feature of high-data rate mobile wireless systems. In that case, two phenomena disturb the symbol detection. Firstly, due to the relative transmitter-receiver motion and a difference between the local oscillator (LO) frequency at the transmitter and the receiver, a carrier frequency offset (CFO) affects the received signal. This leads to an intercarrier interference (ICI). Secondly, several versions of the transmitted signal are received due to the wireless propagation channel. These unwanted phenomena must be taken into account when designing a receiver. As estimating the multipath channel and the CFO is essential, this PhD deals with several CFO and channel estimation methods based on optimal filtering.

Firstly, as the estimation issue is nonlinear, we suggest using the extended Kalman filter (EKF). It is based on a local linearization of the equations around the last state estimate. However, this approach requires a linearization based on calculations of Jacobians and Hessians matrices and may not be a sufficient description of the nonlinearity. For these reasons, we can consider the sigma-point Kalman filter (SPKF), namely the unscented Kalman Filter (UKF) and the central difference Kalman filter (CDKF). The UKF is based on the unscented transformation whereas the CDKF is based on the second order Sterling polynomial interpolation formula. Nevertheless, the above methods require an exact and accurate *a priori* system model as well as perfect knowledge of the additive measurement-noise statistics. Therefore, we propose to use the H_∞ filtering, which is known to be more robust to uncertainties than Kalman filtering. As the state-space representation of the system is non-linear, we first evaluate the "extended H_∞ filter", which is based on a linearization of the state-space equations like the EKF. As an alternative, the "unscented H_∞ filter", which has been recently proposed in the literature, is implemented by embedding the unscented transformation into the "extended H_∞ filter" and carrying out the filtering by using the statistical linear error propagation approach.

The above techniques have been implemented in different multicarrier contexts: Firstly, we address the estimation of the multiple CFOs and channels by means

of a control data in an uplink orthogonal frequency division multiple access (OFDMA) system. To reduce the amount of control data, the optimal filtering techniques are combined in an iterative way with the so-called minimum mean square error successive detector (MMSE-SD) to obtain an estimator that does not require pilot subcarriers.

Then, as the SPKF gives a better compromise between computational complexity and estimation performances when the noise characteristics are available, we use this filter in a dynamic bandwidth allocation context. In that case, network resources are dynamically adjusted to give the appropriate bandwidth to each user at any time. This plays a key role in cognitive radio systems where the spectrum that is not used by licensed (primary) users must be detected in order to be shared with unlicensed (secondary) users. However, harmful narrow band interferences (NBI) produced by a cognitive radio system may appear. Therefore, we propose to combine the estimation of the CFOs and channels by means of SPKF with a statistical test to check whether there are interferences or not. Two statistical tests, namely the binary hypothesis test (BHT) and the cumulative sum (CUSUM) test, are studied.

Secondly, we deal with a system that combines orthogonal frequency division multiplexing (OFDM) and the interleaved division multiple access (IDMA). The OFDM-IDMA systems achieve a very high single-user capacity. However, the complexity in the correction of the CFO effects is higher than in OFDMA systems. For that reason, we propose to modify the iterative architecture of the IDMA receiver by using the estimations performed by a SPKF. In addition, an iterative space-time block coding (STBC) OFDM-IDMA receiver is proposed.

The above optimal-filtering based architectures in the OFDMA and OFDM-IDMA are compared with existing estimation methods. Simulation results clearly show the efficiency of the proposed algorithms in terms of CFO estimation, channel estimation and bit error rate performances.

Contents

Acronyms and Abbreviations

1,2,3,4G	1st, 2nd, 3rd, 4th Generation Mobile Wireless Systems
3GPP	3rd Generation Partnership Project
3GPP2	3rd Generation Partnership Project 2
A/D	Analog-Digital
ADD CP	ADDition of a Cyclic Prefix
AF	Amplify-and-Forward
AMPS	Advanced Mobile Phone Service
AWGN	Additive White Gaussian Noise
BHT	Binary Hypothesis Test
BPF	Band-Pass Filter
BPSK	Binary Phase-Shift Keying
BS	Base Station
CAS	Carrier Allocation Strategy
CDKF	Central Difference Kalman Filter
CDMA	Code Division Multiple Access
CDMA EVDO	CDMA EVolution-Data Optimized
CFO	Carrier Frequency Offset
CIR	Channel Impulse Response
CP	Cyclic Prefix
CR	Cognitive Radio
CR-NBI	Cognitive Radio Narrow-Band Interference
CSI	Channel State Information
CUSUM	CUmulative SUM
D/A	Digital-Analog
DAB	Digital Audio Broadcasting
DDF	Divided Difference Filter
DEC	DECoder
DF	Decode-and-Forward
DFT	Discrete Fourier Transform
DVB-T	Digital Video Broadcasting Terrestrial
EDGE	Enhanced Data rates for GSM Evolution
EDGEev	Enhanced Data rates for GSM Evolution evolved
EKF	Extended Kalman Filter

Acronyms and Abbreviations

EM	Expectation-Maximization
ENC	low-data rate ENCoder
EQU	channel EQUalizer
ESE	Elementary Signal Estimator
FCC	Federal Communications Commission
FDMA	Frequency Division Multiple Access
FFT	Fast Fourier Transform
GPRS	General Packet Radio Service
GRV	Gaussian Random Variable
GSM	Global System for Mobile Communications
HSDPA	High-Speed Downlink Packet Access
HSPA+	High-Speed Packet Access Plus
HSUPA	High-Speed Uplink Packet Access
IBI	Inter Block Interference
IC	Interference Cancellation
ICI	Inter Carrier Interference
IDFT	Inverse Discrete Fourier Transform
IDMA	Interleaved Division Multiple Access
IEEE	Institute of Electrical and Electronics Engineers
IEKF	Iterative Extended Kalman Filter
IFFT	Inverse Fast Fourier Transform
ISI	Inter Symbol Interference
ITU	International Telecommunication Union
KF	Kalman Filter
LLR	Logarithm Likelihood Ratio
LMS	Least Mean Squares
LO	Local Oscillator
LS	Least-Squares
LTE	Long Term Evolution
LTE-A	LTE Advanced
M-PSK	M-ary Phase-Shift Keying
MAI	Multiple Access Interference
MAP	Maximum *A Posteriori*
MC-CDMA	Multi Carrier CDMA
MC-DS-CDMA	Multi Carrier Direct Sequence CDMA
MIMO	Multiple-Input Multiple-Output
ML	Maximum Likelihood
MMSE	Minimum Mean Square Error
MMSE-SD	Minimum Mean Square Error Successive Detection
MRC	Maximum Ratio Combining
NAMTS	Nippon Automatic Mobile Telephone System

NBI	Narrow-Band Interference
OFDM	Orthogonal Frequency Division Multiplexing
OFDMA	Orthogonal Frequency Division Multiple Access
OQAM	Offset Quadrature Amplitude Modulation
P/S	Parallel-Serial converter
PDC	Personal Digital Cellular
PU	Primary User
QKF	Quadrature Kalman Filter
QPSK	Quadrature Phase-Shift Keying
RF	Radio Frequency
RLS	Recursive Least Squares
SAGE	Space Alternating Generalized Expectation-maximization
SC-FDMA	Single Carrier Frequency Division Multiple Access
SIR	Signal-to-Interference Ratio
SNR	Signal-to-Noise Ratio
SOEKF	Second-Order Kalman Filter
SPKF	Sigma-Point Kalman Filter
SPKF-BHT	Sigma-Point Kalman Filter combined with a BHT
SPKF-CT	Sigma-Point Kalman Filter combined with a CUSUM Test
SR-UKF	Square-Root UKF
STBC	Space Time Block Code
TACS	Total Access Communication System
TDMA	Time Division Multiple Access
UKF	Unscented Kalman Filter
UMB	Ultra Mobile Broadband
UMTS	Universal Mobile Telecommunication System
WCDMA	Wideband CDMA
WiMAX	Worldwide Interoperability of Microwave Access
WLAN	Wireless Local Area Network

List of Figures

List of Tables

Notations

$\mathbf{A}$	OFDMA symbol vector after the convolution with the channel
$\mathbf{B}$	Additive white Gaussian noise vector
$\mathbf{E}_u$	CFO matrix of the uth user
ϵ_u	Normalized CFO of the uth user
$\hat{\epsilon}_u$	Estimation of ϵ_u
ϵ_u^{pu}	Normalized CFO of the uth user in the PU-OFDMA system
$\hat{\epsilon}_u^{pu}$	Estimation of ϵ_u^{pu}
$\mathbf{F}$	Fourier matrix
$\mathbf{F}^H$	Inverse Fourier matrix
$\mathbf{h}_u$	CSI vector of the uth user
$\hat{\mathbf{h}}_u$	Estimation of $\mathbf{h}_u$
$\mathbf{h}_u^{pu}$	CSI vector of the uth user in the PU-OFDMA system
$\hat{\mathbf{h}}_u^{pu}$	Estimation of $\mathbf{h}_u^{pu}$
$\mathbf{I}_x$	Identity matrix of size $x \times x$
K	Number of subcarriers
K^{pu}	Number of subcarriers of the PU-OFDMA system
K^{cr}	Number of subcarriers of the CR system
$\mathbf{K}(n)$	Kalman gain at time n
$\mathbf{K}^{\infty}(n)$	H$_{\infty}$ gain at time n
L	Number of paths of the channel
L_u	Number of paths of the channel associated to the uth user
L_u^{pu}	Number of paths of the channel associated to the uth user of the PU-OFDMA system
$\mathbf{P}(n\|n-1)$	Covariance matrix of the *a priori* estimation error, when using Kalman filtering
$\mathbf{P}(n\|n)$	Covariance matrix of the *a posteriori* estimation error, when using Kalman filtering
$\mathbf{P}^{\infty}(n\|n)$	Recursive estimate of the Ricatti equation solution in a H$_{\infty}$ setting

P_{fa}	Probability of false alarm
$R(n)$	nth sample of the received OFDMA or OFDM-IDMA symbol
$R(m^{pu}, n)$	nth sample of the received m^{pu}th PU-OFDMA symbol
$\mathbf{S}$	Symbol (M-PSK symbol) vector
T	OFDMA symbol time
T_s	Symbol time
T_{samp}	Sampling time, $T_{samp} = T_s$ in the OFDM case
T_c	Channel coherence time
$\mathbf{X}$	OFDMA or OFDM-IDMA modulated symbol vector
$\mathbf{x}(n)$	State vector containing the channels and the CFOs
W	Transmitted-signal bandwidth
W_c	Channel coherence bandwidth
W^{pu}	PU-OFDMA transmitted signal bandwidth
W^{cr}	CR transmitted signal bandwidth
$\mathbf{Y}(n, \mathbf{x}(n))$	Observation vector, storing the real and the imaginary parts of $R(n)$ or $R(m^{pu}, n)$
$\mathfrak{J}^{sd}$	Number of iterations when using the OFDMA non-pilot receiver
$\mathfrak{J}^{idma}$	Number of iterations when using the OFDM-IDMA receiver
Ξ^2	Prescribed noise attenuation level
β	Factor improving the detection of the disturbance
$\mathcal{P}_b\{.\}$	Probability distribution of $\{.\}$
$\mathbb{E}\{.\}$	Expectation of $\{.\}$
$\text{Var}\{.\}$	Variance of $\{.\}$
$\propto$	Proportional to
$\text{diag}\{.\}$	Diagonal matrix with entries in the main diagonal of $\{.\}$
$Im\{.\}$	Imaginary part of $\{.\}$
$Re\{.\}$	Real part of $\{.\}$
$\{.\}^H$	Hermitian matrix of $\{.\}$
$\{.\}^T$	Transpose matrix of $\{.\}$
$\{.\}^*$	Conjugate of $\{.\}$
$tr\{.\}$	Trace of $\{.\}$
$\|.\|$	Euclidean norm of $\{.\}$
$\lfloor.\rfloor$	Integer part of $\{.\}$

Introduction

For more than 25 years, a great deal of interest has been paid to mobile communication systems and the design of new schemes to transmit and receive information. Engineers and researchers have worked much and exchanged on that topic.

Several PhD in the signal group at the UMR CNRS 5218 IMS have dealt with channel estimation and symbol detection in multicarrier systems involving several users. In [Jamo 07b], the channel was assumed to be an autoregressive (AR) process. Jamoos suggested estimating both the channel and its AR parameters by using training sequences and optimal filtering. To avoid an approach dedicated to the non-linear estimation issue, mutually interactive optimal filters were used. One filter aimed at estimating the channel, whereas the other updated the estimation of the AR parameters. H_∞ and Kalman filtering were tested and the resulting approaches were studied in a multicarrier direct-sequence code division multiple access system (MC-DS-CDMA). In [Grol 07], the channel was modeled by a sinusoidal stochastic process or a low-pass filter version of an AR process. Then, both the symbols and the Rayleigh fading channel were jointly estimated in MC-DS-CDMA systems by using a Rao-Blackwellized particle filter cross-coupled with a Kalman filter.

Despite the great success of the CDMA as a multiple access technique, the current trend is to use the orthogonal frequency division multiple access (OFDMA) and the orthogonal frequency division multiplexing-interleaved division multiple access (OFDM-IDMA). In that case, the input data stream is split into a number of streams that are transmitted in parallel over a large number of orthogonal subcarriers. The frequency-selective fading over the entire bandwidth of the transmitted signal has hence the advantage of being converted in frequency-flat fading over each subcarrier. It should be noted that these schemes are particularly well adapted to mobile wireless communication to provide high-data rate services, e.g. [3GPP 09], [IEEE 06].

However, there are two unwanted phenomena:

1/ the channel remains unknown and hence has to be estimated.

2/ The relative transmitter-receiver motion and a difference between the local-oscillator (LO) frequencies at the transmitter and the receiver lead to a carrier frequency offset (CFO). These CFOs that affect the received signal no longer guarantee orthogonality between subcarriers. To avoid the resulting intercarrier interference (ICI), a CFO estimation/correction step must be introduced at the receiver.

In the literature, some authors focus their attentions on the CFO estimation [More 04], [Zhao 06], [Jing 08], while others address the joint estimation of the CFOs and the channels. More specifically, a conventional expectation-maximization (EM) algorithm is proposed in [Pun 04a] for an OFDMA uplink system. Then, to reduce the computational cost of the EM algorithm, the authors use the space alternating generalized expectation-maximization (SAGE) algorithm. Instead of addressing a multidimensional optimization issue, the so-called alternating projection estimator is used in [Pun 06]. This method consists in iteratively estimating the CFO of one user, by means of an exhaustive grid search over the possible range of the CFO value and by setting the other CFOs to their last updated values. In [Fu 06], Fu *et al.* propose two iterative estimation approaches using the SAGE method. In [Sezg 08], Sezginer *et al.* propose an iterative sub-optimal method. It is based on an approximation of a maximum likelihood (ML) estimator to reduce the computational complexity of the EM-based algorithms. Nevertheless, an initialization step is required in the above algorithms. Another drawback of those methods is the high computational cost due to the iterative estimation and the exhaustive grid search.

In this PhD dissertation, our contribution is twofold:

1/ from the estimation point of view: as the joint estimation of the CFO and the channel is a non-linear estimation problem, we propose to use variants of the Kalman filter and H_∞ filter. Based on a comparative study, we evaluate the performance of the approaches in two uplink multicarrier contexts: the OFDMA and the OFDM-IDMA systems. Various criteria are taken into account, such as the minimum mean square error (MMSE) on the CFO and the channel estimates, and the computational cost.

2/ From the digital-communication system point of view: we propose to combine the above estimation methods with:

- the minimum mean square error successive detector (MMSE-SD) [Hou 08] to increase the data rate for an OFDMA system [Pove 09a], [Pove 09b], [Pove 11c].

- a statistical test, e.g. the binary hypothesis test (BHT) or the cumulative sum (CUSUM) test, to detect the beginning and the end of the disturbances induced by another system [Pove 11b], [Pove 11d]. This happens with cognitive radio (CR) systems where the spectrum that is not used by licensed (primary) users must be detected in order to be shared with unlicensed (secondary) users[1].

- a modified version of the iterative IDMA receiver [Ping 02a] to design a new receiver scheme for an OFDM-IDMA system [Pove 12].

- a space time block code (STBC) and a new variant of the iterative IDMA receiver [Pove 11a].

The PhD dissertation is organized as follows:

In the first chapter, we present different multiuser scenarios and then focus our attention on those based on a multicarrier modulation. Thus, we look at two mobile wireless communication systems: the conventional ones [IEEE 99], [IEEE 06] and the cognitive radio (CR) systems [Mito 00]. The brief presentation of these wireless systems allows us to introduce both the multipath propagation channel, its statistical properties and the Doppler shifts. We also define the received faded signal that is a superposition of several delayed and attenuated copies of the transmitted signal.

Then, we present the multicarrier multiple access schemes that can be used in these systems. Among them, we give details about multicarrier multiple access schemes. We first present the OFDMA, which results from the combination between the frequency division multiple access (FDMA) and the OFDM.

---

[1]In that case, physical-layer parameters are dynamically adjusted to give the appropriate bandwidth to each user at any time.

Then, we look at the OFDM-IDMA scheme initially proposed by Mahafeno *et al.* [Maha 06].

Whatever the multicarrier systems, the transmitted signals are subject to a CFO and the multipath propagation channel. Therefore, we have to design new receivers taking into account both unwanted phenomena.

In chapter 2, we propose and compare several CFO and channel estimation methods based on optimal filtering techniques [Pove 10]. As the relation between the CFO and the received signal is non-linear, a linearized version of the Least-Squares (LS) approach can be first used to estimate the CFO. More generally, we suggest using an extended Kalman filter (EKF). The EKF consists in analytically propagating the estimation through the system dynamics, by means of a first-order Taylor expansion of the functions defining the state-space representation of the system. However, as the approximation may not be sufficient to describe the non-linearity, the EKF may sometimes diverge. To solve this problem, a second-order linearization can be considered and leads to the second-order EKF (SOEKF) [Bar 01]. Another solution is to use the iterative extended Kalman filter (IEKF). In the IEKF, the measurement model is linearized around the updated state vector, instead of the predicted state vector. Then, the process is iterated until the state vector estimate does not change much.

As the above approaches require the computation of the Jacobians and the Hessians matrices for the first-order and the second-order linearizations respectively, we also look at the sigma-point Kalman filter (SPKF) [VdMe 04a], namely the unscented Kalman Filter (UKF) and the central difference Kalman filter (CDKF). In that case, the state distribution is approximated by a Gaussian distribution, which is characterized by the so-called sigma points. Then, the sigma points are propagated through the non-linear system. A weighted combination of the resulting values makes it possible to estimate the mean and the covariance matrix of the transformed random variable. The UKF is based on the unscented transformation whereas the CDKF is based on the second-order Sterling polynomial interpolation formula.

Nevertheless, Kalman algorithms require an accurate system model as well as perfect knowledge of the noise statistics. Therefore, we also propose to evaluate

the performance of the H_∞ filtering, which has been very popular in the field of control and is more and more used in signal processing (see for instance [Shen 99], [Laba 05] and [Gire 09]). This approach is designed to be robust against uncertainties. In addition, no Gaussian assumption on the additive noise and the model noise in the state-space representation of the system is required. Here, we analyze the relevance of the "extended H_∞ filter", based on Taylor expansion like the EKF and the "unscented H_∞ filter" in which an unscented transformation is embedded into the "extended H_∞ filter" [Li 10].

Then, the above techniques are combined with different processing blocks to design new receiver schemes:

Firstly, the optimal filtering techniques are combined with the so-called MMSE-SD [Hou 08] in an iterative way to obtain a CFO estimator that does not require pilot subcarriers [Pove 09a], [Pove 09b], [Pove 11c].

Secondly, we use the SPKF in a dynamic bandwidth allocation context. The SPKF is combined with a statistical test, either the BHT or the CUSUM test. This approach allows the CFOs and the channels to be jointly estimated and the beginning and the end of a narrow-band interference (NBI) produced by a CR system to be detected [Pove 11b], [Pove 11d].

In chapter 3, we address the CFO and channel estimation problems in an OFDM-IDMA context. Although this access technique has the potential to solve the constant growth on the user density per cell, CFO and channel estimations have not been widely addressed. The IDMA conventional receiver consists of an elementary signal estimator (ESE) and several *a posteriori* probability decoders (DECs) for the different users in the system. The ESE operation is based on the constraint of the *a priori* knowledge of the multipath channels. However, few papers deal with the channel estimation in IDMA systems. The reader may refer to [Suya 08] and [Rehm 08] for channel estimation in OFDM-IDMA systems, where the system is assumed to be perfectly frequency synchronized. To our knowledge, the frequency synchronization issue has never been addressed in an OFDM-IDMA system.

Thus, we propose a new scheme, which operates in two steps. Firstly, CFOs and channels are estimated for each user in the system, by using control data

of one OFDM-IDMA symbol and a SPKF. Secondly, the OFDM demodulation is performed without any CFO correction on the received signal [Pove 12]. The resulting signal is inserted in a modified version of the iterative IDMA receiver, initially proposed by [Ping 02a]. The second part of the chapter 3 deals with a STBC-OFDM-IDMA receiver. In that case, we show how to modify the IDMA iterative receiver by taking advantage of the spatial diversity introduced by the multiple inputs [Pove 11a].

In each case, simulation results confirm the efficiency of the proposed architectures in terms of CFO estimation, channel estimation, computational complexity and BER performance.

Finally, conclusions and perspectives are given.

To help the reader, we also present six appendices:

- In the first one, we recall the main results about the Kalman filter in the linear case.

- In the second appendix, the H_∞ filtering in the linear case is presented.

- In the third one, we present a theoretical comparison between the Kalman and the H_∞ filters.

- In the fourth appendix, we introduce the EKF, the SOEKF and the IEKF.

- The fifth appendix is about the SPKF.

- Finally, the last appendix deals with the H_∞ filtering for non-linear cases. The "extended H_∞ filter" and the "unscented H_∞ filter" are presented.

Chapter **1**

Multicarrier High-Data Rate Mobile Wireless Systems

Contents

1.1 Introduction

The purpose of this chapter is first to give general information about wireless communication systems. Then, we present the unwanted phenomena that may appear when transmitting wireless information. More particularly, the channel plays a key role. Its statistical properties may also vary and depend on the existence of a line-of-sight (LoS) between the transmitter and the receiver. Notions of frequency-selective fading or flat-fading channels are recalled. In the second part of this chapter, we introduce the various access schemes. After recalling what FDMA, time division multiple access (TDMA) and code division multiple access (CDMA) are all about, OFDMA and OFDM-IDMA are presented.

1.2 Wireless Communication Systems

A great deal of interest has been paid to wireless communications for more than hundred years. At the end of the 19th and the beginning of the 20th century, Marconi was at the origin of the first radio transmission [Hanz 98], and wireless communications began.

During the second half of the 20th century, successive modifications in wireless communications were performed, and correspond to the development of the data transmission over telephone networks, the creation of wireless local area networks (WLANs) and the evolution of mobile wireless communications systems.

Today, these transformations in the field of wireless communications still continue. Conventional wireless systems, (e.g. WLANs or cellular networks) that are usually based on a static frequency allocation are evolving to an intelligent concept, where a dynamic frequency allocation can be allowed. Intelligent wireless systems known as cognitive radio (CR) systems [Mito 99] are solutions proposed to improve wireless communications.

This PhD dissertation thesis is devoted to two kinds of wireless communication systems: conventional systems and CR systems. In the following subsections, both types of systems are defined.

1.2.1 Conventional Systems

A conventional system corresponds to a current wireless system. Common examples of these systems can be WLANs, digital video broadcasting terrestrial (DVB-T) or 3G cellular networks. For more details on the conventional wireless systems, the reader is referred to [Rapp 02] and [Stal 05].

These types of systems use a static and predetermined frequency band allocation. Moreover, each terminal is programmed to a limited number of tasks.

Even if conventional systems provide high-data rate services, the exponential increase of data rates and the number of users have produced an overload of the frequency spectrum. For instance, in December 2008, there were 4 billion of mobile subscriptions [ITU 08] worldwide. In 2013, the number of 4G subscribers worldwide is expected to exceed 90 million. To keep on providing high-data rate services, developers and researchers have to find alternative technologies. The next subsection deals with CR systems. This is a technology proposed as a solution to correct this frequency spectrum overload.

1.2.2 Cognitive Radio Systems

Mitola was the first one to employ the concept of CR [Mito 99] and defined it as: "a radio that employs model-based reasoning to achieve a specified level of competence in radio-related domains".

CR systems have emerged as a new technology to improve the utilization of the limited radio bandwidth. The key features of those systems are their awareness and intelligence, which are achieved through learning via a cognition cycle (observe, decide and act). This intelligence allows CR systems to tune the system parameters such as power, carrier frequency, and modulation at the physical layer, and higher-layer protocol parameters to improve their utilization.

Nowadays, there is an overload of the frequency spectrum assigned to the conventional systems. However, at the same time there is an underutilization of this assigned frequency spectrum [Mito 00]. CR may be a solution to this issue. It can be achieved by a spectrum shared by primary and secondary users. The sharing techniques can be classified into underlay and overlay spectrum sharing. On the one hand, when using underlay systems, the primary and secondary users share
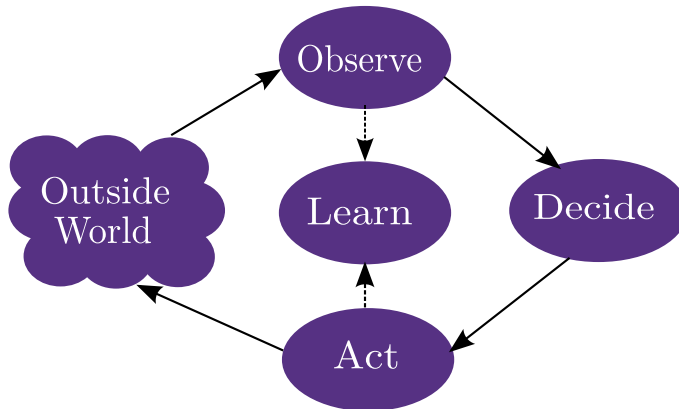
Figure 1.1: Cognition cycle

the same frequency spectrum. However, secondary users should transmit the signal with a low power that does not exceed an interference threshold [Pali 10]. On the other hand, in overlay systems the secondary users have to find out the bands that are not used by the primary users (PUs). Then, secondary users can utilize these unused portions of the spectrum. For this purpose, the secondary users need information about the spectrum allocation of the PUs by regularly performing spectrum sensing techniques. Various spectrum sensing techniques have been proposed [Arsl 07]. Some of them aim at identifying the characteristics of the transmission whereas others distinguish the signal type. The most common are the matched filter, the cyclostationary feature detection and the energy detection [Arsl 07]. For more details about CR systems, the reader is referred to [Pali 10]. Understanding that CR systems have the potential to exploit the underutilized conventional system frequency bands by spectrum sharing, the Federal Communications Commission (FCC) released a second report in which unlicensed devices are allowed to operate in the unused portions of the TV-spectrum in 2008.

CR systems will be considered in this PhD dissertation, in chapter 2, section 2.5. In the following section, we present one of the more challenging tasks when designing a wireless system, taking into account the influence of the propagation channel.

1.3   Propagation Channel Model

In mobile wireless communication systems, the transmitted signal arrives at the receiver from different propagation paths. Such phenomenon occurs due to the obstacles such as buildings, mountains, trees, etc., between the transmitter and the receiver, as shown in figure 1.2.
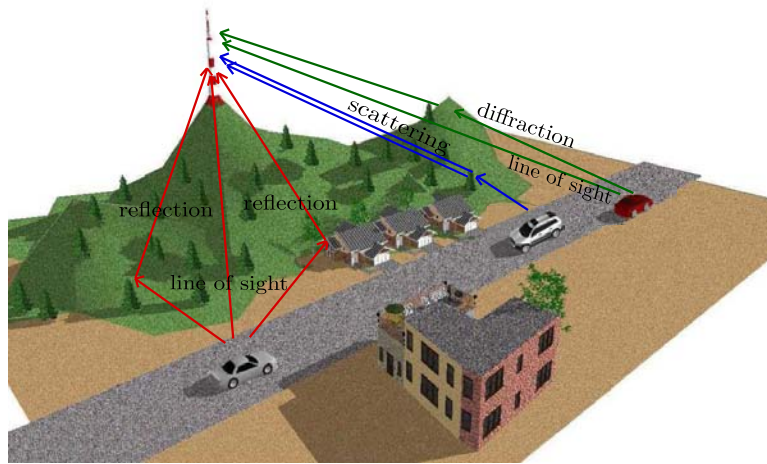
Figure 1.2: Multipath propagation channel

Due to these obstacles, the transmitted signal is subject to:

- reflection: it arises when the plane waves are incident upon a surface with dimensions that are very large compared to the wavelength.

- diffraction: it occurs when there is an obstruction between the transmitter and receiver antennas. Secondary waves are then generated behind the obstruction.

- scattering: it happens when the plane waves are incident upon an object, the dimensions of which are of the order of a wavelength or less, and causes the energy to be redirected in many directions.

Given these three mechanisms, a wireless propagation can be roughly characterized by some independent phenomena: path loss variation, shadowing and multipath fading. Mathematically, the path loss is only distance dependent, whereas

the other two phenomena are statistically described. In the following, let us focus our attention on the multipath effect.

The received signal is a superposition of several delayed and attenuated copies of the transmitted signal. By considering a stationary propagation, the channel propagation model $h(\tau)$ at time τ can be mathematically expressed as:

$$h(\tau) = \sum_{l=0}^{L-1} \mathcal{A}(l)\delta(\tau - \tau_l) \tag{1.1}$$

where L is defined as the number of paths, $\mathcal{A}(l)$ and $\tau_l = lT_{samp}$ are the amplitude and the time delay associated to the lth path, respectively. In addition, T_{samp} is the sampling time.

Thus, the coefficients of the discrete-time channel impulse response (CIR) can be stored in the following vector:

$$\mathbf{h} = [h(0), h(1), \ldots, h(l), \ldots, h(L-1)] \tag{1.2}$$

Figure 1.3 shows an example of a CIR, where τ_{max} represents the maximum channel delay spread in seconds.
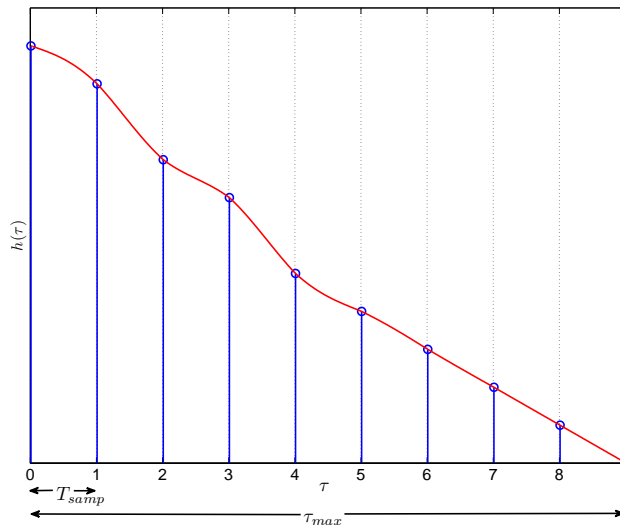
Figure 1.3: Channel impulse response with $L = 9$

The fading that modifies the transmitted signal depends on the characteristics of the channel and the nature of the transmitted signal. Moreover, the statistical model of the channel is slightly different if the transmitter is in LoS with the receiver. The multipath fading channel can be hence classified by looking at its probability density distribution and its frequency response in the transmitted signal bandwidth.

These classifications of fading are investigated in the next subsections.

1.3.1   Rician and Rayleigh Fading Channels

Due to the existence of a great variety of propagation environments, several statistical distributions have been proposed for channel modeling. However, in the following let us consider the two most commonly used distributions: the Rayleigh and Rician distributions.

In wireless systems, a predominant component of the transmitted signal is sometimes present at the receiver. If this predominant component can be the LoS wave for instance, each coefficient of the CIR follows a Rician distribution [Jake 74].

Let us look at this case more carefully. When the received signal consists of a large number of plane waves with different phases, it can be treated as a complex Gaussian random process $\alpha_r(n) = \alpha_I(n) + j\alpha_Q(n)$, where $\alpha_I(n)$ and $\alpha_Q(n)$ are Gaussian random variables (GRVs) with non-zero means μ_I and μ_Q, respectively. The processes are assumed to be uncorrelated and the GRVs have the same variance σ_r^2. Then, the magnitude of the received signal has the following Rician distribution:

$$\mathcal{P}_{df}(x) = \frac{x}{\sigma_r^2} e^{-\frac{x^2+\mu_r^2}{2\sigma_r^2}} \mathcal{I}_0\left(\frac{x\mu_r}{\sigma_r^2}\right) \quad x \geq 0 \tag{1.3}$$

where $\mu_r^2 = \mu_I^2 + \mu_Q^2$ is called the non-centrality parameter and $\mathcal{I}_0\left(\frac{x\mu_r}{\sigma_r^2}\right)$ is the zero-order modified Bessel function[1] of the first kind [Stub 02].

---

[1]The zero-order modified Bessel function of the first kind is defined as:

$$\mathcal{I}_0(y) \triangleq \frac{1}{2\pi} \int_0^{2\pi} e^{-y cos(z)} dz$$

1. Multicarrier High-Data Rate Mobile Wireless Systems

The received signal distribution can be rewritten by using the Rice factor defined by:

$$\mathcal{K}_{rice} = \mu_r^2/2\sigma_r^2 \tag{1.4}$$

and the average envelope power

$$\mathbb{E}\{|\alpha_r(t)|^2\} = \Omega_r = \mu_r^2 + 2\sigma_r^2 \tag{1.5}$$

Therefore, the distribution can be expressed as follows[1]:

$$\mathcal{P}_{df}(x) = \frac{2x(\mathcal{K}_{rice}+1)}{\Omega_r} e^{-\mathcal{K}_{rice} - \frac{(\mathcal{K}_{rice}+1)x^2}{\Omega_r}} \mathcal{I}_0\left(2x\sqrt{\frac{\mathcal{K}_{rice}(\mathcal{K}_{rice}+1)}{\Omega_r}}\right) \quad x \geq 0 \tag{1.6}$$

Figure 1.4 shows examples of Rician distributions for differents values of $\mathcal{K}_{rice}$. It should be noted that μ_r^2 characterizes the LoS wave. Therefore, if there is non LoS wave, $\mu_r^2 = 0$, i.e. $\mathcal{K}_{rice} = 0$. This is the case of a Rayleigh model.
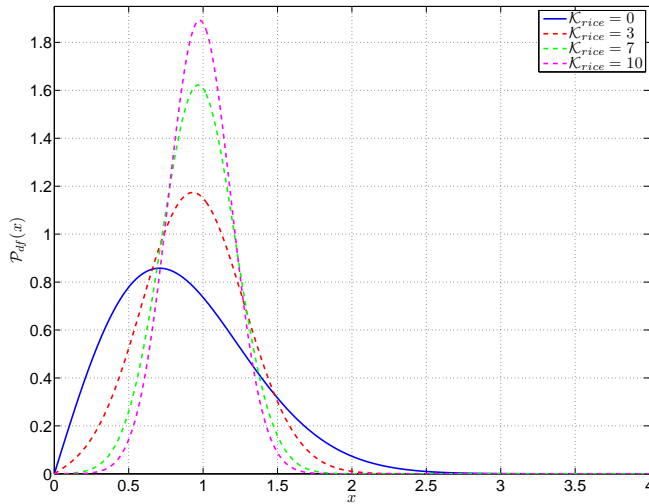
Figure 1.4: Rician distribution

Rayleigh channel model is the most common assumption in wireless systems. In this case, propagation path consists of a two dimensional isotropic scattering. The

---

[1]It should be noted that: $\mu_r^2 = \frac{\mathcal{K}_{rice}\Omega_r}{\mathcal{K}_{rice}+1}$ and $\sigma_r^2 = \frac{\Omega_r}{2(\mathcal{K}_{rice}+1)}$

plane waves arrive from many directions with equal probability without a direct LoS component. Then, each coefficient of the CIR follows a Rayleigh distribution [Jake 74]. Therefore, given (1.3) and under these assumptions, the magnitude of the received signal has the following Rayleigh distribution:

$$\mathcal{P}_{df}(x) = \frac{2x}{\Omega_r} e^{-\frac{x^2}{\Omega_r}} \quad x \geq 0 \tag{1.7}$$

where $\Omega_r = \mathbb{E}\{|\alpha_r(t)|^2\} = 2\sigma_r^2$ is the average envelope power [Stub 02]. Figure 1.5 shows examples of Rayleigh distribution for different values of Ω_r. In the following subsection, we present the frequency-selective and the time-varying channels.
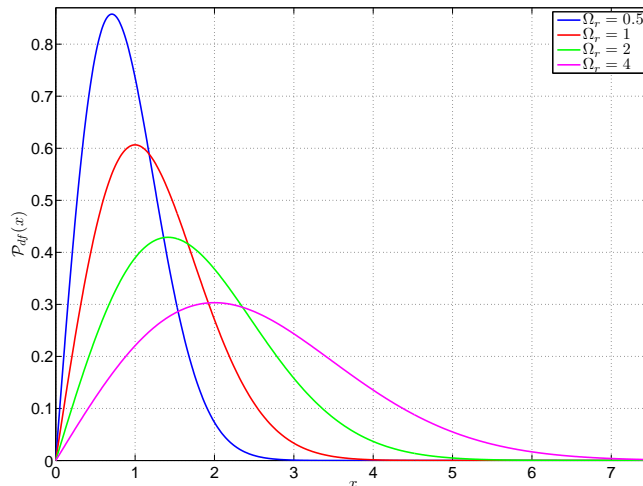
Figure 1.5: Rayleigh distribution

1.3.2 Frequency-Selective and Time-Varying Fading Channels

The fading model can also be characterized by the nature of the transmitted signal and the relative speed between the transmitter and the receiver. It can be classified by the relationship between the transmitted signal bandwidth W,

that is proportional to the inverse of the symbol[1] (M-PSK symbol) time T_s, (i.e. $W \propto \frac{1}{T_s}$) and the channel frequency response in this bandwidth.

Let us define the channel coherence bandwidth W_c as:

$$W_c = \frac{1}{\tau_{max}} \tag{1.8}$$

On the one hand, if all the multipaths arrive at the receiver within the symbol duration, the fading channel is considered as a frequency non-selective fading or flat-fading channel. Then, the channel coherence bandwidth is higher than the transmitted signal bandwidth:

$$W << W_c \tag{1.9}$$

i.e.

$$\tau_{max} << T_s \tag{1.10}$$

At the receiver, without the noise contribution, the signal is an attenuated copy of the transmitted signal:

$$r(n) = hs(n) \tag{1.11}$$

where $s(n)$ is the received symbol, h is the CIR coefficient and $r(n)$ is the received symbol.

On the other hand, if the multipaths are spread outside the symbol duration, i.e. the maximum channel delay spread is higher than the symbol time, the fading channel is considered as a frequency-selective fading channel. In this case, the transmitted signal bandwidth is higher than the channel coherence bandwidth:

$$W >> W_c \tag{1.12}$$

i.e.

$$\tau_{max} >> T_s \tag{1.13}$$

Therefore, without the noise contribution, the received signal is a superposition of several transmitted attenuated and delayed signals. Mathematically, it can be

---

[1]In this PhD dissertation we consider M-ary phase shift keying (M-PSK) as the modulation technique. It consists in changing the phase of the carrier frequency, where M is the number of possible phases. For example, when using BPSK modulation the set of symbols is $\{-1, +1\}$ and when using QPSK the set of symbols can be $\{e^{j\frac{\pi}{4}}, e^{j\frac{3\pi}{4}}, e^{j\frac{5\pi}{4}}, e^{j\frac{7\pi}{4}}\}$.

expressed as the convolution between the transmitted signal and the CIR:

$$r(n) = \sum_{l=0}^{L} h(l)s(n-l) \tag{1.14}$$

The received signal is spread in time and this leads to the so-called inter symbol interference (ISI). Figure (1.6) shows the frequency response of a frequency-selective fading channel.

In both cases, estimating and correcting the CIR, also called channel equalization, is usually performed using a known signal at the receiver, called pilot signal. Given (1.11) and (1.14), we can expect a higher complexity of the equalization when dealing with frequency-selective channel.
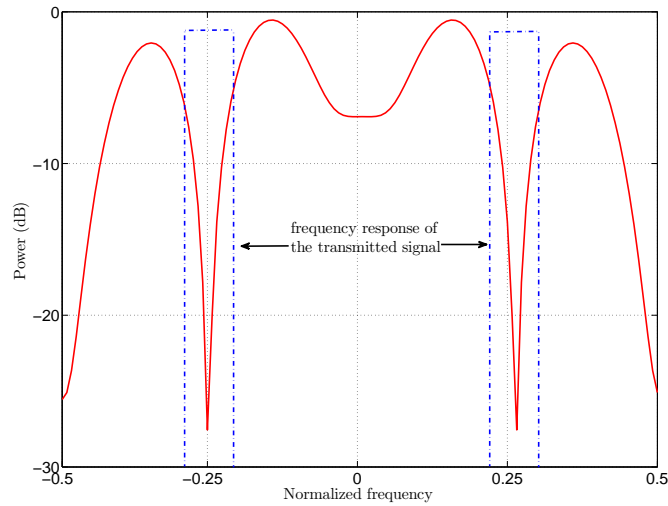
Figure 1.6: Frequency-selective fading channel

Furthermore, there is sometimes a relative motion between the transmitter and the receiver in wireless systems. This results in a time-varying channel. The channel can be divided in two categories depending on the ratio between the transmitted symbol time T_s and the channel coherence time T_c.

Let us define the channel coherence time T_c as follows:

$$T_c = \frac{1}{f^{\text{DOP}}} = \frac{c}{vf_c} \tag{1.15}$$

where the Doppler shift $f^{\text{DOP}} = v\frac{f_c}{c}$ is the maximum measure in Hertz of a relative frequency shift between the transmitted and the received signal, v is the relative speed between the transmitter and the receiver, f_c is the frequency carrier and c is the speed of the light.

The Doppler shift is caused not only by the transmitter-receiver relative motion, but also by the movement of surrounding objects. It leads to frequency offsets at the receiver.

If the channel coherence time is higher than the transmitted symbol time:

$$T_s < T_c \tag{1.16}$$

the channel is considered as a slow-fading channel.

If the transmitted symbol time is higher than channel coherence time:

$$T_s > T_c \tag{1.17}$$

the channel is considered a fast-fading channel.

Table 1.1 shows a classification of the fading channels according to the nature of the transmitted signal and the relative speed between the transmitter and the receiver

	slow-fading channel	fast-fading channel
flat-fading channel	$\tau_{max} << T_s$ $T_s < T_c$	$\tau_{max} << T_s$ $T_s > T_c$
frequency-selective channel	$\tau_{max} >> T_s$ $T_s < T_c$	$\tau_{max} >> T_s$ $T_s > T_c$

Table 1.1: Fading channel classification

In both cases, at the receiver, the frequency offset caused by the Doppler shift has to be estimated in order to recover the original transmitted signal.

The design of a mobile wireless system implies the above technical challenges. In the following, we present some schemes that have been proposed during the last years to take into account the impact of the fading effects.

1.4 Multiple Access Techniques for Mobile Systems

In mobile wireless systems, a big challenge is to choose the multiple access technology that will efficiently share the available bandwidth among a large number of users and that will be robust against the channel propagation effects. For the past decades, the mobile wireless communication industry has searched for different techniques to allocate the communication resources to the different users. The first public cellular radio system, known as advanced mobile phone service (AMPS), was introduced at the end of the '70s in the United States, shortly followed by the Nordic mobile telephone system and the total access communication system (TACS) in Europe. At the same time, the Japaneses introduced the Nippon automatic mobile telephone system (NAMTS) [Hanz 98]. These systems were analog and are known as the 1st generation mobile wireless systems (1G). All of them used FDMA as their multiple access scheme. In FDMA, the allocated spectrum is divided into several frequency bands where each band is assigned to one user, i.e. each user can communicate at the same time. See figure 1.7. Multiple users using separate frequency bands can access system on the same time without significant interference from other users simultaneously operating in the system [Stub 02].
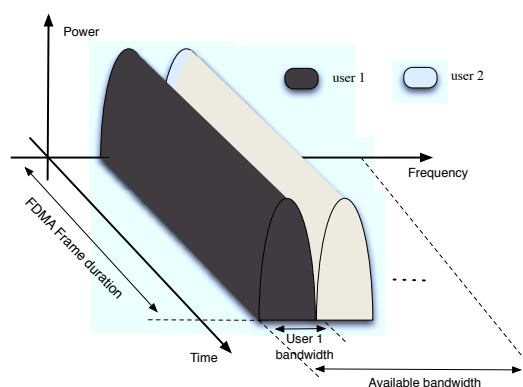
Figure 1.7: FDMA

1. Multicarrier High-Data Rate Mobile Wireless Systems

At the beginning of the '90s, the 2nd generation mobile wireless systems (2G) were developed, such as the digital AMPS in the United States, the global system for mobile communications (GSM) in Europe and the personal digital cellular (PDC) system in Japan [Hanz 98]. These systems employed TDMA as their multiple access scheme. When using TDMA, the whole bandwidth is assigned and the time-domain transmission frame is divided into time slots, each assigned to one user to transmit the data information [Stub 02]. See figure 1.8. TDMA is used in the evolution of the 2G GSM standard, namely the general packet radio service (GPRS) and the enhanced data rates for GSM Evolution (EDGE) systems.
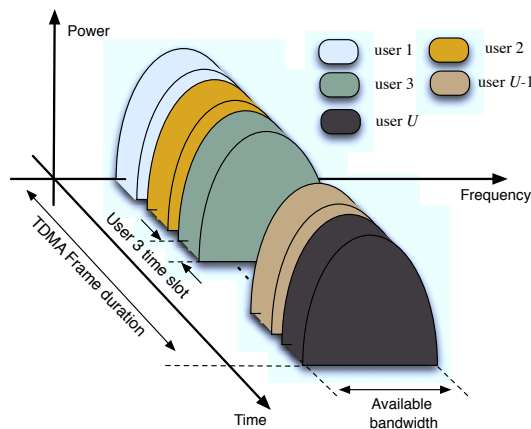
Figure 1.8: TDMA

Nevertheless in FDMA and TDMA, the number of frequency bands or time slots is fixed for a given system, and one frequency band/time slot is assigned to one user during the whole period of communications. This guarantees the service quality for real-time and constant-bit-rate voice telephony. However, as the number of services is increasing from simple voice to multimedia traffic with different requirements, fixed frequency band or time slot assignments have shown their limitations, especially with the increasing number of users in the system. For that reason, CDMA scheme, based on spread spectrum technology, has emerged. In CDMA systems, the relatively narrow-band users information is spread into a much wider spectrum using a high chip rate spreading code. When using different

codes, multiple user information can be transmitted on the same frequency band at the same time. See figure 1.9. The spreading code of each user is orthogonal[1] to the codes of all other users to minimize the multiple access interference (MAI) produced by other users [Schu 05]. The 2G American system IS-95 was the first mobile cellular communication system to use CDMA technology followed by the CDMA 2000 technology [Stub 02].
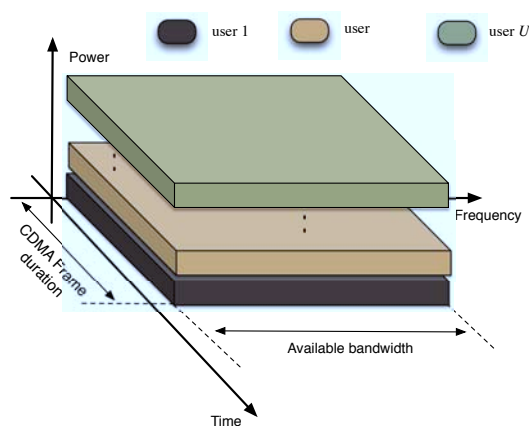
Figure 1.9: CDMA

The digital 2G has shown higher transmission capacity and better voice quality than the analog 1G. Like the 1G, 2G was primarily designed to support voice communication. In the last releases of these standards, capabilities were introduced to support data transmission. However, the data rates were generally lower than those supported by the existent bandwidth. Thus, an initiative of the international telecommunication union (ITU) laid the way for evolution to 3rd generation mobile wireless systems (3G). Requirements such as a specific high-data rate and support for vehicular mobility were established. Both the GSM and CDMA camps formed their own separate 3G partnership projects, the 3GPP and 3GPP2, respectively. Within the 3GPP evolution track, the 2G GSM/GPRS/EDGE family is based on TDMA and FDMA, whereas the 2G IS-95/CDMA 2000 is based on TDMA and CDMA in the 3GPP2. See table 1.2.

---

[1]Two vectors $\mathbf{x}(n)$ and $\mathbf{y}(n)$ are orthogonal if their dot product $\langle\mathbf{x}(n),\mathbf{y}(n)\rangle=\sum_{-\infty}^{\infty}\mathbf{x}(n)\mathbf{y}(n)$ is equal to zero.

The 3G in the 3GPP was first referred to the universal mobile telecommunication system wideband CDMA (UMTS WCDMA). Then, it evolved in the high-speed downlink and uplink packet access (HSDPA and HSUPA) enhancements and in the high-speed packet access plus (HSPA+) enhancement. Meanwhile in the 3GPP2, the 3G was known as the CDMA evolution-data optimized (CDMA EVDO) [Sesi 09]. All these systems use CDMA as their multiple access technique. The number of orthogonal codes used for uplink transmission[1] from one user is limited to a few codes or complex techniques are used to limit the uplink signal peakiness and to improve the low noise amplifier efficiency[2]. In addition, CDMA usually employs a rake receiver [Proa 95] technique to suppress multipath effects and the related cost increases with the number of paths. Therefore, the complexity of the receiver can be very high for a high-data rate mobile wireless systems.

1.4.1   About Multicarrier Multiple Access Techniques

One solution to transmit the signal over a multipath frequency-selective and time-varying fading channel, without ISI, is to choose a transmitted signal bandwidth very higher than the Doppler shift and much lower than the channel coherence bandwidth, $f_d << W << W_c$, i.e $\tau_{max} << T_s << T_c$. See section 1.3.2.

This hypothesis is true for low data rate and low mobility systems. When a high data rate system is considered usually, one has:

$$T_s << \tau_{max} << T_c \tag{1.18}$$

To avoid the ISI, a solution could be to divide the entire bandwidth W in several subbands of size $\Delta f << W_c$ and to send a large number of narrow-band signals over several parallel subcarriers in the frequency band assigned to the transmission. This is the concept of a multicarrier modulation.

The preferred case of multicarrier modulation is the one that uses an orthogonal

---

[1]In the uplink transmission, the transmitter is the user and the receiver is the base station.
[2]For example, when using CDMA for an uplink transmission, a complex successive interference cancellation method is required to improve the performance of the receiver.

Family	Generation	Standard	Peak Data Rates		Radio Access
			Downlink (Mbits/s)	Uplink (Mbits/s)	
3GPP	2G	GSM	0.04	0.01	FDMA, TDMA
		GPRS	0.17	0.13	
		EDGE	0.47	0.36	
		EDGEev	1.89	1.42	
	3G	UMTS WCMA	0.38	0.38	CDMA, OFDMA, SC-FDMA
		HSDPA	14.4	—	
		HSUPA	—	5.76	
	4G	HSPA+	42.2	11.5	
		LTE	300	50	
		LTE-A	1000	500	
IEEE	3G	WiMAX 802.16e	128	56	OFDMA
		WiMAX 802.16m	300	135	
	4G	WiMAX 2	1000	500	
3GPP2	2G	IS-95	0.115	0.115	TDMA, CDMA
		CDMA 2000	0.307	0.307	
	3G	CDMA EVDO	73.5	27	

Table 1.2: Mobile standards evolution from 2G to 4G.

basis, namely the orthogonal frequency division multiplexing (OFDM)[1] [Bing 90]. In this scheme, the input symbols are transmitted at the same time over orthogonal subcarriers [Wein 71]. See figure 1.10. The main idea of OFDM is to convert a frequency-selective channel in the time domain into a collection of frequency-flat channels in the frequency domain.

OFDM increases robustness against multipath distortions, making the system robust against ISI. In addition, OFDM systems use a cyclic prefix (CP) to combat interblock interference (IBI). The CP consists in prefixing the OFDM symbol with the end of it[2]. The above advantages allow the channel equalization to be easily performed in the frequency and time domains through a bank of one-tap multipliers [Cimi 85]. Furthermore, OFDM exploits the spectral diversity and allows an independent selection over each subcarrier of resources, such as power, constellation size and necessary bandwidth [Kell 00], in order to maximize the

---

[1]Orthogonality between two frequencies f_k, $f_{k'}$ is defined as $\langle e^{j2\pi f_k t}, e^{j2\pi f_{k'} t} \rangle = \delta_{k,k'}$, where $\delta_{k,k'} = 0$ if $k = k'$, and $\delta_{k,k'} = 1$ if $k \neq k$.

[2]The CP is detailed in subsection 1.4.2.1.
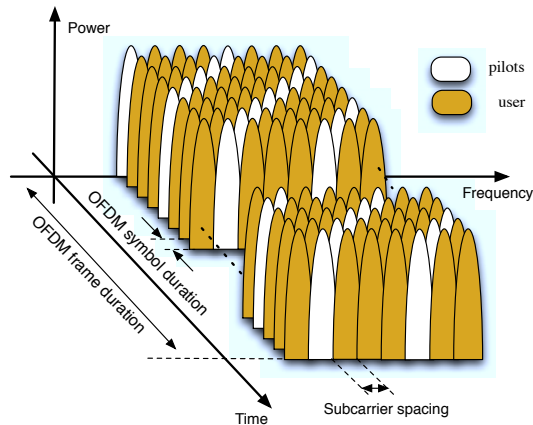
Figure 1.10: OFDM

link efficiency.

OFDM has been adopted in several communication standards such as digital audio broadcasting (DAB) [ETSI 95], DVB-T [ETSI 97], and the WLAN IEEE 802.11a [IEEE 99].

The OFDM concept has been extended to multiuser communication scenarios. In the following subsections three different multiple access schemes based on OFDM are presented:

- OFDMA,

- single carrier frequency division multiple access (SC-FDMA),

- and OFDM-IDMA.

1.4.1.1   About OFDMA

This scheme was originally suggested for cable TV (CATV) networks [Sari 98] and in the uplink communication of the Interaction Channel for Digital Terrestrial Television (DVB-RCT) [ETSI 01]. The institute of electrical and electronics engineers (IEEE) 3G project, called the mobile worldwide interoperability of microwave access (WiMAX) [IEEE 06] uses ODFMA technology. The last releases of the 3GPP and 3GPP2, known as the long term evolution (LTE) and ultra

mobile broadband (UMB) respectively, are based on OFDMA[1]. Note that LTE uses OFDMA in the downlink communication[2] [3GPP 09].

In this scheme, unlike the OFDM case where all subcarriers are assigned to a single user, subcarriers are divided in several mutually exclusive subchannels and they are exclusively assigned to a particular user in an OFDMA network. See figure 1.11.

OFDMA inherits from OFDM the flexibility for simultaneous transmissions and frequency allocation algorithms aim at exploiting the spectral diversity to allocate the communication resources to the different users. In addition, OFDMA inherits the ability to compensate channel distortions in the frequency domain without computationally demanding time domain equalizers.

In subsection 1.4.2, more details about the OFDMA system are presented.
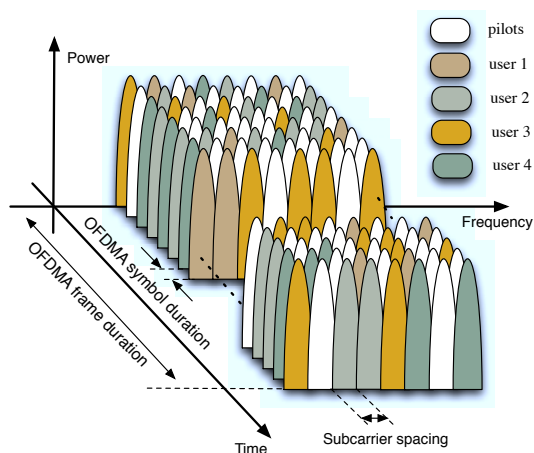
Figure 1.11: OFDMA

1.4.1.2 About SC-FDMA

SC-FDMA is a modified form of OFDMA with similar throughput performance and complexity. It is used as multiple access technique in the LTE uplink com-

---

[1]The 3GPP2 announced it was ending development of the UMB technology, favoring LTE instead.

[2]In the downlink transmission, the transmitter is the base station and the receiver is the user.

munication [3GPP 09]. In this multiple access scheme, the symbols pass through a discrete Fourier transform before going through the standard OFDMA modulation. This is often viewed as a DFT-coded OFDM. Thus, SC-FDMA inherits all the advantages of OFDMA over other well-known techniques such as TDMA and CDMA. SC-FDMA brings additional benefit of low peak-to-average power ratio (PAPR) compared to OFDMA, making it suitable for uplink transmissions [Sesi 09]. The SC-FDMA transceiver has similar structure as a typical OFDMA system except the addition of a new DFT block before subcarrier mapping. Hence, SC-FDMA can be considered as an OFDMA system with a DFT mapper.

1.4.1.3 About OFDM-IDMA

When using OFDMA and SC-FDMA, an MAI free transmission can be achieved by allocating different subcarriers to different users. Thus, if there are more than one user in the system, the entire bandwidth has to be shared by all the users. This may limit the data rate.

In 2002, Ping *et al.* [Ping 02a] proposed the interleave-Division Multiple Access (IDMA) for asynchronous[1] spread-spectrum mobile systems. Whereas transmitters can be defined by using different orthogonal codes in CDMA systems, they are distinguished by a different chip-level interleaver in IDMA systems. While CDMA allows the MAI to be suppressed using the different codes, IDMA requires an iterative process. Like CDMA, the entire bandwidth can be allocated to a single user, achieving a very high single-user capacity when using IDMA.

IDMA systems require a method to suppress multipath effects and avoid the ISI. One solution may be to use an ISI cancellation method as in [Ping 06]. However, the corresponding computational cost of this method increases linearly with the number of paths and may be unsuitable for high-data rate systems.

To solve this constraint, a scheme that combines OFDM and IDMA has been proposed by Mahafeno *et al.* [Maha 06]. This architecture combines most of the advantages of the OFDM and the IDMA and avoids their individual disadvantages. When an OFDM-IDMA is considered, ISI is resolved by an OFDM

---

[1]The users of an IDMA system do not have to be time-synchronized one to another.

modulation and MAI is suppressed by the IDMA iterative reception.

In the next subsection, we focus our attention on the OFDMA system. Then, in subsection 1.4.3, the OFDM-IDMA system will be presented in details.

1.4.2 OFDMA System

Basically, the OFDMA system is equivalent to an OFDM system. The difference is that each OFDMA symbol simultaneously carries the information for multiple users while OFDM system carries data of a single specific user.

Let us consider an OFDMA system consisting of a single base station (BS) and U simultaneously users performing an uplink communication[1].

The U users share the bandwidth W, divided in K subcarriers to perform a transmission. The users are numbered from 1 to U, i.e $u \in \{1, \ldots U\}$. In the following the subscript u denotes the information associated to the uth user. In addition, the overall subcarriers are numbered from 0 to $K-1$, i.e $k \in \{0, \ldots K-1\}$. The subcarriers are grouped in $\mathfrak{K}$ subchannels. One or more subchannels may be allocated to the same user depending on its requested data rate. As the maximum number of users that the system can simultaneously support is limited to $\mathfrak{K}$, it is assumed that $U \leq \mathfrak{K}$.

1.4.2.1 OFDMA Uplink Transmitter

This subsection describes the OFDMA transmitter model. After channel coding and modulation, the symbols are grouped into blocks of length $\mathcal{K}_u < K$, where $\sum_{u=1}^{U} \mathcal{K}_u = K$.

Carrier Allocation Strategy (CAS)

The OFDMA transmitter performs the CAS. Three possible strategies [Wang 04] to distribute subcarriers among the active users have been proposed:

---

[1]In the OFDMA uplink communication, the receiver is the BS. Then, the received signal is a superposition of the signals transmitted by each user. Thus, the synchronization and the equalization in this case are more difficult than in the downlink case, where the user only receives the signal transmitted by the BS.

- Subband CAS: each subchannel is composed by a group of $\mathcal{K}_u$ adjacent subcarriers. The main drawback of this scheme is that it does not exploit the frequency diversity of the multipath channel since a large fading might strike a substantial number of subcarriers for a given user. See figure 1.12.
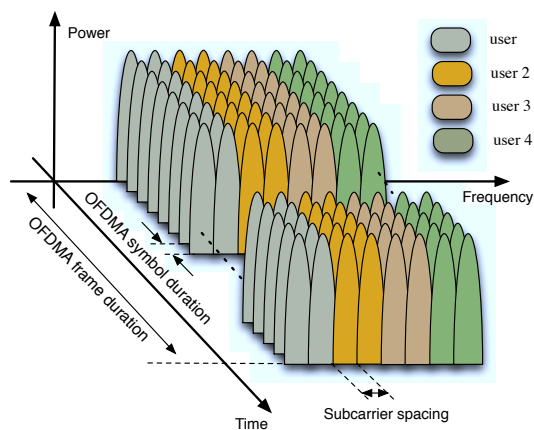
Figure 1.12: Subband CAS

- Interleaved CAS: the subcarriers of each user are uniformly spaced over the signal bandwidth at a distance $\mathcal{K}$ from each other. This method can exploit the channel frequency diversity. See figure 1.13.
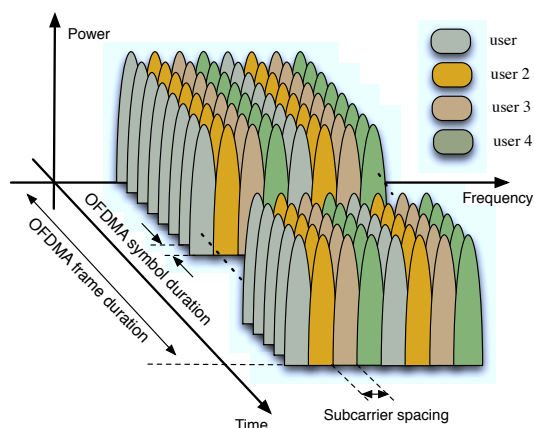
Figure 1.13: Interleaved CAS

- Generalized CAS: each user can select the best subcarriers that are currently available, e.g. those with the highest signal-to-noise ratios (SNRs). In this allocation strategy, there is no rigid association between subcarriers and users; the generalized CAS allows dynamic resource allocation and provides more flexibility than the other CAS. When using generalized CAS, *a priori* knowledge of the propagation channel is necesssary, i.e. the transmitter needs a channel feedback. See figure 1.14.
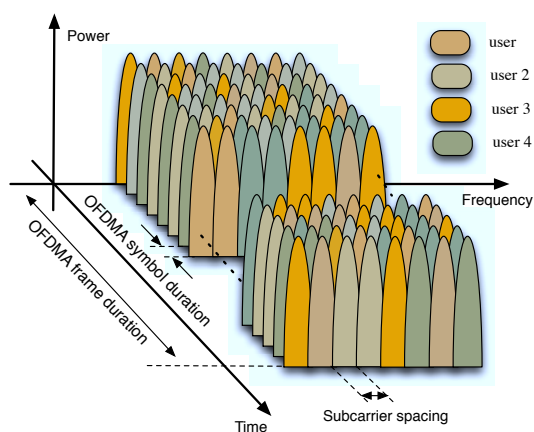
Figure 1.14: Generalized CAS

Then, the CAS maps the $\mathcal{K}_u$ symbols (M-PSK symbols) of each block to the subcarriers assigned to the uth user. This operation is easily performed by extending the block with the insertion of $K - \mathcal{K}_u$ zeros. The resulting column vector of dimension K is defined as follows:

$$\mathbf{S}_u \triangleq [S_u(0), S_u(1), \ldots, S_u(k), \ldots S_u(K-1)]^T \qquad (1.19)$$

according to the frequency allocation of each user, $S_u(k)$ is non-zero if the kth subcarrier is allocated to the uth user. $S_u(k)$ is the symbol associated to the kth subcarrier. The resulting block has a time duration $T = KT_s$. In the following let T be the OFDMA symbol time duration.

1. Multicarrier High-Data Rate Mobile Wireless Systems

Inverse Fast Fourier Transform (IFFT)

To obtain the OFDMA symbol, the symbols are sent in parallel over orthogonal subcarriers by using a K-dimensional IFFT step [Wein 71] as follows:

$$X_u(n) = \sum_{k=0}^{K-1} S_u(k) e^{j2\pi \frac{kn}{K}} \quad 0 \leq n \leq K - 1 \tag{1.20}$$

Then, the IFFT output samples are gathered into a vector, resulting in the OFDMA symbol:

$$\begin{aligned}
\mathbf{X}_u &\triangleq [X_u(0), X_u(1), \ldots, X_u(n), \ldots, X_u(K-1)]^T \\
&= \mathbf{F}^H \mathbf{Q}_u \mathbf{S}_u
\end{aligned} \tag{1.21}$$

where $\mathbf{F}^H$ is the $K \times K$ IFFT matrix and $\mathbf{F}$ is the $K \times K$ fast Fourier transform (FFT) matrix defined as[1]:

$$\mathbf{F} = \begin{bmatrix}
1 & 1 & 1 & \ldots & 1 \\
1 & e^{-\frac{j2\pi}{K}} & e^{-\frac{j4\pi}{K}} & \ldots & e^{-\frac{j2(K-1)\pi}{K}} \\
1 & e^{-\frac{j4\pi}{K}} & e^{-\frac{j8\pi}{K}} & \ldots & e^{-\frac{j4(K-1)\pi}{K}} \\
\vdots & \vdots & \vdots & \ddots & \vdots \\
1 & e^{-\frac{j2(K-1)\pi}{K}} & e^{-\frac{j4(K-1)\pi}{K}} & \ldots & e^{-\frac{j2(K-1)^2\pi}{K}}
\end{bmatrix} \tag{1.22}$$

In addition, $\mathbf{Q}_u$ is the CAS diagonal matrix where the kth coefficient of the main diagonal is given by:

$$\mathbf{Q}_u(k, k) = \begin{cases} 1 & \text{if } S_u(k) \neq 0 \\ 0 & \text{elsewhere} \end{cases} \tag{1.23}$$

Adding a Cyclic Prefix (CP)

At the receiver due to the multipaths, the lth copy of a determined OFDMA symbol[2] arrives with a time delay τ_l, where $l \in \{0, \ldots L_u - 1\}$ and L_u is number of paths of the channel. See section 1.3. Then, some samples of the OFDMA symbol interfere with the adjacent OFDMA symbol causing IBI.

The next step of the OFDMA transmitter consists in introducing the cyclic prefix (CP), that is a repetition of the N_g last samples of the vector $\mathbf{X}_u$ at the beginning of it. The CP makes the OFDMA symbol robust to IBI. By inserting a CP of

---

[1]It should be noted that $\mathbf{F}\mathbf{F}^H = \mathbf{I}_K$.

[2]The users are assumed to be time-synchronized one another.
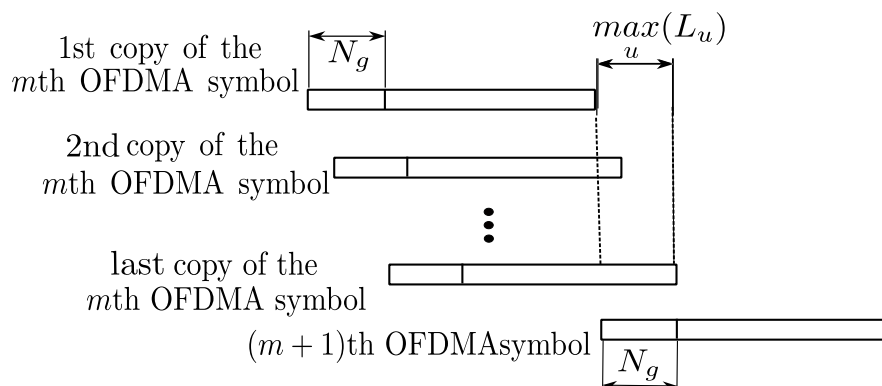
Figure 1.15: Cyclic prefix, where m denotes the OFDMA symbol index

size $N_g \geq \max\limits_{u}(L_u)$, the interferences between adjacent OFDMA symbols are avoided. To maintain acceptable data throughput, the CP length must be chosen just greater than the CIR length. See figure 1.15 which shows the advantage of adding the CP.

Thus, a CP of size N_g is inserted to $\mathbf{X}_u$ such that:

$$X_u(n) = X_u(n + K) \text{ for } -N_g \leq n < -1 \tag{1.24}$$

Then, the OFDMA symbol to be transmitted of size $K_T = K + N_g$ is expressed as:

$$\mathbf{X}_u^{\text{CP}} \triangleq [X_u(K - N_g), \ldots, X_u(K - 1), X_u(0), \ldots, X_u(K - 1)]^T \tag{1.25}$$

Parallel/Serial Converter (P/S)

The OFDMA symbols pass through a parallel-serial converter (P/S) and are stored to compose the OFDMA frame to be transmitted. A simplified OFDMA transmitter scheme is shown in figure 1.16.

The OFDMA frame is then inserted in a digital/analog (D/A) converter and the output signal is modulated to the carrier frequency of the local oscillator (LO). Finally, the signal passes through the power amplifier and it is transmitted over the channel. Figure 1.17 shows the OFDMA spectrum. It should be noted that the distance in the frequency domain between two adjacent subcarriers is $\Delta f = \frac{1}{KT_s} = \frac{1}{T}$.

As an example, table 1.3 shows the IEEE 802.16 OFDMA Wireless MAN system

parameters, which uses OFDMA for the uplink transmisssion.

In the following, let us look at the OFDMA uplink receiver.
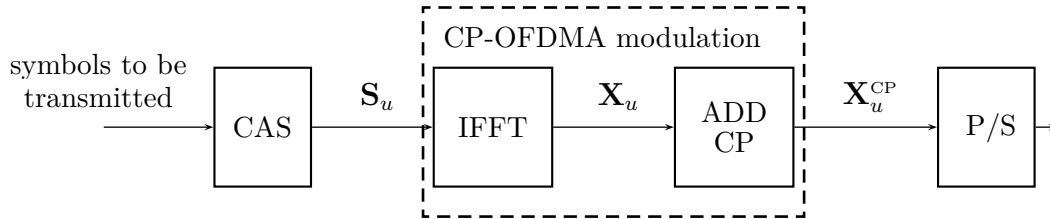
Figure 1.16: Simplified OFDMA transmitter for the uth user, where $\mathbf{X}_u$ is the OFDMA symbol
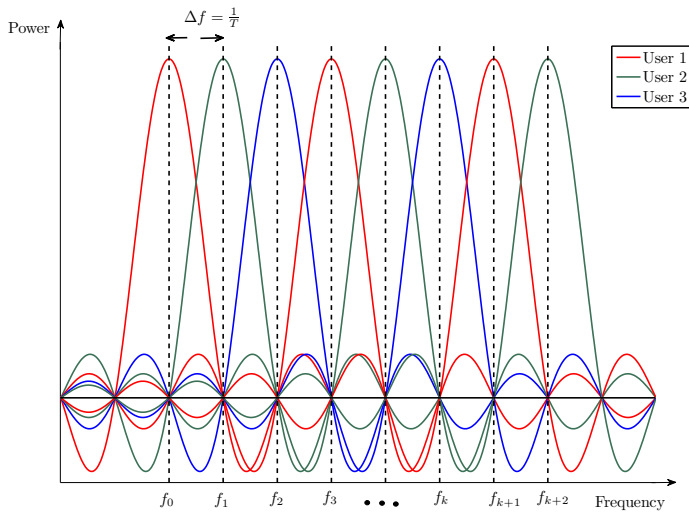
Figure 1.17: OFDMA spectrum, where f_k is the subcarrier frequency

System parameters	Mode 1	Mode 2	Mode 3	Mode 4	Mode 5
System bandwidth (MHz)	1.25	2.5	5.0	10	20
Sampling frequency (MHz)	1.429	2.857	5.714	11.429	22.857
Sampling period (ns)	700	350	175	88	44
FFT size	128	256	512	1024	2048
Subcarrier spacing	11.16 kHz				
CP duration	11.2 μs				
OFDMA symbol duration	100.8 μs				

Table 1.3: Physical layer parameters of IEEE 802.16 Wireless MAN

Tolerance=$\frac{f_u^{\text{LO}}}{f_c}$ (ppm)	f_u^{LO} (kHz)	$f_u^{\text{DOP}} + f_u^{\text{LO}}$ (kHz)	ϵ_u
4	10.40	11.12	0.9966
3	7.80	8.52	0.7636
2	5.20	5.92	0.5306
1	2.60	3.32	0.2977
0.5	1.30	2.02	0.1812

Table 1.4: CFO values for different values of LO tolerance, using the IEEE 802.16 Wireless MAN system parameters, $v_u = 300$ km/h and f_c=2.6 GHz

1.4.2.2 OFDMA Uplink Receiver

After down-conversion and low-pass filtering, the received signal passes into an analog-to-digital (A/D) converter, where it is sampled at the frequency $F_s = \frac{1}{T_s}$. The signal received by the BS is a superposition of the contributions from the U active users. After the time synchronization, the received OFDMA symbol of size K_T can be expressed as:

$$\mathbf{R}^{\text{CP}} = \sum_{u=1}^{U} \mathbf{R}_u^{\text{CP}} + \mathbf{B}^{\text{CP}} \tag{1.26}$$

where $\mathbf{B}^{\text{CP}}$ is a zero-mean AWGN vector with variance $\sigma_B^2 \mathbf{I}_{K^T}$ and

$$\mathbf{R}_u^{\text{CP}} \triangleq [R_u(K - N_g), \dots, R_u(K - 1), R_u(0), \dots, R_u(K - 1)]^T \tag{1.27}$$

At the BS, the signal transmitted by each user has been affected each propagation channel, thus:

$$R_u^{\text{CP}}(n) = e^{j2\pi\frac{\epsilon_u n}{K}} \sum_{l=0}^{L_u-1} h_u(l)X_u(n - l) \quad -N_g \leq n \leq K - 1 \tag{1.28}$$

where $h_u(l)$ is the lth coefficient of the CIR, $\epsilon_u = K(f_u^{\text{DOP}} + f_u^{\text{OSC}})T_s$ is the carrier frequency offset (CFO) normalized to the subcarrier spacing, f^{DOP} is the Doppler shift and f_u^{OSC} is the frequency difference in Hertz between the carrier frequencies of the LOs . Tables 1.4 and 1.5 show examples of the CFO magnitudes.

Then, at the OFDMA uplink receiver a CFO estimation/correction is necessary (See chapter 2). Let us consider that this step is performed perfectly. Then,

relative speed (km/h)	f_u^{DOP} (Hz)	ϵ_u
300	722.22	0.0647
200	481.48	0.0431
100	240.74	0.0216
80	192.59	0.0173
60	144.44	0.0129

Table 1.5: CFO values for different relative speeds, using the IEEE 802.16 Wireless MAN system parameters and $f_u^{\mathrm{LO}} = 0$ Hz

removing the CP, the contribution from each user to the nth sample of the received OFDMA symbol can be expressed as:

$$R_u(n) = \sum_{l=0}^{L_u-1} h_u(l)X_u(n-l) \quad 0 \le n \le K-1 \tag{1.29}$$

Then, the contribution from each user to the received OFDMA symbol at the BS satisfies:

$$\begin{aligned}
\mathbf{R}_u &\triangleq [R_u(0), R_u(1), \ldots, R_u(n), \ldots, R_u(K-1)]^T \\
&= \mathfrak{h}_u \mathbf{X}_u
\end{aligned} \tag{1.30}$$

where $\mathfrak{h}_u$ is a $K \times K$ circulant matrix[1] defined as:

$$\mathfrak{h}_u = \begin{bmatrix}
h_u(0) & 0 & \ldots & 0 & h_u(L_u-1) & \ldots & h_u(1) \\
h_u(1) & h_u(0) & \ddots & 0 & 0 & \ddots & h_u(2) \\
\vdots & \ddots & \ddots & \ddots & \ddots & \ddots & \vdots \\
h_u(L_u-1) & h_u(L_u-2) & \ddots & h_u(0) & 0 & \ddots & 0 \\
0 & h_u(L_u-1) & \ddots & h_u(1) & h_u(0) & \ddots & \vdots \\
\vdots & \ddots & \ddots & \ddots & \ddots & \ddots & \vdots \\
0 & 0 & \ldots & h_u(L_u-1) & h_u(L_u-2) & \ldots & h_u(0)
\end{bmatrix} \tag{1.31}$$

---

[1]Due to the CP, at the reception, the convolution between the transmitted signal and the channel can be expressed a circular convolution.

Finally, given (1.30) the received OFDMA symbol can be expressed as:

$$\begin{aligned}
\mathbf{R} &\triangleq [R(0), R(1), \ldots, R(n) \ldots, R(K-1)]^T \\
&= \sum_{u=1}^{U} \mathbf{R}_u + \mathbf{B} \\
&= \sum_{u=1}^{U} \mathfrak{h}_u \mathbf{X}_u + \mathbf{B}
\end{aligned} \tag{1.32}$$

where $\mathbf{B} = [B(0), B(1), \ldots, B(n) \ldots, B(K-1)]^T$ is a zero-mean AWGN vector with variance $\sigma_B^2 \mathbf{I}_K$.

Then, to recover the transmitted symbols, an FFT step is performed over the received OFDMA symbol $\mathbf{R}$ as follows:

$$\begin{aligned}
\mathbf{r} &\triangleq [r(0), r(1), \ldots, r(k), \ldots, r(m, K-1)]^T \\
&= \mathbf{F}\mathbf{R} \\
&= \sum_{u=1}^{U} \mathbf{F}\mathfrak{h}_u \mathbf{X}_u + \mathbf{b}
\end{aligned} \tag{1.33}$$

where $\mathbf{b} = \mathbf{F}\mathbf{B}$.

Then, given (1.21), (1.22) and (1.23), (1.33) can be rewritten as:

$$\begin{aligned}
\mathbf{r} &= \sum_{u=1}^{U} \underbrace{\mathbf{F}\mathfrak{h}_u\mathbf{F}}_{\mathbf{H}_u} \mathbf{Q}_u \mathbf{S}_u + \mathbf{b} \\
&= \sum_{u=1}^{U} \mathbf{H}_u \mathbf{Q}_u \mathbf{S}_u + \mathbf{b}
\end{aligned} \tag{1.34}$$

where $\mathbf{H}_u = \text{diag}\{[H_u(0), h_u(1), \ldots, H_u(K-1)]\}$ is the channel frequency response matrix, the entries of which are the channel frequency responses associated to the kth subcarrier:

$$H_u(k) = \sum_{l=0}^{L-1} h_u(l) e^{-j2\pi \frac{kl}{K}} \tag{1.35}$$

Then, $r(k)$ can be expressed as:

$$r(k) = \sum_{u=1}^{U} H_u(k) S_u(k) + b(k) \tag{1.36}$$

where $S_u(k) \neq 0$ if the kth subcarrier is allocated to the uth user and $b(k) = \sum_{n=0}^{K-1} B(n) e^{-j2\pi \frac{nk}{K}}$.

After subcarrier selection, the symbols $r(k)$ pass through channel equalizers (EQU) to obtain the transmitted symbols. It should be noted that due to the diagonal scheme of the matrix $\mathbf{H}_u$ the channel equalization can "easily" be performed. The OFDMA uplink receiver block scheme is shown in figure 1.18.
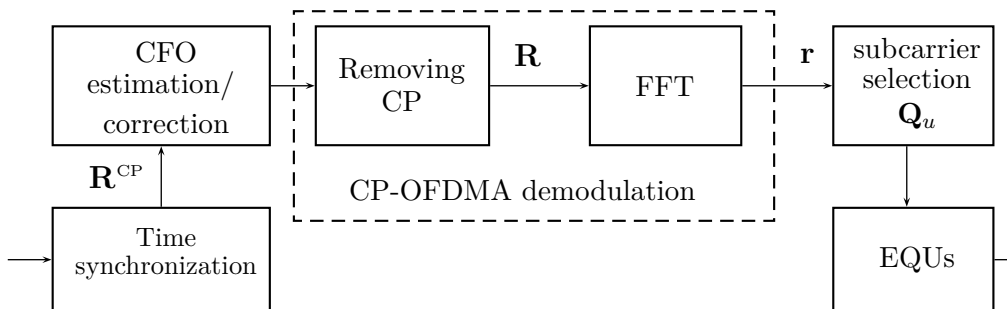
Figure 1.18: OFDMA uplink receiver

In this subsection, we assume a perfect CFO estimation/correction. In addition, we do not give details about the channel equalization. The CFO estimation/correction and channel equalization are usually performed using a preamble and/or pilot subcarriers. The preamble is a training sequence known by the receiver, whereas the pilot subcarriers are frequency subcarriers with high power that carry a sequence known by the receiver. Those important issues have to be considered in the design of an OFDMA mobile wireless system. In chapter 2, we propose several techniques for the frequency synchronization and channel equalization.

In the following subsection, the OFDM-IDMA scheme is presented.

1.4.3   OFDM-IDMA System

The main difference between OFDM-IDMA and OFDMA is that the entire bandwidth of the system can be allocated to all users at the same time. Therefore, CAS is not necessary, reducing the complexity of the OFDM-IDMA transmitter. Let us define an OFDM-IDMA system consisting of a single BS and U simultaneously users performing an uplink communication, as defined in section 1.4.2. The U users share the bandwidth W, divided in K subcarriers to perform a transmission. The users are numbered from 1 to U, i.e $u \in \{1, \dots U\}$. In the following

the subscript u denotes the information associated to the uth user. In addition, the overall subcarriers are numbered from 0 to $K - 1$, i.e $k \in \{0, \ldots K - 1\}$.

1.4.3.1 OFDM-IDMA Uplink Transmitter

IDMA transmitter

The bits of the uth user to be transmitted are encoded by a low-rate encoder (ENC), which consists of an association of channel coding[1] and spreading code of size $\mathbb{S}$. The encoded bits pass through the interleaver $\prod_u$ and then are modulated. The symbols are divided into blocks of length K; the resulting IDMA modulated block is:

$$\mathbf{S}_u \triangleq [S_u(0), S_u(1), \ldots, S_u(k), \ldots S_u(K-1)]^T \tag{1.37}$$

CP-OFDM Modulation

An IFFT is performed over the IDMA modulated symbol as in (1.20) resulting in the OFDM-IDMA symbol:

$$\mathbf{X}_u \triangleq [X_u(0), X_u(1), \ldots, X_u(k), \ldots X_u(K-1)]^T \tag{1.38}$$

At that time, a CP is inserted as in (1.24). The OFDM-IDMA symbols pass through a P/S and are stored to compose the OFDM-IDMA frame to be transmitted. The basic principles of an OFDM-IDMA transmitter is shown in figure 1.19. Finally, as for the OFDMA transmitter, the OFDM-IDMA frame is inserted in a D/A converter, modulated to the carrier frequency of the LO, amplified and transmitted over the channel.

1.4.3.2 OFDM-IDMA Uplink Receiver

As in the OFDMA uplink receiver, after down-conversion and low-pass filtering, the received signal passes into an A/D converter. At the BS, it has been affected by the propagation channel. Thus, the transmitted OFDM-IDMA symbol is affected by the different CFOs and multipath channels. As presented in subsection

---

[1]Depending on the targeted system performance, the channel coding can be inserted or not.
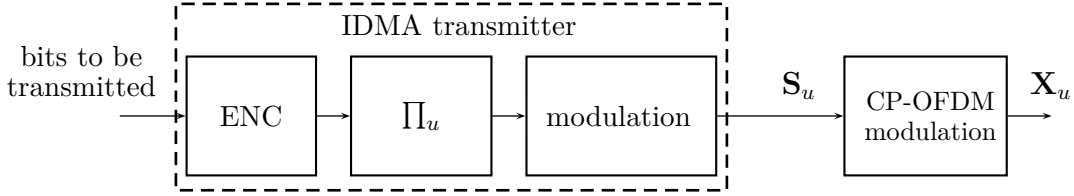
Figure 1.19: OFDM-IDMA transmitter for the uth user, where $\prod_u$ represents the interleaver

1.4.2.2, the OFDM-IDMA received symbol after time-synchronization, frequency synchronization and CP removing can be expressed as follows:

$$\begin{aligned}
\mathbf{R} &= \sum_{u=1}^{U} \mathbf{R}_u + \mathbf{B} \\
&= \sum_{u=1}^{U} \mathfrak{h}_u \mathbf{X}_u + \mathbf{B}
\end{aligned} \tag{1.39}$$

where $\mathbf{B} = [B(0), B(1), \ldots, B(n) \ldots, B(K-1)]^T$ is zero-mean AWGN vector with variance $\sigma_B^2 \mathbf{I}_K$ and $\mathfrak{h}_u$ is the channel circulant matrix as is expressed in (1.31). Thus, after the FFT step the received symbol can be expressed as:

$$\begin{aligned}
\mathbf{r} &\triangleq [r(0), r(1), \ldots, r(k), \ldots, r(K-1)]^T \\
&= \mathbf{F}\mathbf{R} \\
&= \sum_{u=1}^{U} \mathbf{F}\mathfrak{h}_u \mathbf{X}_u + \mathbf{b}
\end{aligned} \tag{1.40}$$

with $r(k)$ defined in (1.36).

The receiver consists of an ESE and U *a posteriori* probability DECs, one for each user. The two steps are considered separately. The results are then combined by using an iterative process. The DECs produce hard decisions to obtain the estimations of the transmitted bits during the final iteration[1].

Let us denote the *a priori* extrinsic logarithm likelihood ratios (LLRs) about $S_u(k)$ by:

$$g_u(k) \triangleq \log\left(\frac{\mathcal{P}_b\{S_u(k) = +1\}}{\mathcal{P}_b\{S_u(k) = -1\}}\right) \tag{1.41}$$

---

[1] It should be noted that the IDMA receiver may be applied to real and complex signals [Maha 07]. However, for the sake of simplicity, let us consider a BPSK modulation.

where $\mathcal{P}_b\{.\}$ is the probability distribution of $\{.\}$.

In the following let us distinguish $g_u^{\text{ESE}}(k)$ and $g_u^{\text{DEC}}(k)$ the *a priori* LLRs used by the ESE and DECs, respectively.

The ESE uses $r(k)$ and $g_u^{\text{ESE}}(k)$ as inputs and only the channel frequency response $\mathbf{H}_u = [H_u(0), \ldots, H_u(k), \ldots, H_u(K-1)]$ is considered. Knowing $\mathbf{H}_u$, the *a posteriori* LLRs about $S_u(k)$ are defined as[1]:

$$
\begin{aligned}
\log\left(\frac{\mathcal{P}_b\{S_u(k) = +1|r(k), \mathbf{H}_u\}}{\mathcal{P}_b\{S_u(k) = -1|r(k), \mathbf{H}_u\}}\right) &= \log\left(\frac{\mathcal{P}_b\{S_u(k) = +1|\mathbf{H}_u\}}{\mathcal{P}_b\{S_u(k) = -1|\mathbf{H}_u\}}\right) \\
&\quad + g_u^{\text{ESE}}(k) \\
&= \mathfrak{g}_u^{\text{ESE}}(k) + g_u^{\text{ESE}}(k)
\end{aligned}
\tag{1.42}
$$

where $\mathfrak{g}_u^{\text{ESE}}(k)$ is the extrinsic LLR about $S_u(k)$ based on the channel observation and the *a priori* information of the other users, excluding the uth treated user. Then, if $\mathbf{g}_u^{\text{DEC}} = [g_u^{\text{DEC}}(0), \ldots, g_u^{\text{DEC}}(k), \ldots, g_u^{\text{DEC}}(K-1)]$ are the inputs of the uth user DEC, the *a posteriori* LLRs about $S_u(k)$ are generated based on the code ENC as:

$$
\begin{aligned}
\log\left(\frac{\mathcal{P}_b\{S_u(k) = +1|\text{ENC}, \mathbf{g}_u^{\text{DEC}}\}}{\mathcal{P}_b\{S_u(k) = -1|\text{ENC}, \mathbf{g}_u^{\text{DEC}}\}}\right) &= \log\left(\frac{\mathcal{P}_b\{S_u(k) = +1|\tilde{\mathbf{g}}_u^{\text{DEC}}\}}{\mathcal{P}_b\{S_u(k) = -1|\tilde{\mathbf{g}}_u^{\text{DEC}}\}}\right) + g_u^{\text{DEC}}(k) \\
&= \mathfrak{g}_u^{\text{DEC}}(k) + g_u^{\text{DEC}}(k)
\end{aligned}
\tag{1.43}
$$

where $\tilde{\mathbf{g}}_u^{\text{DEC}}$ is obtained by setting $g_u^{\text{DEC}}(k) = 0$ in $\mathbf{g}_u^{\text{DEC}}$. The outputs of the DEC for the uth user consists of the extrinsic LLRs $\mathfrak{g}_u^{\text{DEC}}(k)$.

During the iterative process, the extrinsic information generated by the ESE $\mathfrak{g}_u^{\text{ESE}}(k)$ after deinterleaving is used as the *a priori* information in the DEC:

$$
\mathfrak{g}_u^{\text{ESE}}(k) \overset{\prod_u^{-1}}{\Rightarrow} g_u^{\text{DEC}}(k)
\tag{1.44}
$$

where $\overset{\prod_u^{-1}}{\Rightarrow}$ represents the deinterleaving process and $\prod_u^{-1}$ is the deinterleaver. Furthermore, the extrinsic information generated by the DEC $\mathfrak{g}_u^{\text{DEC}}(k)$ after interleaving is used as the *a priori* information in the ESE:

$$
\mathfrak{g}_u^{\text{DEC}}(k) \overset{\prod_u}{\Rightarrow} g_u^{\text{ESE}}(k)
\tag{1.45}
$$

---

[1]In Bayesian statistics, the *a posteriori* probability distribution of a random variable x based on the observations of $\mathbf{y}$ is expressed as follows: $\mathcal{P}_b\{x|\mathbf{y}\} = \frac{\mathcal{P}_b\{\mathbf{y}|x\}\mathcal{P}_b\{x\}}{\mathcal{P}_b\{\mathbf{y}\}}$, where $\mathcal{P}_b\{x\}$ is the so-called *a priori* probability distribution of x. As the denominator does not depend on x, the so-called *a posteriori* probability distribution can be rewritten as: $\mathcal{P}_b\{x|\mathbf{y}\} = \mathcal{P}_b\{\mathbf{y}|x\}\mathcal{P}_b\{x\}$

where $\overset{\prod_u}{\Rightarrow}$ represents the interleaving process. As there is any *a priori* information at the first iteration, the initial values of all $g_u^{\text{ESE}}(k)$ are set to zeros.

On the one hand, the *a posteriori* probability DEC is a standard function that depends on the ENC, such as convolutional or turbo codes [Ping 01], [Berr 93]. The reader may refer to [Ping 01] and [Berr 93] for more details about the DECs. On the other hand, let us present details about the ESE. The ESE generates coarse estimates of the symbol $S_u(k)$. The symbol is treated as a random variable and the *a priori* LLR $g_u^{\text{ESE}}(k)$ about $S_u(k)$ is obtained by updating $\mathfrak{g}_u^{\text{DEC}}(k)$ as shown in (1.45). Given (1.41) we have [Maha 06]:

$$\mu_u(k) = \mathbb{E}\{S_u(k)\} \triangleq \frac{e^{g_u^{\text{ESE}}(k)} - 1}{e^{g_u^{\text{ESE}}(k)} + 1} = \tanh\left(\frac{g_u^{\text{ESE}}(k)}{2}\right) \quad \forall u, k \quad (1.46)$$

$$v_u(k) = \text{Var}\{S_u(k)\} \triangleq 1 - (\mu_u(k))^2 \quad \forall u, k \quad (1.47)$$

where $\mathbb{E}\{.\}$ and $\text{Var}\{.\}$ represents the mean and the variance of $\{.\}$, respectively. For the initialization process, $g_u^{\text{ESE}}(k) = 0$ for $i = 1$, where i denotes the iteration number with $i \in \{1, \ldots, \mathfrak{I}^{idma}\}$, where $\mathfrak{I}^{idma}$ is the maximum number of iterations. Let us recall the expression of the received symbol $r(k)$ done for the OFDMA uplink receiver in (1.36):

$$r(k) = \sum_{u=1}^{U} H_u(k)S_u(k) + b(k) \quad (1.48)$$

where $S_u(k) \neq 0 \; \forall k$.

Let us rewrite (1.48) as:

$$r(k) = H_u(k)S_u(k) + \varsigma_u(k) \quad (1.49)$$

where $\varsigma_u(k) = \sum_{\substack{u'=1 \\ u' \neq u}}^{U} H_u'(k)S_{u'}(k) + b(k)$ represents the interference-plus-noise component in $r(k)$.

Then, assuming that $\mathbf{S}_u$ are independent and identically distributed random variables, and applying the central limit theorem[1], a Gaussian approximation for $\varsigma_u(k)$

---

[1]The central limit theorem states that the mean of a very large number of independent random variables, each one with finite mean and variance, can be approximated by a Gaussian distribution.

and $r(k)$ can be considered. Thus, $\varsigma_u(k)$ can be completely characterized by its mean and variance:

$$
\begin{align}
\mathbb{E}\{\varsigma_u(k)\} &= \mathbb{E}\{r(k)\} - H_u(k)\mu_u(k) \quad \forall u,k \tag{1.50}\\
\mathrm{Var}\{\varsigma_u(k)\} &= Var\{r(k)\} - (H_u(k))^2 \upsilon_u(k) \quad \forall u,k \tag{1.51}
\end{align}
$$

where

$$
\begin{align}
\mathbb{E}\{r(k)\} &= \sum_{u=1}^{U} H_u(k)\mu_u(k) \quad \forall u,k \tag{1.52}\\
\mathrm{Var}\{r(k)\} &= \sigma_B^2 + \sum_{u=1}^{U} (H_u(k))^2 \upsilon_u(k) \quad \forall u,k \tag{1.53}
\end{align}
$$

Then, the value of $\mathfrak{g}_u^{\mathrm{ESE}}(k)$ can be obtained as follows [Maha 06]:

$$
\mathfrak{g}_u^{\mathrm{ESE}}(k) = 2H_u(k) \times \frac{r(k) - \mathbb{E}\{\varsigma_u(k)\}}{\mathrm{Var}\{\varsigma_u(k)\}} \quad \forall u,k \tag{1.54}
$$

The ESE is summarized in algorithm 1.

Then, $\mathfrak{g}_u^{\mathrm{ESE}}(k)$ is updated as $g_u^{\mathrm{DEC}}(k)$ and inserted in the DEC. The DEC provides $\mathfrak{g}_u^{\mathrm{DEC}}(k)$, this value is updated as $g_u^{\mathrm{ESE}}(k)$ and the ESE process is again performed. During the final iteration the DECs produce hard decisions and the transmitted

---

Algorithm 1 ESE

Require: $r(k)$, σ_B^2, $H_u(k)$, $\mathfrak{J}^{\mathrm{idma}}$

　Initialization step:

　$g_u^{\mathrm{ESE}}(k) = 0 \quad \forall u,k$

　Iterative process

　for $i = 1$ to $\mathfrak{J}^{\mathrm{idma}}$ **do**

　　$\mu_u(k) = \mathbb{E}\{S_u(k)\} = tanh\left(\frac{g_u^{\mathrm{ESE}}(k)}{2}\right) \quad \forall u,k$

　　$\upsilon_u(k) = Var\{S_u(k)\} = 1 - (\mu_u(k))^2 \quad \forall u,k$

　　$\mathbb{E}\{r(k)\} = \sum_{u=1}^{U} H_u(k)\mu_u(k) \quad \forall u,k$

　　$Var\{r(k)\} = \sigma_B^2 + \sum_{u=1}^{U} (H_u(k))^2 \upsilon_u(k) \quad \forall u,k$

　　$\mathbb{E}\{\varsigma_u(k)\} = \mathbb{E}\{r(k)\} - H_u(k)\mu_u(k) \quad \forall u,k$

　　$Var\{\varsigma_u(k)\} = Var\{r(k)\} - (H_u(k))^2 \upsilon_u(k) \quad \forall u,k$

　　$\mathfrak{g}_u^{\mathrm{ESE}}(k) = 2H_u(k) \times \frac{r(k) - \mathbb{E}\{\varsigma_u(k)\}}{Var\{\varsigma_u(k)\}} \quad \forall u,k$

　end for

---

bits are estimated[1].

The block scheme of an OFDM-IDMA uplink receiver is shown in figure 1.20. It should be noted that again we considered a perfectly frequency synchronized. However, this is a very strong hypothesis for a real wireless communication system. The effects of the propagation channel on the OFDM-IDMA received signal are the same as the ones presented for an OFDMA system in subsection 1.18. Therefore, the estimation of the CFOs can be implemented as in an OFDMA system, but not the CFO correction. In an OFDM-IDMA system, all the users use all the subcarriers at the same time. Thus, the CFO correction of one user may destroy the orthogonality of the other users. In addition the IDMA receiver needs the *a priori* knowledge of the CIRs. Hence, a channel estimation is required.
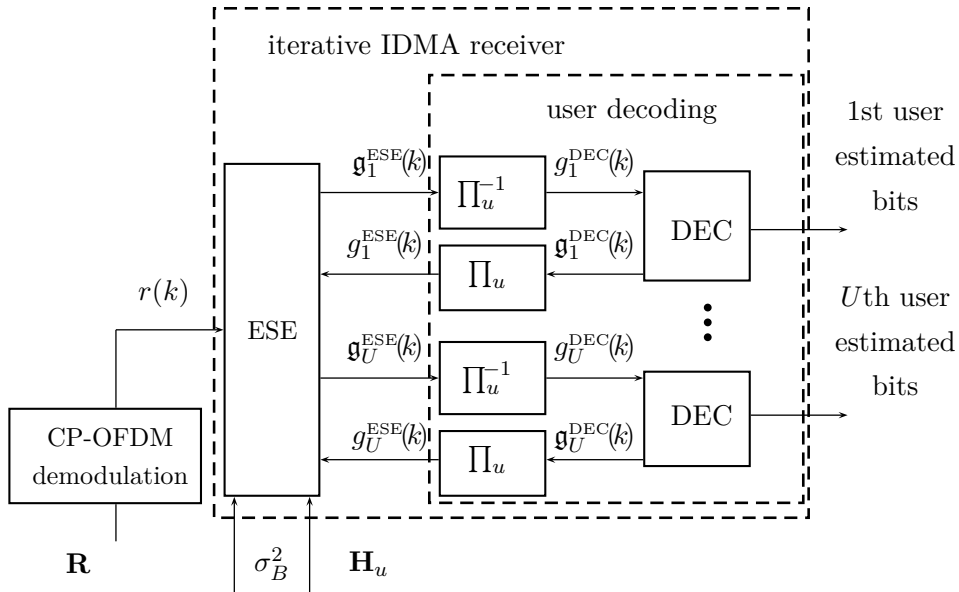
Figure 1.20: OFDM-IDMA uplink receiver [Maha 06], where ESE is the elementary signal estimator and DEC is the *a posteriori* probability decoder

---

[1]In this PhD dissertation we consider a parallel processing of the users in the IDMA receiver.

1.5 Conclusions

In this chapter, our purpose was to present the multicarrier high-data rate mobile wireless systems. We recall various properties of the system such as: 1/ the influence of the propagation channel leading to various kinds of channels (slow or fast fading channel, flat-fading or frequency-selective channel), 2/ the various multiple access techniques that have been derived: FDMA, TDMA, CDMA, SC-FDMA, OFDMA and OFDM-IDMA.

Then, we focus our attention on two systems. We first present in detail the OFDMA uplink transmitter and receiver, by giving the expression of the input and the output of each block in the processing chain. We also look at the OFDM-IDMA system and present the uplink receiver proposed in [Maha 06]

In both cases, we point out the importance of the estimation of the CFO and the channel.

In chapter 2, we are going to propose several methods based on Kalman Filtering and H_∞ filtering to carry out the frequency synchronization and channel equalization.

In chapter 3, we will propose some modifications of the conventional OFDM-IDMA uplink receiver to counteract the effect of the multiple CFOs and the channel in the received OFDM-IDMA signal.

Chapter 2

Frequency Synchronization and Channel Equalization of OFDMA Uplink Systems

Contents

2. Frequency Synchronization and Channel Equalization of OFDMA Uplink Systems

2.1 Introduction

As mentioned in chapter 1, in OFDMA uplink systems, estimating CFO and channel plays a key role. This chapter deals with the frequency synchronization and the channel equalization, and presents our contributions in that field.

The chapter is organized as follows: a state of the art dedicated to the CFO and channel estimation in OFDMA uplink systems is given. We first focus our attention on the estimation of the CFO for systems with interleaved and generalized CAS [More 04], [Zhao 06], [Jing 08]. The estimation can be done in the frequency domain or in the time domain. Then, we present the existing methods dealing with the joint estimation of the CFO and the channel [Pun 04a], [Pun 06], [Sezg 08]. At that stage, we suggest a recursive estimation of the CFO and the channel by using optimal filtering, i.e. Kalman filtering and H_∞ filtering (and their variants). These approaches are derived:

- in combination with an MMSE-SD to increase the data rate in the system;

- in combination with a statistical test, i.e. the BHT and the CUSUM test, to design a robust CFO estimator that detects the beginning and the end of the disturbances induced by another system.

2.2 State of the Art on the OFDMA Uplink Systems - Carrier Frequency Offset (CFO) and Channel Estimation

In an OFDMA uplink system, the signal received at the BS is affected by several CFOs and multipath channels. Indeed, the signal transmitted by each user propagates through different propagation channels. Estimating/correcting the CFO and the channel is necessary. More particularly, without CFO estimations/corrections, orthogonality between subcarriers is no longer satisfied. It results in ICI as well as MAI. These multiple frequency offsets make the CFO

estimation more "complex" than the one in a downlink communication[1].

The CFO estimation problem for OFDMA uplink transmissions using control data[2] has been recently addressed in several papers. Thus, in [More 07], Morelli *et al.* present a tutorial that illustrates various schemes for uplink CFO estimation among different CAS.

More specifically, when using subband CAS (See chapter 1 in section 1.4.2.1), CFO can be estimated by inserting unused subcarriers among subchannels to provide frequency guard intervals as shown in figure 2.1.
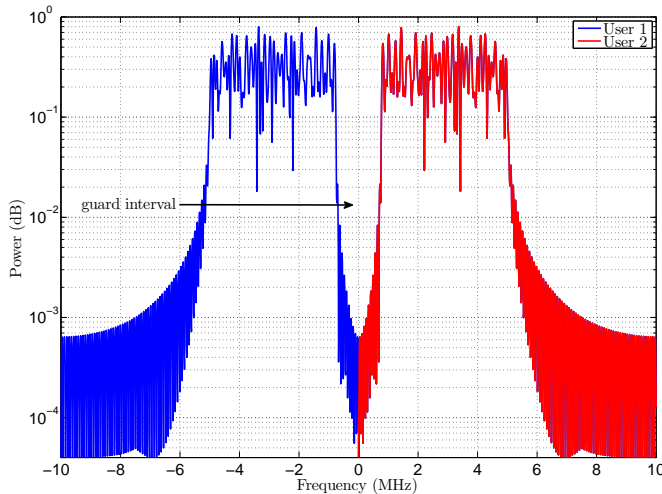
Figure 2.1: OFDMA spectrum when using subband CAS

If the CFOs are smaller than the guard intervals, the received signals can be separated at the BS by passing through a bank of digital band-pass filters (BPFs), each one selecting a subband. Therefore, CFO-estimation methods used in OFDM or OFDMA downlink transmission can be used. For example, the method proposed in [Moos 94] to estimate the CFO in an OFDM transmission can be performed.

---

[1]Indeed, in an OFDMA downlink communication, the receiver is the user. Thus, one user has to estimate only a single CFO and a single channel. Then, the CFO estimation can be performed by using the methods proposed for OFDM single-user communications [Moos 94], [VdBe 99].

[2]The control data are composed by known training sequences called "preambles" and/or pilot subcarriers.

The CFO is estimated by calculating a phase shift in the frequency domain between two successive identical OFDM symbols. The repetitive OFDM symbol remains identical after passing through the channel except for a phase shift produced by the CFO. In [Huan 10a], the authors use control data having a tile structure in the frequency domain. Then, a high-resolution subspace method allows the CFO to be estimated. In [VdBe 99], Van de Beek *et al.* take advantage of the CP and estimate the CFOs by calculating the phase shifts in the time domain between the N_g last samples of the received OFDMA symbols and the CP of each user.

In OFDMA uplink systems with interleaved or generalized CAS, it is impossible to take advantage of the frequency guard intervals. In those systems the CFO estimation is a challenging task. When using control data, several methods have been proposed. In [More 04], the CFO is estimated in the ML sense. However, it requires an exhaustive grid search over all the possible values of the CFO, leading to a high computational cost. For that reason, Morelli also proposes a reduced-complexity frequency estimator, that compares the phase shifts of several identical received OFDMA symbols in the frequency domain. Nevertheless, the author assumes that all the active users, except the first one, are already synchronized in frequency. In [Zhao 06], Zhao *et al.* use an EKF to estimate the CFO. In addition, Jing *et al.* propose an extended H_∞ filter to combat intercarrier interference for an OFDM system [Jing 08]. However, in both approaches, the channels are preliminary estimated and this assumption cannot be necessarily satisfied in real cases. Indeed, during the uplink CFO-synchronization stage, channel state information[1] (CSI) is not available, and hence has to be estimated either jointly with the CFO or after CFO compensation.

In order to correct the MAI, the CFO has to be compensated. In the single-user detector method, shown in figure 2.2, the CFOs are compensated by multiplying the complex envelope of the signal before the CP-OFDMA demodulation at the receiver. However, the number of FFTs increases linearly with the number of users as well as the computational complexity of the receiver. As an alternative, new correction methods have been proposed. More particularly in [Dai 07], the

---

[1]The CSI refers to known channel properties of a communication link. It is usually associated to the CIR.

2. Frequency Synchronization and Channel Equalization of OFDMA Uplink Systems
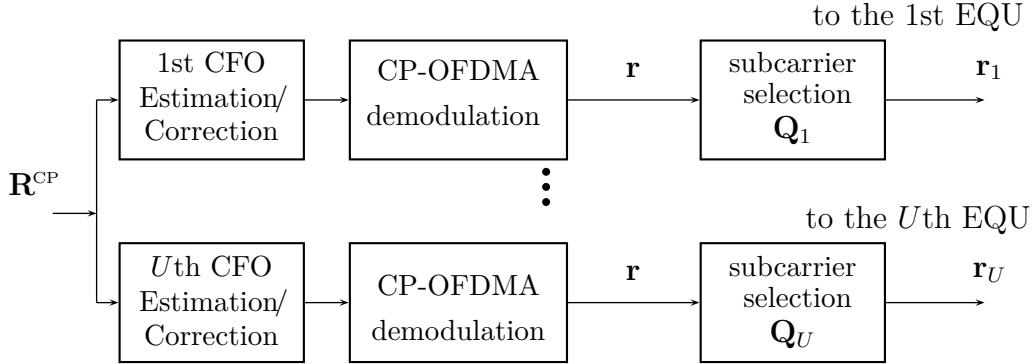
Figure 2.2: Single-user detector

CFO is compensated by mitigating the effects of the major lobes and the side lobes of the frequency response of the signals received from each user. The CFO estimation can be obtained by calculating the phase shifts of two identical received OFDMA symbols in the time domain. In [Choi 00], CFO compensation is based on a circular convolution after the CP-OFDMA demodulation[1], as shown in figure 2.3. The authors suggest using the method presented in [Moos 94] to estimate the CFOs. However, both methods only work for subband CAS. Consequently, in [Huan 05], the authors extend the concept proposed in [Choi 00] and use it in a system with interleaved or generalized CAS. In that case, the
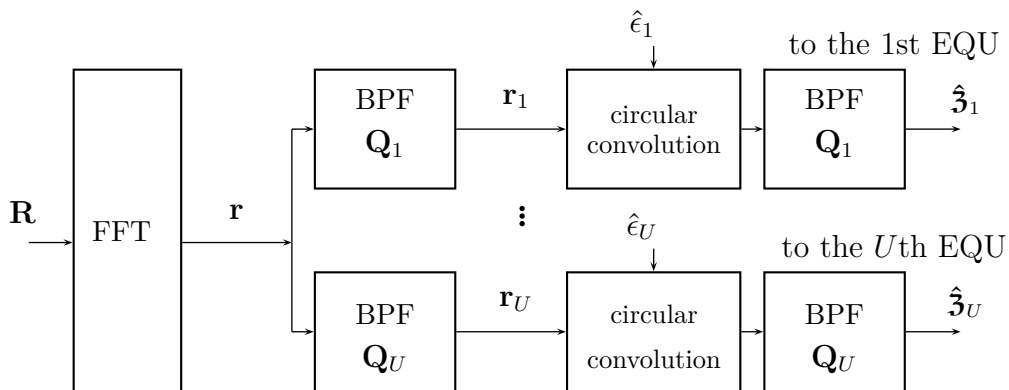
Figure 2.3: CFO correction by means of a circular convolution after the FFT

---

[1]Due to the CP, the received signal without CFO correction after the CP-OFDMA demodulation can be expressed as: $\mathbf{r} = \sum_{u=1}^{U} \mathbf{F}\mathbf{E}_u \otimes \mathfrak{Z}_u + \mathbf{b}$, where $\mathfrak{Z}_u = \mathbf{F}\mathfrak{h}_u\mathbf{X}_u$, $\mathbf{E}_u$ is the CFO matrix and $\otimes$ represents a circular convolution.

Algorithm 2 Circular convolution + IC [Choi 00]

Require: $\mathbf{r} = \sum_{u=1}^{U} \mathbf{FE}_u \otimes \mathbf{3}_u + \mathbf{b}$, $\mathbf{3}_u = \mathbf{F}\mathfrak{h}_u \mathbf{X}_u$, $\hat{\mathbf{E}}_u$, $\otimes$: circular convolution

   Initialization step:

   $\hat{\mathbf{3}}_u = \mathbf{Q}_u \{ \mathbf{Q}_u \mathbf{r} \otimes \mathbf{F}\hat{\mathbf{E}}_u^H \}$

   Circular convolution + IC step:

   for $i = 1$ to $I_{\max}$ **do**

      $\tilde{\mathbf{3}}_u = \mathbf{r} - \sum_{\substack{u'=1 \\ u' \neq u}}^{U} \hat{\mathbf{3}}_u \otimes \mathbf{F}\hat{\mathbf{E}}_u$ and

      $\hat{\mathbf{3}}_u = \mathbf{Q}_u \{ \mathbf{Q}_u \tilde{\mathbf{3}}_u \otimes \mathbf{F}\hat{\mathbf{E}}_u^H \}$

   end for

CFOs are corrected via a circular convolution after the CP-OFDMA demodulation, but an iterative interference-cancellation (IC) step is required, as shown in algorithm 2. The authors suggest again using the method presented in [Moos 94]. In [Cao 04a], the CFO is corrected by means of a linear detection, whereas the CFO is estimated using a high-resolution subspace method, i.e. the multiple signal classification (MUSIC) method [Ther 92]. More recently, Hou *et al.* have proposed a minimum mean square error successive detector (MMSE-SD) to suppress the MAI, but the CFO is assumed to be known [Hou 08].

In the above approaches, channel estimation is not included. The joint estimation of the CFO and the channel has been also investigated. In [Pun 04a] and [Pun 06], the authors study how to obtain the joint ML estimations of the channels and the CFOs of multiple users. Thus in [Pun 04a], a conventional EM is first proposed: during the E-step, the received signals transmitted by each user, namely the "complete data", are estimated. During the M-step, all the CFOs and the channels are jointly estimated by using these complete data. To simplify the optimization issue, the value of the channel is replaced by its expression depending on the CFO in the criterion to be minimized. Therefore, only the CFO of each user has to be estimated. Even if the criterion is explicitly given, the authors do not mention the estimation method they used. For instance, exhaustive grid search could be considered as suggested by the same authors in [Pun 04b]. To reduce the computational cost, the authors in [Pun 04a] use the SAGE algorithm.

2. Frequency Synchronization and Channel Equalization of OFDMA Uplink Systems

In that case, instead of simultaneously estimating every-user parameters, one iteration of the EM algorithm is dedicated to one user. Instead of addressing a multidimensional optimization issue, the so-called alternating projection estimator is used in [Pun 06]. This method consists in iteratively estimating the CFO of one user, by means of an exhaustive grid search over the possible range of the CFO value and by setting the other CFOs to their last updated values. In [Fu 06], Fu *et al.* propose two iterative estimation approaches using the SAGE method. In addition, in [Saem 07] Saemi *et al.* propose two EM-based algorithms. The first one estimate the CFO without the CSI whereas the second one estimate jointly the CFO and the channel. Nevertheless, the EM-based algorithms do not necessarily converge to the global extremum. Like any EM algorithm, an initialization step is required. Another drawback of the above methods is the high computational cost due to the iterative estimation and the exhaustive grid search. For a large number of subcarriers, the EM-based algorithms are impractical. For that reason, Sezginer *et al.* [Sezg 08] proposed an iterative suboptimal method. It is based on an approximation of an ML estimator to reduce the computational complexity of the EM-based algorithms. However, it is still based on an exhaustive grid search and an iterative architecture.

To reduce the amount of control data, alternative estimation techniques have been proposed. If a subband CAS OFDMA uplink system is considered, the method presented in [Cibl 04] can be considered. Thus, Ciblat *et al.* have developed a blind[1] CFO estimation for an OFDM single-user system based on offset quadrature amplitude modulation (OQAM). The CFO is estimated by searching the maximum of the periodogram of the received signal. Nevertheless, this is a single-parameter estimation method and cannot be implemented for interleaved and/or generalized CAS. For that reason, in [Cao 04b], the authors propose a subspace method based blind CFO estimation algorithm for an interleaved CAS OFDMA uplink system. It consists of a high-resolution signal-processing technique to estimate the CFO without control data. Nevertheless, more subchannels than users are required. In addition when the values of the different CFOs are close one another, the grid search approach leads to a suboptimal estimation. In

---

[1]A blind CFO estimation is an estimation of the CFO that does not require control data.

[Mova 08], a blind method to estimate CFOs based on a linear precoder is proposed. Using two OFDMA symbols, the idea is to find a time correlation using a precoder which gives a second-order moment based CFO estimation for each user.

Several approaches using ML estimation of the CFO and channel estimation in multicarrier systems have been proposed. However, only few approaches are based on optimal recursive filtering to perform the CFO and channel estimation in OFDMA uplink systems. One feature is that this multiparameter estimation solution can be implemented recursively. In particular, each updated estimate is computed from the previous estimate and the current observation. Therefore, only the previous estimation has to be stored. The optimal filtering is hence computationally more efficient than algorithms that compute the estimation using the entire past observed data at each step of the estimation process.

In the following, different optimal filtering techniques aiming at estimating the CFO and the channel are proposed for conventional and CR environments.

2.3 A Joint CFO/Channel Estimator for OFDMA Systems

Due to the propagation channels and the radio frequency (RF) effects, the uplink signals at the BS are plagued by synchronization and estimation errors. Therefore at the BS, synchronization and equalization process has to be done. These processes usually require control data. Commonly, the synchronization process is performed before the CIR estimation. However, if a time-synchronized OFDMA uplink system is considered, the CFO and the channel can be jointly estimated. Then, for a time-synchronized system the nth sample of the received OFDMA symbol at the BS after CP removing is:

$$R(n) = e^{j2\pi \frac{\epsilon_u n}{K}} \sum_{u=1}^{U} \sum_{l=0}^{L_u - 1} h_u(l) X_u(n - l) + B(n) \quad 0 \le n \le K - 1 \qquad (2.1)$$

Then, the received OFDMA symbol can be expressed as follows:

$$\mathbf{R} \triangleq [R(0), R(1), \ldots, R(n), \ldots, R(K-1)]^T$$

$$= \sum_{u=1}^{U} \underbrace{\mathbf{E}_u \mathfrak{h}_u \mathbf{X}_u}_{\mathbf{R}_u} + \mathbf{B} \tag{2.2}$$

where $\mathbf{E}_u = \operatorname{diag}\left\{\left[1, e^{j2\pi\epsilon_u/K}, \ldots, e^{j2\pi(K-1)\epsilon_u/K}\right]\right\}$ (See chapter 1 in section 1.4.2.2). In order to restore orthogonality among each user subcarrier, both the CFO-synchronization error vector $\boldsymbol{\epsilon}$ and the CSI vector $\mathbf{h}$ have to be estimated at the BS.

Let us define the vector $\boldsymbol{\epsilon}$ of size U and the vector $\mathbf{h}$ of size $L = \sum_{u=1}^{U} L_u$ by storing the CFOs and the CSIs of the U users in the system as follows:

$$\boldsymbol{\epsilon} = [\epsilon_1, \epsilon_2, \ldots, \epsilon_u, \ldots, \epsilon_U] \tag{2.3}$$

$$\mathbf{h} = [\mathbf{h}_1, \mathbf{h}_2, \ldots, \mathbf{h}_u, \ldots, \mathbf{h}_U] \tag{2.4}$$

where $\mathbf{h}_u = [h_u(0), h_u(1), \ldots, h_u(l), \ldots, h(L_u - 1)]$.

In this section, a joint estimation of the CFOs and the CSIs using Kalman and H$_\infty$ filtering is proposed [Pove 10]. The Kalman filter requires an exact and accurate system model as well as perfect knowledge of the noise statistics. In contrast, the H$_\infty$ filtering is more robust against model uncertainty and does not need any *a priori* knowledge of the noise statistics. It should be noted that the work presented in this section is complementary to the study done in [Kang 07], that presents a joint CFO/channel estimation in a single-user scenario using an UKF. As both Kalman and the H$_\infty$ filtering are based on a state-space representation of the system, the next subsection briefly recalls the equation updating the state vector and the observation equation.

2.3.1   State-Space Representation of the System

The state-space representation of the system (2.1)-(2.2) is the representation of what happens during the OFDMA frame[1].

---

[1]The OFDMA frame has been introduced in chapter 1 in section 1.4.2.1; it is a block composed of several OFDMA symbols.

Let us define the vector $\mathbf{x}(n)$ of size $\mathcal{U} = U + 2L$, which is the state vector of the system (2.1)-(2.2):

$$\mathbf{x}(n) = \begin{bmatrix} \boldsymbol{\epsilon}(n) & Re\left\{\mathbf{h}(n)\right\} & Im\left\{\mathbf{h}(n)\right\} \end{bmatrix}^T \tag{2.5}$$

In order to improve the performance of the proposed algorithm [Kang 07], a separate estimation of the real and the imaginary parts of the state-vector is proposed[1]. Let $\mathbf{Y}$ be the $2 \times K$ observation matrix that stores the real and the imaginary parts of the received OFDMA symbol[2] $\mathbf{R}$:

$$\begin{aligned} \mathbf{Y}(\boldsymbol{\epsilon}, \mathbf{h}) &= \mathbf{C}(\boldsymbol{\epsilon}, \mathbf{h}) + \mathbb{B} \\ &= [\mathbf{Y}(0, \boldsymbol{\epsilon}, \mathbf{h}), \mathbf{Y}(1, \boldsymbol{\epsilon}, \mathbf{h}), \dots, \mathbf{Y}(n, \boldsymbol{\epsilon}, \mathbf{h}), \dots, \mathbf{Y}(K-1, \boldsymbol{\epsilon}, \mathbf{h})] \end{aligned} \tag{2.6}$$

where $\mathbf{C}(\boldsymbol{\epsilon}, \mathbf{h})$ is a $2 \times K$ matrix that stores the real and the imaginary parts of the contributions of alls users to the received OFDMA symbol:

$$\begin{aligned} \mathbf{C}(\boldsymbol{\epsilon}, \mathbf{h}) &= \begin{bmatrix} Re\left\{\sum_{u=1}^{U} \mathbf{R}_u\right\}^T \\ Im\left\{\sum_{u=1}^{U} \mathbf{R}_u\right\}^T \end{bmatrix} \\ &= [\mathbf{C}(0, \boldsymbol{\epsilon}, \mathbf{h}), \mathbf{C}(1, \boldsymbol{\epsilon}, \mathbf{h}), \dots, \mathbf{C}(n, \boldsymbol{\epsilon}, \mathbf{h}), \dots, \mathbf{C}(K-1, \boldsymbol{\epsilon}, \mathbf{h})] \end{aligned} \tag{2.7}$$

and

$$\mathbb{B} = \begin{bmatrix} Re\{\mathbf{B}(n)\}^T \\ Im\{\mathbf{B}(n)\}^T \end{bmatrix} = [\boldsymbol{\mathcal{B}}(0), \boldsymbol{\mathcal{B}}(1), \dots, \boldsymbol{\mathcal{B}}(K-1)] \tag{2.8}$$

$\boldsymbol{\mathcal{B}}(n)$ is an AWGN vector with zero-mean and covariance matrix $\frac{\sigma_B}{2}\mathbf{I}_2$.

Now, let us introduce the state-space representation of the system (2.1)-(2.2) to estimate the CFO and the channel:

State equation:

$$\mathbf{x}(n) = \mathbf{x}(n-1) + \mathbf{w}(n) \quad \forall \quad n \in [0, K-1] \tag{2.9}$$

Measurement equation:

$$\mathbf{Y}(n) = \mathbf{C}(n, \mathbf{x}(n)) + \boldsymbol{\mathcal{B}}(n) \quad \forall \quad n \in [0, K-1] \tag{2.10}$$

---

[1]As an optimal filtering estimation is proposed, one solution could be to use a complex Kalman filter [Dash 00] or a complex H_∞ filter [Nish 99]. However, in order to guarantee the stability of the filter [Dini 10], we have chosen to separate the estimation of the real and the imaginary parts.

[2]$\mathbf{C}(\boldsymbol{\epsilon}, \mathbf{h})$ indicates that the matrix $\mathbf{C}$ depends on these vectors.

where $\mathbf{w}(n)$ is an AWGN matrix with zero-mean and covariance matrix $\sigma_w^2 \mathbf{I}_{\mathcal{U}}$. It should be noted that σ_w^2 is very low and can even be equal to 0. In this latter case, the CFO and the channel are assumed to be constant during one OFDMA symbol.

2.3.2   Kalman Filtering in the Non-Linear Case

When dealing with the non-linear state-space representation (2.9)-(2.10) of the system and if there is no model noise in the state-equation, methods such as the linearized recursive least squares (RLS) can be considered [Hayk 96]. More generally, if there is a model noise in equation (2.9) the EKF [Hayk 96] presented in appendix D can be used. However, due to the first-order approximation, the EKF may sometimes diverge when evaluating the mean and the covariance matrix of the random variable that undergoes the non-linear transform. To address this approximation issue, a second-order linearization can be considered and leads to the SOEKF [Bar 01] presented as well in appendix D. In that case, the Jacobian matrix must be computed for the first-order linearization, but also the Hessian matrix for the second-order linearization. As an alternative, the IEKF presented in appendix D linearizes the measurement model around the updated state, instead of the predicted state. At each time step, this linearization around the estimate can be done several times (e.g. 2 to 5 times). It should be noted that in [Grew 10], another kind of EKF is presented to address numerical issues of the EKF. However, these derivations may be unstable and do not necessarily guarantee the convergence of the filter. For that reason, the SPKF presented in appendix E, namely the UKF or the CDKF, are considered in this thesis [VdMe 04a]. The UKF is based on the unscented transformation [Wan 01], whereas the CDKF is based on the second-order Sterling polynomial [Ito 00]. The main advantages of the SPKF over the EKF is that they do not require calculations of Jacobians or Hessians. See table 2.1.

In this section, these five types of Kalman filters (KFs) are used to recursively estimate the state-vector.

Non-linear Estimation		
No model noise	**Model noise**	
Linearized RLS	**Kalman filter**	
	Linearization	**Gaussian approximation**
	EKF	UKF
	SOEKF	CDKF $\Big\}$ SPKF
	IEKF	

Table 2.1: Gaussian non-linear estimation methods

2.3.3 H$_\infty$ Filtering in the Non-Linear Case

In the above approaches, *a priori* knowledge on the model noise $\mathbf{w}$ and the measurement noise $\mathbb{B}$ characteristics is required. To relax the assumption on the model noise and additive measurement noise, we suggest investigating the relevance of the H$_\infty$ filter. H$_\infty$ filter is known to be more robust to uncertainties than Kalman filtering-based estimation [Hass 99]. The H$_\infty$ theory purpose is to minimize the worst possible effects of the disturbances on the estimation error. No statistical assumptions have to be made on the model and the measurement noises. They are just assumed to have finite energies.

Let us introduce a third state-space equation to focus on a linear combination of the state-vector components:

$$\mathbf{z}(n) = \mathcal{L}\mathbf{x}(n) \tag{2.11}$$

where $\mathcal{L} = \mathbf{I}_{\mathcal{U}}$. The reader is referred to appendix B, where the state-space representation is linear and to appendix F, where the state-space representation is non-linear.

In this section, two types of H$_\infty$ filters are proposed to estimate the state vector in a recursive way:

- like the EKF, the "extended H$_\infty$ filter" consists of a first-order expansion of the state-space functions around the last available estimation of the state vector [Burl 98];

- the unscented H$_\infty$ filter [Li 10], which is based on the unscented transformation embedded into the "extended H$_\infty$ filter" architecture.

The reader is referred to table 2.2. In addition, appendix C deals with a comparison between the equations that define Kalman filtering and H_∞ filtering.

	No linearization	No statistical assumptions
EKF	✗	✗
SPKF	✓	✗
Extended H_∞ filter	✗	✓
Unscented H_∞ filter	✓	✓

Table 2.2: The KF vs the H_∞ filter in a non-linear case, ✓ represents a fulfilled option whereas ✗ represents a not fulfilled option

In the following subsection, simulation results show the efficiency of the proposed optimal filtering algorithms.

2.3.4   Simulation Results

In the following, a comparative study is carried out between:

- the EKF, the SOEKF, the IEKF, presented in appendix D;

- the UKF, the CDKF, presented in appendix E;

- the "extended H_∞ filter", the "unscented H_∞ filter" presented in appendix F;

- and the methods presented in [Pun 04a] and [Pun 06] where a grid search approach is used to update the CFO estimation.

Simulation protocol:
An OFDMA IEEE 802.16 WirelessMAN$^{\text{TM}}$ uplink system composed of $U = 4$ users sharing $K = 128$ subcarriers and with a cyclic prefix $N_g = K/8 \geq \underset{u}{max}(L_u)$ is considered. A transmission over a Rayleigh slow-fading frequency-selective

channel composed of $L_u = 3 \ \forall u$ multipaths is supposed. BPSK is used to modulate the information bits. The carrier frequency is at $f_c = 2.6$GHz and the bandwidth is set to $W = 20$MHz. The users' normalized CFO errors are randomly and uniformly generated in the interval [-1,1]. Then, let us define SNR= $10\log(\frac{\sigma_u^2}{\sigma_B^2})$, where σ_u^2 is the mean power of the received signal from the uth user.

When using H_∞ filtering: $\Xi = 10^2$, $\mathbf{\mathcal{V}} = \frac{\sigma_B^2}{2}\mathbf{I}_2$ and $\mathbf{\mathcal{W}} = \mathbf{I}_{\mathcal{U}}\sigma_w^2$. One assumes that there is a state noise $\mathbf{w}(n)$ with very small variance, e.g. $\sigma_w^2 = 10^{-3}$. For the CFO, the initialization parameters of the algorithm is $\hat{\epsilon}_u(0) = 0 \ \forall u$.

The grid search algorithms proposed in [Pun 04a] and [Pun 06] are based on $\mathfrak{I}^{em} = 20$ iterations and a grid search precision equal to 10^{-4}; this means that $\mathfrak{b} = \frac{2}{10^{-4}} + 1 = 20001$ values of CFO are studied in the grid search algorithm. The estimations are obtained by using control data of one OFDMA symbol.

2.3.4.1 Estimation Performance

We focus our attention on the first user in the system. First of all, our approaches provide similar results when UKF and CDKF are used. Therefore, in the following, we make reference to SPKF filtering performance.

Figure 2.4 and 2.5 show the results in terms of CFO and channel MMSE considering a perfect knowledge of the noise statistics. When the noise characteristics are available, the EKF provides quite similar results in comparison with the "extended H_∞ filter" and there is no real difference between the SPKF and the "unscented H_∞ filter". For that reason, in figure 2.4 and 2.5, we only show the results of the Kalman approaches. In addition, the algorithms in [Pun 04a] and [Pun 06] provide similar results after a given number of iterations. Thus, figure 2.4 and 2.5 show only the performance of the EM-based algorithm presented in [Pun 04a].

The IEKF gives the best estimation performance. However, due to the calculation of the Jacobian matrix at each iteration, the computational complexity is the highest among the proposed approaches. The SPKF algorithms give better CFO and channel estimations than the SOEKF and the EKF.
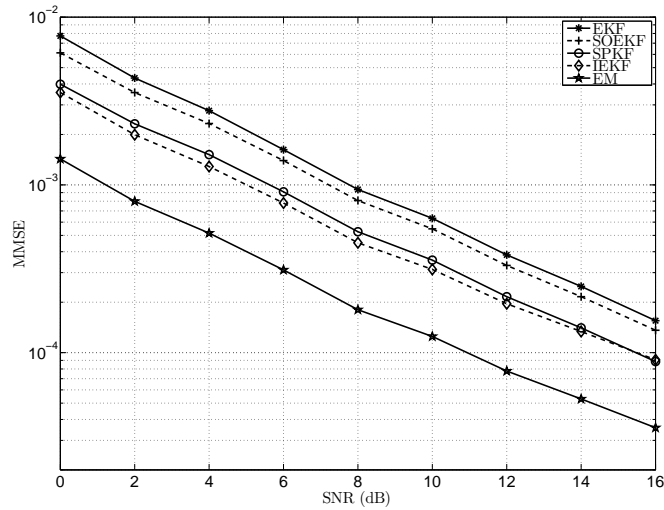
Figure 2.4: CFO estimation performance for a joint channel/CFO estimation when the noise statistics are available
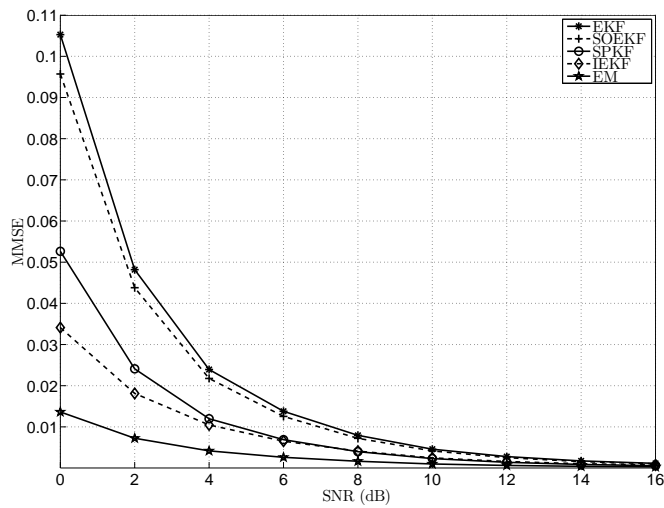
Figure 2.5: Channel estimation performance for a joint channel/CFO estimation when the noise statistics are available

Figure 2.6 shows that the IEKF converges faster than the other Kalman approaches. In addition, the SPKF seem to require less observations than the EKF
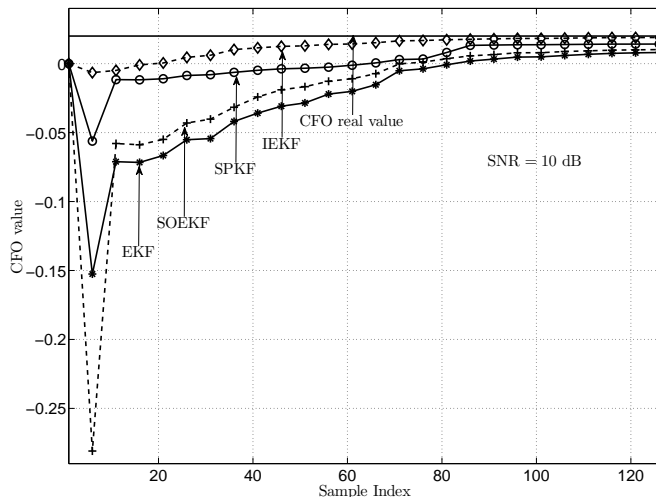
Figure 2.6: Recursive CFO estimation for a joint CFO/channel estimation using optimal filtering, when the noise statistics are available

and the SOEKF to estimate the CFOs.

Let us now look at the H_∞ based approaches. Figure 2.7 shows the robustness of the H_∞ filtering to uncertainties. For an error of 5dB over the variance, the H_∞ filtering approaches converge faster than the Kalman ones. However, the computational complexity of the H_∞ filtering approaches is higher than the SPKF. It should be noted that when using the extended H_∞ and the unscented H_∞ approaches, the choice of the noise attenuation level Ξ plays a key role. If it is set to a high value, there is no real difference between the Kalman algorithm and the H_∞ based approach, whereas no H_∞ solution may exist if Ξ is set to a small value.

Based on the above considerations, we think that among our algorithms the SPKF gives the best compromise in terms of estimation performance, computational complexity and number of parameters to be *a priori* tuned.

The grid search algorithms proposed in [Pun 04a] and [Pun 06] provide better performance in terms of MMSE. Nevertheless, the estimation error of the SPKF is small enough to guarantee bit error rates (BERs) that are similar to the ones obtained when the grid search algorithms are used, as shown in table 2.3.
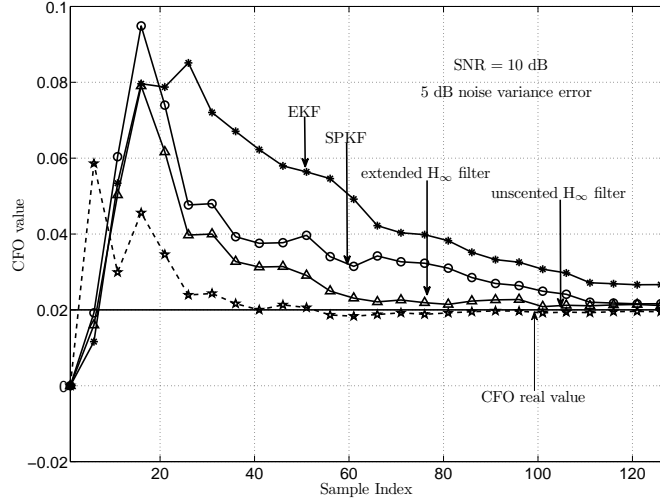
Figure 2.7: Comparison between the Kalman filtering approaches and the H_∞ filtering approaches in terms of convergence speed, when the noise statistics are not available

SNR (dB)	theoretical BER	BER (grid search)	BER (SPKF)
0	1.464×10^{-1}	1.469×10^{-1}	1.584×10^{-1}
5	6.418×10^{-2}	6.452×10^{-2}	6.681×10^{-2}
10	2.327×10^{-2}	2.361×10^{-2}	2.395×10^{-2}

Table 2.3: BER performance when a joint channel/CFO estimation is considered

2.3.4.2 Computational Complexity

One of the goals in the design of wireless communication systems is to reduce the energy consumption of the system. In current wireless communication systems, only a few Go/s are dedicated to the channel estimation and the synchronization. So, in the following let us have a look at the computational cost of the EM algorithm and the SPKF algorithm. These approaches provide similar results in terms of BER, but the EM-based algorithm have a higher computational complexity due to the exhaustive grid search over the possible range of CFOs and the iterative estimation.

Table 2.4 shows the number of arithmetic operations performed by the EM; N^{ob}

denotes the number of observations for the algorithms and it is set to $N^{ob} = K$. The computational cost of the EM approach depends on the number of $\mathfrak{J}^{em}$ iterations and on the number of $\mathfrak{b}$ tested values. The M-step is based on the inversions of U matrices of size $L_u \times L_u$. In addition, the decision test has to be done to decide which is the best value of the CFO. Table 2.5 shows the number

EM algorithm		
E-step		
additions and subtractions	$\mathfrak{J}^{em} N_{ob} U + \mathfrak{J}^{em} U(2L_u + 6)$	1.1200×10^4
multiplications and divisions	$\mathfrak{J}^{em} N_{ob} U + \mathfrak{J}^{em} U(U + 2L_u)$	1.1040×10^4
M-Step		
add./sub. for the grid search	$\mathfrak{J}^{em} \mathfrak{b} N^{ob} U L_u + \mathfrak{J}^{em} \mathfrak{b} U L_u(1 + L_u) - \mathfrak{J}^{em} \mathfrak{b} U$	6.2271×10^7
mult./div. for the grid search	$\mathfrak{J}^{em} \mathfrak{b} U N_{ob}(3U L_u + L_u)$ $+ \mathfrak{J}^{em} \mathfrak{b} U(L_u^2 + 15U + 2L_u + 1)$	8.0040×10^7
other add./sub.	$\mathfrak{J}^{em} N^{ob} U L_u + \mathfrak{J}^{em} U L_u^2$	1.1366×10^6
other mult./div.	$\mathfrak{J}^{em} N^{ob} U(3U L_u + L_u) + \mathfrak{J}^{em} U(L_u^2 + 15U + L_u)$	3.9329×10^6
Total arithmetic operations		1.4740×10^8

Table 2.4: Number of arithmetic operations performed by the EM joint channel/CFO estimator, 20001 tested CFO values and 20 iterations.

of arithmetic operations performed by the SPKF. The first step of the algorithm, corresponding to the selection of the sigma points requires the Cholesky decomposition[1] of a matrix of size $\mathcal{U} \times \mathcal{U}$. As the observation vector length is equal to 2, the measurement update also requires the inversion of a 2×2 matrix.

Table 2.6 shows the number of Giga-operations per second (Go/s) performed by the EM for different grid search precisions.

Table 2.7 shows the number of Go/s for different numbers of users in the system with a channel composed of 3 multi-paths. In addition, table 2.7 shows the number of Go/s for different number of channel multipaths with 4 users in the system.

---

[1]When using the SPKF and by considering $\mathcal{U}$ the length of the state vector, a $\mathcal{U} \times \mathcal{U}$ Cholesky decomposition is necessary to obtain the "square root" of the error covariance matrix.

2. Frequency Synchronization and Channel Equalization of OFDMA Uplink Systems

SPKF algorithm		
step 1: calculation of the sigma points		
additions and subtractions	$2N^{ob}U^2(4L_u^2 + 4L_u + 1)$	2.0070×10^5
multiplications and divisions	$2N^{ob}U^2(4L_u^2 + 4L_u + 1)$	2.0070×10^5
step 2: estimation update		
additions and subtractions	$2N^{ob}U(8U^2L_u^3 + 12U^2L_u^2 + 6U^2L_u$ $12UL_u^2 + U^2 + 12UL_u + 3U + 2L_u + 1)$	6.2290×10^6
multiplications and divisions	$N^{ob}U(16U^2L_u^3 + 24U^2L_u^2 + 12U^2L_u$ $20UL_u^2 + 2U^2 + 20UL_u + 5U + 4L_u + 2)$	6.1286×10^6
step 3: measurement update		
additions and subtractions	$N^{ob}U(44UL_u + 19U + 13)$ $+N^{ob}U(28UL_u^2 + 96L_u)$	1.8348×10^5
multiplications and divisions	$2N^{ob}U(12UL_u + 7U + 27) + 2N^{ob}$ $+2N^{ob}U(4UL_u^2 + 50L_u)$	2.9651×10^5
Total arithmetic operations		1.3239×10^7

Table 2.5: Number of arithmetic operations performed by the SPKF joint channel/CFO estimator

The computational complexity of the EM increases faster when the number of users (or the number of channel multipaths) increases. Indeed the EM-based algorithms work in blocks in an iterative way whereas the SPKF is recursive.

It is clearly seen by the results, that the computational complexity of the EM is higher than the one of the SPKF. When 4 users in the system and a channel composed of 3 multipaths are considered, the SPKF algorithm requires only 9% of the number of operations required by the EM.

The approach presented in [Pun 06] required less iterations than the one proposed in [Pun 04a]. In addition, an improvement to those iterative architectures has been proposed [Sezg 08]. Here, the authors propose to reduce the number of the iterations and the complexity of the matrix inversions. However, if only one iteration is considered using a grid search precision of 10^{-4}, the grid search architecture required 7.1378×10^7 Go/s, the value is still higher than the one presented in table 2.5. Due to the grid search, the above approaches implementation is relatively difficult in real environments;

grid search precision	♭	Go/s
10^{-1}	21	0.0066
10^{-2}	201	0.0194
10^{-3}	2001	0.1474
10^{-4}	20001	1.3239

Table 2.6: Number of Go/s performed by the EM joint channel/CFO estimator for different grid search precisions

4 users in the system			3 multi-paths		
Multipaths	Go/s(EM)	Go/s(SPKF)	Number of users	Go/s(EM)	Go/s(SPKF)
1	0.5349	0.0130	2	0.6751	0.0192
2	0.9780	0.0516	3	1.0417	0.0588
3	1.4276	0.1324	4	1.4276	0.1324
4	1.8835	0.2712	5	1.8328	0.2505
5	2.3459	0.4838	6	2.2573	0.4238
6	2.8147	0.7859	7	2.7011	0.6626
7	3.2899	1.1931	8	3.1643	0.9777
8	3.7715	1.7213	9	3.6468	1.3794
9	4.2596	2.3861	10	4.1486	1.8784
10	4.7540	3.2033	11	4.6698	2.4852
11	5.2549	4.1885	12	5.2102	3.2103

Table 2.7: Number of Go/s performed by the EM and the SPKF joint channel/CFO estimators

2.3.5   Conclusions

The architectures proposed in this section require control data to perform the estimation, but they do not need an initialization step. The robustness to uncertainties of the H_∞ filtering has been confirmed, but the selection of the noise attenuation level remains quite difficult. When the noise characteristics are available, the best estimation performance have been obtained by the IEKF among the proposed estimators. However, the computational complexity is the highest among the proposed algorithms. SPKF gives the best compromise between computational complexity and estimation performance. They have lower computational cost than the grid search methods. This advantage is crucial, because one of the goals in the design of wireless systems is to reduce the energy con-

sumption of the system. In current wireless communication systems, only a few Go/s are dedicated to the channel estimation and the synchronization. These proposed approaches are completely applicable to practical environments, unlike the EM-based methods.

In the next subsection, to reduce the amount of control data in the transmitted signal, we propose to combine the optimal filtering techniques with the so-called MMSE-SD in an iterative way.

2.4 An OFDMA Non-Pilot Aided Iterative CFO Estimator

As an alternative to this classic scheme, shown in figure 2.8 and in order to reduce the amount of control data, a non-pilot aided estimator based on an iterative architecture [Pove 11c] is proposed in this section.

In an OFDMA transmission, the OFDMA frame duration may be higher than the coherence time T_c of the channel. In this case, the CSIs need to be updated by using pilot subcarriers. In this section, we suggest using a shorter OFDMA frame so that the CSIs do not change. The subcarriers are no longer necessary to update the CSI and hence they can be removed. The data rate is increased, but the CFO may vary from one symbol to another. It should be noted that the preamble is kept in order to perform the time synchronization, to estimate the
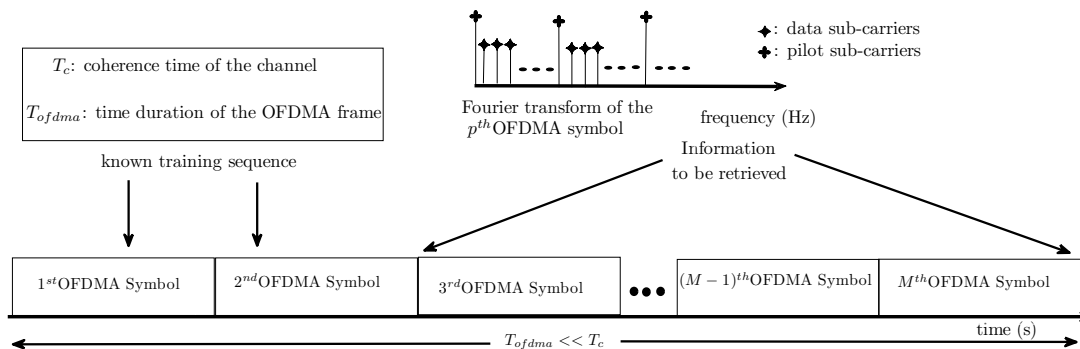
Figure 2.8: Example of an OFDMA frame composed of M OFDMA symbols with a preamble composed of two OFDMA symbols and a determined number of pilot subcarriers

CSI for the whole frame and to provide an initial estimation of the CFO. See figure 2.9.

2.4.1   Problem Formulation
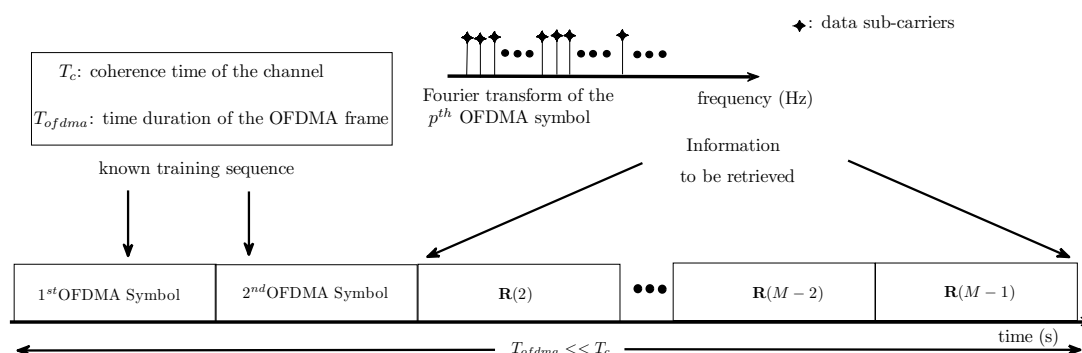
Figure 2.9:   Example of an OFDMA frame composed of M OFDMA symbols with a preamble composed of two OFDMA symbols and no pilot subcarriers, where **R** is the received OFDMA symbol

The idea of the proposed receiver is to correct the MAI and to estimate the signals sent from all users in the system by using an MMSE-SD. These estimated signals called the "MMSE-SD preambles" play the role of the preambles and are used to estimate the CFOs by means of the optimal filter. The iterative architecture is shown in figure 2.10.

The frequency synchronization in an uplink communication can be seen as a multiparameter estimation problem. A solution is to distinguish one user from the others before starting the synchronization process. After the estimation of the U "MMSE-SD preambles", each one is inserted in U optimal filtering processes, i.e. U Kalman filters or U H_∞ filters. See figure 2.11. Finally, the CFOs between the BS and each user are estimated independently, thanks to the optimal filter and an additional MAI cancellation process.
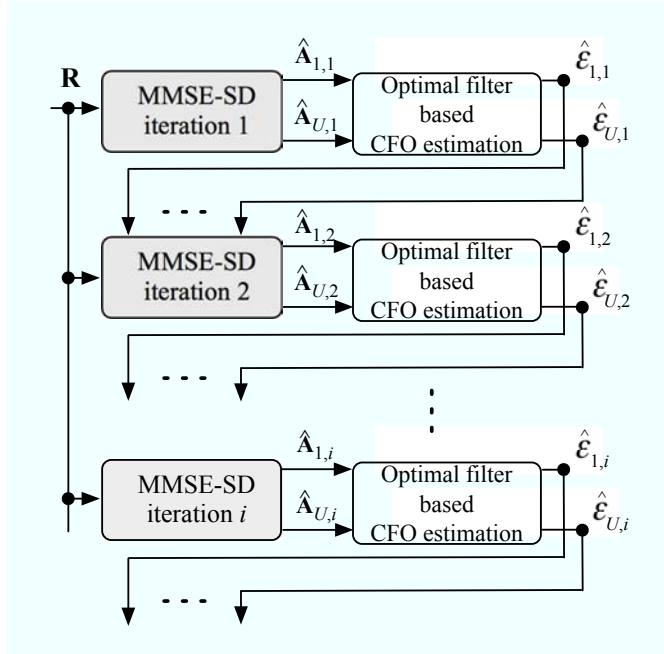
Figure 2.10: Proposed OFDMA non-pilot aided iterative receiver using optimal filtering

2.4.2 User Detection - The Minimum Mean Square Error Successive Detector (MMSE-SD)

The first step of the iterative architecture is to estimate the preambles by using the MMSE-SD. According to [Hou 08], the MMSE-SD is robust against near-far effect[1], produced by the strong MAI. These phenomena are induced by the difference that may exist between two users in terms of the propagation loss. Instead of a joint multiuser decoding, a combination between an MMSE pre-detection scheme with an ordered successive detection is proposed. The detection of the transmitted OFDMA signal components operates in two major steps:

- interference cancellation (IC): during this step, the previous "detected" OFDMA signal components are subtracted out of the received signal. Indeed, let $\hat{\mathbf{S}}_{\tilde{u},i}$ be the estimation of the signal sent by the $\tilde{u}$th user at the ith

---

[1]The near-far effect is a condition in which a strong power received signal does not allow the receiver to detect a weak power received signal.
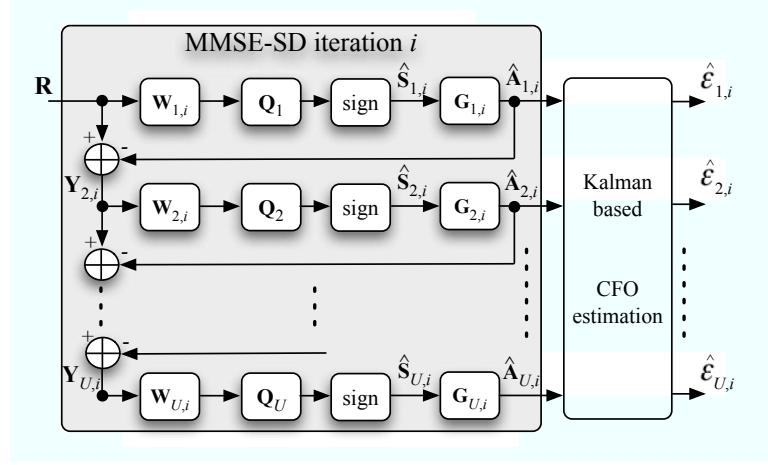
Figure 2.11: Iterative MMSE-SD using a Kalman filtering based estimator and a MAI suppression for BPSK modulation

iteration of the MMSE-SD, where $1 \leq i \leq \mathfrak{J}^{sd}$ and $\mathfrak{J}^{sd}$ denotes the maximum iteration number. The user's decoding order is denoted as $\tilde{u}$ where $\tilde{u} \in \{1, \ldots, U\}$; when $\tilde{u} = 1$, it is associated with the maximum signal to interference-plus-noise ratio[1] (SINR) among the users whereas $\tilde{u} = U$ represents the user with the lowest SINR. In addition the so-called $(\tilde{u} + 1)$th order MMSE-SD residual at the ith iteration $\mathbf{Y}_{\tilde{u}+1,i} \; \forall \tilde{u} \neq 1$ is the difference between the received signal $\mathbf{R}$ and the components transmitted by the detected users[2] (namely those corresponding to the $\tilde{u}$ highest SINRs) and $\mathbf{Y}_{1,i} = \mathbf{R} \; \forall i$. See figure 2.11.

The IC steps can be summarized as follows:

$$\begin{aligned}
\mathbf{Y}_{\tilde{u}+1,i} &= \mathbf{Y}_{\tilde{u},i} - \hat{\mathbf{G}}_{\tilde{u},i}\hat{\mathbf{S}}_{\tilde{u},i} & (2.12) \\
&= \mathbf{R} - \sum_{l=1}^{\tilde{u}} \hat{\mathbf{G}}_{l,i}\hat{\mathbf{S}}_{l,i} & (2.13)
\end{aligned}$$

$$\text{with } \hat{\mathbf{G}}_{\tilde{u},i} = \begin{cases} \sum_{\tilde{u}=1}^{U} \hat{\mathbf{E}}_{\tilde{u},i}\mathbb{H}_{\tilde{u}}\mathbf{Q}_{\tilde{u}} & \text{if } \tilde{u} = 1 \\ \hat{\mathbf{G}}_{\tilde{u}-1,i}\left(\mathbf{I}_K - \mathbf{Q}_{\tilde{u}-1}\right) & \text{if } 2 \leq \tilde{u} \leq U \end{cases} \qquad (2.14)$$

---

[1] As the BS calculates the different SINRs, the signal can be decoded in an ordered way.

[2] Given (1.21), (1.22) and (1.23), the received OFDMA symbol can be expressed as $\mathbf{R} = \sum_{u=1}^{U} \mathbf{G}_u\mathbf{S}_u + \mathbf{B}$, where $\mathbf{G}_u = \mathbf{E}_u\mathbf{F}^H\mathbf{H}_u\mathbf{Q}_u$, See chapter 1 in section 1.4.2.2.

2. Frequency Synchronization and Channel Equalization of OFDMA Uplink Systems

where $\mathbb{H}_{\tilde{u}} = \mathbf{F}^H \mathbf{H}_{\tilde{u}}$, $\mathbf{H}_{\tilde{u}}$ is the channel frequency response matrix associated to the $\tilde{u}$th user[1], $\mathbf{Q}_{\tilde{u}}$ is the CAS matrix associated to the $\tilde{u}$th user defined in (1.23), and $\hat{\mathbf{S}}_{\tilde{u},i}$ is the vector at the ith iteration that contains the estimated symbols sent by the $\tilde{u}$th user:

$$\hat{\mathbf{S}}_{\tilde{u},i} = \left[\hat{S}_{\tilde{u},i}(0), \hat{S}_{\tilde{u},i}(1), \ldots, \hat{S}_{\tilde{u},i}(k), \ldots, \hat{S}_{\tilde{u},i}(K-1) \right] \qquad (2.15)$$

$\hat{\mathbf{E}}_{\tilde{u},i} = diag \left\{ \left[1, e^{j2\pi\hat{\epsilon}_{\tilde{u},i-1}/K}, \ldots, e^{j2\pi(K-1)\hat{\epsilon}_{\tilde{u},i-1}/K} \right] \right\}$ and $\hat{\epsilon}_{\tilde{u},i}$ is the estimation of the CFO associated with the $\tilde{u}$th user at the ith iteration. A new iteration begins when all the users have been processed and when the estimation $\hat{\epsilon}_{\tilde{u},i}$, using the recursive estimator approach proposed in subsection 2.4.3, has been done.

- interference suppression (IS): this step aims at removing the interference stemming from the as-yet undecoded components. The purpose of this step is hence to filter the $\tilde{u}$th order MMSE-SD residual $\mathbf{Y}_{\tilde{u},i}$. By denoting σ_s^2 the signal power allocated on each of the subcarriers, the suppression weight matrix $\mathbf{W}_{\tilde{u},i}$ for the selected $\tilde{u}$th user at the ith iteration satisfies [Hou 08]:

$$\mathbf{W}_{\tilde{u},i} = \left(\frac{\sigma_B^2}{\sigma_s^2} \mathbf{I}_K + \mathbf{G}_{\tilde{u},i}^H \mathbf{G}_{\tilde{u},i} \right)^{-1} \mathbf{G}_{\tilde{u},i}^H \qquad (2.16)$$

Then, (2.16) is used to decode the selected user and to obtain the estimated signal sent by uth user[4].

$$\hat{S}_{\tilde{u},i}(k) = \underset{\Omega_m \in \boldsymbol{\Omega}}{\operatorname{argmin}} \| T_{\tilde{u},i}(k) - \Omega_m \|^2 \qquad (2.17)$$

$$\text{with}: \mathbf{T}_{\tilde{u},i} = \mathbf{Q}_{\tilde{u}} \mathbf{W}_{\tilde{u},i} \mathbf{R} \quad \tilde{u} = 1$$
$$\mathbf{T}_{\tilde{u},i} = \mathbf{Q}_{\tilde{u}} \mathbf{W}_{\tilde{u},i} \mathbf{Y}_{\tilde{u},i} \quad \tilde{u} > 1 \qquad (2.18)$$
$$\mathbf{T}_{\tilde{u},i} = [T_{\tilde{u},i}(0), T_{\tilde{u},i}(1), \ldots, T_{\tilde{u},i}(k), \ldots, T_{\tilde{u},i}(K-1)]$$

where $\boldsymbol{\Omega} = \{\Omega_1, \Omega_2, \ldots \Omega_m, \ldots \Omega_M\}$ is the modulation constellation. At that stage, (2.17) makes it possible to obtain the estimated signal of the $\tilde{u}$th user.

$$\hat{\mathbf{A}}_{\tilde{u},i} = \mathbb{H}_{\tilde{u}} \mathbf{Q}_{\tilde{u}} \hat{\mathbf{S}}_{\tilde{u},i} = \left[\hat{A}_{\tilde{u},i}(0), \hat{A}_{\tilde{u},i}(1) \ldots \hat{A}_{\tilde{u},i}(K-1) \right] \qquad (2.19)$$

---

[1]The matrix $\mathbb{H}_{\tilde{u}}$ is assumed to be known.
[4]For example in BPSK modulation $\hat{\mathbf{S}}_{\tilde{u},i} = \text{sign} \left(\mathbf{Q}_{\tilde{u}} \mathbf{W}_{\tilde{u},i} \mathbf{Y}_{\tilde{u},i} \right)$

In the next subsection, those estimated signals the "MMSE-SD preambles" are used to estimate the CFO of each user.

2.4.3   CFO Estimation with the MMSE-SD Preambles

In order to restore orthogonality among each user subcarrier, the synchronization error vector $\boldsymbol{\epsilon}$ defined in (2.4) has to be estimated. Here, we suggest a recursive method. However, each CFO ϵ_u is estimated independently. In each recursion, the results of these independent estimations are used together for MAI cancellation.

Let us introduce the state-space model to estimate the CFO, that is the representation of what happens during one OFDMA symbol. It is defined by the following state-space model:

State equation:

$$\epsilon_{\tilde{u},i}(n) = \epsilon_{\tilde{u},i}(n-1) + w(n) \tag{2.20}$$

Measurement equation:

$$
\begin{aligned}
\hat{R}_{\tilde{u},i}(n) &= \hat{A}_{\tilde{u},i}(n)e^{j2\pi\frac{\epsilon_{\tilde{u},i}n}{K}} + B_{\tilde{u}}(n) \\
&= f(\epsilon_{\tilde{u},i}(n)) + B_{\tilde{u}}(n)
\end{aligned}
\tag{2.21}
$$

where $\hat{R}_{\tilde{u},i}(n)$ is the estimated received signal from each user (see subsection 2.4.3.1). In addition, w and $B_{\tilde{u}}$ are white zero-mean gaussian noises with variances assumed to be σ_w^2 and $\sigma_{\tilde{u}}^2$ respectively. It should be noted that σ_w^2 is very low and can even be equal to 0. In this latter case, the CFO is assumed to be constant during one OFDMA symbol.

Let us introduce a third state-space equation that is used in the general case for H_∞ filtering to focus on a linear combination of the state-vector components. Here, as the dimension of the state vector is equal to 1, one has:

$$z_{\tilde{u},i}(n) = \mathcal{L}\epsilon_{\tilde{u},i}(n) \tag{2.22}$$

where $\mathcal{L}$ is equal to 1.

As the state-space model is non-linear due to (2.21), the study of several kinds of algorithms is proposed:

- the EKF approaches including the EKF, the SOEKF and the IEKF, presented in appendix D,

- the SPKF, including the UKF and the CDKF, presented in appendix E,

- the "extended H$_\infty$ filter" and the "unscented H$_\infty$ filter" presented in appendix F.

2.4.3.1   Multiple Access Interference Cancellation Process

To improve the estimation, an MAI cancellation strategy as in [Zhao 06] is proposed. The results from the $(n-1)$th recursion are used to estimate and eliminate different users' signals in the nth recursion.

$$\text{MAI estimation: } \hat{R}_{\tilde{u},i}^{(est)}(n) = \hat{A}_{\tilde{u},i}(n)e^{j2\pi n\hat{\epsilon}_{\tilde{u},i}(n-1)/K} \tag{2.23}$$

$$\text{MAI correction: } \hat{R}_{\tilde{u},i}(n) = R(n) - \sum_{j=1,j\neq\tilde{u}}^{U} \hat{R}_{\tilde{u},i}^{(est)}(n) \tag{2.24}$$

After some recursions, the algorithm makes its possible to estimate the value of the uth user CFO.

2.4.4   Simulation Results

In the following, a comparative study is carried out. Three kinds of tests are considered to evaluate the performance of the algorithms.

Simulation protocol: An OFDMA IEEE 802.16 WirelessMAN$^{\text{TM}}$ uplink system, which involves $U = 4$ users sharing $K = 512$ subcarriers and with a cyclic prefix set to $N_g = K/8 \geq \underset{u}{max}(L_u)$ is considered. The carrier frequency is at $f_c = 2.6\text{GHz}$ and the bandwidth is set to $W = 20\text{MHz}$. $T_{ofdma} << T_c$, where T_c is the coherence time of the channel and T_{ofdma} is the OFDMA frame duration. A transmission over a Rayleigh slow-fading frequency-selective channel composed of $L_u = 3 \; \forall u$ multipaths is supposed. QPSK is used to modulate the information bits. Then, $E_b/N_o = 10\log(\frac{\sigma_u^2}{\sigma_{\tilde{u}}^2})$ where σ_u^2 is the mean power of the received signal from the $\tilde{u}$th user.

When using H_∞ filtering: $\Xi = 10^2$, $\mathcal{V} = \sigma_{\tilde{u}}^2$ and $\mathcal{W} = \sigma_w^2$. One assumes that there is a state noise $w(n)$ with very small variance, e.g. and $\sigma_w^2 = 10^{-3}$. It is assumed that the channel estimation and a CFO pre-estimation have been performed using a preamble. The algorithm estimates the "MMSE-SD preambles" of the 4 users, and then estimates the CFOs for each OFDMA symbol so that the coherent detection can be robust against variations over all the OFDMA frame.
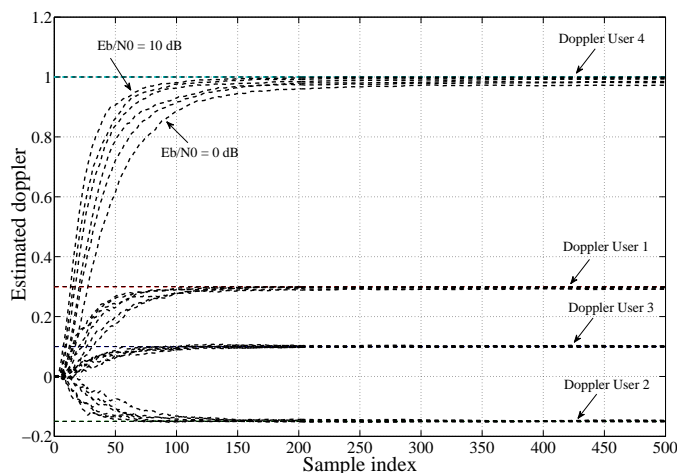
Figure 2.12: CDKF based approach for CFO estimation with a known preamble

2.4.4.1 Test 1: Recursive Estimation Using Perfectly Estimated MMSE-SD Preambles

In this first case, it is assumed that the MMSE-SD preambles have been perfectly estimated at the receiver. The CFO estimation algorithms for users with different CFO are tested. The users' CFO estimation errors are considered fixed during one OFDMA symbol. 500 montecarlo runs are performed.

Based on preliminary tests, it was noticed that the Kalman filtering approaches, "the extended H_∞ filter" and the "unscented H_∞ filter" provide very similar results. In the following, we choose the SPKF and the unscented H_∞ filter to perform the CFO estimation, in order to avoid the linearization step. Therefore, in figure 2.12, we only show the results obtained when using a CDKF. According
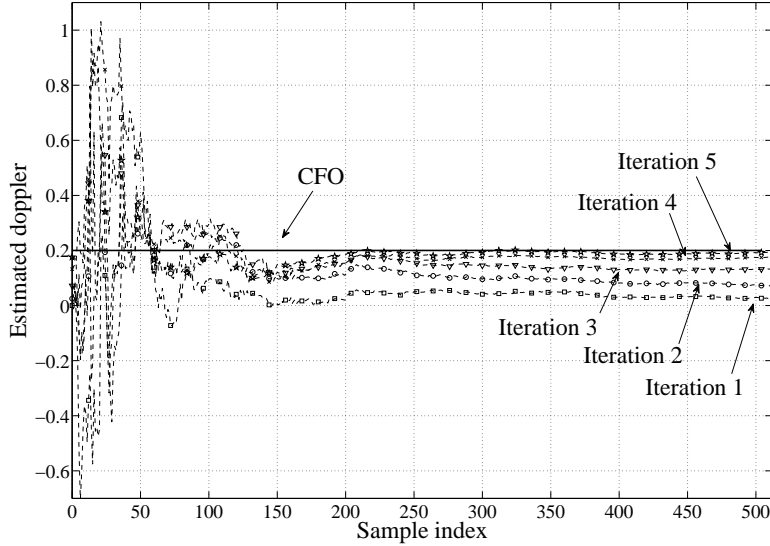
Figure 2.13: MMSE-SD combined with an UKF based approach for CFO estimation

to figure 2.12, our approach makes it possible to accurately estimate the CFO recursively. It should be noted that this is the recursive CFO estimation over only one OFDMA symbol.

2.4.4.2 Test 2: Non-Pilot Aided Estimation

In this second case, the receiver estimates the MMSE-SD preambles. The simulation results deal with the first user of the system. The users' CFO errors vary between the different OFDMA symbols (but they are considered fixed during one OFDMA symbol). They are modeled as independent zero-mean Gaussian random variables with a variance of σ_{cfo}^2. Figure 2.13 shows the results in terms of CFO estimation over one OFDMA symbol. The proposed algorithm provides an estimation of the CFO in an iterative way. As expected, the first iteration leads to poor performance, but iterating our approach especially up to 5 times leads to good performance.

In figure 2.14, the performance of our algorithm in terms of BER are shown; the estimation is done by using either the Kalman filtering with an error of 3 dB over the variance or the H_∞ filtering. In the following, we choose "the unscented H_∞
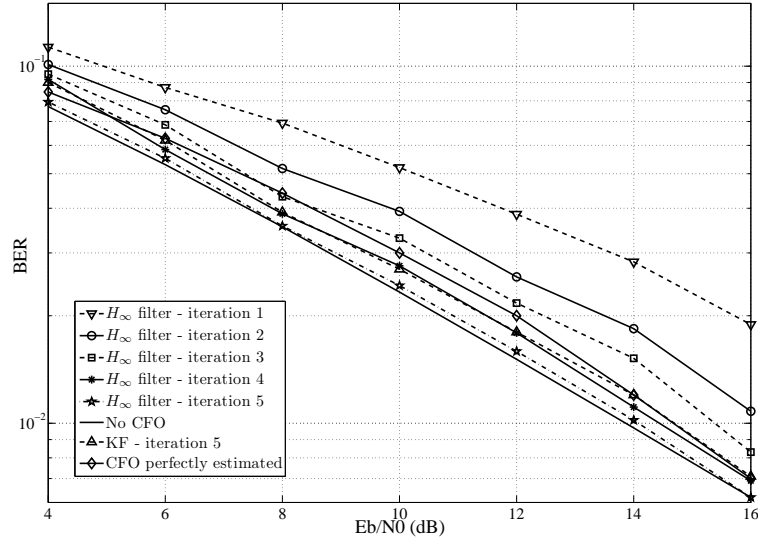
Figure 2.14: BER performance, uniformly distributed CFO, 5 iterations, when a non-pilot aided estimation is considered

filter" to perform the CFO estimation, in order to avoid the linearization step. In addition, we show the results when a single-user detector is used by considering a perfectly estimated CFOs. According to figure 2.14, the results of the proposed method are better after performing the fourth iteration. A gain of around 1 dB for a BER of 10^{-2} is obtained when using the proposed method with the "unscented H_∞ filter" at the fifth iteration in comparison with the single-user detector. In [Huan 05] and [Cao 04a], the algorithms tend to the theoretical value. However, in [Huan 05] more subchannels than users are required. In addition, in [Cao 04a] a training sequence is necessary.

In figure 2.15, the results in terms of MMSE are shown. Based on previous tests, it was seen that the results in [Mova 08] are better than the results in [Cao 04b] in terms of CFO estimation performance. So, we propose a comparative study with the multiuser interference resilient (MUI) approach [Cao 04b]. Note that the algorithm presented in [Cao 04b] needs two OFDMA symbols for the estimation. A gain of 4 dB for an MMSE of 10^{-4} is obtained between the MUI method and the proposed method at the third iteration when using a SPKF. In addition, figure 2.16 compares the SPKF and the "unscented H_∞ filter" in terms of convergence speed, for a $E_b/N_o = 10$ dB, for different errors over the noise variance
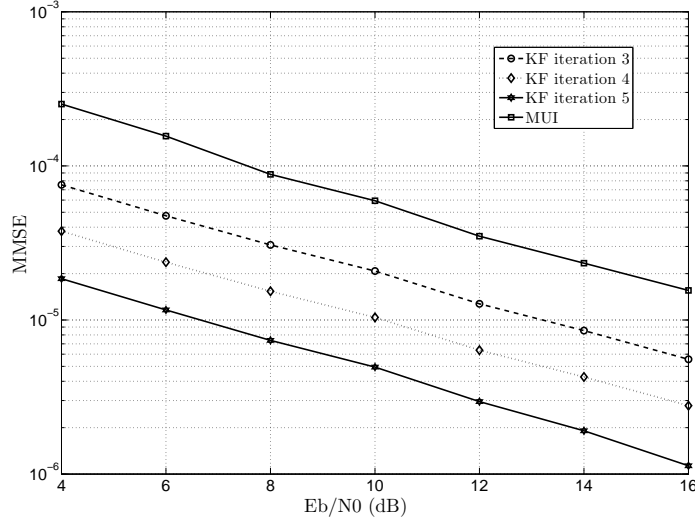
Figure 2.15: CFO estimation performance for a non-pilot aided CFO estimation

when using the SPKF and for different values of Ξ when using the H_∞ filtering. Firstly, one considers an error over the variance of 3dB and 5dB; secondly, no error over the variance is assumed. It can be seen that the convergence speed of the SPKF is affected by the variance noise error. For the lowest values of Ξ, the convergence may be slightly faster. If the value of Ξ increases, the "unscented H_∞" filter performance tend to be the same as the SPKF ones.

2.4.4.3 Test 3: Influence of the CIR Estimations

In this third case, we propose to analyze the influence of the CSIs variations over the receiver performance. The CFO estimation is performed by a SPKF, provided that the noise characteristics are known. The simulation results are focused on the first user of the system. It is assumed that the CSIs have small variations in time over the OFDMA frame. $\hat{\mathbf{h}}_u$ denotes the estimated channel impulse response for each user using the preamble and $\mathbf{h}_{\tilde{u}}$ is the value of the channel response for each user. In a first test, the following normalized random error over each channel is considered $|\hat{\mathbf{h}}_u - \mathbf{h}_{\tilde{u}}| < \mathbf{I}_{L_u \times 1} 10^{-2}$, where $\mathbf{I}_{L_u \times 1}$ is a $L_u \times 1$ vector composed of ones. In the second test $|\hat{\mathbf{h}}_u - \mathbf{h}_{\tilde{u}}| < \mathbf{I}_{L_u \times 1} 10^{-1}$. The results obtained at the fifth iteration for the different BER with a different error over the channels are shown

in figure 2.17. One can notice that the performance of the architecture are not really affected by small variations on the channel.
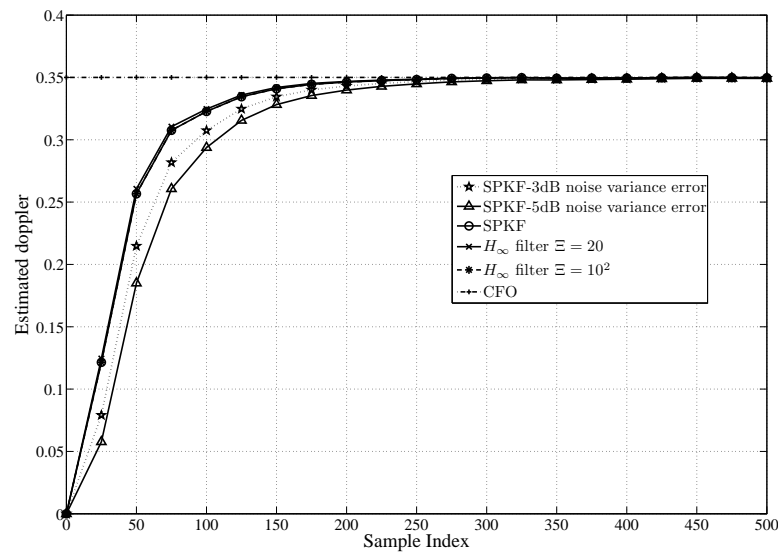
(a)
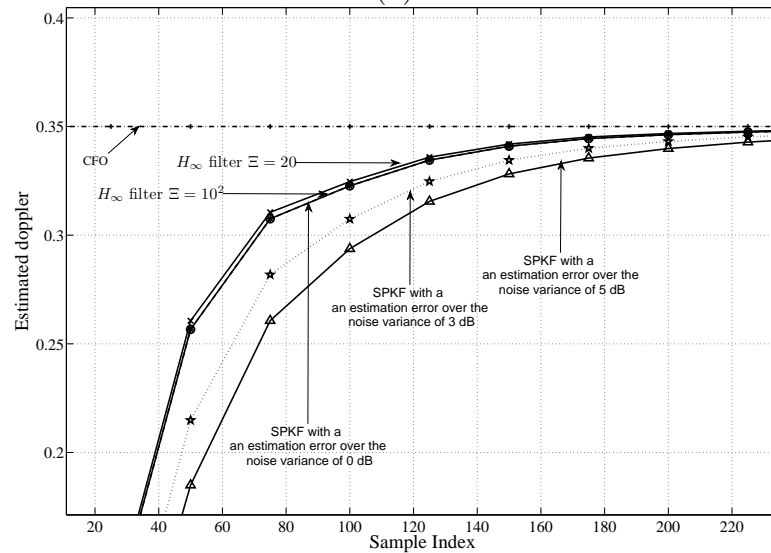
(b)

Figure 2.16: Comparison between the SPKF and the "unscented H$_\infty$ filter" in terms of convergence speed
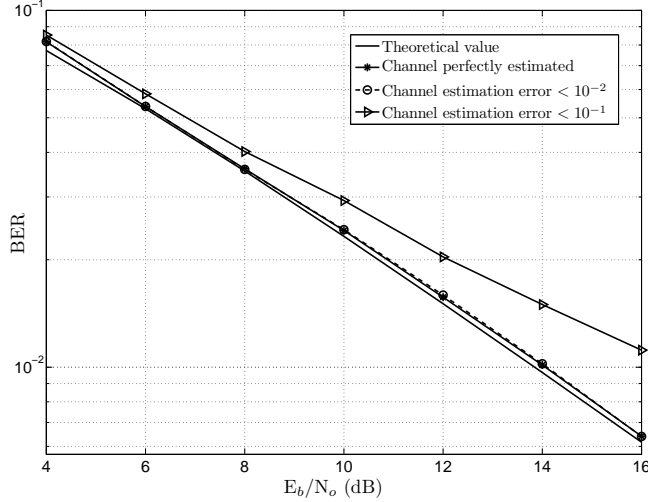
Figure 2.17: BER performance when the channel is estimated and a non-pilot aided CFO estimation is considered

2.4.4.4 Computational Complexity

Now let us look at the complexity of the frequency synchronization scheme. Concerning with the MMSE-SD step, at each iteration and for each user, the MMSE-SD is based on the inversion of a matrix of size $K \times K$ in order to calculate the suppression weight matrix $\mathbf{W}_{\tilde{u},i}$. This matrix inversion requires $\mathcal{O}(K^3)$ operations. Thus, the overall complexity of the MMSE-SD step is $\mathcal{O}(\mathfrak{I}^{sd}UK^3)$.

Then, concerning the estimation step, as the dimension of the state vector is equal to 1, the optimal filtering step requires the computation of $\mathcal{O}(1)$ operations for each user and for each iteration. Thus, the overall complexity of the estimation step is $\mathcal{O}(\mathfrak{I}^{sd}U)$.

Therefore, we can conclude that the overall complexity of the proposed iterative architecture is $\mathcal{O}(\mathfrak{I}^{sd}UK^3)$.

2.4.5 Conclusions

The non-pilot aided MAI suppression scheme for an OFDMA uplink transmission followed by the CFO estimation algorithm based on optimal filtering can estimate

and detect each user's CFO and frame respectively, with no need of pilot sub-carriers. This leads to a maximum transmission data rate.

In addition, simulation results confirm that the proposed scheme can effectively suppress the MAI caused by a relatively large CFO, sufficiently robust to CFO variations. The decoding of OFDMA signal is an ordered serial processing that combines interference suppression and interference cancellation techniques. The iterative decoding applies simple hard interference cancellation techniques, resulting in moderate complexity. The CFO estimation performance of the different approaches give quite similar results. On the one hand, one advantage of the SPKF is that it does not need the calculations of Jacobians or Hessians. In those cases, the computational complexity is lower. On the other hand, when using the H_∞ filter, no information about the noise statistics is required, but the selection of the noise attenuation level may be a problem.

2.5 An OFDMA Robust CFO Estimator

The above algorithms provide accurate estimation as long as the received signal is only disturbed by the propagation channel and an AWGN, whereas significant degradations are expected in the presence of an NBI [Mare 06].

When CR systems are used, the PU has to be detected. When dealing with multi-carrier transmissions and if the cognitive devices have no *a priori* information about the PU signal, energy detection has been suggested as the spectrum sensing technique [Ferr 10], [Quan 08], [Cabr 04]. Nevertheless, when an energy detector is used, deep PU fading must be counteracted to guarantee the PU detection [Cabr 04]. Otherwise, the PU signal may be disturbed by an undesirable NBI caused by the CR that shares the same frequency band. This may lead to an inaccurate estimation of the CFO and hence increases the BER. Therefore, NBI has to be detected and taken into account to deduce the CFO.

The NBI detection has been widely studied [Broe 03], [Li 07]. In particular, the approach proposed in [Li 07] consists of a repetitive pilot block in the time domain to detect an NBI localized in time. Hence, this method cannot be used in the presence of CFO. Since the two duplicated parts remain identical after passing through the channel, their subtraction at the receiver provides the contribution

of the noise-plus-interference, which is then easily detected.

To our knowledge, the CFO estimation in presence of an NBI has not been widely addressed. In [More 08], Morelli *et al.* propose a novel scheme that jointly estimates the CFO and the interference power on each subcarrier. They take advantage of an IFFT property to estimate the CFO, by transmitting pilot symbols over some specific subcarriers while setting the others to zero. By performing the IFFT step, a block composed of several identical parts is obtained and used to estimate the CFO. However to perform the frequency error estimation, an exhaustive grid search is considered over the possible range of the CFO, leading to a high computational cost. In addition, the CFO estimation is very sensitive to the number of subcarriers disturbed by the NBI.

This section shows how to jointly estimate the PU-CFOs and to detect the cognitive radio-NBI (CR-NBI) in an OFDMA PU-system, damaged by a CR-NBI localized in time [Pove 11d], [Pove 11b]. The approach is again based on the SPKF, with an additional step using the innovation energy to detect a variation of the measurement noise covariance matrix [Foki 09], [Bian 05]. Knowing the innovation distribution, two algorithms are proposed to detect the CR-NBI. The first one is based on a binary hypothesis test (BHT), whereas the second consists in comparing the derivate of a cumulative sum (CUSUM) to a threshold. In addition, an alternative way to use these tests is proposed.

2.5.1   System Description

First, let us consider a multicarrier CR system network with an available bandwidth W^{cr} divided among K^{cr} subcarriers. In addition, the uplink PU-OFDMA system consists of a single BS and U simultaneously independent users. Then, the available bandwidth $W^{pu} = \alpha W^{cr}$ of the PU-OFDMA system is divided among $K^{pu} \leq K^{cr}$ subcarriers, with $0 < \alpha < \frac{K^{pu}}{K^{cr}} \leq 1$. The PU and CR bandwidths are shown in figure 2.18.

In the following, let us associate the subscript u to the uth user in the PU-OFDMA system, with $u \in \{1, \ldots, U\}$. Let $S_u^{pu}(m^{pu}, k^{pu})$ be the emitted PU-symbol with a time duration T^{pu} at the k^{pu}th subcarrier associated to the m^{pu}th PU-OFDMA symbol, where M^{pu} is the number of emitted PU-OFDMA symbols.
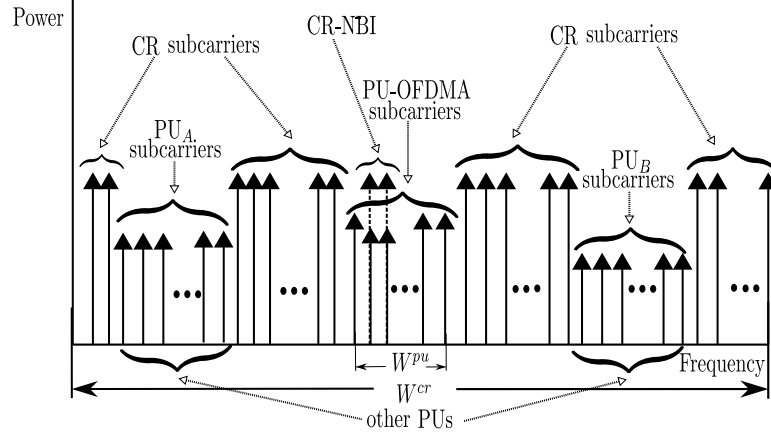
Figure 2.18: PU and CR system spectrum, where PU_A and PU_B denote the frequency bands used by other PUs

Each PU-OFDMA symbol is composed of K^{pu} PU-symbols and has a time duration[1] T_{ofdma}^{pu}. See figure 2.19. In addition, $S_{u,k^{pu}}^{pu}(m^{pu}) = 0$ if the k^{pu}th subcarrier is not assigned to the uth user.

Remark: All the subcarriers are assumed to be used. For this reason, the number of samples in one OFDMA symbol corresponds to the number of subcarriers.

The PU-channel impulse response is defined as follows:

$$\mathbf{h}_u^{pu} = [h_u^{pu}(0), h_u^{pu}(1), \ldots, h_u^{pu}(l^{pu}), \ldots, h_u^{pu}(L_u^{pu}-1)] \tag{2.25}$$

where L_u^{pu} is the length of the maximum channel delay spread.

To help the reader, the PU system parameters are summarized in table 2.8.

At the receiver, due to the propagation conditions, time offset and CFO are induced in the signal. The nth sample of the mth PU-OFDMA received symbol after time synchronization and cyclic prefix removal can be written as follows (See chapter 1 in section 1.4.2.2):

$$R_u(m^{pu}, n) = e^{j2\pi \frac{\epsilon_u n}{K^{pu}}} \sum_{k^{pu}=0}^{K^{pu}-1} S_u^{pu}(m^{pu}, k^{pu}) H_u^{pu}(k^{pu}) e^{j2\pi \frac{k^{pu} n}{K^{pu}}} \tag{2.26}$$

---

[1]It should be noted that T_{ofdma}^{pu} is the time duration of one PU-OFDMA symbol and is not the time duration of one PU-OFDMA frame.

2. Frequency Synchronization and Channel Equalization of OFDMA Uplink Systems

Description	Parameter
Bandwidth	W^{pu}
Symbol time	$T^{pu} = \frac{1}{W^{pu}}$
Number of subcarriers	K^{pu}
Number of emitted OFDMA symbols	M^{pu}
Subcarrier index	$k^{pu} \in \{0, \dots K^{pu} - 1\}$
OFDMA emitted symbol index	$m^{pu} \in \{0, \dots M^{pu} - 1\}$
Emitted symbol at the k^{pu}th subcarrier associated to the m^{pu}th PU-OFDMA symbol	$S^{pu}_{u,k^{pu}}(m^{pu})$
OFDMA symbol time	$T^{pu}_{ofdma} = K^{pu}T^{pu}$
Channel delay spread index	$l^{pu}_u \in \{0, \dots, L^{pu}_u - 1\}$
l^{pu}th coefficient of the channel impulse response	$h^{pu}_{u,l^{pu}}$
Maximum channel delay spread length	L^{pu}_u
Channel frequency response	$H^{pu}_{u,k^{pu}}$

Table 2.8: PU system parameters for the uth user

where $n \in \{0, 1, \dots, K^{pu} - 1\}$, ϵ_u is the normalized PU-CFO and $H^{pu}_u(k^{pu}) = \sum_{l^{pu}=0}^{L^{pu}_u-1} h^{pu}_u(l^{pu}) e^{-j2\pi \frac{l^{pu} k^{pu}}{K^{pu}}}$ is the channel frequency response associated to the k^{pu}th subcarrier.

The normalized PU-CFOs row vector $\boldsymbol{\epsilon}$ is defined in (2.4). Let us now define the row vector that contains the PU-channel impulse responses of each user, respectively:

$$\mathbf{h}^{pu} = [\mathbf{h}^{pu}_1, \mathbf{h}^{pu}_2, \dots, \mathbf{h}^{pu}_u, \dots, \mathbf{h}^{pu}_U] \tag{2.27}$$

Concerning the CR-signal, the analog baseband signal emitted $I(t)$ by the CR-antenna, without cyclic prefix, at time t is given by:

$$I(t) = \sum_{k^{cr}=0}^{K^{cr}-1} S^{cr}(m^{cr}, k^{cr}) e^{j2\pi f^{cr}_k (t - m^{cr} T^{cr}_{ofdm})} \tag{2.28}$$

where $S^{cr}_{k^{cr}}(m^{cr})$ is the emitted CR-symbol with a time duration T^{cr} at the k^{cr}th subcarrier associated to the m^{cr}th CR-OFDM symbol, where M^{cr} is the number of emitted CR-OFDM symbols. Moreover, $S^{cr}_{k^{cr}}(m^{cr}) = 0$ if the spectrum sensing decides that the k^{cr}th subcarrier is busy and $m^{cr} T^{cr}_{ofdm} \leq t < (m^{cr} + 1) T^{cr}_{ofdm}$. T^{cr}_{ofdm} is the CR-OFDM symbol time and f^{cr}_k is the baseband frequency of the k^{cr}th subcarrier.

At the PU-BS antenna, the CR-received signal after the convolution with the

Description	Parameter
Bandwidth	W^{cr}
Symbol time	$T^{cr} = \frac{1}{W^{cr}}$
Number of subcarriers	K^{cr}
Number of emitted OFDM symbols	M^{cr}
Subcarrier index	$k^{cr} \in \{0, \dots K^{cr} - 1\}$
OFDM emitted symbol index	$m^{cr} \in \{0, \dots M^{cr} - 1\}$
Emitted symbol at the k^{cr}th subcarrier associated to the m^{cr}th CR-OFDM symbol	$S^{cr}_{k^{cr}}(m^{cr})$
OFDM symbol time	$T^{cr}_{ofdm} = K^{cr} T^{cr}$
Baseband frequency of the subcarrier	$f^{cr}_k = \frac{k}{T^{cr}_{ofdm}} = \frac{k}{K^{cr} T^{cr}}$
Channel delay spread index	$l^{cr} \in \{0, \dots, L^{cr} - 1\}$
l^{cr}th coefficient of the channel impulse response	$h^{cr}_{l^{cr}}$
Maximum channel delay spread length	L^{cr}
Channel frequency response	$H^{cr}_{k^{cr}}$

Table 2.9: CR system parameters

Description	Parameter
Bandwidth	$W^{cr} = W^{pu}/\alpha$
Symbol time	$T^{cr} = \alpha T^{pu}$
OFDM symbol time	$T^{cr}_{ofdm} = \gamma T^{pu}_{ofdma} = \alpha(K^{cr}/K^{pu}) T^{pu}_{ofdma}$

Table 2.10: Relations between PU and CR system parameters

channel can be expressed as:

$$V(t) = \sum_{l^{cr}=0}^{L^{cr}-1} h^{cr}(l^{cr}) \sum_{k^{cr}=0}^{K^{cr}-1} S^{cr}(m^{cr}, k^{cr}) e^{j2\pi f^{cr}_k(t - m^{cr} T^{cr}_{ofdm} - l^{cr} T^{pu})} \qquad (2.29)$$

where $h^{cr}_{l^{cr}}$ are the coefficients of the CR-channel impulse response, $l^{cr} \in \{0, 1, \dots, L^{cr} - 1\}$ and L^{cr} is the length of the maximum channel delay spread.

Once again, to help the reader, the CR system parameters are summarized in table 2.9. In addition, table 2.10 shows the relations between the PU and the CR-system parameters.

The received signal is sampled at the sampling frequency:

$$f_s = \frac{1}{T^{pu}} \qquad (2.30)$$

Then, using (2.29), (2.30) and tables 2.8-2.10, the unknown downsampled CR-NBI[1] produced by a fault of spectrum sensing detection can be expressed as follows:

$$
\begin{aligned}
V(m^{cr}, n) = Z(m^{cr}T^{cr}_{ofdm} + \frac{n}{f_s}) &= \sum_{l^{cr}=0}^{L^{cr}-1} h^{cr}(l^{cr}) \sum_{k^{cr}=0}^{K^{cr}-1} S^{cr}(m^{cr}, k^{cr}) e^{j2\pi f_k^{cr}(\frac{n}{f_s} - l^{cr}T^{pu})} \\
&= \sum_{k^{cr}=0}^{K^{cr}-1} S^{cr}(m^{cr}, k^{cr}) \sum_{l^{cr}=0}^{L^{cr}-1} h^{cr}(l^{cr}) e^{-j2\pi \frac{k^{cr}l^{cr}T^{pu}}{K^{cr}T^{cr}}} e^{j2\pi \frac{k^{cr}nT^{pu}}{K^{cr}T^{cr}}} \\
&= \sum_{k^{cr}=0}^{K^{cr}-1} S^{cr}(m^{cr}, k^{cr}) H^{cr}_{k^{cr}} e^{j2\pi \frac{k^{cr}n}{\alpha K^{cr}}}
\end{aligned}
$$

(2.31)

where $H^{cr}(k^{cr}) = \sum_{l^{cr}=0}^{L^{cr}-1} h^{cr}(l^{cr}) e^{-j2\pi \frac{k^{cr}l^{cr}}{\alpha K^{cr}}}$ represents the unknown CR-channel frequency response associated to the k^{cr}th subcarrier.

Thus, the PU-OFDMA received signal at the BS satisfies:

$$
R(m^{pu}, n) = \begin{cases} f(m^{pu}, n, \boldsymbol{\epsilon}, \mathbf{h}^{pu}) + V(m^{cr}, n) + B(m^{pu}, n) & \text{if } n_1 \leq n \leq n_2 \\ f(m^{pu}, n, \boldsymbol{\epsilon}, \mathbf{h}^{pu}) + B(m^{pu}, n) & \text{otherwise} \end{cases}
$$

(2.32)

where $f(m^{pu}, n, \epsilon_u, \mathbf{h}^{pu}_u) = \sum_{u=1}^{U} R_u(m^{pu}, n)$ and $B(m^{pu}, n)$ is a zero-mean complex AWGN with variance σ_B^2. In addition, $n_1 \in \{0, 1, \ldots, K^{pu}(1-\gamma)\}$ is the first sample of the CR-NBI and $n_2 = n_1 + \gamma K^{pu} - 1$ is the last sample of the CR-NBI, with $0 \leq \gamma \leq 1$. The time-domain representation of the signals is shown in figure 2.19. To have a clearer idea, a time-frequency domain representation of the received signal at the BS is shown in figure 2.20.

2.5.2 Joint Disturbance Detection and CFO Estimation

Now, we suggest jointly detecting the CR-NBI and estimating both the PU-CFOs and channels. A preamble of one OFDMA symbol is used for the channel/CFOs estimation. It is assumed that the system is synchronized in time and that the PU-channels and the PU-CFOs do not vary over the OFDMA symbols of the OFDMA frame.

---

[1]CRs may likely use wide bands. However, due to the fault of spectrum sensing, a CR-NBI is produced over some subcarriers allocated to the PU.
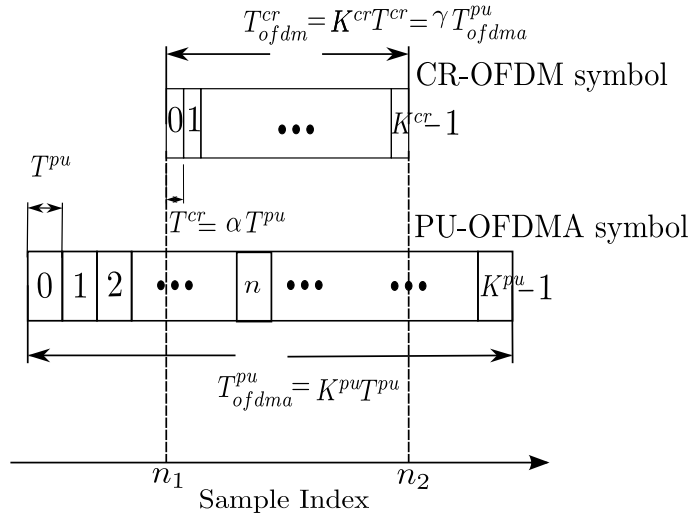
Figure 2.19: Time representation of the PU and CR-NBI signals
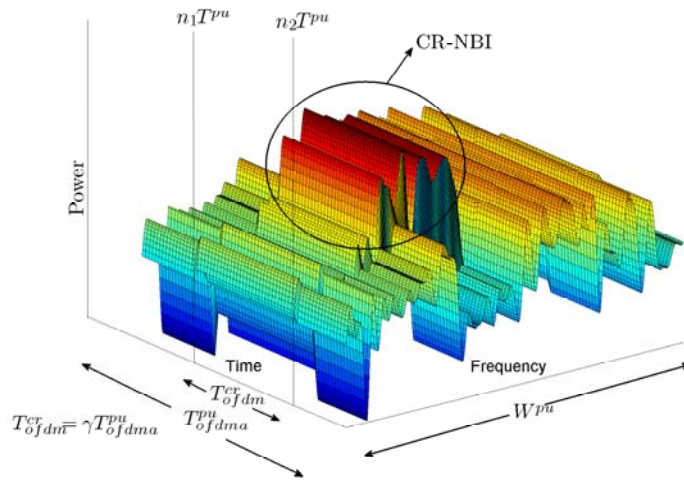
Figure 2.20: Time-frequency representation of the m^{pu}th PU-OFDMA received symbol at the BS

2. Frequency Synchronization and Channel Equalization of OFDMA Uplink Systems

First of all, let us define the following state vector:

$$\mathbf{x}(n) = \left[\begin{array}{ccc} \boldsymbol{\epsilon}(n) & Re\left\{\mathbf{h}^{pu}(n)\right\} & Im\left\{\mathbf{h}^{pu}(n)\right\} \end{array} \right]^T \tag{2.33}$$

that satisfies the following state equation:

$$\mathbf{x}(n) = \mathbf{x}(n-1) \quad \forall n \tag{2.34}$$

Secondly, let $\mathbf{Y}(n)$ be the observation column vector that stores the real and the imaginary parts of the PU-OFDMA received signal $R(m^{pu}, n)$:

$$\mathbf{Y}(n) = \begin{cases} \mathbf{C}(n, \mathbf{x}(n)) + \mathbf{V}(n) + \boldsymbol{\mathcal{B}}(n) & \text{if } n_1 \leq n \leq n_2 \\ \mathbf{C}(n, \mathbf{x}(n)) + \boldsymbol{\mathcal{B}}(n) & \text{otherwise} \end{cases} \tag{2.35}$$

where

$$\mathbf{C}(n, \mathbf{x}(n)) = \left[Re\left\{f(n, \epsilon, \mathbf{h}^{pu})\right\} Im\left\{f(n, \epsilon, \mathbf{h}^{pu})\right\} \right]^T,$$

$\boldsymbol{\mathcal{B}}(n) = \left[Re\left\{B(n)\right\} Im\left\{B(n)\right\} \right]^T$ is a 2×1 white Gaussian noise vector with covariance matrix $(\sigma_B^2/2)\mathbf{I}_2$ and $\mathbf{V}(n) = \left[Re\left\{V(n)\right\} Im\left\{V(n)\right\} \right]^T$ is the 2×1 zero-mean Gaussian CR-NBI vector with covariance matrix $(\sigma_V^2/2)\mathbf{I}_2$. The CR-NBI signal can be considered as a zero-mean Gaussian vector due to the large number of subcarriers K^{cr} [Huan 10b].

The SPKF provide "accurate" estimations as long as the received signal is only disturbed by the AWGN [Pove 10], whereas significant degradations are expected in the presence of the CR-NBI. To maintain the estimation performance, it is proposed to jointly detect the CR-NBI and estimate the PU-CFOs.

The approach operates for the nth sample in three steps:

1. estimating the state vector $\hat{\mathbf{x}}(n|n)$ by means of SPKF from the observations $\{\mathbf{Y}(0), \mathbf{Y}(1), \ldots, \mathbf{Y}(K^{pu}-1)\}$

2. calculating the innovation energy $||\tilde{\mathbf{Y}}(n)||^2$ where $\tilde{\mathbf{Y}}(n) = \mathbf{Y}(n) - \hat{\mathbf{Y}}(n)$, $\hat{\mathbf{Y}}(n) = \left[Re\left\{\hat{R}(m^{pu}, n)\right\} Im\left\{\hat{R}(m^{pu}, n)\right\} \right]^T = \mathbf{C}(n, \hat{\mathbf{x}}(n|n))$ is the estimation of $\mathbf{Y}(n)$,

3. testing whether there is CR-NBI or not by using the innovation energy. Indeed, $||\tilde{\mathbf{Y}}(n)||^2$ increases much when there is CR-NBI. See figure 2.21. This gap is due to the received signal variance that jumps from σ_B^2 to $\sigma_B^2 + \sigma_V^2$.

In the following, let us define the SNR expressed in dB as SNR= $10 \log(\frac{\sigma_u^2}{\sigma_B^2})$, where $\mathbb{E}\{|R(m^{pu}, n)|^2\} = \sigma_u^2$ is the mean power of the received signal from the uth user. In addition, we define the signal-to-interference ratio (SIR) expressed in dB as SIR = $10 \log(\frac{\sigma_u^2}{\sigma_V^2})$.

Remark: If the CR-NBI is assumed to appear at the nth sample, the estimated state vector at time $n - 1$ and its covariance matrix are kept stored: $\hat{\mathbf{x}}^{nu} = \hat{\mathbf{x}}(n - 1|n - 1)$ and $\mathbf{P}^{nu} = \mathbf{P}(n - 1|n - 1)$. They will be used as a new starting point for the CFO and channel estimation once the CR-NBI is considered to have disappeared. During the CR-NBI perturbation, SPKF provides an estimation of the state vector that is not reliable, but useful to detect the presence of the CR-NBI.

In the next subsections, two tests to detect the CR-NBI are presented.
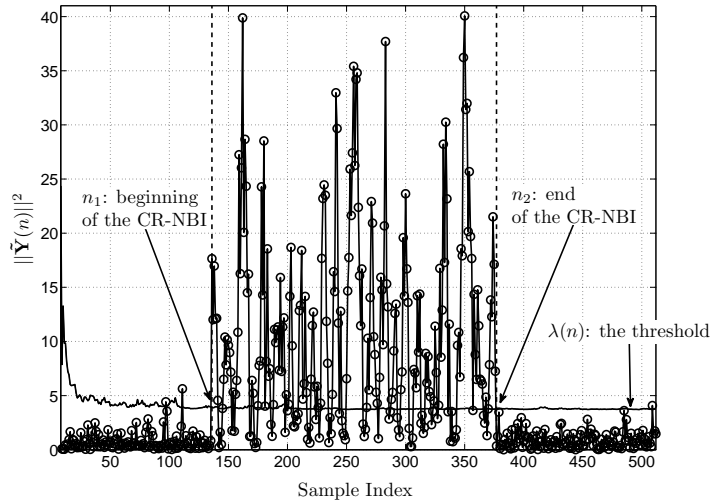
Figure 2.21: Time representation of the innovation energy

2. Frequency Synchronization and Channel Equalization of OFDMA Uplink Systems

2.5.2.1 Combining SPKF and Binary Hypothesis Test (SPKF-BHT)

To decide whether there is CR-NBI in the OFDMA symbol or not, the following binary hypothesis is tested:

$$\begin{cases} \mathcal{H}_0 : \mathbf{C}(n, \mathbf{x}(n)) + \mathbf{V}(n) + \boldsymbol{\mathcal{B}}(n) \\ \mathcal{H}_1 : \mathbf{C}(n, \mathbf{x}(n)) + \boldsymbol{\mathcal{B}}(n) \end{cases} \tag{2.36}$$

The complex residual $\tilde{R}(m^{pu}, n)$ is a zero-mean Gaussian process with variance $tr\left\{\mathbf{P}^{\mathbf{YY}}(n)\right\}$ where $\mathbf{P}^{\mathbf{YY}}(n)$ denotes the innovation covariance matrix obtained by the SPKF at the nth sample. Then, the probability of false alarm can be defined as:

$$\begin{aligned} P_{fa} &= P(|\tilde{R}(n)|^2 > \lambda(n)|\mathcal{H}_1) = P(||\tilde{\mathbf{Y}}(n)||^2 > \lambda(n)|\mathcal{H}_1) \\ &= 2P(||\tilde{\mathbf{Y}}(n)|| > \sqrt{\lambda(n)}|\mathcal{H}_1) \\ &= 2(1 - P(||\tilde{\mathbf{Y}}(n)|| < \sqrt{\lambda(n)}|\mathcal{H}_1)) \\ &= 2(1 - cdf(\sqrt{\lambda(n)})) \end{aligned} \tag{2.37}$$

where $\lambda(n)$ is a threshold at the nth sample set by the practitioner and $cdf(.)$ is the cumulative density function (CDF) of (.).
Using $||\tilde{\mathbf{Y}}(n)||$ the properties and the CDF of the Rayleigh distribution[1], one has:

$$\lambda(n) = tr\left\{\mathbf{P}^{\mathbf{YY}}(n)\right\}ln(\frac{2}{P_{fa}}) \tag{2.38}$$

If $||\tilde{\mathbf{Y}}(n)||^2 \leq \lambda(n)$, no CR-NBI is assumed to be present. When $||\tilde{\mathbf{Y}}(n)||^2 > \lambda(n)$, the CR-NBI is supposed to be at the nth sample. The CR-NBI detection and the PU estimation algorithm is summarized in figure 2.22.

2.5.2.2 Combining SPKF and CUSUM Test (SPKF-CT)

As an alternative to the BHT, a change detection algorithm known as the CUSUM test [Bass 93] is also proposed to be combined with the SPKF. The CUSUM test is an accumulative sum of a data sequence. It aims at detecting abrupt changes in

---

[1]$\tilde{R}(n)$ is Gaussian distributed, so $||\tilde{\mathbf{Y}}(n)|| = \sqrt{Re\{\tilde{R}(n)\}^2 + Im\{\tilde{R}(n)\}^2}$ is Rayleigh distributed. Then $cdf(\sqrt{\lambda(n)}) = 1 - e^{-\frac{\lambda(n)}{tr\{\mathbf{P}^{\mathbf{YY}}(n)\}}}$.
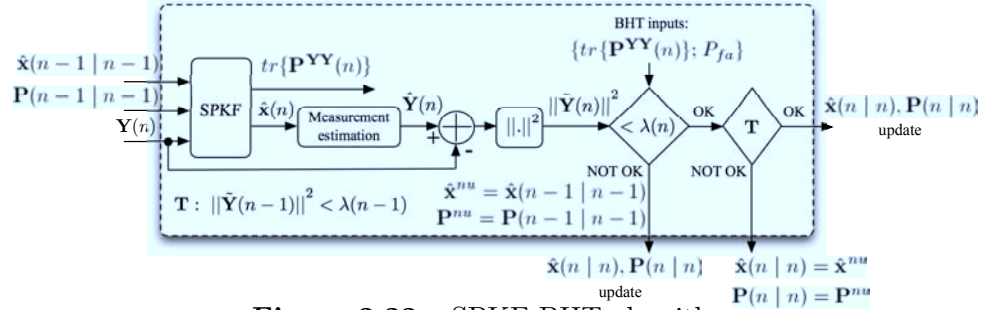
Figure 2.22: SPKF-BHT algorithm

the mean of the sequence. When using the CUSUM, if the mean increases much, the cumulative sum also increases. It has been used in various applications such as information sciences [Huan 11] and biomedicine [Yang 10].

To decide wheter the CR-NBI is present or not, we now suggest using the upper control limit of the CUSUM test defined as follows:

$$
\begin{aligned}
C^+(n) &= max(0, C^+(n-1)) + ||\tilde{\mathbf{Y}}(n)||^2 - tr\left\{\mathbf{P}_{\tilde{\mathbf{Y}}\tilde{\mathbf{Y}}}(n)\right\} \\
&= max(0, C^+(n-1)) + \tilde{\mathbf{Y}}^H(n)\tilde{\mathbf{Y}}(n) - \mathbb{E}\{\tilde{\mathbf{Y}}^H(n)\tilde{\mathbf{Y}}(n)\}
\end{aligned}
\tag{2.39}
$$

Given (2.39) and fixing a threshold, the CUSUM test makes it possible to detect when the CR-NBI begins, but does not give information when it ends. See figure 2.23.

Thus, it is proposed to look at the slope of the curve $C^+(n)$:

$$
\frac{\delta(C^+(n))}{\delta n} = C^+(n) - C^+(n-1)
\tag{2.40}
$$

Two cases can be considered.

1/ Let us assume that $C^+(n-1) > 0$; if the PU-OFDMA symbol is disturbed by the CR-NBI, one has:

$$
tr\left\{\mathbf{P^{YY}}(n)\right\} << ||\tilde{\mathbf{Y}}(n)||^2
\tag{2.41}
$$

Given (2.39) and (2.40), this leads to:

$$
\frac{\delta(C^+(n))}{\delta n} \approx ||\tilde{\mathbf{Y}}(n)||^2
\tag{2.42}
$$

Otherwise, if the PU-OFDMA is not disturbed by the CR-NBI:

$$
tr\left\{\mathbf{P^{YY}}(n)\right\} \approx ||\tilde{\mathbf{Y}}(n)||^2
\tag{2.43}
$$

89

hence one has:

$$\frac{\delta(C^+(n))}{\delta n} = ||\tilde{\mathbf{Y}}(n)||^2 - tr\left\{\mathbf{P^{YY}}(n)\right\} \approx 0 \tag{2.44}$$

2/ Let us now assume that $C^+(n-1) \leq 0$. Then if the PU-OFMDA symbol is disturbed by the CR-NBI and given (2.39), (2.40) and (2.41) one has:

$$\frac{\delta(C^+(n))}{\delta n} = ||\tilde{\mathbf{Y}}(n)||^2 - C^+(n-1) > ||\tilde{\mathbf{Y}}(n)||^2 \tag{2.45}$$

Otherwise if there is no CR-NBI distortion, given (2.39), (2.40) and (2.43) one has:

$$\begin{aligned}\frac{\delta(C^+(n))}{\delta n} &= ||\tilde{\mathbf{Y}}(n)||^2 - tr\left\{\mathbf{P^{YY}}(n)\right\} + C^+(n-1) \\ &\approx C^+(n-1)\end{aligned} \tag{2.46}$$

Therefore, one has to compare $\frac{\delta(C^+(n))}{\delta n}$ to a threshold in order to detect the end of the CR-NBI in the PU-OFDMA symbol. The CR-NBI is assumed to be present provided that $\frac{\delta(C^+(n))}{\delta n}$ is higher than the threshold.

Concerning the choice of the threshold, we suggest the one defined in (2.38).
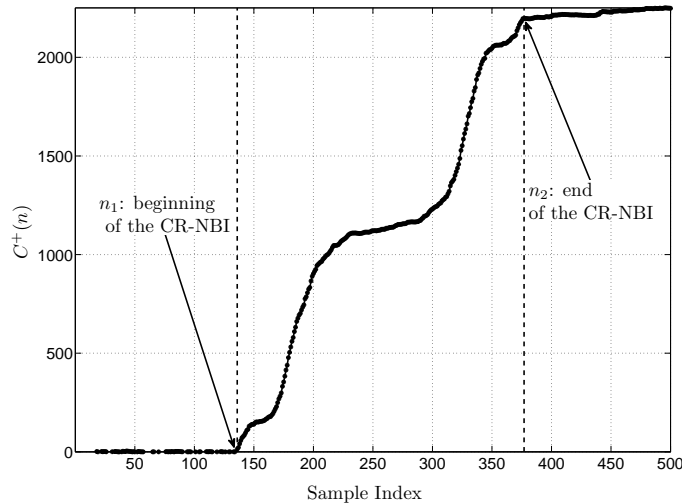
Figure 2.23: Time representation of C in the CUSUM test

2.5.2.3 Improving the Disturbance Detection

In this subsection, the goal is to reduce the gap between the CR-NBI probability of detection $\mathcal{P}_d^{cr} = P(||\tilde{\mathbf{Y}}(n)||^2 > \lambda(n)|\mathcal{H}_0)$ and the PU probability of detection $\mathcal{P}_d^{pu} = P(||\tilde{\mathbf{Y}}(n)||^2 < \lambda(n)|\mathcal{H}_1)$, in order to obtain better estimation performance when using the SPKF-BHT and the SPKF-CT. If the CR-NBI probability of detection $\mathcal{P}_d^{cr}$ increases, the PU probability of detection P_d^{pu} decreases. Therefore, there are less samples available to perform the CFO estimation. This hence may lead to poor estimation of the CFO. The PU probability of detection P_d^{pu} determines the values that are not disturbed by the CR-NBI and that are going to be used in the estimation task.

When looking at figure 2.21, the values of $||\tilde{\mathbf{Y}}(n)||^2$ are not always higher than the threshold between n_1 and n_2 sample indexes. In addition, the values of $||\tilde{\mathbf{Y}}(n)||^2$ may sometimes exceed the threshold outside the interval $[n_1, n_2]$. To improve the CR-NBI and the PU detections when using the BHT, we propose to take into account the evolution of $||\tilde{\mathbf{Y}}(n)||^2$ over several samples. Therefore, we suggest defining a new residual value $||\tilde{\mathbf{Y}}_{mean}(p)||^2$ as follows:

$$||\tilde{\mathbf{Y}}_{mean}(p)||^2 = \frac{1}{\beta} \sum_{q=\beta p}^{\beta(p+1)-1} ||\tilde{\mathbf{Y}}(q)||^2 \tag{2.47}$$

where $p \in \{0, \dots \mathfrak{P} - 1\}$, $\mathfrak{P} = \left\lfloor \frac{K^{pu}}{\beta} \right\rfloor$ and $\lfloor . \rfloor$ is the integer part of $\{.\}$.
If $\frac{K^{pu}}{\beta} \neq \left\lfloor \frac{K^{pu}}{\beta} \right\rfloor$, i.e. $\frac{K^{pu}}{\beta} \notin \mathbb{Z}$, the last sample of the new residual value is:

$$||\tilde{\mathbf{Y}}_{mean}(\mathfrak{P})||^2 = \frac{1}{K^{pu} - \beta\mathfrak{P}} \sum_{q=\beta\mathfrak{P}}^{K^{pu}-1} ||\tilde{\mathbf{Y}}(q)||^2 \tag{2.48}$$

If the value of $||\tilde{\mathbf{Y}}_{mean}(p)||^2$ exceeds the value of the threshold, the algorithm decides that the CR-NBI is present during the corresponding samples. See algorithm 3.

Based on the same idea, to improve the detection performance when using the CUSUM test, we propose to keep only $\mathfrak{P} - \left\lfloor \mathfrak{P} - \frac{K^{pu}}{\beta} \right\rfloor$ (i.e $\mathfrak{P}$ or $\mathfrak{P} + 1$) samples as follows:

$$C_{mean}^+(\mathfrak{p}) = C^+(\beta\mathfrak{p} - 1) \tag{2.49}$$

with $\mathfrak{p} \in \{1, \dots \mathfrak{P} - 1\}$, $C_{mean}^+(0) = C^+(0)$ and if $\frac{K^{pu}}{\beta} \notin \mathbb{Z}$ then $C_{mean}^+(\mathfrak{P}) = C^+(K^{pu} - 1)$. See figure 2.24.

Algorithm 3 Calculate $||\tilde{\mathbf{Y}}_{mean}(p)||^2$

Require: $||\tilde{\mathbf{Y}}(q)||^2$, K^{pu}, β

  for $p = 0$ to $\frac{K^{pu}}{\beta} - 1$ **do**

    $||\tilde{\mathbf{Y}}_{mean}(p)||^2 = \frac{1}{\beta}\sum_{q=\beta p}^{\beta(p+1)-1} ||\tilde{\mathbf{Y}}(q)||^2$

  end for

  if $\frac{K^{pu}}{\beta} \neq \left\lfloor \frac{K^{pu}}{\beta} \right\rfloor$ **then**

    $||\tilde{\mathbf{Y}}_{mean}\left(\left\lfloor \frac{K^{pu}}{\beta} \right\rfloor\right)||^2 = \frac{1}{K^{pu}-\beta\left\lfloor \frac{K^{pu}}{\beta} \right\rfloor} \sum_{q=\beta\left\lfloor \frac{K^{pu}}{\beta} \right\rfloor}^{K^{pu}-1} ||\tilde{\mathbf{Y}}(q)||^2$

  else

  end if
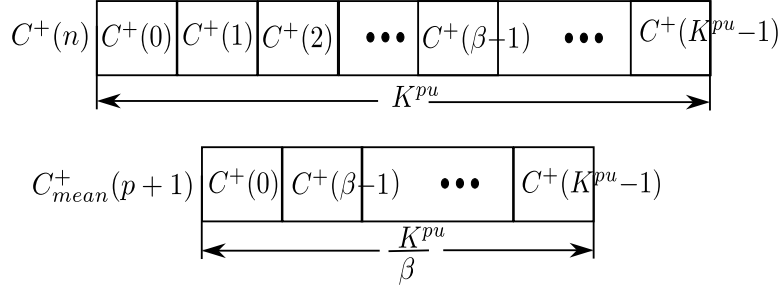
Figure 2.24: $C_{mean}^+(p+1)$ and $C^+(n)$ with $\frac{K^{pu}}{\beta} \in \mathbb{Z}$

If the value of $\frac{\delta(C_{mean}^+(\mathfrak{p}))}{\delta p} = \frac{C^+(\mathfrak{p})-C^+(\mathfrak{p}-1)}{\beta}$ exceeds the value of the threshold, the algorithm decides that the CR-NBI is present in the corresponding samples.

In the next subsection, simulation results show the relevance of our algorithms and their improvements to jointly detect the CR-NBI and estimate the PU-CFOs.

2.5.3 Simulation Results

This section presents computer simulations to validate the performance of the SPKF-BHT and the SPKF-CT estimators. Firstly, the simulation protocol is presented. Secondly, simulations present how to choose the parameter β presented in subsection 2.5.2.3. Finally, the last subsection shows a comparative study in terms of CFO estimation with already existing estimators [More 08], the influence of CR-NBI power on the CFO estimation performance and the channel estimation performance of the proposed algorithms.

Simulation protocol: A PU-OFDMA WirelessMAN™system, which is composed of $U = 4$ users sharing $K^{pu} = 512$ subcarriers and with a cyclic prefix $N_g = K^{pu}/32 \geq \max_u(L_u^{pu})$ is considered. QPSK is used to modulate the information bits. The carrier frequency is at $f_c = 2.6$GHz and the bandwidth is set to $W^{pu} = 5$MHz. A CR-NBI affects $K^{nbi} = 40$ subcarriers of the PU-OFDMA system bandwidth. It is supposed a transmission over a normalized Rayleigh slow-fading frequency-selective channel composed of $L_u^{pu} = 7$ $\forall u$ multipaths.

For very low values of SIR, as $||\tilde{\mathbf{Y}}(n)||^2 >> 0$ during the CR-NBI presence, its detection can be easy. In addition for high values of SIR, i.e SIR> 0dB the difference between σ_B^2 and $(\sigma_B^2 + \sigma_V^2)$ may be negligible and would not affect the Kalman filter estimation performance. Therefore the case when SIR$= -10$ dB is studied. The CR-NBI can begin anywhere in the PU-OFDMA received symbol. For comparison reasons with [More 08], the CR-NBI is supposed to affect only the subcarriers assigned to one PU.
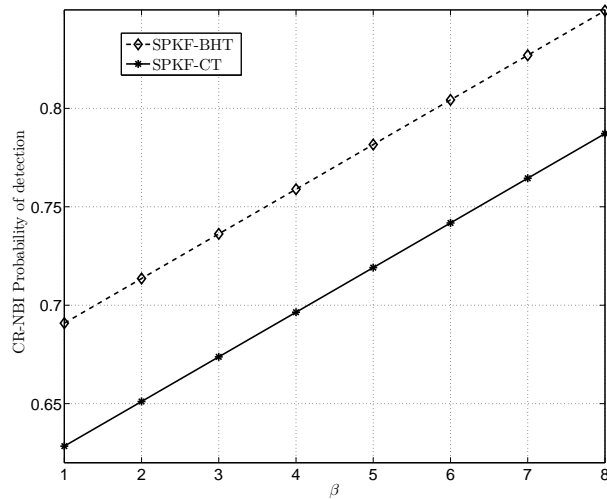
Figure 2.25: CR-NBI detection, SNR$= 0$ dB, SIR$= -10$ dB, $P_{fa} = 0.05$ and $\gamma = 0.5$

2.5.3.1 How to Improve the Disturbance Detection?

This subsection presents how to select a "well suited" value of β, which is the parameter presented in subsection 2.5.2.3, to reduce the gap between the CR-NBI probability of detection $\mathcal{P}_d^{cr}$ and the PU probability of detection $\mathcal{P}_d^{pu}$.

Firstly the impact of β in the CFO estimation performance is shown. The SNR is set to 0 dB and the P_{fa} is set to 0.05.

Let us consider that the CR-NBI disturbs half of the PU-OFDMA symbol ($\gamma = 0.5$). Figure 2.25 shows the CR-NBI probability of detection $\mathcal{P}_d^{cr}$ for different values of β. We clearly see that if β increases, the CR-NBI probability of detection $\mathcal{P}_d^{cr}$ increases and the CFO estimation should normally be improved. However, when looking at figure 2.26 we can see that the PU probability of detection $\mathcal{P}_d^{pu}$ does not increase with the value of β as the CR-NBI probability of detection $\mathcal{P}_d^{cr}$. For both proposed algorithms, there are "well suited" values of β in terms of PU probability of detection. For the SPKF-BHT, the "well suited" value of β is between 4 and 6 whereas the "well suited" value of β is between 2 and 3 when using the SPKF-CT. The CR-NBI probability of detection $\mathcal{P}_d^{cr}$ and the PU probability of detection $\mathcal{P}_d^{pu}$ has been increased, then better estimation performance should be obtained by using this optimal β parameter.
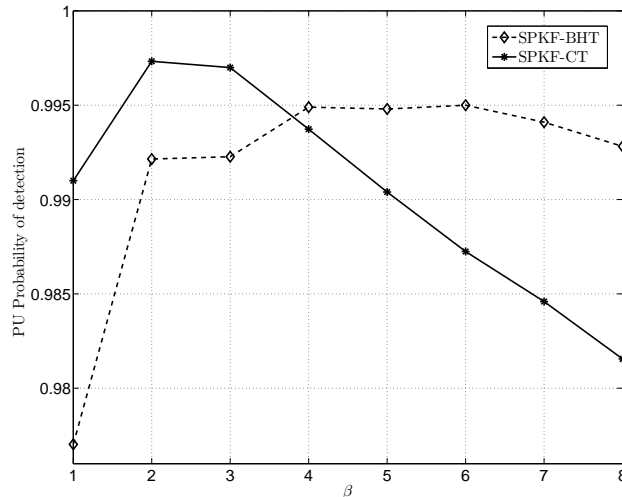
Figure 2.26: PU detection, SNR= 0 dB, SIR= -10 dB, $P_{fa} = 0.05$ and $\gamma = 0.5$

Tables 2.11 and 2.12 show the CFO estimation performance in terms of MMSE for different values of β and duration of the CR-NBI over the symbol. It should be noted that the duration of the CR-NBI over the PU-OFDMA symbol does not change the influence of β in the algorithm. For different durations of the CR-NBI over the symbol, we can see that better performance in terms of CFO estimation are obtained for values β between 4 and 6 for the SPKF-BHT. In addition, it can be seen that the "well suited" value of β in terms of probability of detection is between 2 and 3 for the SPKF-CT.

SNR = 0 dB SIR = −10 dB			
γ	0.47060	0.5333	0.6154
$\beta = 1$	1.124×10^{-3}	1.257×10^{-3}	2.103×10^{-3}
$\beta = 2$	8.517×10^{-4}	9.526×10^{-4}	1.593×10^{-3}
$\beta = 3$	7.949×10^{-4}	8.891×10^{-4}	1.487×10^{-3}
$\beta = 4$	5.735×10^{-4}	6.414×10^{-4}	1.073×10^{-3}
$\beta = 5$	5.962×10^{-4}	6.668×10^{-4}	1.115×10^{-3}
$\beta = 6$	$\mathbf{5.678 \times 10^{-4}}$	$\mathbf{6.350 \times 10^{-4}}$	$\mathbf{1.062 \times 10^{-3}}$
$\beta = 7$	6.814×10^{-4}	7.621×10^{-4}	1.274×10^{-3}
$\beta = 8$	7.382×10^{-4}	8.256×10^{-4}	1.381×10^{-3}

Table 2.11: SPKF-BHT CFO estimation performance for different values of γ and β, $P_{fa} = 0.05$

SNR = 0 dB SIR = −10 dB			
γ	0.47060	0.5333	0.6154
$\beta = 1$	1.569×10^{-3}	1.755×10^{-3}	2.934×10^{-3}
$\beta = 2$	$\mathbf{7.471 \times 10^{-4}}$	$\mathbf{8.356 \times 10^{-4}}$	$\mathbf{1.397 \times 10^{-3}}$
$\beta = 3$	8.218×10^{-4}	9.191×10^{-4}	1.537×10^{-3}
$\beta = 4$	1.494×10^{-3}	1.671×10^{-3}	2.795×10^{-3}
$\beta = 5$	1.644×10^{-3}	1.838×10^{-3}	3.074×10^{-3}
$\beta = 6$	1.718×10^{-3}	1.922×10^{-3}	3.214×10^{-3}
$\beta = 7$	1.793×10^{-3}	2.005×10^{-3}	3.353×10^{-3}
$\beta = 8$	1.868×10^{-3}	2.089×10^{-3}	3.493×10^{-3}

Table 2.12: SPKF-CT CFO estimation performance for different values of γ and β, $P_{fa} = 0.05$

In figure 2.27, we can see the performance in terms of CR-NBI probability of detection. Like the previous tests, better performance are obtained when the BHT is used. When $\beta = 1$ and $P_{fa} = 0.05$, the CR-NBI probability of detection for the SPKF-BHT is higher than the CR-NBI probability of detection for the SPKF-CT. The difference is around 0.08. In addition, when $P_{fa} = 0.05$, the CR-NBI probability of detection for the SPKF-BHT $\beta = 6$ is higher than the CR-NBI probability of detection for SPKF-CT $\beta = 2$. The difference is around 0.15. Again it can be seen that the detection is improved when using $\beta \neq 1$; it confirms the results shown in tables 2.11 and 2.12. Figure 2.28 shows the detection performance in terms of PU probability of detection. In this test, better detection performance are obtained with the CUSUM test.

It should be noted that the choice of an appropriate P_{fa} is a key point in the development of the algorithms.
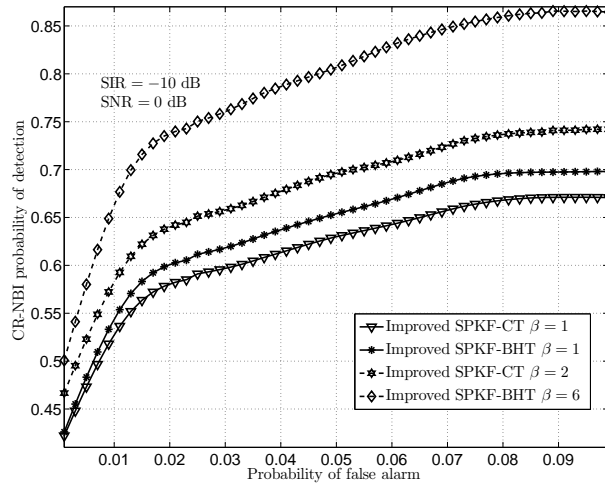
Figure 2.27: CR-NBI detection, SNR= 0 dB, SIR= -10 dB and $\gamma = 0.5$

2.5.3.2 Comparative Study: Influence of the Disturbance Power over the CFO Estimation and Channel Estimation Performance

Figure 2.29 shows the estimation performance in terms of MMSE for different durations of the CR-NBI over the PU-OFDMA symbol. The SNR is again set to
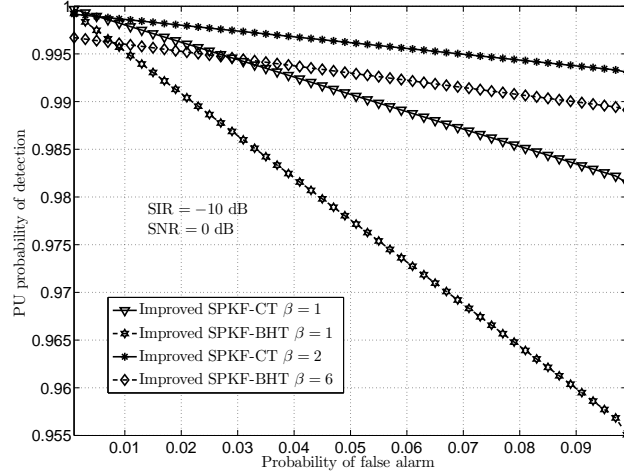
Figure 2.28: PU detection, SNR= 0 dB, SIR= -10 dB and $\gamma = 0.5$
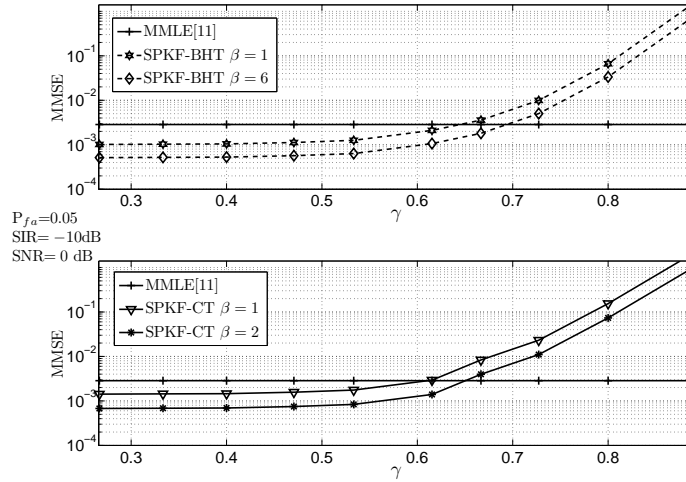
Figure 2.29: Robust CFO estimation performance, SIR= -10 dB, SNR= 0 dB and $P_{fa} = 0.05$

0 dB. We clearly see that the proposed algorithms provide better CFO estimation performance since $\gamma < 0.6$ in comparison with [More 08].

Figure 2.30 shows the CFO estimation performance in terms of MMSE. The CR-NBI disturbs half of the PU-OFDMA symbol ($\gamma = 0.5$).

In comparison with the modified ML estimator (MMLE) proposed in [More 08], an improvement of 2 dB is obtained using the SPKF-CT using $\beta = 1$ and 7 dB is obtained when using the SPKF-BHT using $\beta = 6$, for an MMSE of 10^{-3}.
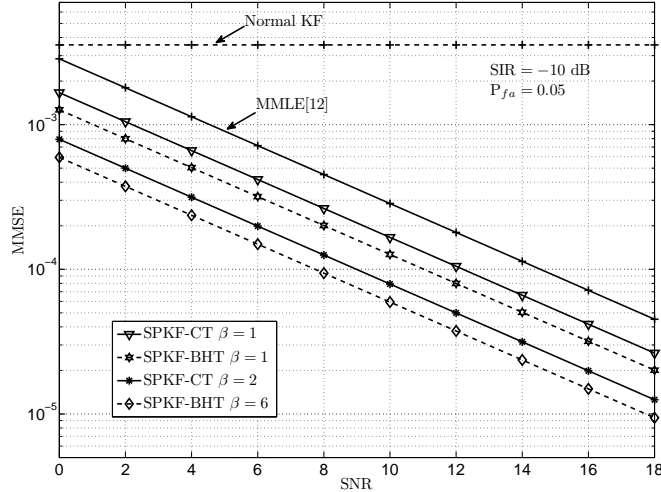
Figure 2.30: Robust CFO estimation performance, SIR$= -10$ dB, $P_{fa} = 0.05$ and $\gamma = 0.5$

Table 2.13 shows the estimation performance in terms of MMSE for different values of SIR. It should be noted that the proposed algorithms are not disturbed by the power of the CR-NBI.

MMSE			
SNR$= 0$ dB			
SIR	-30 dB	-20 dB	-10 dB	0 dB
SPKF	0.43520	0.08150	0.003557	0.00172
SPKF-CT $\beta = 1$	0.0028500		
SPKF-BT $\beta = 1$	0.0012670		
SPKF-CT $\beta = 2$	0.0008217		
SPKF-BT $\beta = 6$	0.0003958		

Table 2.13: Robust CFO estimation performance, $P_{fa} = 0.05$ and $\gamma = 0.5$

Since $\hat{\mathbf{h}}^{pu}$ is determined by the values $\hat{\boldsymbol{\epsilon}}$, one can conclude that the proposed estimators achieve accurate channel estimation. Figure 2.31 confirms the channel

estimation performance of the algorithm. We can see a gain of 12 dB between the SPKF-CT using $\beta = 1$ and the SPKF-BHT using $\beta = 6$.
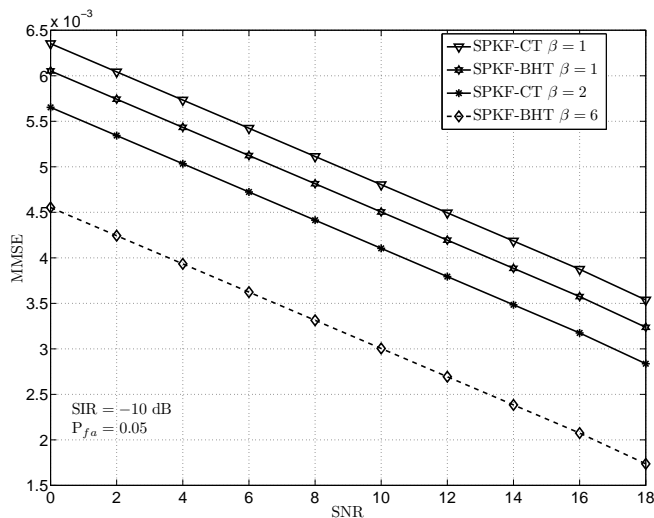
Figure 2.31: Robust channel estimation performance, SIR= -10 dB, $P_{fa} = 0.05$ and $\gamma = 0.5$

2.6 Conclusions

In this chapter we proposed to jointly estimate the CFOs and the channels for an OFDMA uplink system by using a recursive approach. On the one hand, the EKF, the SOEKF, the IEKF and the SPKF including the UKF and the CDKF were considered. On the other hand, to relax the assumptions on the model and measurement noise, the "extended H_∞ filter" and the "unscented H_∞ filter" filter were studied.

Then, the above techniques have been combined with an MMSE-SD to obtain a non-pilot aided CFO estimator for an OFDMA uplink. In addition, as the SPKF give the best compromise between computational complexity and estimation performance, it has been chosen to be combined with two statistical tests: the BHT and the CUSUM test, to design two OFDMA robust CFO estimators.

Both SPKF-based algorithms are used to estimate the CFOs and the channels of different users in a PU-OFDMA system disturbed by a localized in time CR-NBI.

2. Frequency Synchronization and Channel Equalization of OFDMA Uplink Systems

The proposed estimators operate in the time domain unlike other approaches that estimate the CFO in presence of an NBI in the frequency domain [More 08].

By using a SPKF and without increasing the computational complexity, we take advantage of the innovation to detect a sharp variation of the measurement noise covariance matrix when there is CR-NBI. The SPKF enable the state vector to be estimated and the innovation energy to be calculated. Then, a test detects the variation of the measurement-noise covariance matrix by comparing the innovation energy with a threshold set by the practitioner.

When using the BHT, better performance are obtained in terms of the CR-NBI probability of detection. However, when using the CUSUM, better performance in terms of PU probability of detection are obtained. To reduce the gap between the CR-NBI probability of detection and the PU probability of detection, a technique is then proposed. It consists in improving both probabilities of detection by watching the evolution of the innovation energy.

Our method outperforms other existing methods [More 08]. However, the proposed estimators are sensitive to the duration in time of the CR-NBI.

The next chapter still deals with the constraints addressed in this chapter, i.e. frequency synchronization and channel equalization, but in the context of the uplink OFDM-IDMA systems.

Frequency Synchronization and Channel Equalization of OFDM-IDMA Uplink Systems

Contents

3.1 Introduction

The OFDM-IDMA technique initially proposed by Mahafeno *et al.* [Maha 06] has been introduced in chapter 1.

Firstly, OFDM-IDMA can be seen as a special case of multicarrier CDMA (MC-CDMA). IDMA inherits many advantages from CDMA, in particular, its robustness against different kinds of interferences. In addition, the autocorrelation properties of the IDMA transmitted signal make it possible to take advantage of the multipath fading channel diversity[1]. The key principle of IDMA is that the spreading code is the same for all users, unlike CDMA[2]. The user distinction is done by using different interleavers. They are generated independently and randomly, allowing BER to be near the theoretical values of single-user systems. Secondly, OFDM-IDMA can be seen as a special case of OFDMA. OFDM-IDMA inherits the robustness to ISI from OFDMA. In addition, the multicarrier scheme allows the frequency allocation algorithms to improve the spectral efficiency by exploiting the spectral diversity. The main difference between these techniques is that the entire bandwidth can be allocated to a single user for all the OFDM-IDMA frame duration. This may lead to a very high single-user capacity. Indeed, if we assume an OFDMA system with U users and K subcarriers all used, each user can transmit $\frac{K}{U}$ symbols at the same time. Now if one also consider an OFDM-IDMA system with a spreading factor[3] $\mathbb{S} = \log_2(U)$, each user can transmit $\frac{K}{\mathbb{S}} = \frac{K}{\log_2(U)}$ symbols at the same time. We clearly see that $\log_2(U) < U$; thus the users in the OFDM-IDMA system can transmit more symbols at the same time than in an OFDMA system.

Furthermore, an OFDM-IDMA scheme may improve the duty cycle of a single-user transmission[4] in comparison with an OFDMA system. Indeed, in an OFDMA

---

[1]In chapter 1 in section 1.3, we show that the received signal is a superposition of several delayed and attenuated copies of the transmitted signal, due to the multipath fading channel. This diversity may be exploited by a combination of the different copies using a rake receiver [Proa 95].

[2]In chapter 1 in section 1.4.3.1, we present that the ENC of the OFDM-IDMA transmitter incorporates a spreading code.

[3]$\mathbb{S} = \log_2(U)$ is the lowest spreading factor to allow U users transmit at the same time.

[4]The duty cycle of a single-user transmission is defined as the ratio between the duration of one user frame and the time between two successive frames.

system, the maximum number of users allowed by the system to transmit at the same time is $U = K$. In that case, each user transmits one symbol at the same time. In an OFDM-IDMA system, the maximum number of users allowed by the system to transmit at the same time is $U = 2^{\mathbb{S}}$. In addition, to transmit one symbol at the same time, it is necessary that $K = \mathbb{S}$. Then, the maximum number of users allowed by an OFDM-IDMA system to transmit one symbol at the same time is $U = 2^K$. We clearly see that $2^K > K$; the OFDM-IDMA enables more users to perform a transmission at the same time.

Today, the OFDM-IDMA scheme is not used as the multiple access technique by mobile wireless standards, but for the above reasons, it can be seen as a promising technique for the future mobile wireless standards.

To become one of the multiple access schemes of future mobile standards, several constraints have to be addressed, such as the channel equalization. Nevertheless, few papers deal with this issue in IDMA systems. Thus, Zhou *et al.* develop an iterative channel estimation process that uses pilot subcarriers [Zhou 07]. The authors propose two different approaches: the first one is based on an unbiased LS estimator whereas the second is based on the maximum ratio combining (MRC) method. In [Song 09], the authors propose an EM estimation method to obtain the CSIs. More specifically, in [Suya 08], Suyama *et al.* insert a least mean square (LMS) estimator in the iterative process of an OFDM-IDMA receiver. In addition, the authors in [Rehm 08] present a low-complexity uplink channel estimation. By taking advantage of the channel coding, the transmitter creates a training sequence in order to estimate the channel through a linear detection at the receiver.

However, in the above approaches, a perfectly frequency synchronized system is considered. In wireless communication systems with multicarrier modulation, this assumption is usually not true. Therefore, a CFO estimation/correction has to be considered at the receiver.

Several approaches of the frequency synchronization in multicarrier systems have been proposed in the last years. More particularly, in MC-CDMA systems, Chien *et al.* present a blind recursive estimation of the CFOs by using an EM algorithm [Chie 07]. In [Thia 07], the authors take advantage of the knowledge of the

second-order statistics of the received signal. They suggest a two-stage CFO estimation. The first one involves a grid search to obtain the initialization of the CFO estimations, whereas the second consists of a CFO estimation based on the LMS algorithm. In [Chen 10], the CFOs are estimated by searching the peaks of the correlation function of the received signal. In addition, the reader can look at the frequency synchronization techniques for OFDMA systems, [Pun 04a], [Pun 06] and [Sezg 08] presented in chapter 2.

In the above methods, the CFO correction can be performed before or after the CP-OFDM demodulation. The CFO correction methods can take advantage of the orthogonal codes in MC-CDMA systems, whereas the CFO correction methods usually utilize the CAS[1] in OFDMA systems. The CFO estimation/correction issue in the particular OFDM-IDMA scheme becomes a challenging task[2]. In [Cao 04a], Cao *et al.* propose to correct the CFO in an OFDMA uplink system after the CP-OFDMA demodulation through a linear detection[3], without taking advantage of the CAS. This CFO correction method can be completely applied to OFDM-IDMA systems. However, CFOs and CSIs are assumed to be perfectly known. Although frequency synchronization has been addressed in MC-CDMA and OFDMA, it has never been studied in an OFDM-IDMA system to our knowledge.

Given the above considerations, our contribution in this chapter is twofold:

1. We propose two SPKF based receivers: the first one is a modification of the OFDM-IDMA receiver proposed by [Maha 06], whereas the second uses a STBC to take advantage of the space diversity. The proposed OFDM-IDMA receivers aim at jointly estimating the CFO and the channel of each user in the system, by using a preamble of one OFDM-IDMA symbol.

---

[1]In chapter 2 in section 2.2, we present several CFO correction methods that take advantage of the CAS such as the single-user detector method and the methods presented in [Choi 00] and [Huan 05].

[2]Let us recall that in an OFDM-IDMA system all users may use the same spreading code and a subcarrier is allocated to all users at the same time.

[3]In subsection 3.2, we show that after the CP-OFDM demodulation, the received OFDM-IDMA symbol can be expressed as a multiplication between a function depending on the CFO and a function depending on the symbols and channel frequency responses.

2. Both receivers operate in two steps. Firstly, the OFDM demodulation is performed without any correction over the received signal. Then, the resulting signal is inserted in the new versions of the IDMA receiver. Finally, taking into account the interference produced by the CFO and knowing all the CFOs and the CSIs, the IDMA iterative process is able to cancel both the ICI and the MAI, and to recover the sent symbols.

3.2 OFDM-IDMA Modified Receiver

Like the OFDMA uplink system, the signal received at the BS is affected by several CFOs and CSIs in an OFDM-IDMA uplink system. The nth sample of received OFDM-IDMA symbol after time-synchronization and CP removing can be expressed as:

$$R(n) = \sum_{u=1}^{U} e^{j2\pi \frac{\epsilon_u n}{K}} \sum_{l=0}^{L_u-1} h_u(l) X_u(n-l) + B(n) \quad 0 \le n \le K-1 \qquad (3.1)$$

where we recall that $h_u(l)$ is the lth coefficient of the CIR, ϵ_u is the normalized CFO, $X_u(n)$ is the nth sample of the transmitted OFDM-IDMA symbol and $B(n)$ is a zero-mean AWGN with variance σ_B^2.

Then, the received OFDM-IDMA symbol can be expressed as follows:

$$\begin{aligned} \mathbf{R} &\triangleq [R(0), R(1), \dots, R(n), \dots, R(K-1)]^T \\ &= \sum_{u=1}^{U} \underbrace{\mathbf{E}_u \mathfrak{h}_u \mathbf{X}_u}_{\mathbf{R}_u} + \mathbf{B} \end{aligned} \qquad (3.2)$$

where $\mathbf{E}_u = \text{diag}\left\{ \left[1, e^{j2\pi \epsilon_u/K}, \dots, e^{j2\pi(K-1)\epsilon_u/K} \right] \right\}$ is the CFO matrix, $\mathfrak{h}_u$ is the channel circulant matrix defined in (1.31), $\mathbf{X}_u$ is the transmitted OFDM-IDMA symbol defined in (1.21) and $\mathbf{B}$ is a zero-mean AWGN vector with covariance matrix $\sigma_B^2 \mathbf{I}_K$ (See chapter 1 in section 1.4.3.2).

Given (1.20), it should be noted that (3.1) can be rewritten as follows:

$$R(n) = \sum_{u=1}^{U} e^{j2\pi \frac{\epsilon_u n}{K}} \sum_{k'=0}^{K-1} H_u(k') S_u(k') e^{j2\pi \frac{k'n}{K}} + B(n) \quad 0 \le n \le K-1 \qquad (3.3)$$

3. Frequency Synchronization and Channel Equalization of OFDM-IDMA Uplink Systems

where $H_u(k') = \sum_{l=0}^{L-1} h_u(l)e^{-j2\pi\frac{k'l}{K}}$ is the channel frequency response associated to the k'th subcarrier and $S_u(k')$ is the symbol transmitted over the k'th subcarrier.

Given (3.3), although the effect of the CFO of one user or another can be eliminated, they cannot be suppressed all at the same time before the CP-OFDM demodulation. Whatever the strategy chosen by the receiver to compensate the CFO, there are still some interferences. Therefore, we suggest introducing the CFO correction after the CP-OFDM demodulation.

After the CP-OFDM demodulation, the received symbol $r(k)$ can be expressed as follows:

$$
\begin{aligned}
r(k) &= \sum_{n=0}^{K-1} R(n)e^{-j2\pi\frac{kn}{K}} + b(k) \\
&= \sum_{n=0}^{K-1} \sum_{u=1}^{U} e^{j2\pi\frac{\epsilon_u n}{K}} \sum_{k'=0}^{K-1} H_u(k')S_u(k')e^{j2\pi\frac{(k'-k)n}{K}} + b(k) \\
&= \sum_{u=1}^{U} \sum_{k'=0}^{K-1} \sum_{n=0}^{K-1} e^{j2\pi\frac{(k'-k+\epsilon_u)n}{K}} H_u(k')S_u(k') + b(k) \\
&= \sum_{u=1}^{U} \sum_{k'=0}^{K-1} \mathcal{F}(k'-k+\epsilon_u)H_u(k')S_u(k') + b(k)
\end{aligned}
\tag{3.4}
$$

where[1]

$$
\mathcal{F}(x) = \frac{sin(x\pi)}{sin(\frac{x\pi}{K})}e^{j\pi\frac{x(K-1)}{K}}
\tag{3.5}
$$

and

$$
b(k) = \sum_{n=0}^{K-1} B(n)e^{-j2\pi\frac{kn}{K}}
\tag{3.6}
$$

Then, (3.4) can be rewritten as:

$$
r(k) = \sum_{u=1}^{U} \mathcal{F}(\epsilon_u)H_u(k)S_u(k) + \underbrace{\sum_{u=1}^{U} \sum_{\substack{k'=0 \\ k'\neq k}}^{K-1} \mathcal{F}(\epsilon_u + k' - k)H_u(k')S_u(k')}_{ICI(k)} + b(k)
\tag{3.7}
$$

---

[1]Let us recall that $\sum_{n=0}^{K-1} e^{j2\pi\frac{nx}{K}} = \frac{1-e^{j2\pi x}}{1-e^{j2\pi\frac{x}{K}}} = \frac{sin(x\pi)}{sin(\frac{x\pi}{K})}e^{j\pi\frac{x(K-1)}{K}}$.

If we look at the received signal from the uth user point of view, (3.7) can be expressed as a summation of a useful term and an interference term as follows:

$$
\begin{aligned}
r(k) &= \mathcal{F}(\epsilon_u)H_u(k)S_u(k) + \sum_{\substack{u'=1 \\ u'\neq u}}^{U} \mathcal{F}(\epsilon_{u'})H_{u'}(k)S_{u'}(k) + ICI(k) + b(k) \\
&= H_u^{(\mathrm{eq})}(k)S_u(k) + \sum_{\substack{u'=1 \\ u'\neq u}}^{U} H_{u'}^{(\mathrm{eq})}(k)S_{u'}(k) + ICI(k) + b(k) \\
&= H_u^{(\mathrm{eq})}(k)S_u(k) + \varsigma_u(k)
\end{aligned}
\tag{3.8}
$$

where

$$
H_u^{(\mathrm{eq})}(k) = \mathcal{F}(\epsilon_u)H_u(k) \quad \forall u \in \{1,\ldots,U\}
\tag{3.9}
$$

$$
\varsigma_u(k) = \sum_{\substack{u'=1 \\ u'\neq u}}^{U} H_{u'}^{(\mathrm{eq})}(k)S_{u'}(k) + ICI(k) + b(k)
\tag{3.10}
$$

and $ICI(k)$ is a zero-mean ICI with variance $\sigma_{\mathrm{ICI}}^2 = \mathbb{E}\{|ICI(\boldsymbol{\epsilon},k)|^2\}$, caused by the CFOs [Moos 94]. This interference can be considered as a Gaussian vector due to the large number of subcarriers [Huan 10b]. It should be noted that the ICI is included in $\varsigma_u(k)$, the characteristics of which are used by the IDMA receiver to estimate the transmitted bits (See chapter 1 in section 1.4.3.2).

In the following, we will show that the transmitted bits can be recovered by taking into account the ICI characteristics in the IDMA receiver. In addition, as $r(k)$ in (3.8) is a function of $\epsilon_{u'}$ and $H_{u'}^{(\mathrm{eq})}(k)$, it is necessary to know the CFOs and the CSIs values at the IDMA receiver. In the next subsection, the estimations of these vectors are presented.

3.2.1   Multiple CFO and Channel Estimation

Let us define the vector $\boldsymbol{\epsilon}$ of size U and the vector $\mathbf{h}$ of size $L = \sum_{u=1}^{U} L_u$ by storing the CFOs and the CSIs of the U users in the system as follows:

$$
\begin{aligned}
\boldsymbol{\epsilon} &= [\epsilon_1, \epsilon_2, \ldots, \epsilon_u, \ldots, \epsilon_U] \\
\mathbf{h} &= [\mathbf{h}_1, \mathbf{h}_2, \ldots, \mathbf{h}_u, \ldots, \mathbf{h}_U]
\end{aligned}
\tag{3.11}
\tag{3.12}
$$

3. Frequency Synchronization and Channel Equalization of OFDM-IDMA Uplink Systems

where $\mathbf{h}_u = [h_u(0), h_u(1), \ldots, h_u(l), \ldots, h(L_u - 1)]$.

In order to restore orthogonality among each user subcarrier, both the CFO-synchronization error vector $\boldsymbol{\epsilon}$ and the CSI vector $\mathbf{h}$ have to be estimated at the BS.

The state-space representation of the system (3.1)-(3.2) is the representation of what happens during one OFDM-IDMA frame[1].

Let us define the vector $\mathbf{x}(n)$ of size $\mathcal{U} = U + 2L$, which is the state vector of the system (3.1)-(3.2):

$$\mathbf{x}(n) = \left[\begin{array}{ccc} \boldsymbol{\epsilon}(n) & Re\left\{\mathbf{h}(n)\right\} & Im\left\{\mathbf{h}(n)\right\} \end{array}\right]^T \tag{3.13}$$

Let $\mathbf{Y}$ be the $2 \times K$ observation matrix that stores the real and the imaginary parts of the received OFDM-IDMA symbol $\mathbf{R}$:

$$\begin{aligned} \mathbf{Y}(\boldsymbol{\epsilon}, \mathbf{h}) &= \mathbf{C}(\boldsymbol{\epsilon}, \mathbf{h}) + \mathbb{B} \\ &= [\mathbf{Y}(0, \boldsymbol{\epsilon}, \mathbf{h}), \mathbf{Y}(1, \boldsymbol{\epsilon}, \mathbf{h}), \ldots, \mathbf{Y}(n, \boldsymbol{\epsilon}, \mathbf{h}), \ldots, \mathbf{Y}(K - 1, \boldsymbol{\epsilon}, \mathbf{h})] \end{aligned} \tag{3.14}$$

where $\mathbf{C}(\boldsymbol{\epsilon}, \mathbf{h})$ is a $2 \times K$ matrix that stores the real an the imaginary parts of the contribution of all users to the received OFDM-IDMA symbol:

$$\begin{aligned} \mathbf{C}(\boldsymbol{\epsilon}, \mathbf{h}) &= \left[\begin{array}{c} Re\left\{\sum_{u=1}^{U}\mathbf{R}_u\right\}^T \\ Im\left\{\sum_{u=1}^{U}\mathbf{R}_u\right\}^T \end{array}\right] \\ &= [\mathbf{C}(0, \boldsymbol{\epsilon}, \mathbf{h}), \mathbf{C}(1, \boldsymbol{\epsilon}, \mathbf{h}), \ldots, \mathbf{C}(n, \boldsymbol{\epsilon}, \mathbf{h}), \ldots, \mathbf{C}(K - 1, \boldsymbol{\epsilon}, \mathbf{h})] \end{aligned} \tag{3.15}$$

and

$$\begin{aligned} \mathbb{B} &= \left[\begin{array}{c} Re\{\mathbf{B}(n)\}^T \\ Im\{\mathbf{B}(n)\}^T \end{array}\right] \\ &= [\boldsymbol{\mathcal{B}}(0), \boldsymbol{\mathcal{B}}(1), \ldots, \boldsymbol{\mathcal{B}}(K - 1)] \end{aligned} \tag{3.16}$$

$\boldsymbol{\mathcal{B}}(n)$ is an AWGN vector with zero-mean and covariance matrix $\frac{\sigma_B^2}{2}\mathbf{I}_2$.

Now let us introduce the state-space representation of the system to estimate the CFO and the channel:

State equation:

$$\mathbf{x}(n) = \mathbf{x}(n - 1) + \mathbf{w}(n) \quad \forall \quad n \in [0, K - 1] \tag{3.17}$$

---

[1]The OFDM-IDMA frame is a block composed of several OFDM-IDMA symbols.

Measurement equation:

$$\mathbf{Y}(n) = \mathbf{C}(n, \mathbf{x}(n)) + \boldsymbol{\mathcal{B}}(n) \quad \forall \quad n \in [0, K-1] \tag{3.18}$$

where $\mathbf{w}(n)$ is an AWGN matrix with zero-mean and covariance matrix $\sigma_w^2 \mathbf{I}_{\mathcal{U}}$. It should be noted that σ_w^2 is very low and can even be equal to 0.

The SPKF detailed in appendix E is used to estimate the CFOs and the channels, after the time synchronization and CP removal. Then, the OFDM demodulation is performed without any CFO correction and the resulting samples are used in the modified IDMA receiver presented in the next subsection.

3.2.2 Modified IDMA Receiver

At the IDMA receiver, an *a priori* knowledge of $H_u^{(\mathrm{eq})}(k)$ is required. In addition, it is necessary to characterize the interference term $\varsigma_u(k)$ and the noise $b(k)$.

Given (3.9) and the estimated values of the CFO $\hat{\epsilon}_u$ and the CSI $\hat{\mathbf{h}}_u$, we can obtain $\hat{H}_u^{(\mathrm{eq})}(k)$ which is an estimation of $H_u^{(\mathrm{eq})}(k)$.

Then, given the output $r(k)$ of the OFDM demodulation, the values of $\hat{H}_u^{(eq)}(k)$, the additive-noise variance σ_B^2, the ICI variance σ_{ICI}^2 and $g_u^{\mathrm{ESE}}(k)$, the IDMA reception can be performed[1].

Let us view the transmitted symbol $S_u(k)$ as a random variable. Given (1.41), the modified ESE computes the mean and the covariance of $S_u(k)$ as in (1.46) and (1.47) respectively. For the initialization process, $g_u^{\mathrm{ESE}}(k) = 0$ for $i = 1$, where i denotes the iteration number with $i \in \{1, \dots, \mathcal{J}^{idma}\}$ and $\mathcal{J}^{idma}$ is the maximum number of iterations. Then, assuming that $\mathbf{S}_u$ are independent and identically distributed, and applying the central limit theorem, we can consider a Gaussian approximation for $\varsigma_u(k)$ and $r(k)$. Thus, they can be completely characterized by their means and variances.

Given (3.8) and by replacing $H_u^{(\mathrm{eq})}(k)$ by its estimate, one has:

$$\mathbb{E}(\varsigma_u(k)) = \mathbb{E}(r(k)) - \hat{H}_u^{(\mathrm{eq})}(k)\mu_u(k) \quad \forall u, k$$
$$Var(\varsigma_u(k)) = Var(r(k)) - (\hat{H}_u^{(\mathrm{eq})}(k))^2 v_u(k) \quad \forall u, k \tag{3.19}$$

---

[1]The proposed IDMA receiver may be applied to real and complex signals. For the sake of simplicity, let us consider a BPSK modulation.

It should be noted that (3.8) can be rewritten as:

$$r(k) = \sum_{u=1}^{U} H_u^{(eq)}(k)S_u(k) + ICI(k) + b(k) \tag{3.20}$$

Then, given (3.20) and by replacing $H_u^{(eq)}(k)$ by its estimate, one has:

$$\mathbb{E}(r(k)) = \sum_{u=1}^{U} \hat{H}_u^{(eq)}(k)\mu_u(k) \quad \forall u, k$$

$$Var(r(k)) = \sigma_Z^2 + \sum_{u=1}^{U} (\hat{H}_u^{(eq)}(k))^2 \upsilon_u(k) \quad \forall u, k \tag{3.21}$$

with $\sigma_Z^2 = \sigma_{ICI}^2 + \sigma_B^2$.

Unlike a conventional IDMA receiver, the interference-plus-noise is now a combination of the MAI, the ICI produced by the CFOs and the Gaussian noise. The modified ESE process for the uth user at the ith iteration generates the value of the *a posteriori* LLR as follows (See chapter 1 in section 1.4.3.2):

$$\mathfrak{g}_u^{\text{ESE}}(k) = 2\hat{H}_u^{(eq)}(k) \times \frac{r(k) - \mathbb{E}(\varsigma_u(k))}{Var(\varsigma_u(k))} \quad \forall u, k \tag{3.22}$$

The outputs of the modified ESE are inserted in the user decoding process (See
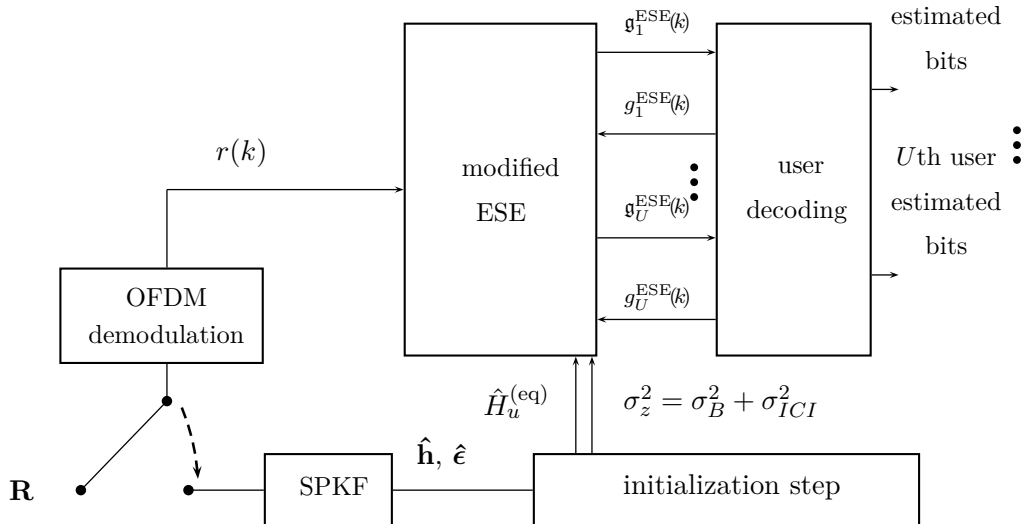
Figure 3.1: Proposed OFDM-IDMA uplink receiver, where the user decoding is the same as in figure 1.20

Algorithm 4 Modified ESE

Require: $r(k)$, σ_B^2, σ_{ICI}^2, $\hat{H}_u^{(\text{eq})}(k)$, $\mathcal{J}^{\text{idma}}$

Initialization step:
$g_u^{\text{ESE}}(k) = 0 \quad \forall u, k$

Iterative process

for $i = 1$ to $\mathcal{J}^{\text{idma}}$ **do**

$\quad \mu_u(k) = \mathbb{E}(S_u(k)) = tanh\left(\frac{g_u^{\text{ESE}}(k)}{2}\right) \quad \forall u, k$

$\quad \upsilon_u(k) = Var(S_u(k)) = 1 - (\mu_u(k))^2 \quad \forall u, k$

$\quad \mathbb{E}(r(k)) = \sum_{u=1}^{U} \hat{H}_u^{(\text{eq})}(k)\mu_u(k) \quad \forall u, k$

$\quad Var(r(k)) = \sigma_Z^2 + \sum_{u=1}^{U} (\hat{H}_u^{(\text{eq})}(k))^2 \upsilon_u(k) \quad \forall u, k$

$\quad \mathbb{E}(\varsigma_u(k)) = \mathbb{E}(r(k)) - \hat{H}_u^{(\text{eq})}(k)\mu_u(k) \quad \forall u, k$

$\quad Var(\varsigma_u(k)) = Var(r(k)) - (\hat{H}_u^{(\text{eq})}(k))^2 \upsilon_u(k) \quad \forall u, k$

$\quad \mathfrak{g}_u^{\text{ESE}}(k) = 2\hat{H}_u^{(\text{eq})}(k) \times \frac{r(k) - \mathbb{E}(\varsigma_u(k))}{Var(\varsigma_u(k))} \quad \forall u, k$

end for

---

chapter 1 in section 1.4.3.2). Then, at the ith iteration for $i < \mathcal{J}^{idma}$, the outputs of the decoding process are the values of $g_u^{\text{ESE}}(k)$, that are reinserted in the ESE. The ESE process is again performed. Finally, the decoding process produces hard decisions to obtain the estimations of the transmitted bits during the final iteration $\mathcal{J}^{idma}$. See algorithm 4, where the modified ESE is summarized. Figure 3.1 shows the modified OFDM-IDMA uplink receiver.

3.2.3 Simulation Results

Simulation protocol:

We consider an OFDM-IDMA uplink system composed of $U = 4, 8, 16$ users over $K = 1024$ subcarriers. The spreading factor is $\mathbb{S} = 64$. BPSK is used to modulate the information bits. The carrier frequency is at $f_c = 2.6\text{GHz}$ and the channel bandwidth is set to $W = 10\text{MHz}$. We consider that the ENC consists only of the insertion of a spreading code. We define the SNR= $10\log(\frac{\sigma_u^2}{\sigma_B^2})$, where σ_u^2 is the mean power of the received signal from the uth user, and the SIR= $10\log(\frac{\sigma_u^2}{\sigma_{ICI}^2})$. We consider a transmission over a normalized Rayleigh slow-fading frequency selective channel channel composed of $L_u = 1, 3, 5 \ \forall u$. The CFOs are modeled as

random variables with a normal distribution with zero-mean and variance 0.1. The estimations are obtained by using control data of one OFDM-IDMA symbol. Figure 3.2 shows the convergence speed of the SPKF for a different number of users in the system. We can see that the number of users in the system does not really affect the estimation performance of the SPKF. This is a key point in OFDM-IDMA systems that allow a large number of users to transmit at the same time. However, the computational complexity of the SPKF increases with the number of users in the system. Then, we fix the number of user to $U = 4$. Figure 3.3 shows the CFO estimation performance in terms of MMSE of one user in the system. The SPKF allows the CFO and the channel of the users to be estimated. The MMSE for an AWGN channel and for channels with different length are presented. The channel estimation for different channel lengths give the same estimation performance, around 10^{-2} for a SNR= 0dB. Previous studies in [Ping 02a] and [Maha 06] show the performance of the IDMA receiver for different number of multipaths, for different number of users and different number of iterations. It has been already proved that the performance of the IDMA receiver in terms of BER are better when the number of multipaths and iterations increases and also when the number of users decreases [Ping 02a], [Maha 06]. For
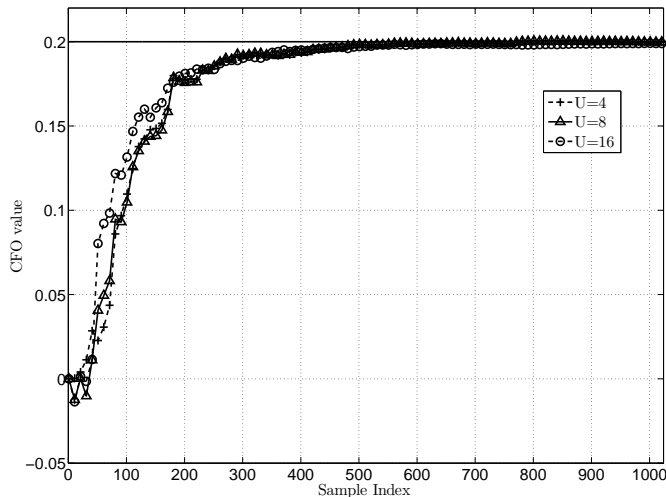
Figure 3.2: SPKF convergence speed
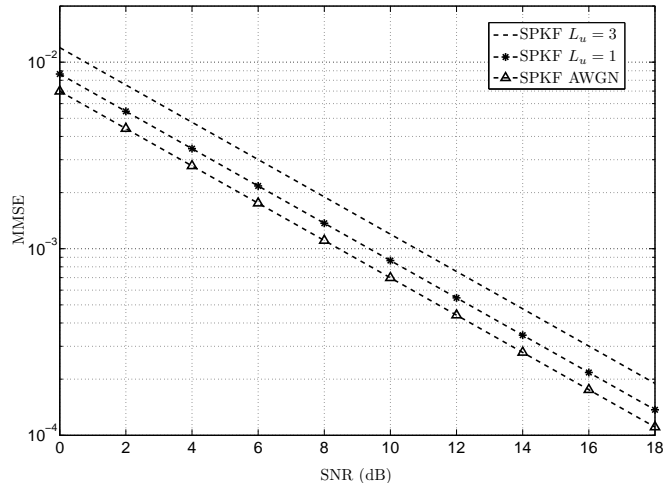
Figure 3.3: CFO estimation performance in terms of MMSE, SIR= 0dB

this reason, we keep the number of users equal to $U = 4$, and the number of iterations to 3. The following results are the average of 5000 OFDM-IDMA symbols. Figure 3.4 shows the BER for a transmission over a normalized Rayleigh slow-fading frequency selective channel channel composed of $\forall u \ L_u = 1$ and $L_u = 3$ multipaths. The efficiency of the algorithm is confirmed. Indeed, we can see that for $L_u = 1$ and a BER $= 10^{-1}$ the difference between the results of the proposed scheme and the perfect case is lower than 1dB. In addition, we can notice that for $L_u = 3$ and a BER$= 10^{-2}$ the difference between the results of the proposed scheme and the perfect case is less than 1 dB. In both cases ($L_u = 1$ and $L_u = 3$), that the proposed scheme gives a gain of around 3dB for BER$= 10^{-1}$ in comparison with the linear detection method presented in [Cao 04a]. Figure 3.5 shows the BER for a transmission over a normalized Rayleigh slow-fading frequency selective channel channel composed of $\forall u \ L_u = 5$ multipaths. We can see that the difference between the results of the proposed scheme and the perfect case is lower than 1 dB. In addition, the proposed scheme gives a gain of around 2dB for BER$= 10^{-2}$ in comparison with the linear detection method presented in [Cao 04a]. It should be noticed that the performance for $L_u = 5$ are better than for $L_u = 3$ and $L_u = 1$. The IDMA receiver takes advantage of the diversity introduced by the propagation channel.
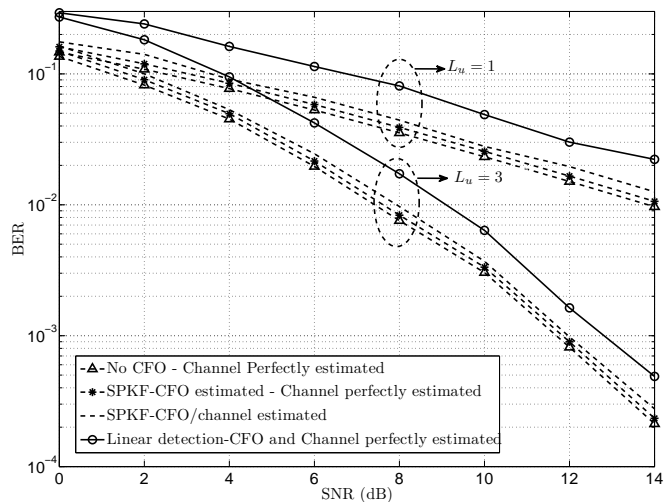
Figure 3.4: BER performance for a channel with $L_u = 1$ and $L_u = 3$
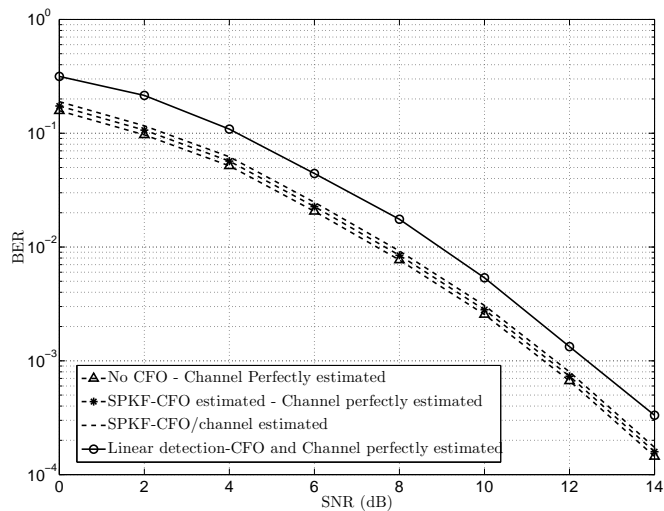
Figure 3.5: BER performance for a channel with $L_u = 5$

3.2.4 Conclusions

In this section, a modified OFDM-IDMA receiver is proposed. The receiver is robust against ISI due to the OFDM modulation and it is robust against the MAI due to the IDMA scheme. Unlike common approaches, the IDMA scheme allows the CFO correction step to be skipped. After the OFDM demodulation, the CFOs and the channels are jointly estimated by using a SPKF. Then, the OFDM demodulation is performed without any CFO correction. Finally, the modified IDMA receiver accurately estimates the transmitted bits of the uth user, by taking into account the estimations of the SPKF and the interference produced by the CFO. The proposed IDMA receiver is able to cancel the ICI produced by the CFOs , as well as the MAI produced by the other users in the system. Simulation results clearly show the efficiency of the proposed OFDM-IDMA receiver. In addition, we show that the proposed receiver outperforms existent CFO correction methods such as [Cao 04a].

In the next section, we show that the proposed scheme can be extended to the multiple-input multiple-output (MIMO) case.

3.3 Space-Time Block Code OFDM-IDMA Receiver

Space-time coding is an effective method to reach the capacity of multiple input multiple output (MIMO) wireless channels. It can supply transmit diversity and power gain without limiting the bandwidth efficiency [Taro 97]. STBC is a kind of space-time coding with simple encoding structure. It allows a simple ML decoding algorithm based on linear signal processing at the receiver [Taro 99].

Given the advantages of the STBC, it has been combined with IDMA. More specifically, in [Wu 03] and [Ping 02b], interleaving is used to separate signals from different antennas. If P denotes the number of transmit antennas, $U \times \mathsf{P}$ interleavers are required by the transmitter. Then, to reduce the complexity of the transmitter, Yang *et al.* [Yang 08] propose a STBC-IDMA system which uses only U interleavers. However, the authors do not aim at estimating the channel. In [Shik 10], Suyama *et al.* propose a MIMO-OFDM IDMA system that uses
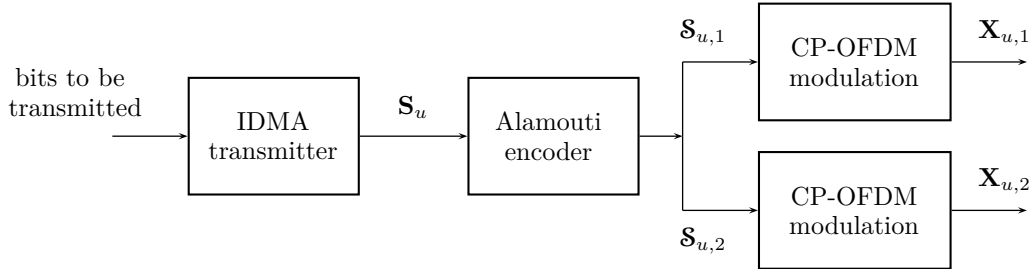
Figure 3.6: OFDM-IDMA-STBC transmitter for the uth user, the IDMA transmitter is the same as in figure 1.19, $\mathbf{S}_{u,\mathsf{p}}$ are the IDMA symbols and $\mathbf{X}_{u,\mathsf{p}}$ are the CP-OFDM-IDMA symbols

U interleavers and address the channel estimation by inserting an LMS in the iterative architecture of the IDMA receiver. Nevertheless, the authors consider a frequency synchronized system.

To our knowledge the frequency synchronization in a STBC-OFDM-IDMA scheme has never been addressed. Therefore, in this section we suggest a joint CFO and channel estimation by using a SPKF in a STBC-OFDM-IDMA system.

3.3.1 System Description

In the following, let us consider an STBC-OFDM-IDMA system consisting of U simultaneously users who transmit information toward a single BS. The available bandwidth W is divided among K subcarriers. We assume that the transmitter uses $\mathsf{P} = 2$ antennas to transmit the information.

As the CSIs are unknown and in order to increase the space diversity, each couple of antennas transmits information from one user by using the Alamouti scheme [Alam 98]. In the following, let us associate the subscript (u, p) to the pth antenna and to the uth user in the system, with $\mathsf{p} \in \{1, 2\}$ and $u \in \{1, \ldots U\}$. As shown in figure 3.6, the STBC-OFDM-IDMA transmitter works as follows:

The IDMA modulated symbols after the IDMA transmitter are denoted as:

$$\mathbf{S}_u \triangleq [S_u(0), S_u(1), \ldots, S_u(K-1)]^T \tag{3.23}$$

The Alamouti code is implemented. Then, the OFDM modulation is performed. The resulting STBC-OFDM-IDMA symbols are:

$$\mathbf{X}_{u,1} = \mathbf{F}^H \mathbf{S}_{u,1} \triangleq \mathbf{F}^H \left[S_u(0), -S_u^*(1), \ldots S_u(K-2), -S_u^*(K-1) \right]^T$$
$$\mathbf{X}_{u,2} = \mathbf{F}^H \mathbf{S}_{u,2} \triangleq \mathbf{F}^H \left[S_u(1), S_u^*(0), \ldots S_u(K-1), S_u^*(K-2) \right]^T \tag{3.24}$$

Let us define the CSI as follows:

$$\mathbf{h}_{u,\mathbf{p}} = [h_{u,\mathbf{p}}(0), h_{u,\mathbf{p}}(1), \ldots, h_{u,\mathbf{p}}(l), \ldots, h_{u,\mathbf{p}}(L_{u,\mathbf{p}}-1)] \tag{3.25}$$

where $L_{u,\mathbf{p}}$ is the length of the channel.

Finally, a CP of size $N_g \geq \max_{u,\mathbf{p}}(L_{u,\mathbf{p}})$ is inserted and the STBC-OFDM-IDMA symbol is transmitted.

Moreover, let us define the row vector of size $2U \times 1$ that contains the normalized CFOs of each user and the row vector of size $L = \sum_{\mathbf{p}=1}^{2} \sum_{u=1}^{U} L_{u,\mathbf{p}}$ that contains the CSIs of each user, respectively:

$$\begin{aligned} \epsilon &= [\boldsymbol{\epsilon}_1, \boldsymbol{\epsilon}_2, \ldots, \boldsymbol{\epsilon}_u, \ldots, \boldsymbol{\epsilon}_U] \\ \mathbf{h} &= [\mathbf{h}_1, \mathbf{h}_2, \ldots, \mathbf{h}_u, \ldots, \mathbf{h}_{\mathbb{S}}] \end{aligned} \tag{3.26}$$

where $\boldsymbol{\epsilon}_u = [\epsilon_{u,1}, \epsilon_{u,2}]$ and $\mathbf{h}_u = [\mathbf{h}_{u,1}, \mathbf{h}_{u,2}]$.

At the receiver, due to the propagation conditions, the multipath channels and the CFOs affect the transmitted signal. Without the noise contribution, after time-synchronization and CP removing, the received STBC-OFDM-IDMA symbol from each user should be written as follows:

$$\begin{aligned} \mathbf{R}_u &\triangleq [R_u(0), \ldots, R_u(n) \ldots, R_u(K-1)] \\ &= \mathbf{E}_{u,1} \mathfrak{h}_{u,1} \mathbf{X}_{u,1} + \mathbf{E}_{u,2} \mathfrak{h} \mathbf{X}_{u,2} \end{aligned} \tag{3.27}$$

where $\mathbf{E}_{u,\mathbf{p}} = \mathrm{diag}\left[1, e^{j2\pi\epsilon_{u,\mathbf{p}}/K}, \ldots, e^{j2\pi(K-1)\epsilon_{u,\mathbf{p}}/K}\right]$, $\epsilon_{u,\mathbf{p}}$ is the normalized CFO and $\mathfrak{h}_{u,\mathbf{p}}$ is the channel circulant matrix defined as follows (See chapter 1 in

3. Frequency Synchronization and Channel Equalization of OFDM-IDMA Uplink Systems

section 1.4.2.2):

$$
\mathfrak{h}_{u,\mathsf{p}} =
\begin{bmatrix}
h_{u,\mathsf{p}}(0) & 0 & \ldots & h_{u,\mathsf{p}}(L_{u,\mathsf{p}}-1) & \ldots & h_{u,\mathsf{p}}(1) \\
h_{u,\mathsf{p}}(1) & h_u(0) & \ddots & 0 & \ddots & h_{u,\mathsf{p}}(2) \\
\vdots & \ddots & \ddots & \ddots & \ddots & \vdots \\
h_{u,\mathsf{p}}(L_u-1) & h_{u,\mathsf{p}}(L_{u,\mathsf{p}}-2) & \ddots & 0 & \ddots & 0 \\
0 & h_{u,\mathsf{p}}(L_u-1) & \ddots & h_{u,\mathsf{p}}(0) & \ddots & \vdots \\
\vdots & \ddots & \ddots & \ddots & \ddots & \vdots \\
0 & 0 & \ldots & h_{u,\mathsf{p}}(L_{u,\mathsf{p}}-2) & \ldots & h_{u,\mathsf{p}}(0)
\end{bmatrix}
\tag{3.28}
$$

Finally, the received signal at the BS is a superposition of the contributions from the U active users:

$$
\begin{aligned}
\mathbf{R} &\triangleq [R(0,\ldots,R(n)\ldots,R(K-1)] \\
&= \sum_{u=1}^{U} \mathbf{R}_u + \mathbf{B}(n)
\end{aligned}
\tag{3.29}
$$

where $\mathbf{B}(n)$ is a zero-mean AWGN noise vector with covariance matrix $\mathbf{I}_K \sigma_B^2$. As in section 3.2, the CP-OFDM is performed without any CFO correction. Then, after some manipulations (See section 3.2), the received samples $r(k)$ and $r(k+1)$ can be expressed can be expressed as:

$$
r(k) = \sum_{u=1}^{U} \{ H_{u,1}^{(eq)}(k) S_u(k) + H_{u,2}^{(eq)}(k) S_u(k+1) \} + ICI(k) + b(k)
$$

$$
\begin{aligned}
r(k+1) = &\sum_{u=1}^{U} \{ -H_{u,1}^{(eq)}(k+1) S_u^*(k+1) + H_{u,2}^{(eq)}(k+1) S_u^*(k) \} \\
&+ ICI(k+1) + b(k+1)
\end{aligned}
$$

where $H_{u,\mathsf{p}}^{(eq)}(k) = \mathcal{F}(\epsilon_{u,\mathsf{p}}) H_{u,\mathsf{p}}(k)$ for $\mathsf{p} \in \{1,2\}$ and $ICI(k)$ is a zero-mean Gaussian ICI with variance $\sigma_{ICI}^2 = \mathbb{E}\{|ICI(\epsilon,k)|^2\}$ caused by all the CFOs. In addition, $b(k) = \sum_{n=0}^{K-1} B(n) e^{-\frac{j2\pi nk}{K}}$, $\mathcal{F}(\epsilon_{u,\mathsf{p}})$ is defined in (3.5) and

$$
H_{u,\mathsf{p}}(k) = \sum_{l=0}^{L_{\mathsf{s},\mathsf{p}}-1} h_{u,\mathsf{p}}(l) e^{-\frac{j2\pi lk}{K}} \quad \text{for} \mathsf{p} \in \{1,2\}
\tag{3.30}
$$

In the following, we show that the transmitted bits can be recovered by taking into account the ICI characteristics in the IDMA receiver. As it is necessary to

know the values of CFOs and the CSIs at the IDMA receiver, the estimation of these vectors is presented in the next subsection.

3.3.2   Multiple CFO and Channel Estimation

Let us define the vector $\mathbf{x}(n)$ of size $\mathcal{U} = 2(U + L)$, which is the state vector of the system (3.29):

$$\mathbf{x}(n) = \left[\begin{array}{ccc} \boldsymbol{\epsilon}(n) & Re\left\{\mathbf{h}(n)\right\} & Im\left\{\mathbf{h}(n)\right\} \end{array} \right]^T \tag{3.31}$$

Now let us introduce the state-space representation[1] of the system estimate the CFO and the channel:

State equation:

$$\mathbf{x}(n) = \mathbf{x}(n-1) + \mathbf{w}(n) \quad \forall \quad n \in [0, K-1] \tag{3.32}$$

Measurement equation:

$$\mathbf{Y}(n) = \mathbf{C}(n, \mathbf{x}(n)) + \boldsymbol{\mathcal{B}}(n) \quad \forall \quad n \in [0, K-1] \tag{3.33}$$

where $\mathbf{w}(n)$ is an AWGN matrix with zero-mean and covariance matrix $\sigma_w^2 \mathbf{I}_{\mathcal{U}}$, $\mathbf{Y}(n)$ is the observation 2×1 vector that stores the real and the imaginary parts of the STBC-OFDM-IDMA symbol $R(n)$, $\boldsymbol{\mathcal{B}}(n)$ is an AWGN matrix with zero-mean and covariance matrix $\sigma_B^2 \mathbf{I}_2$.

The SPKF detailed in appendix E is used to estimate the CFOs and the channels. After the time synchronization and CP removing, the CFOs and channels are estimated. Then, the OFDM demodulation is performed without any CFO correction and the obtained samples are inserted in the MRC receiver presented in the next subsection.

3.3.3   Maximum Ratio Combining Operations

Given the estimates of the CFOs and the channels, we can obtain the value of $\hat{H}_{u,\mathbf{p}}^{(\text{eq})}$. Assume that $S_u(k)$ and $S_u(k+1)$ are two successive symbols. Then, $\hat{S}_u(k)$

---

[1]As in section 3.2.1, the state-space representation represents what happens during one STBC-OFDM-IDMA frame.

and $\hat{S}_u(k+1)$ are the decisions obtained by the MRC of two successive received symbols $r(k)$ and $r(k+1)$, and the channel frequency responses $\hat{H}_u^{(\mathrm{eq})}$ [Alam 98]:

$$\hat{S}_u(k) = \sum_{u'=1}^{U} \{\hat{H}_{u,1}^{(\mathrm{eq})*}(k)\hat{H}_{u',1}^{(\mathrm{eq})}(k) + \hat{H}_{u,2}^{(\mathrm{eq})}(k+1)\hat{H}_{u',2}^{(\mathrm{eq})*}(k+1)\}S_u(k)$$

$$+ \sum_{u'=1}^{U} \{\hat{H}_{u,1}^{(\mathrm{eq})*}(k)\hat{H}_{u',2}^{(\mathrm{eq})}(k) - \hat{H}_{u,2}^{(\mathrm{eq})}(k+1)\hat{H}_{u',1}^{(\mathrm{eq})*}(k+1)\}S_u(k+1)$$

$$+ \hat{H}_{u,1}^{(\mathrm{eq})*}(k)\{ICI(\epsilon,k)+b(k)\} + \hat{H}_{u,2}^{(\mathrm{eq})}(k+1)\{ICI^*(\epsilon,k+1)+b^*(k+1)\}$$

$$(3.34)$$

$$\hat{S}_u(k+1) = \sum_{u'=1}^{U} \{\hat{H}_{u,1}^{(\mathrm{eq})}(k+1)\hat{H}_{u',1}^{(\mathrm{eq})*}(k+1) + \hat{H}_{u,2}^{(\mathrm{eq})*}(k)\hat{H}_{u',2}^{(\mathrm{eq})}(k)\}S_u(k+1)$$

$$+ \sum_{u'=1}^{U} \{\hat{H}_{u,2}^{(\mathrm{eq})*}(k)\hat{H}_{u',1}^{(\mathrm{eq})}(k) - \hat{H}_{u,1}^{(\mathrm{eq})}(k+1)\hat{H}_{u',2}^{(\mathrm{eq})*}(k+1)\}S_u(k)$$

$$+ \hat{H}_{u,2}^{(\mathrm{eq})*}(k)\{ICI(\epsilon,k)+b(k)\}$$

$$+ \hat{H}_{u,1}^{(\mathrm{eq})}(k+1)\{ICI^*(\epsilon,k+1)+b^*(k+1)\}^*$$

$$(3.35)$$

Then, the values $\hat{S}_u(k)$ and $\hat{S}_u(k+1)$ are inserted in the ESE presented in the next subsection.

3.3.4 Modified Elementary Signal Estimator

Then, given the outputs of the MRC $\hat{S}(k)$ and $\hat{S}(k+1)$, the values of $\hat{H}_u^{(eq)}(k)$, the additive-noise variance σ_B^2, the ICI variance σ_{ICI}^2 and $g_u^{\mathrm{ESE}}(k)$, the IDMA reception is performed.

It should be noted that (3.34) and (3.35) can be rewritten as:

$$\hat{S}_u(k) = \{||\hat{H}_{u,1}^{(\mathrm{eq})}(k)||^2 + ||\hat{H}_{u,2}^{(\mathrm{eq})}(k+1)||^2\}S_u(k) + \varsigma_u(k)$$

$$\hat{S}_u(k+1) = \{||\hat{H}_{u,1}^{(\mathrm{eq})}(k+1)||^2 + ||\hat{H}_{u,2}^{(\mathrm{eq})}(k)||^2\}S_u(k+1)$$

$$+\varsigma_u(k+1) \qquad (3.36)$$

and the distortions $\varsigma_u(k)$ and $\varsigma_u(k+1)$ contained in the output values of the MRC can be expressed as:

$$\varsigma_u(k) = \sum_{\substack{u'=1 \\ u'\neq u}}^{U} \{\hat{H}_{u,1}^{\text{(eq)}*}(k)\hat{H}_{u',1}^{\text{(eq)}}(k) + \hat{H}_{u,2}^{\text{(eq)}}(k+1)H_{u',2}^{\text{(eq)}*}(k+1)\}S_u(k)$$

$$+ \sum_{\substack{u'=1 \\ u'\neq u}}^{U} \{\hat{H}_{u,1}^{\text{(eq)}*}(k)H_{u',2}^{\text{(eq)}}(k) - \hat{H}_{u,2}^{\text{(eq)}}(k+1)H_{u',1}^{\text{(eq)}*}(k+1)\}S_u(k+1) \quad (3.37)$$

$$+ \hat{H}_{u,1}^{\text{(eq)}*}(k)\{ICI(\epsilon,k) + b(k)\}$$

$$+ \hat{H}_{u,2}^{\text{(eq)}}(k+1)\{ICI^*(\epsilon,k+1) + b^*(k+1)\}$$

$$\varsigma_u(k+1) = \sum_{\substack{u'=1 \\ u'\neq u}}^{U} \{\hat{H}_{u,1}^{\text{(eq)}}(k+1)H_{u',1}^{\text{(eq)}*}(k+1) + \hat{H}_{u,2}^{\text{(eq)}*}(k)\hat{H}_{u',2}^{\text{(eq)}}(k)\}S_u(k+1)$$

$$+ \sum_{\substack{u'=1 \\ u'\neq u}}^{U} \{\hat{H}_{u,2}^{\text{(eq)}*}(k)H_{u',1}^{\text{(eq)}}(k) - \hat{H}_{u,1}^{\text{(eq)}}(k+1)H_{u',2}^{\text{(eq)}*}(k+1)\}S_u(k)$$

$$+ \hat{H}_{u,2}^{\text{(eq)}*}(k)\{ICI(\epsilon,k) + b(k)\}$$

$$+ \hat{H}_{u,1}^{\text{(eq)}}(k+1)\{ICI^*(\epsilon,k+1) + b^*(k+1)\}$$

$$(3.38)$$

Then, assuming that $\mathbf{S}_u$ are independent and identically distributed, and applying the central limit theorem, a Gaussian approximation for $\varsigma_u(k)$ and $\hat{S}_u(k)$ can be considered. Thus, they can be completely characterized by their means and variances. The modified ESE process for the uth user at the ith iteration generates the value of the *a posteriori* LLR as follows:

$$\mathfrak{g}_u^{\text{ESE}}(k) = 2\{||\hat{H}_{u,1}^{\text{(eq)}}(k)||^2 + ||\hat{H}_{u,2}^{\text{(eq)}}(k)||^2\} \times \frac{\hat{S}_u(k) - \mathbb{E}(\varsigma_u(k))}{Var(\varsigma_u(k))} \quad \forall u \quad (3.39)$$

For the initialization process $g_u^{\text{ESE}}(k) = 0$ for $i = 1$, where i denotes the iteration number with $i \in \{1,\dots,\mathcal{I}^{idma}\}$, with $\mathcal{I}^{idma}$ the maximum number of iterations. The outputs of the modified ESE are inserted in the user decoding process presented in chapter 1 in section 1.4.3.2. Then, at the ith iteration for $i < \mathcal{I}^{idma}$, the outputs of the decoding process are the values of $g_u^{\text{ESE}}(k)$, that are reinserted in the ESE. The ESE process is again performed. Finally, the decoding process produces hard decisions to obtain the estimations of the transmitted bits during

the final iteration $\mathcal{J}^{idma}$. Figure 3.7 shows the proposed STBC-OFDM-IDMA
scheme.
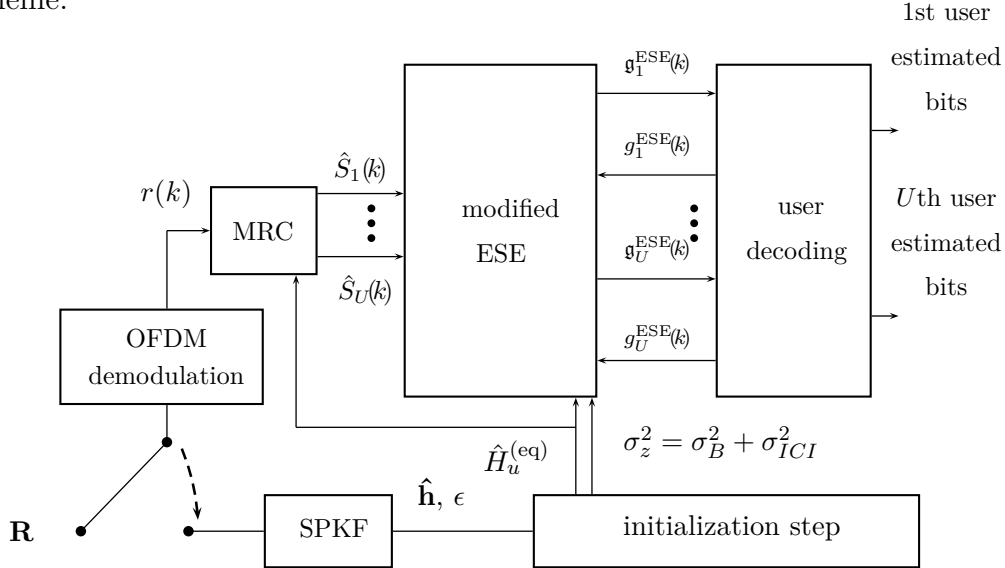
Figure 3.7: Proposed STBC-OFDM-IDMA uplink receiver, where the user decoding is the same as in figure 1.20

3.3.5 Simulation Results

Simulation protocol:

We consider an OFDM-IDMA uplink system composed of $U = 4$ users over
$K = 1024$ subcarriers. The spreading factor is $\mathbb{S} = 64$. BPSK is used to modulate
the information bits. The carrier frequency is at $f_c = 2.6$GHz and the channel
bandwidth is set to $W = 10$MHz. We consider that the ENC consists only
of the insertion of a spreading code. We define the SNR= $10\log(\frac{\sigma_u^2}{\sigma_B^2})$, where
σ_u^2 is the mean power of the received signal from the uth user, and the SIR=
$10\log(\frac{\sigma_u^2}{\sigma_{ICI}^2})$. We consider a transmission over a normalized Rayleigh slow-fading
frequency selective channel composed of $\forall u, \mathsf{p} \ L_{u,\mathsf{p}} = 1, 3$ multipaths. The CFOs
are modeled as random variables with a normal distribution with zero-mean and
variance 0.1. The number of iterations is set to 5. The estimations are obtained
using control data of one OFDM-IDMA symbol.

Figure 3.8 shows the CFO estimation performance in terms of MMSE of one user
in the system. The SPKF allows the CFO and the channel of the users to be

estimated. The MMSE for an AWGN channel and for channels with different length are presented. The channel estimation for different channel lengths give the same estimation performance, around 10^{-2} for a SNR= 0dB. The following
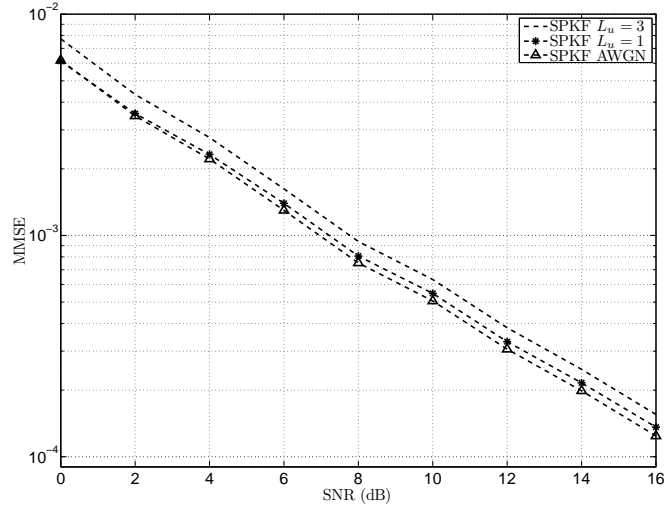
Figure 3.8: CFO estimation performance in terms of MMSE, SIR= 0dB

results are the average of 5000 OFDM-IDMA symbols. Figure 3.9 and 3.10 show the BER for a transmission over a normalized Rayleigh slow-fading frequency selective channel with $L_{u,\mathsf{p}} = 1$ and $L_{u,\mathsf{p}} = 3$ multipaths $\forall u, \mathsf{p}$ respectively. The efficiency of the OFDM-IDMA-STBC proposed scheme is confirmed, we can see that for a BER of 10^{-2} there are less than 1 dB between the curve without CFO and the curve of the proposed estimator. In addition, we can see a gain of around 3dB of the proposed scheme in comparison with the linear detection method presented in [Cao 04a].
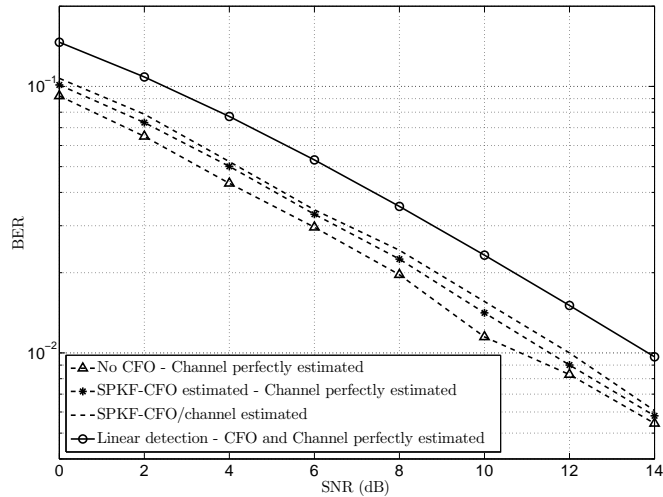
Figure 3.9: BER performance for a channel $L_u = 1$
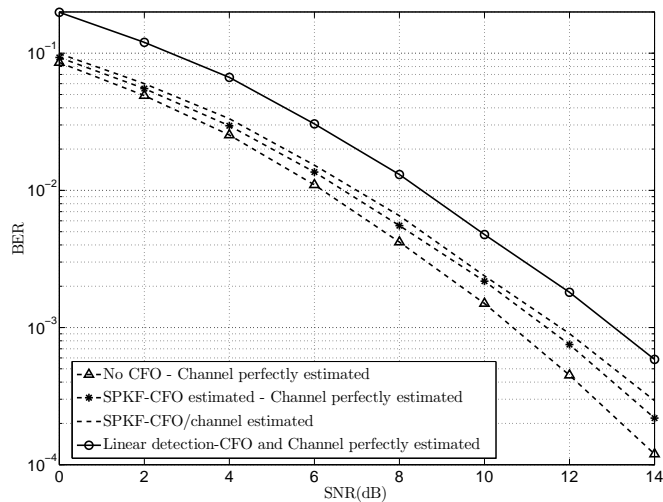
Figure 3.10: BER performance for a channel $L_u = 3$

3.4 Conclusions

In this section, two OFDM-IDMA receivers are proposed. A joint CFO/channel estimation is performed using a SPKF. Then, the estimated parameters are in-

serted in an IDMA iterative receiver. The IDMA receiver accurately estimates the transmitted symbols from all the users; the ICI produced by the CFOs is canceled, as well as the MAI. The receiver is robust against ISI thanks to the OFDM modulation and robust against the MAI due to the IDMA scheme. Unlike common approaches, the IDMA schemes also allow the CFO correction step to be skipped.

OFDM-IDMA systems allow a large number of users to transmit at the same time. We show that the proposed receiver outperforms existing CFO correction methods such as [Cao 04a].

In chapter 1, we mentioned that CR systems may be one solution to the problem induced by the exponential growth of the number of users in the system. As an alternative, OFDM-IDMA could be a solution to the overload produced by the constant increase of the user density per cell in cellular systems.

Conclusions and Perspectives

Estimating the CFOs and channels plays a key role in the design of mobile wireless systems. In this PhD, our purpose was to create new receiver schemes that take into account both phenomena. We have proposed to jointly estimate the CFOs and the channels for an OFDMA uplink system by using a recursive approach [Pove 10]. On the one hand, the EKF, the SOEKF, the IEKF and the SPKF including the UKF and the CDKF were considered. On the other hand, to relax the Gaussian assumptions on the model noise and measurement noise, the "extended H_∞ filter" and the "unscented H_∞ filter" were studied.

From the estimation point of view, we first compared the different Kalman techniques. We can draw the following conclusions:

1/ The SOEKF gives slightly "better" estimates of the CFO and the channels than the EKF in terms of estimation accuracy. Nevertheless, the computational cost of the SOEKF is higher than the EKF one, due to the calculation of the Hessian matrix for the second-order expansion.

2/ Concerning the SPKF, the UKF and the CDKF give the same results in terms of estimation accuracy. In addition, their computational costs are quite similar. They converge faster than the EKF and the SOEKF. They have the advantage of avoiding the calculation of Jacobians and Hessians matrices, but the Cholesky factor of the autocorrelation matrices must be computed.

3/ The IEKF gives the "best" estimation performance in terms of estimation accuracy and convergence speed. It needs less samples to converge to the true value than the other Kalman approaches. However, due to the calculation of the Jacobian matrix at each iteration, the computational complexity is the highest among the proposed approaches.

Let us now look at the relevance of the H_∞ approaches.

1/ the "unscented H_∞ filter" gives better estimation performance than the "extended H_∞ filter". In addition, its convergence is faster than the one of the "extended H_∞ filter".

2/ when the noise characteristics are available, the "extended H_∞ filter" and the

EKF give similar results. In addition, there is no real difference between the "unscented H_∞ filter" and the SPKF. If the noise variances are *a priori* unknown, the H_∞ approaches converge faster than the Kalman algorithms. Nevertheless, the noise attenuation level and the weighting matrices have to be chosen by the practitioner. If the noise attenuation level is set to a value that is too small, a solution to the H_∞ issue may not exist. If the noise attenuation level is set to a high value to guarantee the existence of a solution, the resulting H_∞ filter "looks like" the Kalman filter.

3/ The computational complexity of the "extended H_∞ filter" is slightly higher than the EKF while the computational cost of the "unscented H_∞ filter" is slightly higher than the SPKF.

Then, the above techniques have been compared with the EM-based algorithms proposed in [Pun 04a] and in [Pun 06] in terms of estimation accuracy and computational complexity. Even if the EM-based estimator gives better estimation performance, its computational complexity is much higher than the costs of the SPKF and the "unscented H_∞ filter". Our methods are therefore very useful for practical cases.

Based on the above considerations, we think that the SPKF gives the best compromise in terms of estimation performance, computational complexity and *a priori* information to be tuned.

From the digital communication point of view, the above optimal filtering techniques have been combined with an MMSE-SD to obtain a non-pilot aided CFO estimator for an OFDMA uplink [Pove 09a], [Pove 09b], [Pove 11c]. The MAI suppression scheme followed by the CFO estimation algorithm based on optimal filtering can jointly estimate and detect each user's CFO and symbols respectively. According to the simulations we carried out, the proposed scheme can effectively suppress the MAI caused by a relatively large CFO, and it is sufficiently robust to CFO variations. The iterative decoding applies simple hard interference cancellation techniques, resulting in a moderate complexity.

Then, the SPKF has been chosen to be combined with two statistical tests: the

BHT and the CUSUM test [Pove 11b], [Pove 11d] to detect the beginning and the end of a CR-NBI disturbing the estimation of the CFOs and the channels of different users in a PU-OFDMA system. The proposed estimator operates in the time domain unlike other approaches such as [More 08] that estimate the CFO in presence of an NBI in the frequency domain. By using a SPKF and without increasing the computational complexity, we take advantage of the innovation in the Kalman filter to detect the CR-NBI. When using the BHT, better performance are obtained in terms of the CR-NBI probability of detection. However, when using the CUSUM, better performance in terms of PU probability of detection are obtained. The results show that the SPKF without the statistical tests is not able to estimate the CFO of each user. The proposed estimator outperforms the existing CFO estimation methods such as [More 08] in presence of NBI and it is robust to the NBI power. Nevertheless, the architecture is sensitive to the duration in time of the CR-NBI.

We have also proposed to combine the SPKF with a modified version of an iterative IDMA receiver to design a new OFDM-IDMA receiver [Pove 12]. Simulation results show that the SPKF provides "accurate" estimations of the CFO and the channel of each user. In addition, the modified OFDM-IDMA receiver accurately estimates the transmitted bits of each user, by taking into account the estimations of the SPKF and the interference produced by the CFO. According to the simulation tests we carried out, our receiver outperforms CFO correction methods proposed for other multicarrier systems such as [Cao 04a].

Our last contribution consists in combining the SPKF with a STBC and a new variant of an iterative IDMA receiver to take advantage of the space diversity [Pove 11a]. The simulation results confirm that the SPKF provides accurate estimations of the CFO and the channel. In addition, the STBC-OFDM-IDMA receiver can accurately estimate the transmitted bits of each user. We show that the proposed receiver outperforms existing CFO correction methods such as [Cao 04a].

Currently, we are working on the sensitivity analysis of the optimal filtering techniques in the non-linear case. We are studying the local sensitivity of the Kalman filtering and the H_∞ filtering regarding perturbations. For this purpose

we take advantage of appendix C.

In the future, we propose to address the estimation issue by using a quadrature Kalman filter (QKF) [Ito 00], which avoids the linearization step by using the Gauss-Hermite numerical integration rule. In addition, the relevance of the "second-order H_∞ filter" [Hu 11] could be investigated.

In this PhD, some assumptions have been made. For instance, we suppose that the radio-frequency (RF) power amplifier (PA) is used below its saturation point to guarantee a linear behavior of the PA. However, this may lead to a poor power efficiency, especially when the transmitted signal exhibits high PAPR[1]. One solution would be to use the PA closer to its saturation point, but this induces nonlinear distortion of the transmitted signal. In [Roli 09], non-linear models for the PA such as the Volterra model can be considered. In the future, we could design new architectures to compensate the influence of these non-linearities.

In addition, in the future we propose to investigate an OFDM-IDMA with a sufficiently long CP that allows a transmission in an asynchronous way. We could study this non-optimal characteristic from a point of view of the spectral efficiency to allow all the users to use the same interleaver.

---

[1]Due to the large number of independent modulated subcarriers that are added up coherently, the transmitted signal exhibits a high PAPR.

Kalman Filter - Linear Case

Firstly presented in [Kalm 60] by Rudolf E. Kalman, the Kalman filter (KF) is based on a state-space representation of the system. It has been used in a wide range of applications, from speech enhancement to time-varying autoregressive parameters tracking, from biomedical applications to mobile communications. It uses two equations to describe the system. When the state-space equations are linear and the noises are additive white zero-mean Gaussian processes, they satisfy:

State equation:

$$\mathbf{x}(n) = \mathbf{\Phi}(n-1)\mathbf{x}(n-1) + \mathbf{\Gamma}\mathbf{w}(n) \tag{A.1}$$

Measurement equation:

$$\mathbf{y}(n) = \mathbf{\Psi}(n)\mathbf{x}(n) + \mathbf{b}(n) \tag{A.2}$$

where $\mathbf{x}(n)$ is the state vector[1] of size U at time n and $\mathbf{y}(n)$ is the measurement vector of size K at time n. The model noise $\mathbf{w}$ and the observation noise $\mathbf{b}$ are uncorrelated white zero-mean Gaussian vectors with covariance matrices assumed to be $\mathbf{Q} = \sigma_w^2 \mathbf{I}_U$ and $\mathbf{R} = \sigma_b^2 \mathbf{I}_K$ respectively. In addition, $\mathbf{\Phi}(n-1)$ is the transition matrix of size $U \times U$ from time $n-1$ to n, $\mathbf{\Gamma}$ is the input gain matrix of size $U \times U$ and $\mathbf{\Psi}(n)$ is the measurement matrix $K \times U$ at time n.

The KF operates in two steps: the prediction step and the filtering step.

In the prediction step, the KF uses the estimated state at the previous instant to estimate the current state, without taking into account the current observation. This is the so-called *a priori* estimation of the state vector defined as follows:

$$\hat{\mathbf{x}}(n|n-1) = \mathbb{E}\left[\mathbf{x}(n)|\mathbf{y}(0), \mathbf{y}(1), \ldots, \mathbf{y}(n-1)\right] \tag{A.3}$$

---

[1] The state vector stores the set of parameters of the system, necessary for prediction when the input is known. In practical cases, it usually contains the unknown quantities to be estimated.
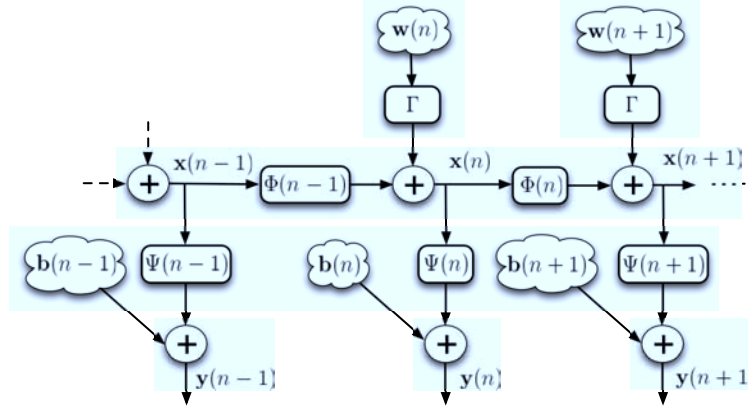
Figure A.1: Kalman filter - system model

Given (A.1) and (A.3) and as **w** is a zero-mean AWGN, the *a priori* estimation of the state vector can be expressed as follows:

$$\hat{\mathbf{x}}(n|n-1) = \boldsymbol{\Phi}(n-1)\hat{\mathbf{x}}(n-1|n-1) \tag{A.4}$$

where $\hat{\mathbf{x}}(n-1|n-1)$ is the estimation of the state vector at time $n-1$ given the set of observations $[\mathbf{y}(0), \mathbf{y}(1), \ldots, \mathbf{y}(n-1)]$.

Then, let us introduce the *a priori* estimation error:

$$\tilde{\mathbf{x}}(n|n-1) = \mathbf{x}(n) - \hat{\mathbf{x}}(n|n-1) \tag{A.5}$$

and its corresponding covariance matrix $\mathbf{P}(n|n-1)$ defined by:

$$\mathbf{P}(n|n-1) = \mathbb{E}\left[\tilde{\mathbf{x}}(n|n-1)\tilde{\mathbf{x}}^{H}(n|n-1)\right] \tag{A.6}$$

Given (A.1) and (A.4), the *a priori* estimation error of the state vector can be rewritten as:

$$
\begin{aligned}
\tilde{\mathbf{x}}(n|n-1) &= \boldsymbol{\Phi}(n-1)\mathbf{x}(n-1) + \boldsymbol{\Gamma}\mathbf{w}(n) - \boldsymbol{\Phi}(n-1)\hat{\mathbf{x}}(n-1|n-1) \\
&= \boldsymbol{\Phi}(n-1)\tilde{\mathbf{x}}(n-1|n-1) + \boldsymbol{\Gamma}\mathbf{w}(n)
\end{aligned}
\tag{A.7}
$$

Then, the covariance matrix of $\tilde{\mathbf{x}}(n|n-1)$ satisfies:

$$
\begin{aligned}
\mathbf{P}(n|n-1) &= \boldsymbol{\Phi}(n-1)\mathbb{E}\left[\tilde{\mathbf{x}}(n-1|n-1)\tilde{\mathbf{x}}^{H}(n-1|n-1)\right]\boldsymbol{\Phi}^{H}(n-1) \\
&\quad + \boldsymbol{\Gamma}\mathbb{E}\left[\tilde{\mathbf{w}}(n)\tilde{\mathbf{w}}^{H}(n)\right]\boldsymbol{\Gamma}^{H} \\
&= \boldsymbol{\Phi}(n-1)\mathbf{P}(n-1|n-1)\boldsymbol{\Phi}^{H}(n-1) + \boldsymbol{\Gamma}\boldsymbol{\Omega}\boldsymbol{\Gamma}^{H}
\end{aligned}
\tag{A.8}
$$

At that stage, the filtering step uses the current observation to correct the *a priori* estimated state vector, in order to obtain the *a posteriori* estimation. To estimate the current state and by following the kind of update equation obtained in the RLS algorithm, one has:

$$\hat{\mathbf{x}}(n|n) = \hat{\mathbf{x}}(n|n-1) + \mathbf{K}(n)\tilde{\mathbf{y}}(n) \tag{A.9}$$

where $\mathbf{K}(n)$ is the Kalman gain and $\tilde{\mathbf{y}}(n)$ is the innovation defined as:

$$\begin{aligned}
\tilde{\mathbf{y}}(n) &= \mathbf{y}(n) - \hat{\mathbf{y}}(n|n-1) \\
&= \mathbf{y}(n) - \mathbf{\Psi}(n)\hat{\mathbf{x}}(n|n-1)
\end{aligned} \tag{A.10}$$

with $\hat{\mathbf{y}}(n|n-1)$ the prediction of $\mathbf{y}(n)$ based on $\hat{\mathbf{x}}(n|n-1)$.

The Kalman gain is defined to obtain the MMSE estimation of the state vector. This means that:

$$\frac{\partial\left(\mathbb{E}\left[\mathbf{x}^H(n|n)\mathbf{x}(n|n)\right]\right)}{\partial\mathbf{K}(n)} = \frac{\partial tr(\mathbf{P}(n|n))}{\partial\mathbf{K}(n)} = \underline{\mathbf{0}} \tag{A.11}$$

and it satisfies:

$$\mathbf{K}(n) = \{\mathbf{P}^{\mathbf{xy}}(n)\}\{\mathbf{P}^{\mathbf{yy}}(n)\}^{-1} \tag{A.12}$$

where $\mathbf{P}^{\mathbf{yy}}(n)$ is the innovation covariance matrix defined as follows:

$$\mathbf{P}^{\mathbf{yy}}(n) = \mathbf{\Psi}(n)\mathbf{P}(n|n-1)\mathbf{\Psi}^H(n) + \mathcal{R} \tag{A.13}$$

and $\mathbf{P}^{\mathbf{xy}}(n)$ is the cross-covariance matrix between $\mathbf{y}(n)$ and the state prediction $\hat{\mathbf{x}}(n|n-1)$ defined as:

$$\mathbf{P}^{\mathbf{xy}}(n) = \mathbf{P}(n|n-1)\mathbf{\Psi}^H(n) \tag{A.14}$$

Finally, by combining (A.9) and (A.12) it can be easily shown that the error estimation covariance matrix is updated as follows:

$$\begin{aligned}
\mathbf{P}(n|n) &= \mathbf{P}(n|n-1) - \mathbf{K}(n)\mathbf{\Psi}(n)\mathbf{P}(n|n-1) \\
&= \{\mathbf{I}_U - \mathbf{K}(n)\mathbf{\Psi}(n)\}\mathbf{P}(n|n-1)
\end{aligned} \tag{A.15}$$

Given (A.8) adjusted to the set of observations $\{\mathbf{y}(1),\ldots,\mathbf{y}(n)\}$ instead of $\{\mathbf{y}(1),\ldots,\mathbf{y}(n-1)\}$, (A.12) and (A.15), the error estimation covariance matrix

satisfies the following Riccati equation[1] for the Kalman filter:

$$\begin{aligned}
\mathbf{P}(n+1|n) &\underset{(A.8)}{=} \mathbf{\Phi}(n)\mathbf{P}(n|n)\mathbf{\Phi}^H(n) + \mathbf{\Gamma}\mathbf{\Omega}\mathbf{\Gamma}^H \\
&\underset{(A.15)}{=} \mathbf{\Phi}(n)\{\mathbf{I}_U - \mathbf{K}(n)\mathbf{\Psi}(n)\}\mathbf{P}(n|n-1)\mathbf{\Phi}^H(n) + \mathbf{\Gamma}\mathbf{\Omega}\mathbf{\Gamma}^H \\
&\underset{(A.12)}{=} \mathbf{\Phi}(n)\{\mathbf{I}_U - \mathbf{P}(n|n-1)\mathbf{\Psi}^H(n)\{\mathbf{\Psi}(n)\mathbf{P}(n|n-1)\mathbf{\Psi}^H(n) + \mathbf{\mathcal{R}}\}^{-1} \\
&\quad \times \mathbf{\Psi}(n)\}\mathbf{P}(n|n-1)\mathbf{\Phi}^H(n) + \mathbf{\Gamma}\mathbf{\Omega}\mathbf{\Gamma}^H
\end{aligned}$$

$$(A.16)$$

The Kalman filter can also be derived from a Bayesian MAP perspective [VdMe 04a]. Indeed, (A.3) can be expressed as:

$$\hat{\mathbf{x}}(n|n-1) = \int \mathbf{x}(n)\mathcal{P}\{\mathbf{x}(n)|\mathbf{Y}(n-1)\}d\mathbf{x}(n) \tag{A.17}$$

where $\mathcal{P}\{\mathbf{x}(n)|\mathbf{Y}(n-1)\} = \mathcal{P}\{\mathbf{x}(n)|\mathbf{y}(0),\mathbf{y}(1),\ldots,\mathbf{y}(n-1)\}$ is the *a priori* probability density of the state vector. As it is Gaussian, it can be completely characterized by its mean and its covariance matrix. Then, by using the Bayes rule the *a posteriori* probability density can be obtained as follows:

$$\begin{aligned}
\mathcal{P}\{\mathbf{x}(n)|\mathbf{Y}(n)\} &= \mathcal{P}\{\mathbf{x}(n)|\mathbf{y}(0),\mathbf{y}(1),\ldots,\mathbf{y}(n)\} \\
&= \frac{\mathcal{P}\{\mathbf{Y}(n)|\mathbf{x}(n)\}\mathcal{P}\{\mathbf{x}(n)\}}{\mathcal{P}\{\mathbf{Y}(n)\}} \\
&= \frac{\mathcal{P}\{\mathbf{y}(n),\mathbf{Y}(n-1)|\mathbf{x}(n)\}\mathcal{P}\{\mathbf{x}(n)\}}{\mathcal{P}\{\mathbf{y}(n),\mathbf{Y}(n-1)\}} \\
&= \frac{\mathcal{P}\{\mathbf{y}(n)|\mathbf{Y}(n-1),\mathbf{x}(n)\}\mathcal{P}\{\mathbf{Y}(n-1)|\mathbf{x}(n)\}\mathcal{P}\{\mathbf{x}(n)\}}{\mathcal{P}\{\mathbf{y}(n)|\mathbf{Y}(n-1)\}\mathcal{P}\{\mathbf{Y}(n-1)\}} \\
&= \frac{\mathcal{P}\{\mathbf{y}(n)|\mathbf{Y}(n-1),\mathbf{x}(n)\}\mathcal{P}\{\mathbf{x}(n)|\mathbf{Y}(n-1)\}\mathcal{P}\{\mathbf{Y}(n-1)\}\mathcal{P}\{\mathbf{x}(n)\}}{\mathcal{P}\{\mathbf{y}(n)|\mathbf{Y}(n-1)\}\mathcal{P}\{\mathbf{Y}(n-1)\}\mathcal{P}\{\mathbf{x}(n)\}} \\
&= \frac{\mathcal{P}\{\mathbf{y}(n)|\mathbf{x}(n)\}\mathcal{P}\{\mathbf{x}(n)|\mathbf{Y}(n-1)\}}{\mathcal{P}\{\mathbf{y}(n)|\mathbf{Y}(n-1)\}}
\end{aligned}$$

$$(A.18)$$

Then, maximizing $\mathcal{P}\{\mathbf{x}(n)|\mathbf{Y}(n)\}$ consists in maximizing the numerator of (A.18).

---

[1]The Riccati equation is defined as: $\mathbf{P} = \mathbf{A}\{\mathbf{I} - \mathbf{P}\mathbf{B}^H(\mathbf{B}\mathbf{P}\mathbf{B}^H + \mathbf{R})^{-1}\mathbf{B}\}\mathbf{P}\mathbf{A}^H + \mathbf{Q}$.

Appendix B

H$_\infty$ Filter - Linear Case

The H$_\infty$ approach was introduced in the field of control in 1981 [Zame 81]. A solution of the H$_\infty$ estimation problem can be based on polynomial decomposition techniques [Grim 90]. Nevertheless, they lead to equations with high-computational cost that cannot be used in practical situations. As an alternative solution, state-space approaches have emerged. In [Gero 99], the author presents a solution of the H$_\infty$ estimation constraint, based on the resolution of a convex optimization problem under linear matrix inequality constraints approaches. In [Shak 92], Shaked *et al.* present a state-space approach solution based on the resolution of a quadratic Riccati-type equation. This algorithm is easy to implement and has a lower computational cost than the above approaches.

The H$_\infty$ filter has been widely used in the field of control. For the last 12 years, several studies have been conducted by the signal processing community.

In [Shen 99], instead of using a Kalman filtering, Shen *et al.* suggest using an H$_\infty$ filter to enhance a speech signal disturbed by an additive noise and recorded from a single microphone. For this purpose, the signal is assumed to be modeled by an AR process. However, the AR parameters are unknown and hence need to be estimated. Shen *et al.* propose to estimate them directly from the noisy observations by using a second H$_\infty$ filter. Therefore, the resulting AR parameter estimates are biased, as pointed out by Labarre *et al.* in [Laba 05], who investigated the relevance of the H$_\infty$ filtering for speech enhancement. To avoid the problem of biased AR parameter estimates that can be obtained in [Shen 99], Labarre *et al.* suggest estimating both the AR model and its parameters. Although this leads to a non-linear estimation issue, they have developed a structure based on two mutually interactive standard H$_\infty$ filters [Laba 07]. The first one aims at estimating the AR model, while the second one updates the estimation of the AR parameters. In addition, in [Jamo 07a], the authors take advantage

of the two mutually interactive H$_\infty$ filter based approach to jointly estimate the fading channel and its AR parameters. However, the authors do not obtain better performance than a KF based method.

Let us now look more carefully at the H$_\infty$ filtering approach. Given the state-space model in (A.1) and (A.2), let us introduce a third state-space equation to focus on a linear combination of the state-vector components:

$$\mathbf{z}(n) = \mathcal{L}\mathbf{x}(n) \tag{B.1}$$

where $\mathcal{L}$ is a linear transformation operator that can be either a matrix of size $U \times U$ or a row vector of size U. $\mathbf{z}(n)$ is hence a vector or a scalar.

Given (A.1), (A.2), (B.1) and figure B.1, the H$_\infty$ filtering provides the estimation of the state vector, by minimizing the H$_\infty$ norm of the transfer operator that maps the discrete-time noise disturbances[1] to the estimation error, as follows:

$$J^\infty = \sup \frac{\sum_{n=0}^{N^{ob}-1} \|\mathbf{e}(n)\|^2}{\mathcal{V}^{-1}\sum_{n=0}^{N^{ob}-1} \|\mathbf{b}(n)\|^2 + \mathcal{W}^{-1}\sum_{n=0}^{N^{ob}-1} \|\mathbf{w}(n)\|^2 + \mathbf{e}^H(n)\mathbf{P}(0)\mathbf{e}(n)} \tag{B.2}$$

where N^{ob} denotes the number of available observations, $\mathbf{e}(n) = \mathbf{z}(n) - \hat{\mathbf{z}}(n)$, and $\mathcal{V}$ and $\mathcal{W}$ are positive weighting matrices tuned by the practitioner to achieve performance requirements.

Figure B.1: Transfer operator from disturbances to estimation error for H$_\infty$-norm based estimation

---

[1]Namely $\mathbf{w}(n)$, $\mathbf{b}(n)$ and the initial conditions on the state vector.

Since the minimization of (B.2) is often impossible, the following sub-optimal H$_\infty$ problem is usually considered:

$$J^\infty < \Xi^2 \tag{B.3}$$

where Ξ^2 is the prescribed noise attenuation level.

At that stage, $\mathbf{P}^\infty(n+1|n)$ satisfies the following Riccati equation for the H_∞ filter:

$$
\begin{aligned}
\mathbf{P}^\infty(n+1|n) &= \boldsymbol{\Phi}(n)\mathbf{P}^\infty(n|n)\boldsymbol{\Phi}^H(n) + \boldsymbol{\Gamma}\mathcal{W}\boldsymbol{\Gamma}^H \\
&= \boldsymbol{\Phi}(n)\mathbf{P}^\infty(n|n-1)\{\mathbf{I}_U - \begin{bmatrix} \boldsymbol{\Psi}^H(n) & \mathcal{L}^H \end{bmatrix} \\
&\quad \times \mathbb{M}^{-1} \begin{bmatrix} \boldsymbol{\Psi}(n) \\ \mathcal{L} \end{bmatrix} \mathbf{P}^\infty(n|n-1)\}\boldsymbol{\Phi}^H(n) + \boldsymbol{\Gamma}\mathcal{W}\boldsymbol{\Gamma}^H
\end{aligned}
\tag{B.4}
$$

where

$$
\begin{aligned}
\mathbb{M} &= \begin{bmatrix} \mathcal{V} & \mathbf{0} \\ \mathbf{0} & -\Xi^2\mathbf{I}_U \end{bmatrix} + \begin{bmatrix} \boldsymbol{\Psi}(n) \\ \mathcal{L} \end{bmatrix} \mathbf{P}^\infty(n|n-1) \begin{bmatrix} \boldsymbol{\Psi}^H(n) & \mathcal{L}^H \end{bmatrix} \\
&= \begin{bmatrix} \boldsymbol{\Psi}(n)\mathbf{P}^\infty(n|n-1)\boldsymbol{\Psi}^H(n) + \mathcal{V} & \boldsymbol{\Psi}(n)\mathbf{P}^\infty(n|n-1)\mathcal{L}^H \\ \mathcal{L}\mathbf{P}^\infty(n|n-1)\boldsymbol{\Psi}^H(n) & \mathcal{L}\mathbf{P}^\infty(n|n-1)\mathcal{L}^H - \Xi^2\mathbf{I}_U \end{bmatrix}
\end{aligned}
\tag{B.5}
$$

Remark: if $\mathcal{L} = \mathbf{I}_U$, one has:

$$
\mathbb{M} = \begin{bmatrix} \boldsymbol{\Psi}(n)\mathbf{P}^\infty(n|n-1)\boldsymbol{\Psi}^H(n) + \mathcal{V} & \boldsymbol{\Psi}(n)\mathbf{P}^\infty(n|n-1) \\ \mathbf{P}^\infty(n|n-1)\boldsymbol{\Psi}^H(n) & \mathbf{P}^\infty(n|n-1) - \Xi^2\mathbf{I}_U \end{bmatrix}
\tag{B.6}
$$

When using the H$_\infty$ filter, the state vector can be estimated recursively as follows:

$$\hat{\mathbf{x}}(n|n) = \hat{\mathbf{x}}(n|n-1) + \mathbf{K}^\infty(n)\tilde{\mathbf{y}}(n) \tag{B.7}$$

where $\mathbf{K}^\infty(n)$ is the H$_\infty$ filter gain defined as:

$$\mathbf{K}^\infty(n) = \{\mathbf{P}^{\mathbf{xy}\infty}(n)\}\{\mathbf{P}^{\mathbf{yy}\infty}(n)\}^{-1} \tag{B.8}$$

where $\mathbf{P}^{\mathbf{yy}\infty}(n)$ is defined as follows:

$$\mathbf{P}^{\mathbf{yy}\infty}(n) = \boldsymbol{\Psi}(n)\mathbf{P}^\infty(n|n-1)\boldsymbol{\Psi}^H(n) + \mathcal{V} \tag{B.9}$$

and $\mathbf{P}^{\mathbf{xy}\infty}(n)$ is:

$$\mathbf{P}^{\mathbf{xy}\infty}(n) = \mathbf{P}^\infty(n|n-1)\boldsymbol{\Psi}^H(n) \tag{B.10}$$

(B.4) is true provided that:

$$\mathbf{P}^\infty(n+1|n)^{-1} + \mathbf{\Psi}^H(n)\mathbf{\Psi}(n) - \Xi^{-2}\mathcal{L}^H\mathcal{L} > 0 \qquad \text{(B.11)}$$

It should be noted that the purpose of the H$_\infty$ filter is to minimize the peak error power in the frequency domain whereas the Kalman filter minimizes the average error power [Grim 90].

Appendix C

Kalman Filter vs H$_\infty$ Filter

In this appendix, our purpose is to compare the H$_\infty$ filter and the KF in the linear case when estimating model parameters, by comparing the Ricatti equations of both algorithms. To our knowledge, there is no work dealing with this kind of comparison.

Let us first assume that:

$$\mathbf{P}^\infty(n|n-1) = \mathbf{P}(n|n-1) \tag{C.1}$$

and

$$\boldsymbol{\mathcal{L}} = \mathbf{I}_U \tag{C.2}$$

In addition, as it is often done when dealing with H$_\infty$ filter in signal processing, let us set $\boldsymbol{\mathcal{W}}$ and $\boldsymbol{\mathcal{V}}$ to $\boldsymbol{\mathcal{Q}}$ and $\boldsymbol{\mathcal{R}}$ respectively. This implies that:

$$\mathbf{K}^\infty(n) = \mathbf{K}(n) \tag{C.3}$$

and

$$\mathbf{P}^{\mathbf{yy}\infty}(n) = \mathbf{P}^{\mathbf{yy}}(n) \tag{C.4}$$

Then, let us compare $\mathbf{P}^\infty(n+1|n)$ and $\mathbf{P}(n+1|n)$. For this purpose, the matrix $\mathbb{M}$ defined in (B.6) must be inverted in (B.4). Among the approaches that could be considered such as the matrix inversion lemma, we suggest using the one based on the Schur complement [Brez 88] for the sake of simplicity[1]. Indeed by defining

---

[1]$\mathbf{M} = \begin{bmatrix} \mathbf{A} & \mathbf{B} \\ \mathbf{C} & \mathbf{D} \end{bmatrix}$, then $\mathbf{M}^{-1} = \begin{bmatrix} \mathbf{I}_K & -\mathbf{A}^{-1}\mathbf{B} \\ \mathbf{0} & \mathbf{I}_U \end{bmatrix} \begin{bmatrix} \mathbf{A}^{-1} & \mathbf{0} \\ \mathbf{0} & \mathbf{S}^{-1} \end{bmatrix} \begin{bmatrix} \mathbf{I}_K & \mathbf{0} \\ -\mathbf{C}\mathbf{A}^{-1} & \mathbf{I}_U \end{bmatrix}$
where $\mathbf{A}$ is matrix of size $K \times K$, $\mathbf{B}$ is matrix of size $K \times U$, $\mathbf{C}$ is matrix of size $U \times K$, $\mathbf{D}$ is matrix of size $U \times U$, $\mathbf{S} = \mathbf{D} - \mathbf{C}\mathbf{A}^{-1}\mathbf{B}$ is the Schur complement of $\mathbf{A}$ in $\mathbf{M}$ and $\underline{\mathbf{0}}$ is a zero matrix.

$\mathbf{\Upsilon}(n)$ the Schur complement of $\mathbf{P^{yy\infty}}(n)$ in $\mathbb{M}$ as follows:

$$\mathbf{\Upsilon}(n) = \{\mathbf{P}^\infty(n|n-1) - \Xi^2\mathbf{I}_U\}$$
$$- \mathbf{P}^\infty(n|n-1)\mathbf{\Psi}^H(n)\{\mathbf{P^{yy\infty}}(n)\}^{-1}\mathbf{\Psi}(n)\mathbf{P}^\infty(n|n-1) \quad \text{(C.5)}$$

Given (A.12), (A.13), (A.15), (C.1) and (C.4), one obtains:

$$\mathbf{\Upsilon}(n) \underset{(C.1),(C.4)}{=} \mathbf{P}(n|n-1)$$
$$- \{\mathbf{P}(n|n-1)\mathbf{\Psi}^H(n)\{\mathbf{P^{yy}}(n)\}^{-1}\}\mathbf{\Psi}(n)\mathbf{P}(n|n-1) - \Xi^2\mathbf{I}_U$$
$$\underset{(A.12),(A.13)}{=} \mathbf{P}(n|n-1) - \mathbf{K}(n)\mathbf{\Psi}(n)\mathbf{P}(n|n-1) - \Xi^2\mathbf{I}_U$$
$$\underset{(A.15)}{=} \mathbf{P}(n|n) - \Xi^2\mathbf{I}_U \quad \text{(C.6)}$$

Then given the previous footnote, $\mathbb{M}^{-1}$ can be expressed as the product of three matrices, the coefficients of which are defined from the coefficients of M and the Schur complement $\mathbf{\Upsilon}(n)$ as follows:

$$\mathbb{M}^{-1} = \begin{bmatrix} \mathbf{I}_K & -\mathbf{K}^H(n) \\ \mathbf{0} & \mathbf{I}_U \end{bmatrix} \begin{bmatrix} \{\mathbf{P^{yy}}(n)\}^{-1} & \mathbf{0} \\ \mathbf{0} & \mathbf{\Upsilon}^{-1} \end{bmatrix} \begin{bmatrix} \mathbf{I}_K & \mathbf{0} \\ -\mathbf{K}(n) & \mathbf{I}_U \end{bmatrix}$$
$$= \mathbb{W}(n)\mathbb{X}(n)\mathbb{Y}(n) \quad \text{(C.7)}$$

At that stage, given (C.7), we can rewrite the Riccati recursion (B.4) as:

$$\mathbf{P}^\infty(n+1|n) = \mathbf{\Phi}(n)\mathbf{P}(n|n-1)\mathbf{\Phi}^H(n) + \mathbf{\Gamma}\mathbf{\Omega}\mathbf{\Gamma}^H \quad \text{(C.8)}$$
$$-\mathbf{\Phi}(n)\mathbf{P}(n|n-1)\begin{bmatrix} \mathbf{\Psi}^H(n) & \mathbf{I}_U \end{bmatrix}\mathbb{W}(n)\mathbb{X}(n)\mathbb{Y}(n)\begin{bmatrix} \mathbf{\Psi}(n) \\ \mathbf{I}_U \end{bmatrix}\mathbf{P}(n|n-1)\mathbf{\Phi}^H(n)$$
$$= \mathbf{\Phi}(n)\mathbf{P}(n|n-1)\mathbf{\Phi}^H(n) + \mathbf{\Gamma}\mathbf{\Omega}\mathbf{\Gamma}^H - \mathbf{\Phi}(n)\begin{bmatrix} \mathbf{P}(n|n-1)\mathbf{\Psi}^H(n) & \mathbf{P}(n|n) \end{bmatrix}$$
$$\times \begin{bmatrix} \{\mathbf{P^{yy}}(n)\}^{-1} & 0 \\ 0 & \mathbf{\Upsilon}^{-1} \end{bmatrix} \begin{bmatrix} \mathbf{\Psi}(n)\mathbf{P}(n|n-1) \\ \mathbf{P}(n|n) \end{bmatrix}\mathbf{\Phi}^H(n)$$

Using (A.12), (A.15) and (C.6), this leads to:

$$\mathbf{P}^\infty(n+1|n) = \mathbf{\Phi}(n)\mathbf{P}(n|n-1)\mathbf{\Phi}^H(n) + \mathbf{\Gamma}\mathbf{\Omega}\mathbf{\Gamma}^H \quad \text{(C.9)}$$
$$-\mathbf{\Phi}(n)\begin{bmatrix} \mathbf{P}(n|n-1)\mathbf{\Psi}^H(n)\{\mathbf{P^{yy}}(n)\}^{-1} & \mathbf{P}(n|n)\mathbf{\Upsilon}^{-1} \end{bmatrix}\begin{bmatrix} \mathbf{\Psi}(n)\mathbf{P}(n|n-1) \\ \mathbf{P}(n|n) \end{bmatrix}\mathbf{\Phi}^H(n)$$
$$\underset{(A.12)}{=} \mathbf{\Phi}(n)\mathbf{P}(n|n-1)\mathbf{\Phi}^H(n) - \mathbf{\Phi}(n)\mathbf{K}(n)\mathbf{\Psi}(n)\mathbf{P}(n|n-1)\mathbf{\Phi}^H(n)$$
$$-\mathbf{\Phi}(n)\mathbf{P}(n|n)\mathbf{\Upsilon}^{-1}\mathbf{P}(n|n)\mathbf{\Phi}^H(n) + \mathbf{\Gamma}\mathbf{\Omega}\mathbf{\Gamma}^H$$
$$\underset{(A.15),(C.6)}{=} \mathbf{\Phi}(n)\mathbf{P}(n|n)\mathbf{\Phi}^H(n) - \mathbf{\Phi}(n)\mathbf{P}(n|n)\{\mathbf{P}(n|n) - \Xi^2\mathbf{I}_U\}^{-1}\mathbf{P}(n|n)\mathbf{\Phi}^H(n) + \mathbf{\Gamma}\mathbf{\Omega}\mathbf{\Gamma}^H$$

Hence, the solution of the Riccati equation when using the H$_\infty$ filter satisfies:

$$\mathbf{P}^\infty(n+1|n) = \boldsymbol{\Phi}(n)\mathbf{P}(n|n)\boldsymbol{\Phi}^H(n) + \mathfrak{Q}^\Xi(n) + \boldsymbol{\Gamma}\mathfrak{Q}\boldsymbol{\Gamma}^H = \boldsymbol{\Phi}(n)\mathbf{P}(n|n)\boldsymbol{\Phi}^H(n) + \mathfrak{Q}^{\Xi w}$$

where

$$\mathfrak{Q}^\Xi(n) = -\boldsymbol{\Phi}(n)\mathbf{P}(n|n)\{\mathbf{P}(n|n) - \Xi^2\mathbf{I}_U\}^{-1}\mathbf{P}(n|n)\boldsymbol{\Phi}^H(n) \tag{C.10}$$

Given, (A.16) and (C.10), one has

$$\mathbf{P}^\infty(n+1|n) = \mathbf{P}(n+1|n) + \mathfrak{Q}^\Xi(n) \tag{C.11}$$

Therefore, H$_\infty$ filtering can be seen as a Kalman filtering with a model-noise covariance matrix equal to $\mathfrak{Q}^{\Xi w} = \mathfrak{Q}^\Xi(n) + \boldsymbol{\Gamma}\mathfrak{Q}\boldsymbol{\Gamma}^H$.

For parameter tracking, the larger the coefficients of the state-noise covariance matrix are, the easier it is to track the parameter variations, especially when the parameters are subject to abrupt variations. Nevertheless, the larger they are, the larger the variance of the estimated parameters over time is.

At that stage, let us introduce the eigenvalue decomposition of $\mathbf{P}(n|n)$:

$$\mathbf{P}(n|n) = \mathbf{G}\begin{bmatrix} \lambda_1 & 0 & \cdots & \cdots & 0 \\ 0 & \lambda_2 & 0 & \cdots & 0 \\ \vdots & 0 & \ddots & \ddots & \vdots \\ \vdots & \vdots & \ddots & \ddots & 0 \\ 0 & 0 & \cdots & 0 & \lambda_U \end{bmatrix}\mathbf{G}^{-1}$$

where $\{\lambda_u\}_{u\in\{1,2,\dots,U\}}$ are the eigenvalues of $\mathbf{P}(n|n)$. Hence, one has:

$$\mathbf{P}(n|n) - \Xi^2\mathbf{I}_U = \mathbf{G}\begin{bmatrix} \lambda_1 - \Xi^2 & 0 & \cdots & \cdots & 0 \\ 0 & \lambda_2 - \Xi^2 & 0 & \cdots & 0 \\ \vdots & 0 & \ddots & \ddots & \vdots \\ \vdots & \vdots & \ddots & \ddots & 0 \\ 0 & 0 & \cdots & 0 & \lambda_U - \Xi^2 \end{bmatrix}\mathbf{G}^{-1}$$

Therefore:

$$\mathfrak{Q}^\Xi(n) = \boldsymbol{\Phi}(n)\mathbf{G}\begin{bmatrix} -\frac{\lambda_1{}^2}{\lambda_1 - \Xi^2} & 0 & \cdots & \cdots & 0 \\ 0 & -\frac{\lambda_2{}^2}{\lambda_2 - \Xi^2} & 0 & \cdots & 0 \\ \vdots & 0 & \ddots & \ddots & \vdots \\ \vdots & \vdots & \ddots & \ddots & 0 \\ 0 & 0 & \cdots & 0 & -\frac{\lambda_U{}^2}{\lambda_U - \Xi^2} \end{bmatrix}(\boldsymbol{\Phi}(n)\mathbf{G})^H \tag{C.12}$$

where $\{-\frac{\lambda_u{}^2}{\lambda_u - \Xi^2}\}_{u \in \{1,2,\dots,U\}}$ are the eigenvalues of $\mathbf{Q}^\Xi(n)$.

It should be noted that when Ξ tends to $+\infty$, $\mathbf{Q}^\Xi(n)$ tends to be a zero matrix and $\mathbf{P}^\infty(n+1|n)$ tends to $\mathbf{P}(n+1|n)$.

If $\Xi^2 > \lambda_u$, for $u \in \{1, 2, \dots, U\}$, $\mathbf{Q}^\Xi(n)$ is a positive-definite matrix. Therefore, the solution to the Ricatti equation for the H$_\infty$ filter can be seen as an upper bound of the Kalman *a priori* error covariance matrix.

Extended Kalman Filter Approaches

When considering a non-linear system, the EKF consists in analytically propagating the estimation through the system dynamics, by means of a first-order linearization using Taylor expansion [Hayk 96].

The non-linear state-space equations that describe the system are:

State equation:

$$\mathbf{x}(n) = \mathbf{\Phi}_n\left(\mathbf{x}(n-1)\right) + \mathbf{\Gamma}\mathbf{w}(n) \tag{D.1}$$

Measurement equation:

$$\mathbf{y}(n) = \mathbf{\Psi}_n(\mathbf{x}(n)) + \mathbf{b}(n) \tag{D.2}$$

where $\mathbf{\Phi}_n$ and $\mathbf{\Psi}_n$ are non-linear functions. As in appendix A, $\mathbf{x}(n)$ is the state vector of size U at time n and $\mathbf{y}(n)$ is the measurement vector of size K at time n. The noises $\mathbf{w}(n)$ and $\mathbf{b}(n)$ are additive white zero-mean Gaussian processes with covariance matrices $\mathbf{Q} = \sigma_w^2\mathbf{I}_U$ and $\mathbf{R} = \sigma_b^2\mathbf{I}_K$ respectively. In addition, $\mathbf{\Gamma}$ is the input gain matrix of size $U \times U$.

Then, the first-order Taylor expansion of (D.1) around $\hat{\mathbf{x}}(n-1|n-1)$ is:

$$
\begin{aligned}
\mathbf{\Phi}_n(\mathbf{x}(n-1)) &\approx \mathbf{\Phi}_n(\hat{\mathbf{x}}(n-1|n-1)) \\
&\quad + \nabla\mathbf{\Phi}_n|_{\hat{\mathbf{x}}(n-1|n-1)}\{\mathbf{x}(n-1) - \hat{\mathbf{x}}(n-1|n-1)\} \\
&\approx \mathbf{\Phi}_n(\hat{\mathbf{x}}(n-1|n-1)) + \nabla\mathbf{\Phi}_n|_{\hat{\mathbf{x}}(n-1|n-1)}\mathbf{x}(n-1) \\
&\quad - \nabla\mathbf{\Phi}_n|_{\hat{\mathbf{x}}(n-1|n-1)}\hat{\mathbf{x}}(n-1|n-1)
\end{aligned} \tag{D.3}
$$

where $\nabla\mathbf{\Phi}_n|_{\hat{\mathbf{x}}(n-1|n-1)}$ is the Jacobian matrix of $\mathbf{\Phi}_n$ evaluated for $\hat{\mathbf{x}}(n-1|n-1)$. Given (D.3), (D.1) can be rewritten as follows:

$$
\begin{aligned}
\mathbf{x}(n) &= \mathbf{\Phi}_n(\hat{\mathbf{x}}(n-1|n-1)) + \nabla\mathbf{\Phi}_n|_{\hat{\mathbf{x}}(n-1|n-1)}\mathbf{x}(n-1) \\
&\quad - \nabla\mathbf{\Phi}_n|_{\hat{\mathbf{x}}(n-1|n-1)}\hat{\mathbf{x}}(n-1|n-1) + \mathbf{\Gamma}\mathbf{w}(n)
\end{aligned} \tag{D.4}
$$

Given (A.3) and (D.4), the *a priori* estimation of the state vector is defined as follows:

$$
\begin{aligned}
\hat{\mathbf{x}}(n|n-1) = {}& \boldsymbol{\Phi}_n(\hat{\mathbf{x}}(n-1|n-1)) \\
& + \nabla\boldsymbol{\Phi}_n|_{\hat{\mathbf{x}}(n-1|n-1)}\mathbb{E}\left[\mathbf{x}(n-1)|\mathbf{y}(0),\mathbf{y}(1),\ldots,\mathbf{y}(n-1)\right] \\
& - \nabla\boldsymbol{\Phi}_n|_{\hat{\mathbf{x}}(n-1|n-1)}\hat{\mathbf{x}}(n-1|n-1)\} \\
& + \boldsymbol{\Gamma}\mathbb{E}\left[\mathbf{w}(n)|\mathbf{y}(0),\mathbf{y}(1),\ldots,\mathbf{y}(n-1)\right]
\end{aligned}
\tag{D.5}
$$

As $\mathbf{w}(n)$ is a white zero-mean Gaussian process, (D.5) can be rewritten as:

$$
\begin{aligned}
\hat{\mathbf{x}}(n|n-1) = {}& \boldsymbol{\Phi}_n(\hat{\mathbf{x}}(n-1|n-1)) \\
& + \nabla\boldsymbol{\Phi}_n|_{\hat{\mathbf{x}}(n-1|n-1)}\hat{\mathbf{x}}(n-1|n-1) \\
& - \nabla\boldsymbol{\Phi}_n|_{\hat{\mathbf{x}}(n-1|n-1)}\hat{\mathbf{x}}(n-1|n-1)
\end{aligned}
\tag{D.6}
$$

So, the *a priori* estimation of the state vector satisfies:

$$
\hat{\mathbf{x}}(n|n-1) = \boldsymbol{\Phi}_n(\hat{\mathbf{x}}(n-1|n-1))
\tag{D.7}
$$

Thus, given (D.4) and (D.7), the *a priori* error estimation can be defined as:

$$
\begin{aligned}
\tilde{\mathbf{x}}(n|n-1) = {}& \mathbf{x}(n) - \hat{\mathbf{x}}(n|n-1) \\
= {}& \boldsymbol{\Phi}_n(\hat{\mathbf{x}}(n-1|n-1)) + \nabla\boldsymbol{\Phi}|_{\hat{\mathbf{x}}(n-1|n-1)}\mathbf{x}(n-1) \\
& - \nabla\boldsymbol{\Phi}_n|_{\hat{\mathbf{x}}(n-1|n-1)}\hat{\mathbf{x}}(n-1|n-1) + \boldsymbol{\Gamma}\mathbf{w}(n) - \boldsymbol{\Phi}_n(\hat{\mathbf{x}}(n-1|n-1)) \\
= {}& \nabla\boldsymbol{\Phi}_n|_{\hat{\mathbf{x}}(n-1|n-1)}\tilde{\mathbf{x}}(n-1|n-1) + \boldsymbol{\Gamma}\mathbf{w}(n)
\end{aligned}
\tag{D.8}
$$

and its corresponding covariance matrix $\mathbf{P}(n|n-1)$ is defined by:

$$
\mathbf{P}(n|n-1) = \nabla\boldsymbol{\Phi}_n|_{\hat{\mathbf{x}}(n-1|n-1)}\mathbf{P}(n-1|n-1)\nabla\boldsymbol{\Phi}_n^H|_{\hat{\mathbf{x}}(n-1|n-1)} + \boldsymbol{\Gamma}\boldsymbol{\mathcal{Q}}\boldsymbol{\Gamma}^H
\tag{D.9}
$$

It should be noted the *a priori* estimation of the state vector (D.7) does not depend on the Jacobian matrix $\nabla\boldsymbol{\Phi}_n|_{\hat{\mathbf{x}}(n-1|n-1)}$. However, $\nabla\boldsymbol{\Phi}_n|_{\hat{\mathbf{x}}(n-1|n-1)}$ is required to calculate the *a priori* error estimation covariance matrix $\mathbf{P}(n|n-1)$.

Now, let us focus our attention on the *a posteriori* estimation of the state vector. For this purpose, it is necessary to calculate the first-order Taylor expansion of (D.2) around $\hat{\mathbf{x}}(n|n-1)$ as follows:

$$
\boldsymbol{\Psi}_n(\mathbf{x}(n)) \approx \boldsymbol{\Psi}_n(\hat{\mathbf{x}}(n|n-1)) + \nabla\boldsymbol{\Psi}_n|_{\hat{\mathbf{x}}(n|n-1)}\{\mathbf{x}(n) - \hat{\mathbf{x}}(n|n-1)\}
\tag{D.10}
$$

where $\nabla \mathbf{\Psi}_n|_{\hat{\mathbf{x}}(n|n-1)}$ is the Jacobian matrix of $\mathbf{\Psi}_n$ evaluated for $\hat{\mathbf{x}}(n|n-1)$.

Then, given (D.2) and (D.10), the innovation can be expressed as:

$$
\begin{aligned}
\mathbf{y}(n) - \mathbf{\Psi}_n(\hat{\mathbf{x}}(n|n-1)) &\approx \mathbf{\Psi}_n(\mathbf{x}(n)) + \mathbf{b}(n) \\
&\quad - \mathbf{\Psi}_n(\mathbf{x}(n)) + \nabla\mathbf{\Psi}_n|_{\hat{\mathbf{x}}(n|n-1)}\{\mathbf{x}(n) - \hat{\mathbf{x}}(n|n-1)\} \quad \text{(D.11)} \\
&\approx \nabla\mathbf{\Psi}_n|_{\hat{\mathbf{x}}(n|n-1)}\{\mathbf{x}(n) - \hat{\mathbf{x}}(n|n-1)\} + \mathbf{b}(n)
\end{aligned}
$$

When looking at the linear case and more particularly (A.10), the innovation is defined as follows:

$$
\mathbf{y}(n) - \mathbf{\Psi}(n)\hat{\mathbf{x}}(n|n-1) = \mathbf{\Psi}(n)\{\mathbf{x}(n) - \hat{\mathbf{x}}(n|n-1)\} + \mathbf{b}(n) \quad \text{(D.12)}
$$

A similarity can be noticed between (D.11) and (D.12). The EKF can be hence easily derived. The way the state-vector estimation can be updated and the definition of the Kalman gain can be obtained similarly as in appendix A, by replacing $\mathbf{\Psi}(n)$ by $\nabla\mathbf{\Psi}_n|_{\hat{\mathbf{x}}(n|n-1)}$.

Thus, to obtain the *a posteriori* estimation of the state vector, one has:

$$
\hat{\mathbf{x}}(n|n) = \hat{\mathbf{x}}(n|n-1) + \mathbf{K}(n)\{\mathbf{y}(n) - \mathbf{\Psi}_n(\hat{\mathbf{x}}(n|n-1))\} \quad \text{(D.13)}
$$

where $\mathbf{K}(n)$ is the Kalman gain defined by:

$$
\mathbf{K}(n) = \{\mathbf{P}^{\mathbf{xy}}(n)\}\{\mathbf{P}^{\mathbf{yy}}(n)\}^{-1} \quad \text{(D.14)}
$$

with $\mathbf{P}^{\mathbf{yy}}(n)$ the innovation covariance matrix defined as follows:

$$
\mathbf{P}^{\mathbf{yy}}(n) = \nabla\mathbf{\Psi}_n|_{\hat{\mathbf{x}}(n|n-1)}\mathbf{P}(n|n-1)\nabla\mathbf{\Psi}_n^H|_{\hat{\mathbf{x}}(n|n-1)} + \mathcal{R} \quad \text{(D.15)}
$$
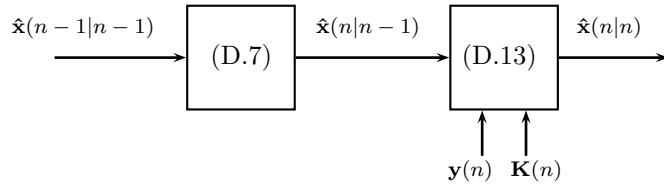
Figure D.1: EKF

and $\mathbf{P^{xy}}(n)$ the cross-covariance matrix between $\mathbf{y}(n)$ and the state prediction $\hat{\mathbf{x}}(n|n-1)$ defined as:

$$\mathbf{P^{xy}}(n) = \mathbf{P}(n|n-1)\nabla\mathbf{\Psi}_n^H|_{\hat{\mathbf{x}}(n|n-1)} \tag{D.16}$$

Figure D.1 shows the block scheme of the EKF.

Finally, by combining (D.13) and (D.14), it can be easily shown that the estimation error covariance matrix is updated as follows:

$$\begin{aligned}
\mathbf{P}(n|n) &= \mathbf{P}(n|n-1) - \mathbf{K}(n)\nabla\mathbf{\Psi}_n|_{\hat{\mathbf{x}}(n|n-1)}(n)\mathbf{P}(n|n-1) \\
&= \{\mathbf{I}_U - \mathbf{K}(n)\nabla\mathbf{\Psi}_n|_{\hat{\mathbf{x}}(n|n-1)}(n)\}\mathbf{P}(n|n-1)
\end{aligned} \tag{D.17}$$

The EKF may sometimes diverge if the first-order approximation is not sufficient to describe the non-linearity. Therefore, a second-order approximation can be used and leads to the SOEKF [Bar 01]. It is still based on a Taylor expansion, but a second-order expansion is considered.

Given the state-space equations in (D.1) and (D.2), let us look at the second-order Taylor expansion of (D.1) around $\hat{\mathbf{x}}(n-1|n-1)$:

$$\begin{aligned}
\mathbf{\Phi}_n(\mathbf{x}(n-1)) &\approx \mathbf{\Phi}_n(\hat{\mathbf{x}}(n-1|n-1)) \\
&\quad + \nabla\mathbf{\Phi}_n|_{\hat{\mathbf{x}}(n-1|n-1)}\{\mathbf{x}(n-1) - \hat{\mathbf{x}}(n-1|n-1)\} + \frac{1}{2}\overline{\mathbf{\Phi}}_n \\
&\approx \mathbf{\Phi}_n(\hat{\mathbf{x}}(n-1|n-1)) + \nabla\mathbf{\Phi}_n|_{\hat{\mathbf{x}}(n-1|n-1)}\tilde{\mathbf{x}}(n-1|n-1) + \frac{1}{2}\overline{\mathbf{\Phi}}_n
\end{aligned} \tag{D.18}$$

where $\nabla\mathbf{\Phi}_n|_{\hat{\mathbf{x}}(n-1|n-1)}$ is the Jacobian matrix of $\mathbf{\Phi}_n$ evaluated at $\hat{\mathbf{x}}(n-1|n-1)$ and

$$\begin{aligned}
\overline{\mathbf{\Phi}}_n &= \sum_{u=1}^{U}\mathbf{\Theta}_u^\Phi\{\mathbf{x}(n-1) - \hat{\mathbf{x}}(n-1|n-1)\}^H\frac{\partial^2\Phi_{n,u}}{\partial\mathbf{x}^2(n)}|_{\hat{\mathbf{x}}(n-1|n-1)} \\
&\quad \times \{\mathbf{x}(n-1) - \hat{\mathbf{x}}(n-1|n-1)\} \\
&= \sum_{u=1}^{U}\mathbf{\Theta}_u^\Phi\overline{\mathbf{\Phi}}_{n,u}
\end{aligned} \tag{D.19}$$

where $\Phi_{n,u}$ is the uth element of $\mathbf{\Phi}_n(\mathbf{x}(n))$ and $\mathbf{\Theta}_u^\Phi$ is a $U \times 1$ vector with zeros everywhere except for the uth element which is equal to 1.

Remark 1: The uth quadratic term of $\overline{\mathbf{\Phi}}_n$ can expressed as follows:

$$
\begin{aligned}
\overline{\Phi}_{n,u} &= tr\{\frac{\partial^2 \Phi_{n,u}}{\partial \mathbf{x}^2(n)}|_{\hat{\mathbf{x}}(n-1|n-1)} \\
&\quad \times \{\mathbf{x}(n-1) - \hat{\mathbf{x}}(n-1|n-1)\}\{\mathbf{x}(n-1) - \hat{\mathbf{x}}(n-1|n-1)\}^H\} \\
&= tr\{\{\mathbf{x}(n-1) - \hat{\mathbf{x}}(n-1|n-1)\}\{\mathbf{x}(n-1) - \hat{\mathbf{x}}(n-1|n-1)\}^H \\
&\quad \times \frac{\partial^2 \Phi_{n,u}}{\partial \mathbf{x}^2(n)}|_{\hat{\mathbf{x}}(n-1|n-1)}\}
\end{aligned}
\tag{D.20}
$$

Remark 2: one can approximate the expectation of $\overline{\Phi}_{n,u}$ given the set of observations $\{\mathbf{y}(0), \ldots, \mathbf{y}(n-1)\}$ by:

$$
\begin{aligned}
\overline{\Phi}_{n,u}^{\text{mean}} &= \mathbb{E}\{\overline{\Phi}_{n,u}|\mathbf{y}(0), \ldots, \mathbf{y}(n-1)\} \\
&\approx tr\{\mathbf{P}(n-1|n-1)\frac{\partial^2 \Phi_{n,u}}{\partial \mathbf{x}^2(n)}|_{\hat{\mathbf{x}}(n-1|n-1)}\}
\end{aligned}
\tag{D.21}
$$

The above approximation of $\overline{\Phi}_{n,u}^{\text{mean}}$ has the advantage of being "easily" computed by using $\mathbf{P}(n-1|n-1)$ and $\frac{\partial^2 \Phi_{n,u}}{\partial \mathbf{x}^2(n)}|_{\hat{\mathbf{x}}(n-1|n-1)}$.

Given (D.19) and (D.21), one has:

$$
\begin{aligned}
\overline{\mathbf{\Phi}}_n^{\text{mean}} &= \mathbb{E}\{\overline{\mathbf{\Phi}}_n|\mathbf{y}(0), \ldots, \mathbf{y}(n-1)\} \\
&= \sum_{u=1}^{U} \mathbf{\Theta}_u^{\Phi} \overline{\Phi}_{n,u}^{\text{mean}}
\end{aligned}
\tag{D.22}
$$

By following the same development as in (D.5) and (D.6), the *a priori* estimation of the state vector can be obtained as follows:

$$
\hat{\mathbf{x}}(n|n-1) = \mathbf{\Phi}_n(\hat{\mathbf{x}}(n-1|n-1)) + \frac{1}{2}\overline{\mathbf{\Phi}}_n^{\text{mean}}
\tag{D.23}
$$

By assuming that $\overline{\mathbf{\Phi}}_n^{\text{mean}} \approx \overline{\mathbf{\Phi}}_n$ and by combining (D.18) and (D.23), the *a priori* estimation error $\tilde{\mathbf{x}}(n|n-1)$ can be expressed as follows:

$$
\tilde{\mathbf{x}}(n|n-1) = \nabla\mathbf{\Phi}_n|_{\hat{\mathbf{x}}(n-1|n-1)}\tilde{\mathbf{x}}(n-1|n-1) + \mathbf{\Gamma}\mathbf{w}(n)
\tag{D.24}
$$

Therefore, the covariance matrix $\mathbf{P}(n|n-1)$ satisfies:

$$
\mathbf{P}(n|n-1) = \nabla\mathbf{\Phi}_n|_{\hat{\mathbf{x}}(n-1|n-1)}\mathbf{P}(n-1|n-1)\nabla\mathbf{\Phi}_n^H|_{\hat{\mathbf{x}}(n-1|n-1)} + \mathbf{\Gamma}\mathbf{Q}\mathbf{\Gamma}^H
\tag{D.25}
$$

Then, the second-order Taylor expansion of (D.2) around $\hat{\mathbf{x}}(n|n-1)$ is:

$$\boldsymbol{\Psi}_n(\mathbf{x}(n)) \approx \boldsymbol{\Psi}_n(\hat{\mathbf{x}}(n|n-1))$$
$$+ \nabla\boldsymbol{\Psi}_n|_{\hat{\mathbf{x}}(n|n-1)}\{\mathbf{x}(n) - \hat{\mathbf{x}}(n|n-1)\} + \frac{1}{2}\overline{\boldsymbol{\Psi}}_n \tag{D.26}$$

where $\nabla\boldsymbol{\Psi}_n|_{\hat{\mathbf{x}}(n|n-1)}$ is the Jacobian matrix of $\boldsymbol{\Psi}_n$ evaluated at $\hat{\mathbf{x}}(n|n-1)$ and

$$\overline{\boldsymbol{\Psi}}_n = \sum_{k=1}^{K} \boldsymbol{\Theta}_k^{\Psi}\{\mathbf{x}(n) - \hat{\mathbf{x}}(n|n-1)\}^H \frac{\partial^2 \Psi_{n,k}}{\partial \mathbf{x}^2(n)}|_{\hat{\mathbf{x}}(n|n-1)}\{\mathbf{x}(n) - \hat{\mathbf{x}}(n|n-1)\} \tag{D.27}$$

where $\Psi_{n,k}$ is the kth element of $\boldsymbol{\Psi}_n(\mathbf{x}(n))$ and $\boldsymbol{\Theta}_k^{\Psi}$ is a $K \times 1$ vector with zeros everywhere except for the kth element which is equal to 1.

Remark 3: Once again, it should be noted that the kth element of $\overline{\boldsymbol{\Psi}}_n$ can be expressed as follows:

$$\overline{\Psi}_{n,k} = tr\{\frac{\partial^2 \Psi_{n,k}}{\partial \mathbf{x}^2(n)}|_{\hat{\mathbf{x}}(n|n-1)}$$
$$\times \{\mathbf{x}(n) - \hat{\mathbf{x}}(n|n-1)\}\{\mathbf{x}(n) - \hat{\mathbf{x}}(n|n-1)\}^H\}$$
$$= tr\{\{\mathbf{x}(n) - \hat{\mathbf{x}}(n|n-1)\}\{\mathbf{x}(n) - \hat{\mathbf{x}}(n|n-1)\}^H$$
$$\frac{\partial^2 \Psi_{n,k}}{\partial \mathbf{x}^2(n)}|_{\hat{\mathbf{x}}(n|n-1)}\} \tag{D.28}$$

Then, given (D.2) and (D.26) the innovation can be expressed as follows:

$$\mathbf{y}(n) - \boldsymbol{\Psi}_n(\hat{\mathbf{x}}(n|n-1)) \approx \nabla\boldsymbol{\Psi}_n|_{\hat{\mathbf{x}}(n|n-1)}\{\mathbf{x}(n) - \hat{\mathbf{x}}(n|n-1)\} + \frac{1}{2}\overline{\boldsymbol{\Psi}}_n + \mathbf{b}(n) \tag{D.29}$$

Unlike the Kalman filter in the linear case or the EKF, the innovation depends on $\overline{\boldsymbol{\Psi}}_n$. Therefore, to obtain the *a posteriori* estimation of the state vector, the following relation can be considered:

$$\hat{\mathbf{x}}(n|n) = \hat{\mathbf{x}}(n|n-1) + \mathbf{K}(n)\{\mathbf{y}(n) - \boldsymbol{\Psi}_n(\hat{\mathbf{x}}(n|n-1)) - \frac{1}{2}\overline{\boldsymbol{\Psi}}_n\} \tag{D.30}$$

where $\mathbf{K}(n)$ is the Kalman gain defined in (D.14) and the error estimation covariance matrix is updated as in (D.17).

However, in practical case $\mathbf{x}(n) - \hat{\mathbf{x}}(n|n-1)$ is not available and hence $\overline{\overline{\mathbf{\Psi}}}_n$ cannot be computed. For this reason, instead of $\overline{\mathbf{\Psi}}_n$ one suggests using:

$$\overline{\overline{\mathbf{\Psi}}}_n = \sum_{k=1}^{K} \mathbf{\Theta}_k^{\Psi} \overline{\Psi}_{n,k}^{\text{mean}} \tag{D.31}$$

where $\overline{\Psi}_{n,k}^{\text{mean}} = tr\{\mathbf{P}(n|n-1)\frac{\partial^2 \Psi_{n,k}}{\partial \mathbf{x}^2(n)}|_{\hat{\mathbf{x}}(n-1|n-1)}\}$.

As consequence, the state vector is updated as follows:

$$\hat{\mathbf{x}}(n|n) = \hat{\mathbf{x}}(n|n-1) + \mathbf{K}(n)\{\mathbf{y}(n) - \mathbf{\Psi}_n(\hat{\mathbf{x}}(n|n-1)) - \frac{1}{2}\overline{\overline{\mathbf{\Psi}}}_n\} \tag{D.32}$$

The IEKF is another alternative that aims at improving the EKF [Gelb 74]. The purpose is to linearize the measurement model around the updated state $\hat{\mathbf{x}}(n|n)$, instead of the predicted state $\hat{\mathbf{x}}(n|n-1)$. Indeed, the Bayesian approach makes it possible to separate the Kalman filter in two steps: the prediction step and the filtering step. The nearer the linearization point is to the real value, the lower the linearization error should be. In addition, after the filtering step, $\hat{\mathbf{x}}(n|n)$ is expected to have a lower error variance than $\hat{\mathbf{x}}(n|n-1)$. For the above reasons, using the IEKF can be of interest.

Given the state-space equations in (D.1) and (D.2), the *a priori* estimation of the state vector and its covariance matrix can be obtained as in (D.7) and (D.9) respectively.

To obtain the *a posteriori* estimation of the state vector, an iterative process is introduced. At the $i+1$th iteration, with $i \in \{0, 1, 2, \ldots, \mathfrak{I}^{kf}\}$, where $\mathfrak{I}^{kf}$ is
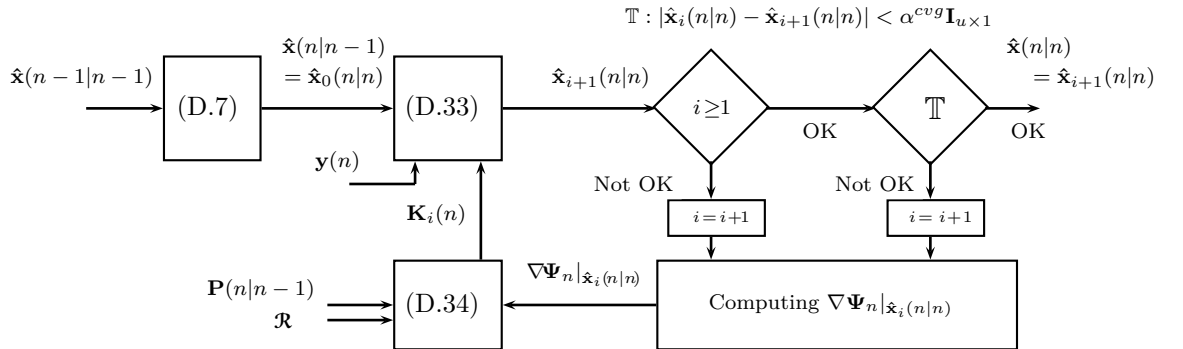
Figure D.2: IEKF

the number of iterations, the $(i+1)$th *a posteriori* estimate of the state vector satisfies:

$$\hat{\mathbf{x}}_{i+1}(n|n) = \hat{\mathbf{x}}(n|n-1) + \mathbf{K}_i(n)\{\mathbf{y}(n) - \mathbf{\Psi}_n(\hat{\mathbf{x}}(n|n-1))\} \tag{D.33}$$

where

$$\mathbf{K}_i(n) = \{\mathbf{P}_i^{\mathbf{xy}}(n)\}\{\mathbf{P}_i^{\mathbf{yy}}(n)\}^{-1} \tag{D.34}$$

$$\mathbf{P}_i^{\mathbf{yy}}(n) = \nabla\mathbf{\Psi}_n|_{\hat{\mathbf{x}}_i(n|n)}\mathbf{P}(n|n-1)\nabla\mathbf{\Psi}_n^H|_{\hat{\mathbf{x}}_i(n|n)} + \boldsymbol{\mathcal{R}} \tag{D.35}$$

$$\mathbf{P}_i^{\mathbf{xy}}(n) = \mathbf{P}(n|n-1)\nabla\mathbf{\Psi}_n^H|_{\hat{\mathbf{x}}_i(n|n)} \tag{D.36}$$

and $\hat{\mathbf{x}}_0(n|n) = \hat{\mathbf{x}}(n|n-1)$. Figure D.2 shows the block scheme of the IEKF. The estimation-error covariance matrix has to be updated as follows:

$$\mathbf{P}_{i+1}(n|n) = \mathbf{P}(n|n-1) - \mathbf{K}_i(n)\nabla\mathbf{\Psi}_n^H|_{\hat{\mathbf{x}}_i(n|n)}\mathbf{P}(n|n-1) \tag{D.37}$$

Then, having a new value of the estimate, the procedure is repeated until the difference between two consecutive estimates is lower than a predefined value α^{cvg}:

$$|\hat{\mathbf{x}}_i(n|n) - \hat{\mathbf{x}}_{i+1}(n|n)| < \alpha^{cvg}\mathbf{I}_{U\times 1} \quad \alpha^{cvg} > 0 \tag{D.38}$$

where $\mathbf{I}_{U\times 1}$ is a $U \times 1$ vector composed of ones.

The relations (D.33)-(D.37) define the IEKF. Nevertheless, it is again a local approximation and the convergence of the estimate is not guaranteed as in the EKF.

Appendix E

Sigma-Point Kalman Filter

When dealing with the SPKF, the state distribution is still approximated by a Gaussian distribution, which is now characterized by a set of points lying along the main eigenaxes of the random variable covariance matrix, as shown in figure E.1.
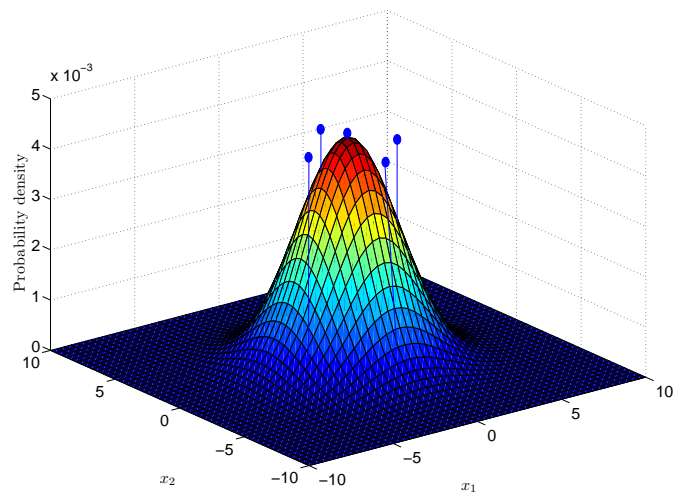
Figure E.1: Gaussian distribution approximated by the sigma-points

These so-called sigma-points are propagated through the non-linear system (D.2), as shown in figure E.2. A weighted combination of the resulting values makes it possible to estimate the mean and the covariance matrix of the transformed random vector, i.e. the Gaussian random variable that undergoes the non-linear transformation.

On the one hand, the UKF is based on the unscented transformation [Wan 01].
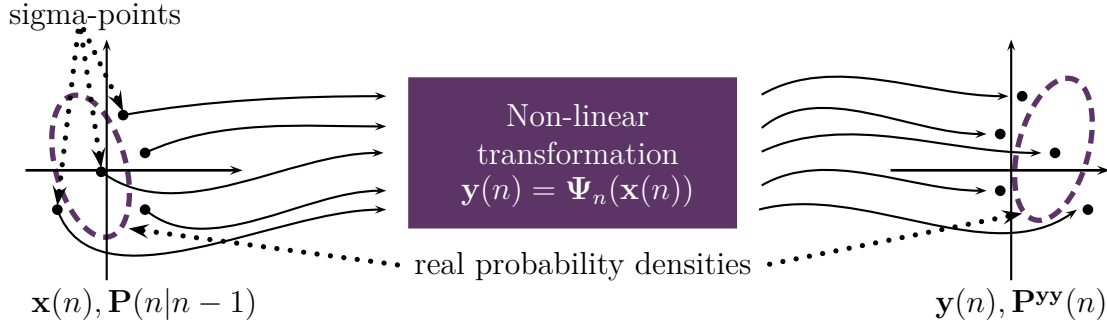
Figure E.2: Non-linear transformation for a random vector of size 2

When the density is odd, the weights are chosen to provide the exact second-order Taylor expansion around the mean of the random variable. The UKF was proposed by their authors as an alternative to the EKF to avoid the linearization step. Nevertheless, Lefebvre *et al.* [Lefe 02] showed that the sigma-point approach corresponds to a weighted statistical linear regression (WSLR). In [VdMe 01], a square-root UKF is presented. It has better numerical properties and guarantees the positive semi-definiteness of the underlying state covariance.

On the other hand, the CDKF is based on the second-order Sterling polynomial interpolation[1] formula [Ito 00]. The linearization is based on Sterling polynomial interpolation around the last available estimate of the state vector. The CDKF can be seen as a Bayesian approach of a second-order divided difference filter (DDF). According to Nörgaard *et al.* [Norg 00], if the last available estimate is "far" from the real value, the Sterling polynomial interpolation approximation of the non-linear function is better than a Taylor expansion approximation.

Let us consider the state-space representation done in (D.1) and (D.2). Thus, as the size of the state vector is U, there are $2U + 1$ sigma-points stored in the following matrix:

$$\mathcal{X}(n-1|n-1) = \begin{bmatrix} \mathcal{X}_0(n-1|n-1) & \mathcal{X}_a(n-1|n-1) & \mathcal{X}_b(n-1|n-1) \end{bmatrix} \quad \text{(E.1)}$$

---

[1]Sterling polynomial interpolation [Boas 64] is the approximation in an infinite sum of terms of a function $y_i = f(x_i)|_{i \in \mathbb{Z}} = f(x_0 + hu)$ around a value x_0, where $u = \frac{x_i - x_0}{h}$ and h is the distance between two points chosen arbitrarily. Thus, the second-order Sterling formula of the function $f(x_i)$ is $y_i = f(x_i) \approx y_0 + \frac{u}{2}(y_1 - y_{-1}) + \frac{u^2}{2}(y_1 + y_{-1} - 2y_0)$.

where

$$\mathcal{X}_0(n-1|n-1) = \hat{\mathbf{x}}(n-1|n-1)$$

$$\mathcal{X}_a(n-1|n-1) = \hat{\mathbf{x}}(n-1|n-1) + \Lambda \left(\sqrt[\star]{\mathbf{P}(n-1|n-1)} \right)_{\mathfrak{m}} \quad \mathfrak{m} \in \{1, \ldots, U\}$$

$$\mathcal{X}_b(n-1|n-1) = \hat{\mathbf{x}}(n-1|n-1) - \Lambda \left(\sqrt[\star]{\mathbf{P}(n-1|n-1)} \right)_{\mathfrak{m}} \quad \mathfrak{m} \in \{U, \ldots, 2U\}$$

$$\text{(E.2)}$$

$(\sqrt[\star]{\mathbf{P}(n-1|n-1)})_{\mathfrak{m}}$ is the $\mathfrak{m}$th column of the matrix square-root, $\sqrt[\star]{(.)}$ is the so-called matrix square-root that can be obtained by using the lower triangular Cholesky decomposition and Λ is a scalar scaling factor that determines the spread of the sigma-points. These points are deterministically chosen so that they completely capture the true mean and the covariance matrix of the Gaussian random variable.

The difference between CDKF and UKF stands in the way the mean and the covariance matrix of the transformed Gaussian random variable are calculated. The CDKF uses only a single scalar scaling parameter Λ, as opposed to three required by the UKF. When using the CDKF, $\Lambda = \sqrt{3}$ [VdMe 04b]. If the UKF is used, one has:

- $\Lambda = \iota^2(U + \kappa) + U$, with $10^{-4} \leq \iota \leq 1$,

- κ is the secondary scaling parameter usually set to 0 or $3 - U$ [Juli 95].

- η is the third scaling parameter used to incorporate prior knowledge of the distribution. For example, when dealing with Gaussian distributions $\eta = 2$ is the optimal value [Wan 01].

Let us define the weight scalar parameters for the UKF [Wan 01] as follows:

$$w_{\circ}^{(c0)} = \frac{\eta}{\eta + U}$$

$$w_{\circ}^{(c1)} = \frac{\eta}{\eta + U} + (1 - \iota^2 + \eta) \qquad \text{(E.3)}$$

$$w_{\mathfrak{m}}^{(c0)} = w_{\mathfrak{m}}^{(c1)} = \frac{1}{2(U + \Lambda)}$$

and for the CDKF [VdMe 04b] as:

$$
\begin{aligned}
w_{\mathfrak{o}}^{(c0)} &= \frac{\Lambda^2 - U}{\Lambda^2} \\
w_{\mathfrak{m}}^{(c0)} &= \frac{1}{2\Lambda^2} \\
w_{\mathfrak{m}}^{(c1)} &= \frac{1}{4\Lambda^2} \\
w_{\mathfrak{m}}^{(c2)} &= \frac{\Lambda^2 - 1}{4\Lambda^4}
\end{aligned}
\tag{E.4}
$$

The sigma-points are propagated through the non-linear $\boldsymbol{\Phi}_n$ as follows:

$$
\boldsymbol{\mathcal{X}}(n|n-1) = \boldsymbol{\Phi}_n\left(\boldsymbol{\mathcal{X}}(n-1|n-1)\right)
\tag{E.5}
$$

Then, the *a priori* mean is obtained as follows:

$$
\hat{\mathbf{x}}^-(n|n-1) = \sum_{\mathfrak{m}=0}^{2U} w_{\mathfrak{m}}^{(c0)}\boldsymbol{\mathcal{X}}_{\mathfrak{m}}(n|n-1)
\tag{E.6}
$$

while the *a priori* estimation error covariance matrix when using the UKF satisfies:

$$
\mathbf{P}(n|n-1) = \sum_{\mathfrak{m}=0}^{2U} w_{\mathfrak{m}}^{(c1)}\left[\boldsymbol{\mathcal{X}}_{\mathfrak{m}}(n|n-1) - \hat{\mathbf{x}}^-(n|n-1)\right]^\star + \boldsymbol{\mathcal{Q}}
\tag{E.7}
$$

where $[(.)]^\star = [(.)] \times [(.)]^H$.

When using the CDKF, one has:

$$
\begin{aligned}
\mathbf{P}(n|n-1) = \sum_{\mathfrak{m}=0}^{U} \{ & w_m^{c1}\left[\boldsymbol{\mathcal{X}}_m(n|n-1) - \boldsymbol{\mathcal{X}}_{\mathfrak{m}+U}(n|n-1)\right]^\star \\
& + w_{\mathfrak{m}}^{c2}[\boldsymbol{\mathcal{X}}_{\mathfrak{m}}(n|n-1) + \boldsymbol{\mathcal{X}}_{\mathfrak{m}+U}(n|n-1) - 2\boldsymbol{\mathcal{X}}_0(n|n-1)]^\star\} + \boldsymbol{\mathcal{Q}}
\end{aligned}
\tag{E.8}
$$

Then, the *a priori* sigma points are calculated as follows:

$$
\boldsymbol{\mathcal{X}}(n|n-1) = \left[\begin{array}{ccc} \boldsymbol{\mathcal{X}}_0(n|n-1) & \boldsymbol{\mathcal{X}}_a(n|n-1) & \boldsymbol{\mathcal{X}}_b(n|n-1) \end{array}\right]
\tag{E.9}
$$

where:

$$
\begin{aligned}
\boldsymbol{\mathcal{X}}_0(n|n-1) &= \hat{\mathbf{x}}(n|n-1) \\
\boldsymbol{\mathcal{X}}_a(n|n-1) &= \hat{\mathbf{x}}(n|n-1) + \Lambda\left(\sqrt[\star]{\mathbf{P}(n|n-1)}\right)_{\mathfrak{m}} \quad \mathfrak{m} \in \{1,\ldots,U\} \\
\boldsymbol{\mathcal{X}}_b(n-1|n-1) &= \hat{\mathbf{x}}(n|n-1) - \Lambda\left(\sqrt[\star]{\mathbf{P}(n|n-1)}\right)_{\mathfrak{m}} \quad \mathfrak{m} \in \{U,\ldots,2U\}
\end{aligned}
\tag{E.10}
$$

Once the *a priori* sigma points are calculated, they are propagated through the non-linear function:

$$\boldsymbol{\mathcal{Y}}(n|n-1) = \boldsymbol{\Psi}_n\left(\boldsymbol{\mathcal{X}}(n|n-1)\right) \tag{E.11}$$

The mean and the covariance of $\mathbf{y}(n)$ are approximated by using the *posterior* sigma points as follows:

$$\hat{\mathbf{y}}^-(n) = \sum_{\mathfrak{m}=0}^{2U} w_{\mathfrak{m}}^{c0} \boldsymbol{\mathcal{Y}}_{\mathfrak{m}}(n|n-1) \tag{E.12}$$

where $\boldsymbol{\mathcal{Y}}_{\mathfrak{m}}(n|n-1) = \boldsymbol{\Phi}_n\left(\boldsymbol{\mathcal{X}}(n|n-1)\right)$.

Then, the state vector is estimated recursively as follows:

$$\hat{\mathbf{x}}(n|n) = \hat{\mathbf{x}}(n|n-1) + \mathbf{K}(n)\{\mathbf{y}(n) - \hat{\mathbf{y}}^-(n)\} \tag{E.13}$$

where $\mathbf{K}(n)$ is the Kalman gain defined as:

$$\mathbf{K}(n) = \{\mathbf{P^{xy}}(n)\}\{\mathbf{P^{yy}}(n)\}^{-1} \tag{E.14}$$

On the one hand, when using the UKF, the covariance matrix $\mathbf{P^{yy}}(n)$ of the innovation $\tilde{\mathbf{y}}(n) = \mathbf{y}(n) - \hat{\mathbf{y}}^-(n)$ and the cross-covariance matrix $\mathbf{P^{xy}}(n)$ between $\mathbf{y}(n)$ and the state prediction error satisfy:

$$\mathbf{P^{yy}}(n) = \sum_{\mathfrak{m}=0}^{2U} w_{\mathfrak{m}}^{c1}\left[\boldsymbol{\mathcal{Y}}_{\mathfrak{m}}(n|n-1) - \hat{\mathbf{y}}^-(n)\right]^\star + \boldsymbol{\mathcal{R}} \tag{E.15}$$

$$\mathbf{P^{xy}}(n) = \sum_{\mathfrak{m}=0}^{2U} w_{\mathfrak{m}}^{c1}\left[\boldsymbol{\mathcal{X}}_{\mathfrak{m}}(n|n-1) - \hat{\mathbf{x}}^-(n)\right] \times \left[\boldsymbol{\mathcal{Y}}_{\mathfrak{m}}(n|n-1) - \hat{\mathbf{y}}^-(n)\right] \tag{E.16}$$

On the other hand, when using the CDKF, the covariance matrix of the innovation and the cross-covariance matrix between $\mathbf{y}(n)$ and the state prediction error satisfy:

$$\begin{aligned}
\mathbf{P^{yy}}(n) = \sum_{\mathfrak{m}=0}^{U} \{&w_{\mathfrak{m}}^{c1}\left[\boldsymbol{\mathcal{Y}}_{\mathfrak{m}}(n|n-1) - \boldsymbol{\mathcal{Y}}_{\mathfrak{m}+U}(n|n-1)\right]^\star \\
&+ w_{\mathfrak{m}}^{c2}[\boldsymbol{\mathcal{Y}}_{\mathfrak{m}}(n|n-1) + \boldsymbol{\mathcal{Y}}_{\mathfrak{m}+U}(n|n-1) - 2\boldsymbol{\mathcal{Y}}_0(n|n-1)]^\star\} + \boldsymbol{\mathcal{R}}
\end{aligned} \tag{E.17}$$

$$\mathbf{P^{xy}}(n) = \sqrt{w_{\mathfrak{m}}^{c1}\mathbf{P}(n|n-1)}\left[\boldsymbol{\mathcal{Y}}_{1:U}(n|n-1) - \boldsymbol{\mathcal{Y}}_{U+1:2U}(n|n-1)\right]^H \tag{E.18}$$

Finally, the estimation error covariance matrix is updated as follows:

$$\mathbf{P}(n|n) = \mathbf{P}(n|n-1) - \mathbf{K}(n)\mathbf{P^{yy}}(n)\mathbf{K}^H(n) \tag{E.19}$$

Appendix F

Extended and Unscented H∞ Filter

When a non-linear estimation issue is addressed, alternatives to the Kalman filtering approaches are the so-called "extended H∞ filter" and the "unscented H∞ filter".

Indeed, initial works about the "extended H∞ filter" were conducted by Burl [Burl 98]. Like the EKF, it consists of a first-order linearization around the last available estimation of the state vector. Since, various authors have used the "extended H∞ filter. See for instance, Giremus *et al.* [Gire 09] who study the relevance of H∞ filtering in the field of the global positioning system navigation. However, the authors do not obtain noticeable improvements in terms of positioning error in comparison with the Kalman filtering.

Let us consider the equations (D.1), (D.2) and (B.1), that define the state-space of the system. The matrix $\mathbf{P}^\infty(n+1|n)$ satisfies the following Riccati equation for the "extended H_∞ filter":

$$
\begin{aligned}
\mathbf{P}^\infty(n+1|n) &= \nabla\boldsymbol{\Phi}_{n+1}^H|_{\hat{\mathbf{x}}(n|n)}\mathbf{P}^\infty(n|n)\nabla\boldsymbol{\Phi}_{n+1}^H|_{\hat{\mathbf{x}}(n|n)} + \boldsymbol{\Gamma}\boldsymbol{\mathcal{W}}\boldsymbol{\Gamma}^H & \text{(F.1)} \\
&= \nabla\boldsymbol{\Phi}_{n+1}|_{\hat{\mathbf{x}}(n|n)}\mathbf{P}^\infty(n|n-1)\{\mathbf{I}_U - \left[\ \nabla\boldsymbol{\Psi}_n^H|_{\hat{\mathbf{x}}(n|n-1)} \quad \boldsymbol{\mathcal{L}}^H\ \right] \\
&\quad \times \mathbb{M}^{-1}\left[\begin{array}{c} \nabla\boldsymbol{\Psi}_n|_{\hat{\mathbf{x}}(n|n-1)} \\ \boldsymbol{\mathcal{L}} \end{array}\right]\mathbf{P}^\infty(n|n-1)\}\nabla\boldsymbol{\Phi}_{n+1}^H|_{\hat{\mathbf{x}}(n|n)} \\
&\quad + \boldsymbol{\Gamma}\boldsymbol{\mathcal{W}}\boldsymbol{\Gamma}^H & \text{(F.2)}
\end{aligned}
$$

where $\nabla\boldsymbol{\Phi}_{n+1}^H|_{\hat{\mathbf{x}}(n|n)}$ is the Jacobian matrix of $\boldsymbol{\Phi}_{n+1}$ evaluated for $\hat{\mathbf{x}}(n|n)$, $\nabla\boldsymbol{\Psi}_n|_{\hat{\mathbf{x}}(n|n-1)}$ is the Jacobian matrix of $\boldsymbol{\Psi}_n$ evaluated for $\hat{\mathbf{x}}(n|n-1)$ and

$$
\begin{aligned}
\mathbb{M} &= \left[\begin{array}{cc} \boldsymbol{\mathcal{V}} & \mathbf{0} \\ \mathbf{0} & -\Xi^2\mathbf{I}_U \end{array}\right] + \left[\begin{array}{c} \nabla\boldsymbol{\Psi}_n|_{\hat{\mathbf{x}}(n|n-1)} \\ \boldsymbol{\mathcal{L}} \end{array}\right]\mathbf{P}^\infty(n|n-1)\left[\ \nabla\boldsymbol{\Psi}_n^H|_{\hat{\mathbf{x}}(n|n-1)} \quad \boldsymbol{\mathcal{L}}^H\ \right] \\
&= \left[\begin{array}{cc} \nabla\boldsymbol{\Psi}_n|_{\hat{\mathbf{x}}(n|n-1)}\mathbf{P}^\infty(n|n-1)\nabla\boldsymbol{\Psi}_n^H|_{\hat{\mathbf{x}}(n|n-1)} + \boldsymbol{\mathcal{V}} & \nabla\boldsymbol{\Psi}_n|_{\hat{\mathbf{x}}(n|n-1)}\mathbf{P}^\infty(n|n-1)\boldsymbol{\mathcal{L}}^H \\ \boldsymbol{\mathcal{L}}\mathbf{P}^\infty(n|n-1)\nabla\boldsymbol{\Psi}_n^H|_{\hat{\mathbf{x}}(n|n-1)} & \boldsymbol{\mathcal{L}}\mathbf{P}^\infty(n|n-1)\boldsymbol{\mathcal{L}}^H - \Xi^2\mathbf{I}_U \end{array}\right] \\
& \hspace{12cm} \text{(F.3)}
\end{aligned}
$$

157

where Ξ^2 is the prescribed noise attenuation level given in (B.3).

When using the "extended H_∞ filter", the state vector can be estimated recursively as follows:

$$\hat{\mathbf{x}}(n|n) = \hat{\mathbf{x}}(n|n-1) + \mathbf{K}^\infty(n)\{\mathbf{y}(n) - \boldsymbol{\Psi}_n(\hat{\mathbf{x}}(n|n-1))\} \tag{F.4}$$

where $\mathbf{K}^\infty(n)$ is the filter gain defined as:

$$\mathbf{K}^\infty(n) = \{\mathbf{P^{xy}}^\infty(n)\}\{\mathbf{P^{yy}}^\infty(n)\}^{-1} \tag{F.5}$$

where $\mathbf{P^{yy}}^\infty(n)$ is defined as follows:

$$\mathbf{P^{yy}}^\infty(n) = \nabla\boldsymbol{\Psi}_n|_{\hat{\mathbf{x}}(n|n-1)}\mathbf{P}^\infty(n|n-1)\nabla\boldsymbol{\Psi}_n^H|_{\hat{\mathbf{x}}(n|n-1)} + \boldsymbol{\mathcal{V}} \tag{F.6}$$

and $\mathbf{P^{xy}}^\infty(n)$ is:

$$\mathbf{P^{xy}}^\infty(n) = \mathbf{P}^\infty(n|n-1)\nabla\boldsymbol{\Psi}_n^H|_{\hat{\mathbf{x}}(n|n-1)} \tag{F.7}$$

Remark 1: when Ξ^2 tends to $+\infty$, the "extended H$_\infty$ filter" reduces to the EKF [Hass 99].

Remark 2: the computational cost of the "extended H$_\infty$ filter" is slightly higher than the EKF.

The "unscented H$_\infty$ filter" was recently proposed by Li *et al.* in [Li 10]. It is implemented by embedding the unscented transformation into the "extended H$_\infty$ filter" architecture. According to the authors, the unscented H$_\infty$ filtering can be carried out by using the statistical linear error propagation approach [Sibl 06]. Like the UKF, the unscented H$_\infty$ filter avoids the linearization step by using an unscented transformation. In [Wang 10], an unscented H$_\infty$ filter is used to provide an initial alignment of an inertial navigation system. The authors show that the H$_\infty$ filtering approach would be an effective method when the measurement noise is colored.

According to [Li 10] and given (D.1), (D.2) and (B.1), when using the "unscented H$_\infty$ filter", the state vector can be estimated as follows:

$$\hat{\mathbf{x}}(n|n) = \hat{\mathbf{x}}(n|n-1) + \mathbf{K}^\infty(n)\{\mathbf{y}(n) - \hat{\mathbf{y}}^-(n)\} \tag{F.8}$$

where $\hat{\mathbf{y}}^-(n)$ is obtained as in (E.12) by performing the same process as in the UKF, but by replacing the matrix $\mathcal{Q}$ by $\mathcal{W}$. The gain $\mathbf{K}^\infty(n)$ is obtained as in (F.5), but $\mathbf{P}^{\mathbf{xy}\infty}(n)$ and $\mathbf{P}^{\mathbf{yy}\infty}(n)$ are now approximated as follows:

$$\mathbf{P}^{\mathbf{yy}\infty}(n) \approx \sum_{\mathfrak{m}=0}^{2U} w_{\mathfrak{m}}^{c1} \left[\boldsymbol{\mathcal{Y}}_{\mathfrak{m}}(n|n-1) - \hat{\mathbf{y}}^-(n)\right]^\star + \boldsymbol{\mathcal{V}} \tag{F.9}$$

and

$$\mathbf{P}^{\mathbf{xy}\infty}(n) \approx \sum_{\mathfrak{m}=0}^{2U} w_{\mathfrak{m}}^{c1} \left[\boldsymbol{\mathcal{X}}_{\mathfrak{m}}(n|n-1) - \hat{\mathbf{x}}^-(n)\right] \times \left[\boldsymbol{\mathcal{Y}}_{\mathfrak{m}}(n|n-1) - \hat{\mathbf{y}}^-(n)\right] \tag{F.10}$$

where the $w_{\mathfrak{m}}^{c1}$, $\boldsymbol{\mathcal{X}}_{\mathfrak{m}}(n|n-1)$, $\hat{\mathbf{x}}^-(n)$ and $\boldsymbol{\mathcal{Y}}_{\mathfrak{m}}(n|n-1)$ are obtained as in (E.3), (E.5), (E.6) and (E.11) respectively, by the using the UKF process.

Considering $\mathcal{L} = \mathbf{I}_U$, given (F.6), (F.7), (F.9) and (F.10) the matrix $\mathbb{M}$ in (F.3) can be rewritten as:

$$\mathbb{M} = \left[\begin{array}{cc} \mathbf{P}^{\mathbf{yy}\infty}(n) & \{\mathbf{P}^{\mathbf{xy}\infty}(n)\}^H \\ \mathbf{P}^{\mathbf{xy}\infty}(n) & \mathbf{P}^\infty(n|n-1) - \Xi^2\mathbf{I}_U \end{array}\right] \tag{F.11}$$

Finally, the matrix $\mathbf{P}^\infty(n|n)$ can be obtained as:

$$\begin{aligned} \mathbf{P}^\infty(n|n) &= \mathbf{P}^\infty(n|n-1) - \left[\begin{array}{cc} \mathbf{P}^{\mathbf{xy}\infty}(n) & \mathbf{P}^\infty(n|n-1) \end{array}\right] \\ &\times \mathbb{M}^{-1} \left[\begin{array}{c} \{\mathbf{P}^{\mathbf{xy}\infty}(n)\}^H \\ \mathbf{P}^\infty(n|n-1) \end{array}\right] \end{aligned} \tag{F.12}$$

Remark 1: the unscented transform is used to approximate the matrices that are involved in the definition of the H$_\infty$ gain.

Remark 2: concerning the work proposed by Li *et al.* in [Li 10], we have decided to look at it and evaluate its performance even if we are not totally convinced by the way the authors have motivated their approach and justified it. On the one hand, in their paper [Li 10], they speak of covariance matrices and define some quantities using the expectation. This should not be done as they are working in an H$_\infty$ setting, where there is not statistical mean to be considered. On the other hand, according to appendix C, we have seen that the equations describing the H$_\infty$ filter could be seen as a kind of Kalman filter. Therefore, we can understand that the authors in [Li 10] consider that the solution of the Ricatti equation in the H$_\infty$ setting can be viewed as a covariance matrix.

References

[3GPP 09] 3GPP Standard. Technical Specification Group Radio Access Network; Evolved Universal Terrestrial Radio Access (E-UTRA); Physical layer procedures (Release 8). *3GPP TS 36.213 V8.8.0*, September 2009. 1, 25, 26

[Alam 98] S. M. Alamouti. A Simple Transmit Diversity Technique for Wireless Communications. *IEEE Journal on Selected Areas in Communications*, Vol. 16, No. 8, pp. 1451–1458, October 1998. 116, 120

[Arsl 07] H. Arslan. *Cognitive Radio, Software Defined Radio, and Adaptive Wireless Systems.* Springer, 2007. 10

[Bar 01] Y. Bar-Shalom, X. R. Li, and T. Kirubarajan. *Estimation With Applications to Tracking and Navigation.* Wiley, 2001. 4, 56, 146

[Bass 93] M. Basseville and I. V. Nikiforov. *Detection of Abrupt Changes: Theory and Application.* Prentice Hall, 1993. 88

[Berr 93] C. Berrou, A. Glavieux, and P. Thitimajshima. Near Shannon Limit Error-Correcting Coding and Decoding: Turbo-codes. *Proceedings of the IEEE International Conference on Communications (ICC '93)*, Vol. 2, pp. 1064–1070, May 1993. 40

[Bian 05] H. Bian, Z. Jin, and W. Tian. Study on GPS Attitude Determination System Aided INS Using Adaptive Kalman Filter. *Measurement Science and Technology*, Vol. 6, No. 10, pp. 2072–2079, September 2005. 80

[Bing 90] J. Bingham. Multicarrier Modulation for Data Transmission: An Idea Whose Time Has Come. *IEEE Communication Magazine*, Vol. 28, pp. 5–14, May 1990. 23

[Boas 64]   R. P. Boas Jr. and R. C. Buck. *Polynomial Expansions of Analytic Functions*. Springer-Verlag, 1964. 152

[Brez 88]   C. Brezinski. Other Manifestations of the Schur Complement. *Linear Algebra and its Applications*, Vol. 111, pp. 231–247, December 1988. 139

[Broe 03]   L. Broetje, S. Vogeler, and K. D. Kammeyer. Blind Bluetooth Interference Detection and Suppression for OFDM Transmission in the ISM Band. *Proceedings of the IEEE Asilomar Conference on Signals, Systems and Computers (ACSSC '03)*, Vol. 1, pp. 703–707, November 2003. 79

[Burl 98]   J. B. Burl. H_∞ Estimation for Nonlinear Systems. *IEEE Signal Processing Letters*, Vol. 5, No. 8, pp. 199–202, August 1998. 57, 157

[Cabr 04]   D. Cabric, S. M. Mishra, and R. W. Brodersen. Implementation Issues in Spectrum Sensing for Cognitive Radios. *Proceedings of the IEEE Asilomar Conference on Signals, Systems and Computers (ACSSC '04)*, Vol. 1, pp. 772–776, November 2004. 79

[Cao 04a]   Z. Cao, U. Tureli, Y. D. Yao, and P. Honan. Frequency Synchronization for Generalized OFDMA Uplink. *Proceedings of the IEEE Global Communications Conference (GLOBECOM '04)*, pp. 1071–1075, December 2004. 51, 75, 104, 113, 115, 123, 125, 129

[Cao 04b]   Z. Cao, U. Tureli, and Y. D. Yao. Deterministic Multiuser Carrier-Frequency Offset Estimation for Interleaved OFDMA Uplink. *IEEE Transactions on Communications*, Vol. 52, No. 9, pp. 1585–1594, September 2004. 52, 75

[Chen 10]   C. J. Chen, T. T. Lin, and T. C. Chen. Blind Joint Frequency Offset and Channel Estimation for MC-CDMA Systems over Multipath Fading Channels. *Proceedings of the Mechanical and Electronics Engineering (ICMEE '10)*, pp. 137–141, August 2010. 104

[Chie 07]   F. T. Chien and C. C. J. Kuo. Blind Recursive Tracking of Carrier Frequency Offset (CFO) Vector in MC-CDMA Systems. *IEEE Transactions on Wireless Communications*, Vol. 6, No. 4, pp. 1246–1255, April 2007. 103

[Choi 00]   J. H. Choi, Y. H. Lee, C. G. Lee, and H. W. Jung. Carrier Frequency Offset Compensation for Uplink of OFDM-FDMA Systems. *Proceedings of the IEEE International Conference on Communications (ICC '00)*, Vol. 1, pp. 425–429, June 2000. 50, 51, 104

[Cibl 04]   P. Ciblat and E. Serpedin. A Fine Blind Frequency Offset Estimator for OFDM/OQAM Systems. *IEEE Transactions on Signal Processing*, Vol. 52, No. 1, pp. 291–296, January 2004. 52

[Cimi 85]   L. J. Cimini. Analysis and Simulation of a Digital Mobile Channel Using Orthogonal Frequency Division Multiplexing. *IEEE Transactions on Communications*, Vol. COM-33, No. 7, pp. 665–675, July 1985. 23

[Dai 07]   X. Dai. Carrier Frequency Offset Estimation and Correction for OFDMA Uplink. *IET Commununications*, Vol. 1, No. 2, pp. 273–281, April 2007. 49

[Dash 00]   P. K. Dash, R. K. Jena, G. G. Panda, and A. Routray. An Extended Complex Kalman Filter for Frequency Measurement of Distorted Signals. *IEEE Transactions on Instrumentation and Measurement*, Vol. 49, No. 4, pp. 746–753, August 2000. 55

[Dini 10]   D. H. Dini and D. P. Mandic. Analysis of the Widely Linear Complex Kalman Filter. *Proceedings of the UDRC Sensor Signal Processing for Defense (SSPD '10)*, pp. 1–4, September 2010. 55

[ETSI 01]   ETSI Standard. Interaction Channel for Digital Terrestrial Television (RCT) Incorporating Multiple Access OFDM. *ETSI DVB RCT*, March 2001. 24

[ETSI 95] ETSI Standard. Radio Broadcasting Systems: Digital Audio Broadcasting to Mobile, Portable and Fixed Receivers. *ETS 300 401, European Telecommunications Standard*, 1995. 24

[ETSI 97] ETSI Standard. Digital Video Broadcasting (DVB-T); Frame Structure, Channel Coding, Modulation for Digital Terrestrial Television. *ETS 300 744, European Telecommunications Standard*, 1997. 24

[Ferr 10] G. Ferré and M. Raoult. Flexible Distributed Wideband Cognitive Radio Network with Double Threshold Energy Detector Combining Cooperative and Spatial Diversity. *Proceedings of the EURASIP European Signal Processing Conference (EUSIPCO '10)*, pp. 880–884, August 2010. 79

[Foki 09] L. Fokin and A. G. Shchipitsyn. Innovation-Based Adaptive Kalman Filter Derivation. *Proceedings of the IEEE International Sierian Conference on Control and Communications (SIBCON '09)*, pp. 318–323, March 2009. 80

[Fu 06] X. Y. Fu, H. Minn, and C. Cantrell. Two Novel Iterative Joint Frequency-Offset and Channel Estimation Methods for OFDMA Uplink. *Proceedings of the IEEE Global Communications Conference (GLOBECOM '06)*, pp. 1–6, November 2006. 2, 52

[Gelb 74] A. Gelb. *Applied Optimal Estimation*. MIT Press, 1974. 149

[Gero 99] J. C. Geromel. Optimal Linear Filtering Under Parameter Uncertainty. *IEEE Transactions on Signal Processing*, Vol. 47, pp. 168–175, January 1999. 135

[Gire 09] A. Giremus, E. Grivel, and F. Castanié. Is H_∞ Filter Relevant for Correlated Noises in GPS Navigation. *Proceedings of the IEEE International Conference on Digital Signal Processing (DSP '09)*, pp. 1–6, July 2009. 5, 157

[Grew 10]   M. S. Grewal and J. Kain. Kalman Filter Implementation with Improved Numerical Properties. *IEEE Transactions on Automatic Control*, Vol. 55, No. 9, pp. 2058–2068, September 2010. 56

[Grim 90]   M. J. Grimble and A. E. Sayed. Solution of the H$_\infty$ Optimal Linear Filtering Problem for Discrete-time Systems. *IEEE Transactions on Acoustics, Speech, and Signal Processing*, Vol. 38, pp. 1092–1104, July 1990. 135, 138

[Grol 07]   J. Grolleau. *Modelès et Estimateurs de Canaux de Rayleigh pour la Detéction de Symboles dans un Système Multiporteuse à Étalement de Spectre*. PhD thesis, under the supervision of E. Grivel and M. Najim, Université Bordeaux 1, Ecole Doctorale des Sciences Physiques et de l'Ingénieur, December 2007. In French. 1

[Hanz 98]   L. Hanzo. Bandwidth-Efficient Wireless Multimedia Communications. *Proceedings of the IEEE*, Vol. 86, pp. 1342–1382, July 1998. 8, 19, 20

[Hass 99]   B. Hassibi, A. H. Sayed, and T. Kailath. *Indefinite-Quadratic Estimation and Control, a Unified Approach to H$_2$ and H$_\infty$ Theories*. Society for Industrial and Applied Mathematics (SIAM), 1999. 57, 158

[Hayk 96]   S. Haykin. *Adaptative Filter Theory*. Prentice Hall, 1996. 56, 143

[Hou 08]   S. W. Hou and C. C. Ko. Intercarrier Interference Suppression for OFDMA Uplink in Time and Frequency Selective Rayleigh Fading Channels. *Proceedings of the IEEE Vehicular Technology Conference (VTC '08)*, pp. 1438–1442, May 2008. 3, 5, 51, 68, 70

[Hu 11]   J. S. Hu and C. H. Yang. Second-Order Extended H$_\infty$ Filter for Nonlinear Discrete-Time Systems Using Quadratic Error Matrix Approximation. *IEEE Transactions on Signal Processing*, Vol. 59, No. 7, pp. 3110–3119, July 2011. 130

[Huan 05] D. Huang and K. B. Letaief. An Interference Cancellation Scheme for Carrier Frequency Offsets Correction in OFDMA Systems. *IEEE Transactions on Communications*, Vol. 53, No. 7, pp. 1155–1165, July 2005. 50, 75, 104

[Huan 10a] Q. F. Huang, M. Ghogho, J. Wei, and P. Ciblat. Practical Timing and Frequency Synchronization for OFDM-Based Cooperative Systems. *IEEE Transactions on Signal Processing*, Vol. 58, No. 7, pp. 3706–3716, July 2010. 49

[Huan 10b] W. C. Huang, C. P. Li, and H. J. Li. An Investigation into the Noise Variance and the SNR Estimators in Imperfectly-Synchronized OFDM Systems. *IEEE Transactions on Wireless Communications*, Vol. 9, No. 3, pp. 1159–1167, March 2010. 86, 107

[Huan 11] Y. Huang, H. Li, K. A. Campbell, and Z. Han. Defending False Data Injection Attack on Smart Grid Network Using Adaptive CUSUM Test. *Proceedings of the IEEE Conference on Information Sciences and Systems (CISS '11)*, pp. 1–6, March 2011. 89

[IEEE 06] IEEE Standard. Part 16: Air Interface for Fixed and Mobile Broadband Wireless Access System; Amendment 2: Physical and Medium Access Control Layers for Combined Fixed and Mobile Operation in Licensed Bands. *IEEE Std. 802.16e-2005*, February 2006. 1, 3, 24

[IEEE 99] IEEE Standard. Part 11: Wireless LAN Medium Access Control (MAC) and Physical Layer (PHY) Specifications; Higher-Speed Physical Layer Extension in the 5 GHz Band. *IEEE Std. 802.11a*, December 1999. 3, 24

[Ito 00] K. Ito and K. Xiong. Gaussian Filters for Nonlinear Filtering Problems. *IEEE Transactions on Automatic Control*, Vol. 5, No. 5, pp. 910–927, May 2000. 56, 130, 152

[ITU 08] ITU Report. ITU Corporate Annual Report 2008. pp. 38–40, June 2008. 9

[Jake 74] W. C. Jakes. *Microwave mobile communications*. Wiley-IEEE Press, 1974. 13, 15

[Jamo 07a] A. Jamoos, J. Grolleau, E. Grivel, H. A. Nour, and M. Najim. Kalman vs H$_\infty$ Algorithms for MC-DS-CDMA Channel Estimation with or without a priori AR Modeling. *Lecture Notes in Electrical Engineering*, 2007. 135

[Jamo 07b] A. Jamoos. *Contribution à la Mise en Œuvre de Récepteurs et de Techniques d'Estimation de Canal pour les Systèmes Mobiles DS-CDMA Multi-porteuse*. PhD thesis, under the supervision of E. Grivel and M. Najim, Université Bordeaux 1, Ecole Doctorale des Sciences Physiques et de l'Ingénieur, June 2007. 1

[Jing 08] Y. Jing, F. L. Yin, and Z. Chen. An H$_\infty$ Filter Based Approach to Combat Inter-Carrier Interference for OFDM Systems. *IEEE Communications Letters*, Vol. 12, No. 6, pp. 453–455, June 2008. 2, 47, 49

[Juli 95] S. J. Julier, J. K. Uhlmann, and H. F. Durrant-Whyte. A New Approach for Filtering Nonlinear Systems. *Proceedings of the IEEE American Control Conference (ACC '95)*, Vol. 3, pp. 1628–1632, June 1995. 153

[Kalm 60] R. E. Kalman. A New Approach to Linear Filtering and Prediction Problems. *Transactions of the ASME - Journal of Basic Engineering*, pp. 34–45, March 1960. 131

[Kang 07] T. H. Kang and R. A. Iltis. Iterative Decoding, Offset and Channel Estimation for OFDM using the Unscented Kalman Filter. *Proceedings of the IEEE Asilomar Conference on Signals, Systems and Computers (ACSSC '07)*, pp. 1828–1732, November 2007. 54, 55

[Kell 00] T. Keller and L. Hanzo. Adaptive Multicarrier Modulation: A Convenient Framework for Time-Frequency Processing in Wireless Communications. *Proceedings of the IEEE*, Vol. 88, No. 5, pp. 611–640, May 2000. 23

[Laba 05] D. Labarre, E. Grivel, M. Najim, and N. Christov. Relevance of H$_\infty$ Filtering for Speech Enhancement. *Proceedings of the IEEE International Conference on Acoustics, Speech, and Signal Processing (ICASSP '05)*, Vol. 4, pp. 169–172, March 2005. 5, 135

[Laba 07] D. Labarre, E. Grivel, M. Najim, and N. Christov. Dual H$_\infty$ Algorithms for Signal Processing-Application to Speech Enhancement. *IEEE Transactions on Signal Processing*, Vol. 55, No. 11, pp. 5195–5208, November 2007. 135

[Lefe 02] T. Lefebvre, H. Bruyninckx, and J. D. Schutter. Comment on a New Method for the Nonlinear Transformation of Means and Covariances in Filters and Estimators. *IEEE Transactions on Automatic Control*, Vol. 7, No. 8, pp. 1406–1408, August 2002. 152

[Li 07] T. Li, W. H. Mow, V. K. N. Lau, M. H. Siu, R. S. Cheng, and R. D. Murch. Robust Joint Interference Detection and Decoding for OFDM-Based Cognitive Radio Systems with Unknown Interference. *IEEE Journal on Selected Areas Communications*, Vol. 25, No. 3, pp. 566–575, April 2007. 79

[Li 10] W. L. Li and Y. M. Jia. H$_\infty$ Filtering for a Class of Nonlinear Discrete-Time Systems based on Unscented Transform. *Signal Processing*, Vol. 90, No. 12, pp. 3301–3307, December 2010. 5, 57, 158, 159

[Maha 06] I. Mahafeno, C. Langlais, and C. Jego. OFDM-IDMA Versus IDMA with ISI Cancellation for Quasi-Static Rayleigh Fading Multipath Channels. *Proceedings of the VDE International Symposium on Turbo Codes in Connection with International ITG-Conference on*

Source and Channel Coding, April 2006. 4, 26, 40, 41, 42, 43, 102, 104, 112

[Maha 07] I. Mahafeno. *Etude de la Technique d'Accès Multiple IDMA (Interleave Division Multiple Access)*. PhD thesis, under the supervision of C. Berrou, Ecole Nationale Supérieure des Télécommunications de Bretagne, May 2007. In French. 38

[Mare 06] H. Marey and M. Steendam. The Effect of Narrowband Interference on Frequency Ambiguity Resolution for OFDM. *Proceedings of the IEEE Vehicular Technology Conference (VTC '06)*, pp. 1–5, September 2006. 79

[Mito 00] J. Mitola III. *An Integrated Agent Architecture for Software Defined Radio*. PhD thesis, under the supervision of G. Q Maguire, Royal Institute of Technology (KTH), May 2000. 3, 9

[Mito 99] J. Mitola III and G. Q. Maguire Jr. Cognitive Radio: Making Software Radios More Personal. *IEEE Personal Communications*, Vol. 6, No. 4, pp. 13–18, August 1999. 8, 9

[Moos 94] P. H. Moose. A Technique for Orthogonal Frequency Division Multiplexing Frequency Offset Correction. *IEEE Transactions on Communications*, Vol. 42, No. 10, pp. 2908–2914, October 1994. 48, 50, 51, 107

[More 04] M. Morelli. Timing and Frequency Synchronization for the Uplink of an OFDMA System. *IEEE Transactions on Communications*, Vol. 52, No. 2, pp. 296–306, February 2004. 2, 47, 49

[More 07] M. Morelli, C. C. J. Kuo, and M. O. Pun. Synchronization Techniques for Orthogonal Frequency Division Multiple Access (OFDMA): A Tutorial Review. *Proceedings of the IEEE*, Vol. 95, No. 7, pp. 1394–1427, July 2007. 48

[More 08] M. Morelli and M. Moretti. Robust Frequency Synchronization for OFDM-Based Cognitive Radio Systems. *IEEE Transactions on Wireless Communications*, Vol. 7, No. 12, pp. 5346–5355, December 2008. 80, 92, 93, 97, 98, 100, 129

[Mova 08] M. Movahedian, M. Yi, and R. Tafazolli. An MUI Resilient Approach for Blind CFO Estimation in OFDMA Uplink. *Proceedings of the IEEE International Symposium on Personal, Indoor and Mobile Radio Communications (PIMRC '08)*, pp. 1–5, September 2008. 53, 75

[Nish 99] K. Nishiyama. Robust Estimation of a Single Complex Sinusoid in White Noise - H$_\infty$ Filtering Approach. *IEEE Transactions on Signal Processing*, Vol. 47, No. 10, pp. 2853–2856, October 1999. 55

[Norg 00] M. Nørgard, N. K. Poulsen, and O. Ravn. New Developments in State Estimation for Nonlinear Systems. *Automatica*, Vol. 36, pp. 1627–1638, November 2000. 152

[Pali 10] J. Palicot. *De la Radio Logicielle à la Radio Intelligente.* Hermes Science, 2010. In French. 10

[Ping 01] L. Ping, W. K. Leung, and K. Y. Wu. Low Rate Turbo-Hadamard Codes. *Proceedings of the IEEE International Symposium on Information Theory*, p. 211, August 2001. 40

[Ping 02a] L. Ping, K. Y. Wu, L. H. Liu, and W. K. Leung. A Simple Unified Approach to Nearly Optimal Multiuser Detection and Space-Time Coding. *Proceedings of the IEEE Information Theory Workshop (ITW '02)*, pp. 53–56, October 2002. 3, 6, 26, 112

[Ping 02b] L. Ping, K. Y. Wu, L. Liu, and W. K. Leung. A Simple, Unified Approach to Nearly Optimal Multiuser Detection and Space-Time Coding. *Proceedings of the IEEE Information Theory Workshop (ITW '02)*, pp. 53–56, October 2002. 115

[Ping 06]   L. Ping, L. H. Liu, K. Y. Wu, and W. K. Leung. Interleave-Division Multiple-Access. *IEEE Transactions on Communications*, Vol. 5, No. 4, pp. 938–947, April 2006. 26

[Pove 09a]   H. Poveda, G. Ferré, and E. Grivel. Estimation Aveugle Itérative par Filtrage H_∞ des Décalages Doppler d'un Système OFDMA Entrelacé en Liaison Montante. *Actes de la Conférence Groupe de Recherche et d'Etudes du Traitement du Signal (GRETSI '09)*, September 2009. In French. 3, 5, 128

[Pove 09b]   H. Poveda, G. Ferré, E. Grivel, and P. Ramos. A Blind Iterative Carrier Frequency Offset Estimator based on a Kalman Approach for an Interleaved OFDMA Uplink System. *Proceedings of the EURASIP European Signal Processing Conference (EUSIPCO '10)*, pp. 378–382, August 2009. 3, 5, 128

[Pove 10]   H. Poveda, G. Ferré, and E. Grivel. Joint Channel and Frequency Offset Estimation Using Sigma-Point Kalman Filter for an OFDMA Uplink System. *Proceedings of the EURASIP European Signal Processing Conference (EUSIPCO '10)*, pp. 855–859, August 2010. 4, 54, 86, 127

[Pove 11a]   H. Poveda, G. Ferré, N. Bouny, and E. Grivel. Estimation Jointe de Multiples Décalages de Fréquence dans un Système Coopératif à Relais OFDM-IDMA. *Actes de la Conférence Groupe de Recherche et d'Etudes du Traitement du Signal (GRETSI '11)*, September 2011. In French. 3, 6, 129

[Pove 11b]   H. Poveda, G. Ferré, and E. Grivel. Frequency Offset and Channel Estimations for an OFDMA Uplink Primary User System Despite a Cognitive Radio Interference. *To be submitted IEEE Transactions on Wireless Communications*, 2011. 3, 5, 80, 129

[Pove 11c]   H. Poveda, G. Ferré, and E. Grivel. A Non-Pilot Aided Iterative Carrier Frequency Offset Estimator Using Optimal Filtering for an

Interleaved OFDMA Uplink System. *Accepted to Wireless Personal Communications*, 2011. 3, 5, 66, 128

[Pove 11d] H. Poveda, G. Ferré, and E. Grivel. Robust Frequency Synchronization for an OFDMA Uplink System Disturbed by a Cognitive Radio System Interference. *Proceedings of the IEEE International Conference on Acoustics, Speech, and Signal Processing (ICASSP '11)*, pp. 3552–3555, May 2011. 3, 5, 80, 129

[Pove 12] H. Poveda, G. Ferré, and E. Grivel. Frequency Synchronization and Channel Equalization for an OFDM-IDMA Uplink system. *Submitted to IEEE International Conference on Acoustics, Speech, and Signal Processing (ICASSP '12)*, March 2012. 3, 6, 129

[Proa 95] J. G. Proakis. *Digital Communications*. McGraw-Hill, 1995. 22, 102

[Pun 04a] M. O. Pun, S. H. Tsai, and C. C. J. Kuo. An EM-Based Joint Maximum Likelihood Estimation of Carrier Frequency Offset and Channel for Uplink OFDMA Systems. *Proceedings of the IEEE Vehicular Technology Conference (VTC '04)*, pp. 598–602, September 2004. 2, 47, 51, 58, 59, 61, 64, 104, 128

[Pun 04b] M. O. Pun, S. H. Tsai, and C. C. J. Kuo. Joint Maximum Likelihood Estimation of Carrier Frequency Offset and Channel for Uplink OFDMA Systems. *Proceedings of the IEEE Global Communications Conference (GLOBECOM '04)*, Vol. 6, pp. 3748–3752, November 2004. 51

[Pun 06] M. O. Pun, M. Morelli, and C. C. J. Kuo. Maximum-Likelihood Synchronization and Channel Estimation for OFDMA Uplink Transmissions. *IEEE Transactions on Communications*, Vol. 54, No. 4, pp. 726–736, April 2006. 2, 47, 51, 52, 58, 59, 61, 64, 104, 128

[Quan 08] Z. Quan, S. G. Cui, A. H. Sayed, and H. Poor. Optimal Multiband Joint Detection for Spectrum Sensing in Cognitive Radio Networks. *IEEE Transactions on Signal Processing*, Vol. 57, No. 3, pp. 1128–1140, March 2008. 79

[Rapp 02]   T. S. Rappaport. *Wireless Communications: Principles and Practice*. Prentice Hall, 2002. 9

[Rehm 08]   H. U. Rehman, I. Zaka, S. Shah, and J. Ahmad. Combined Equalization and Channel Estimation for MC-IDMA Uplink Transmissions. *Proceedings of the IEEE Networking and Communications Conference (INCC '08)*, pp. 34–38, May 2008. 5, 103

[Roli 09]   C. A. Rolim Fernandes. *Nonlinear MIMO Communication Systems: Channel Estimation and Information Recovery using Volterra Models*. PhD thesis, under the supervision of G. Favier and J. C. Mota, Université de Nice Sophia Antipolis, Ecole Doctorale Sciences et Technologies de l'Information et de la Communication, July 2009. 130

[Saem 07]   A. Saemi, J. P. Cances, and V. Meghdadi. Synchronization Algorithms for MIMO OFDMA Systems. *IEEE Transactions on Wireless Communications*, Vol. 6, No. 12, pp. 4441–4451, December 2007. 52

[Sari 98]   H. Sari and G. Karam. Orthogonal Frequency Division Multiple Access and its Application to CATV Networks. *European Transactions on Telecommunications*, Vol. 45, pp. 507–516, November 1998. 24

[Schu 05]   H. Schulze and C. Lüders. *Theory and Applications of OFDM and CDMA*. Wiley, 2005. 21

[Sesi 09]   S. Sesia, I. Toufik, and M. Baker. *LTE, The UMTS Long Term Evolution: From Theory to Practice*. Wiley, 2009. 22, 26

[Sezg 08]   S. Sezginer and P. Bianchi. Asymptotically Efficient Reduced Complexity Frequency Offset and Channel Estimators for Uplink MIMO-OFDMA Systems. *IEEE Transactions on Signal Processing*, Vol. 56, No. 3, pp. 964–979, March 2008. 2, 47, 52, 64, 104

[Shak 92]   U. Shaked and Y. Theodor. H_∞ - Optimal Estimation: A Tutorial. *Proceedings of IEEE Conference on Decision and Control*, Vol. 2, pp. 2278–2286, August 1992. 135

[Shen 99] X. Shen and L. Deng. A Dynamic System Approach to Speech Enhancement Using the H$_\infty$ Filtering Algorithm. *IEEE Transactions on Speech and Audio Processing*, Vol. 7, pp. 391–399, July 1999. 5, 135

[Shik 10] J. Shikida, S. Suyama, H. Suzuki, and K. Fukawa. Iterative Receiver Employing Multiuser Detection and Channel Estimation for MIMO-OFDM IDMA. *Proceedings of the IEEE Vehicular Technology Conference (VTC '10)*, pp. 1–5, May 2010. 115

[Sibl 06] G. Sibley, G. S. Sukhatme, and L. Matthies. The Iterated Sigma-Point Kalman Filter with Applications to Long Range Stereo. *Proceedings of the Robotics: Science and Systems Conference*, pp. 16–19, August 2006. 158

[Song 09] J. Song, J. H. Hu, and X. Z. Xiong. EM Estimation Algorithm for TDR-IDMA Systems in Complex Multipath Channel. *Proceedings of the IEEE International Conference on Communications Technology and Applications (ICCTA '09)*, pp. 671–675, October 2009. 103

[Stal 05] W. Stallings. *Wireless Communications and Networks,*. Prentice Hall, 2005. 9

[Stub 02] G. Stüber. *Principles of Mobile Communication*. Kluwer Academic Publishers, 2002. 13, 15, 19, 20, 21

[Suya 08] S. Suyama, L. Zhang, H. Suzuki, and K. Fukawa. Performance of Iterative Multiuser Detection with Channel Estimation for MC-IDMA and Comparison with Chip-Interleaved MC-CDMA. *Proceedings of the IEEE Global Communications Conference (GLOBECOM '08)*, pp. 1–5, December 2008. 5, 103

[Taro 97] V. Tarokh, N. Seshadri, and A. R. Calderbank. Space-Time Codes For High Data Rate Wireless Communication: Performance Criteria. *Proceedings of the IEEE International Conference on Communications (ICC '97)*, Vol. 1, pp. 299–303, June 1997. 115

[Taro 99] V. Tarokh, N. Seshadri, and A. R. Calderbank. Space-Time Block Codes from Orthogonal Designs. *IEEE Transactions on Information Theory*, Vol. 45, No. 5, pp. 1456–1467, July 1999. 115

[Ther 92] C. W. Therrien. *Discrete Random Signals and Statistical Signal Processing.* Prentice-Hall, 1992. 51

[Thia 07] L. B. Thiagarajan, S. Attallah, and Y. C. Liang. Two-Stage Frequency Synchronization for Uplink MC-CDMA System. *Proceedings of the IEEE Wireless Communications and Networking Conference (WCNC '07)*, pp. 2441–2445, March 2007. 103

[VdBe 99] J. J. Van de Beek, P. O. Börjesson, M. L. Boucheret, D. Landström, J. M. Arenas, O. Ödling, C. Östberg, M. Wahlqvist, and S. K. Wilson. Time and Frequency Synchronization Scheme for Multiuser OFDM. *IEEE Journal on Selected Areas Communications*, Vol. 17, No. 11, pp. 1900–1914, November 1999. 48, 49

[VdMe 01] R. van der Merwe and E. A. Wan. The Square-Root Unscented Kalman Filter for State and Parameter-Estimation. *Proceedings of the IEEE International Conference on Acoustics, Speech, and Signal Processing (ICASSP '01)*, Vol. 6, pp. 3461–3464, May 2001. 152

[VdMe 04a] R. van der Merwe. *Sigma-Point Kalman Filters for Probabilistic Inference in Dynamic State-space Models.* PhD thesis, under the supervision of E. A. Wan, OGI School of Science and Engineering at Oregon Health and Science University, April 2004. 4, 56, 134

[VdMe 04b] R. van der Merwe, E. A. Wan, and S. J. Julier. Sigma-Point Kalman Filters for Nonlinear Estimation and Sensor-Fusion: Applications to Integrated Navigation. *Proceedings of the AIAA Guidance, Navigation and Control Conference (GNC '04)*, pp. 1–30, August 2004. 153, 154

[Wan 01] E. A. Wan and R. van der Merwe. Chapter 7, The Unscented Kalman Filter. *Adaptive and Learning Systems for Signal Processing, Communications and Control*, Wiley, 2001. 56, 151, 153

[Wang 04] H. Wang and B. Chen. A Comparison of the Subcarrier Allocation Schemes for Uplink OFDMA Systems. *Proceedings of the IEEE Conference on Information, Sciences, and Systems (CISS '04)*, March 2004. 27

[Wang 10] J. H. Wang, C. L. Song, X. T. Yao, and J. B. Chen. Sigma-Point H_∞ Filter for Initial Alignment in Marine Strapdown Inertial Navigation System. *Proceedings of the IEEE International Conference on Signal Processing Systems (ICSPS '10)*, Vol. 1, No. 6, pp. 580–584, July 2010. 158

[Wein 71] S. B. Weinstein and P. M. Ebert. Data Transmission by Frequency Division Multiplexing Using the Discrete Fourier Transform. *IEEE Transactions on Communications*, Vol. COM-19, No. 10, pp. 628–634, October 1971. 23, 30

[Wu 03] K. Y. Wu, W. K. Leung, and L. Ping. A Simple Approach to Near-Optimal Multiple Transmit Antenna Space-Time Codes. *Proceedings of the IEEE International Conference on Communications (ICC '03)*, Vol. 4, pp. 2603–2607, May 2003. 115

[Yang 08] S. S. Yang, W. K. Xu, L. Wang, and Q. F. Wei. Performance of STBC-IDMA System over Quasi-static Rayleigh Fading Channel. *Proceedings of the IEEE International Conference on Communications, Circuits and Systems(ICCCAS '08)*, pp. 44–47, May 2008. 115

[Yang 10] P. Yang, G. Dumont, and J. M. Ansermino. A Cusum-Based Multilevel Alerting Method for Physiological Monitoring. *IEEE Transactions on Information Technology in Biomedicine*, Vol. 14, No. 4, pp. 1046–1052, July 2010. 89

[Zame 81] G. Zames. Feedback and Optimal Sensitivity: Model Reference Transformations, Multiplicative Seminorms, and Approximate Inverses. *IEEE Transactions on Automatic Control*, Vol. 26, No. 2, pp. 301–320, April 1981. 135

[Zhao 06]   P. K. Zhao, L. L. Kuang, and J. H. Lu. Carrier Frequency Offset Es-
            timation Using Extended Kalman Filter in Uplink OFDMA Systems.
            *Proceedings of the IEEE International Conference on Communica-
            tions (ICC '06)*, Vol. 6, pp. 2870–2874, June 2006. 2, 47, 49, 72

[Zhou 07]   X. Y. Zhou, Z. N. Shi, and M. C. Reed. Iterative Channel Estima-
            tion for IDMA Systems in Time-Varying Channels. *Proceedings of
            the IEEE Global Communications Conference (GLOBECOM '07)*,
            pp. 4020–4024, November 2007. 103